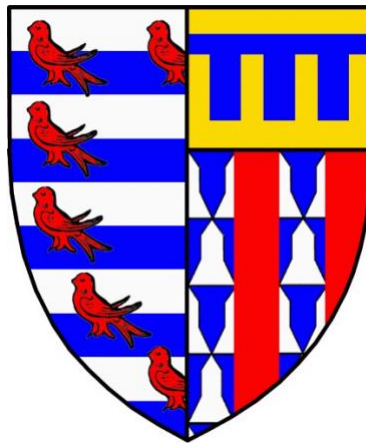


Case Studies in Invertebrate Visual Processing:

I. Spectral and Spatial Processing in the Early Visual System of *Drosophila melanogaster*

II. Binocular Stereopsis in *Sepia officinalis*

Rachael Claire Cashin Feord



Pembroke College

September 2019

This dissertation is submitted for the degree of Doctor of Philosophy

Declaration

This thesis is the result of my own work and includes nothing which is the outcome of work done in collaboration with the exception of the work presented in Chapter 6, which is the product of a study conceived by Dr Paloma Gonzalez-Bellido and Dr Trevor Wardill, who carried out the initial experiments. My contributions to the work are nonetheless substantial and individual contributions to the project are detailed in the acknowledgment section of Chapter 6 (section 6.5)

It is not substantially the same as any that I have submitted, or, is being concurrently submitted for a degree or diploma or other qualification at the University of Cambridge or any other University or similar institution except as declared in the Preface and specified in the text. I further state that no substantial part of my dissertation has already been submitted, or, is being concurrently submitted for any such degree, diploma or other qualification at the University of Cambridge or any other University or similar institution except as declared in the Preface and specified in the text

It does not exceed the prescribed word limit for the relevant Degree Committee.

Abstract

Case Studies in Invertebrate Visual Processing:

- I. **Spectral and Spatial Processing in the Early Visual System of *Drosophila melanogaster***
- II. **Binocular Stereopsis in *Sepia officinalis***

Rachael Claire Cashin Feord

This thesis addresses two aspects of visual processing in two different invertebrate organisms.

The fruit fly, *Drosophila melanogaster*, has emerged as a key model for invertebrate vision research. Despite extensive characterisation of motion vision, very little is known about how flies process colour information, or how the spectral content of light affects other visual modalities. With the aim to accurately dissect the different components of the *Drosophila* visual system responsible for processing colour, I have developed a versatile visual stimulation setup to probe for the combinations of spatial, temporal and spectral visual response properties. Using flies that express neural activity indicators, I can track visual responses to a colour stimulus (i.e. narrow bands of light across the spectrum) via a two-photon imaging system. The visual stimulus is projected on a specialised screen material that scatters wavelengths of light across the spectrum equally at all locations of the screen, thus enabling presentation of spatially structured stimuli. Using this setup, I have characterised spectral responses, intensity-response relationships, and receptive fields of neurons in the early visual system of a variety of genetically modified strains of *Drosophila*. Specifically, I compared visual responses in the medulla of flies expressing either a subset or all photoreceptor opsins, with differing levels of screening pigment present in the eye. I found layer-specific shifts of spectral response properties correlating with projection regions of photoreceptor terminals. I also

found that a reduction in screening pigment shifts the general spectral response in the neuropil towards the longer wavelengths of light. I have also mapped receptive fields across the different layers of the medulla for the peak spectral response wavelength. My results suggest that receptive field dimensions match the expected size predicted by the conservation of a columnar organisation in the medulla, with little variation from layer to layer. In a subset of these cells, we see an elongated receptive field suggestive of static orientation selectivity with an apparent split in the preferred axis of orientation of these receptive fields, with a near-orthogonal angle between the summed vectors of the split populations.

The camera type eyes of vertebrates and cephalopods exhibit remarkable convergence, but it is currently unknown if the mechanisms for visual information processing in these brains, which exhibit wildly disparate architecture, is also shared. I chose to investigate the visual processing mechanism known as stereopsis in the cuttlefish *Sepia officinalis*. Stereoscopic vision is used to assess depth information by comparing the disparity between left and right visual fields. This strategy is commonplace in vertebrates having evolved multiple times independently but has only been demonstrated in one invertebrate: the praying mantis. Cuttlefish require precise distance estimation during their predatory hunt when they extend two tentacles in a ballistic strike to catch their target. Using a 3D perception paradigm whereby the cuttlefish were fitted with anaglyph glasses, I show that these animals use stereopsis to resolve distance to their prey. Although this is not an exclusive depth perception mechanism for hunting, it does shorten the time and distance covered prior to striking at a target. Furthermore, stereopsis in cuttlefish works differently to vertebrates, as cuttlefish can extract stereopsis cues from anti-correlated stimuli.

Acknowledgments

Firstly I would like to express my thanks to my supervisor, Dr Trevor Wardill, for the guidance, support and confidence he has shown me over the course of this project.

I am grateful to the BBSRC Doctoral Training Partnership for funding me over the course of this four-year PhD programme.

I would like to thank Dr Paloma Gonzalez-Bellido for being a mentor to me throughout my PhD, and for all of the invaluable advice she has provided.

Thanks also go to Dr Kristian Franze for kindly stepping in as my Cambridge based supervisor once the lab had moved across the ocean.

A huge thank you goes to my PhD siblings, Jack Supple, Sam Fabian and Sergio Rossoni, as well as Mary Sumner to whom I am very grateful for this shared journey.

I am also very grateful to Dr Kathryn Feller and Dr Camilla Sharkey for their perpetual support, kindness, encouragement, wisdom and sense of fun throughout the project, and to Dr Jorge Blanco for his wizardry with genetics.

I would like to thank the Department of Physiology, Development and Neuroscience for their constant support over the course of my PhD. Special thanks go to the Neural Oscillation Group: Prof Ole Paulsen, Dr Susanna Mierau, Dr Audrey Hay and Dr Ana González-Rueda for taking me under their wing.

Thanks go to the University of Minnesota and to the Marine Biology Laboratory (Woods Hole, MA) for welcoming me into their respective institutions and giving me space and resources for my research.

I would also like to say a special thank you to the community that is Pembroke College, as well as to all the music and choral communities of Cambridge for making my experience at this university much more special and valuable than I could have imagined.

Very importantly, a huge thank you to my truly wonderful parents, Karan and Damian, without whom I would never have made it this far. This thesis is dedicated to them. And thank you to my siblings Helen, Elisabeth and Antony for always lending a sympathetic ear.

And finally, I would like to extend my thanks to all of my friends for their moral and emotional support.

Table of contents

<i>Declaration</i>	<i>1</i>
<i>Abstract</i>	<i>3</i>
<i>Acknowledgments</i>	<i>5</i>
<i>Table of contents</i>	<i>7</i>
<i>List of figures</i>	<i>13</i>
<i>List of tables</i>	<i>15</i>
<i>Chapter 1 – Introduction</i>	<i>17</i>
1.1 STUDYING INVERTEBRATE VISION	17
1.1.1 Who wouldn't want to study invertebrates?	17
1.1.2 The valuable contributions of invertebrate research	17
1.1.3 The case for comparative neurobiology	19
1.1.4 Key contributions to visual research from invertebrates	20
1.1.5 Thesis outline	20
1.2 DROSOPHILA AS A MODEL FOR VISION RESEARCH	21
1.2.1 <i>Drosophila</i> holds many tools for studying neural circuitry	21
1.2.2 Functional imaging: visualising neural activity	22
1.2.3 <i>Drosophila</i> has pioneered motion vision research	24
1.2.4 Colour vision in <i>Drosophila</i>	25
1.2.5 <i>Drosophila white</i> mutant	25
1.3 COLOUR/SPECTRAL PROCESSING IN DROSOPHILA	26
1.3.1 Defining colour vision	26
1.3.2 Phototransduction and light affective parameters	27
1.3.3 Photoreceptors properties	28
1.3.4 Early visual processing	30
1.3.5 Circuitry underlying colour vision	32
1.3.6 Do flies compute colour opponency?	33
1.3.7 The case for investigating fly colour vision	36
1.4 STEREOPSIS	38
1.4.1 Depth perception	38

1.4.2 The principle underlying stereopsis	39
1.4.3 Stereopsis, a remarkable feat of evolution	39
1.5 INVERTEBRATE MODEL ORGANISM: THE CUTTLEFISH.....	41
1.5.1 Cognition, camouflage and brain structure	41
1.5.2 The cuttlefish visual system	42
1.5.3 The cuttlefish predatory hunt.....	43
1.5.4 Depth perception in cuttlefish.....	45
1.5.5 The case for investigating stereopsis in cuttlefish	45
1.6 REFERENCES	46
 <i>Chapter 2 – Methodology for Drosophila visual system two-photon</i>	
<i>imaging</i>	<i>59</i>
2.1 DROSOPHILA PREPARATION METHODOLOGY	59
2.1.1 Fly stocks.....	59
2.1.2 Fly preparation.....	59
2.1.3 Saline solution	60
2.2 VISUAL STIMULATION SETUP	65
2.2.1 Overview of the system	65
2.2.2 Visual field coverage	66
2.2.3 Locating visual responses.....	66
2.3 CALCIUM IMAGING AND DATA ACQUISITION	66
2.3.1 Imaging parameters	66
2.3.2 Fluorescent signal extraction	67
2.4 REFERENCES	68
 <i>Chapter 3 – Development of a novel setup for simultaneous two-photon</i>	
<i>functional imaging of neural activity indicators and precise colour visual</i>	
<i>stimulation in Drosophila.</i>	<i>69</i>
3.1 INTRODUCTION.....	69
3.1.1 Characterising colour vision in <i>Drosophila</i>	69
3.1.2 Producing a stimulus to probe colour vision	69
3.1.3 General experimental requirements.....	70
3.2 EXPERIMENTAL SETUP COMPONENTS.....	71
3.2.1 Microscope and monochromator modifications	71

3.2.2 Light source filtering	72
3.2.3 Imaging pathway light filtering.....	72
3.2.4 The projector/monochromator setup.....	73
3.3 VISUAL STIMULUS PARAMETERS	77
3.3.1 Light measurement methodology.....	77
3.3.2 Transmission properties along the optical path	81
3.3.3 Setup geometry and alignment	82
3.4 SPECTRAL CHARACTERISATION OF THE STIMULATION SETUP	82
3.4.1 Radiance properties of the visual stimulus	82
3.4.2 Stimulus calibration process	85
3.4.3 Visual stimulus stability	87
3.5 SPATIAL CHARACTERISATION OF THE STIMULATION SETUP.....	90
3.5.1 Light scattering is a function of wavelength	90
3.5.2 Intensity distribution across the screen.....	91
3.5.3 Spectral constancy across the screen	91
3.6 REFERENCES	94
<i>Chapter 4 – Spectral Response Properties in the Drosophila Medulla.....</i>	<i>95</i>
4.1 INTRODUCTION.....	95
4.1.1 Detecting the spectral quality of light	95
4.1.2 The functional role of screening pigment.....	96
4.1.3 The advantages spectral information brings to visual processing.....	96
4.1.4 Chapter aims	97
4.2 METHODS.....	98
4.2.1 Fly stocks.....	98
4.2.2 Two-photon imaging	99
4.2.3 Visual stimulation.....	99
4.2.4 Analysis	102
4.3 RESULTS	104
4.3.1 Response profiling across medulla layers	105
4.3.2 General medulla processing	107
4.3.3 Inter-layer variability of intensity-response curve coefficients	115
4.4 DISCUSSION	119

4.4.1 Inner photoreceptor-driven responses	119
4.4.2 Unreported trials of alternative mutant strains	121
4.4.3 The effect of screening pigment on spectral processing	122
4.4.4 Genetically encoded calcium activity indicators	124
4.5 REFERENCES	126
<i>Chapter 5 – Receptive Field Mapping in the Drosophila Medulla</i>	<i>129</i>
5.1 INTRODUCTION	129
5.1.1 Why study receptive fields?	129
5.1.2 Receptive fields of medulla cells	130
5.1.3 Project aims	130
5.2 METHODS	131
5.2.1 Fly stocks	131
5.2.2 Two-photon imaging	131
5.2.3 Visual stimulation	131
5.2.4 Analysis	135
5.3 RESULTS	140
5.3.1 Spatial and temporal response profiles	140
5.3.2 Receptive field dimensions	141
5.3.3 Receptive field orientation preference	145
5.4 DISCUSSION	152
5.4.1 Experimental considerations	152
5.4.2 Receptive fields reflect the columnar structure of the medulla	153
5.4.3 Defining orientation selectivity	153
5.4.4 How does orientation selectivity arise?	154
5.4.5 Compound eye optical axes and preferred orientation	155
5.4.6 Elongated receptive fields could potentially arise from eye movements	156
5.4.7 Previous reports of orientation selectivity in <i>Drosophila</i>	157
5.5 REFERENCES	158
<i>Chapter 6 – Stereoscopic vision in the European cuttlefish</i>	<i>161</i>
6.1 INTRODUCTION	161
6.1.1 Evidence for stereopsis in cuttlefish	161
6.1.2 Project aims	162

6.2 METHODS.....	163
6.2.1 Animals.....	163
6.2.2 Experimental setup.....	163
6.2.3 Behavioural training.....	163
6.2.4 Visual stimuli.....	164
6.2.4 Data digitisation	170
6.2.5 Data analysis	170
6.3 RESULTS.....	172
6.3.1 Cuttlefish are tricked by a stereoscopic illusion	172
6.3.2 Tentacle extension is precisely calculated.....	172
6.3.3 Control parameters of the hunting behaviour	174
6.3.4 Impact of binocular vision on the hunting behaviour	174
6.3.5 ‘Static’ and ‘kinetic’ luminance correlation between eyes.....	178
6.4 DISCUSSION	180
6.4.1 Experimental considerations.....	180
6.4.2 Stereopsis is used in addition to other depth cues	181
6.4.3 Cuttlefish stereopsis requires ‘static’ background disparity.....	182
6.4.4 Stereopsis and eye movement control	182
6.4.5 Alternative depth perception cues.....	183
6.5. ACKNOWLEDGMENTS	184
6.6 REFERENCES	184
<i>Chapter 7 – Concluding remarks and future directions</i>	<i>187</i>
7.1 EXPLORING FACETS OF INVERTEBRATE VISION.....	187
7.1.1 General conclusions.....	187
7.1.2 Future directions for studying fly spectral processing	188
7.1.3 Future directions for studying cuttlefish visual processing	190
7.2 THE BIGGER PICTURE	191
7.2.1 Impact in the field of biological science	191
7.2.2 Impact in the field of technological science	191
7.3 REFERENCES	192
<i>Appendix 1</i>	<i>195</i>
<i>Appendix 2</i>	<i>197</i>

List of figures

Figure 1.1 Imaging neural activity in <i>Drosophila</i>	22
Figure 1.2 Spectral preference of rhodopsins in the <i>Drosophila</i> compound eye.....	29
Figure 1.3 The <i>Drosophila</i> visual system.....	30
Figure 1.4 Photoreceptor terminal projections.....	31
Figure 1.5 Candidate colour neurons.....	33
Figure 1.6 Lateral inhibition of colour photoreceptors.	35
Figure 1.7 Geometry of binocular vision.	40
Figure 1.8 Stages of the hunt.	44
Figure 2.1 Fly preparation for visual system imaging.	60
Figure 2.2 Effect of varying concentrations of buffer on saline pH stability.	62
Figure 2.3 Projector/monochromator and two-photon imaging setup.	65
Figure 3.1 Customised filter system for the monochromator/projector setup.	74
Figure 3.2 Optical equipment warm up time.	76
Figure 3.3 Versatility of monochromator produced light.	76
Figure 3.4 Experimental setup for simultaneous precise colour stimulation and two-photon functional imaging.	79
Figure 3.5 Spectrometer measurement parameters.....	80
Figure 3.6 Maximal optical power capacity of the monochromator/projector system. ..	84
Figure 3.7 Calibrated optical power capacity of the monochromator/projector system.	86
Figure 3.8 Variation in monochromator slit widths across daily calibrations.....	87
Figure 3.9 Assessment of optical power stability.....	89
Figure 3.10 Optical properties for consideration when selecting a screen material.	90
Figure 3.11 Optical power variation across the screen surface.	92
Figure 3.12 Variation in spectral constancy across the screen surface.....	93
Figure 4.1 Spectral sweep stimuli bandwidths.....	101
Figure 4.2 Segmentation process for neuronal signal extraction.	102
Figure 4.3 Layer specific response profiles of summed neural activity.....	106
Figure 4.4 Intensity-response stimulus: example responses.	107
Figure 4.5 Intensity-response relationship comparison across fly strains.....	109
Figure 4.6 Spectral sweep stimulus: example responses.	110
Figure 4.7 Spectral response profiling.	110
Figure 4.8 Spectral response profiling – breakdown for individual wavelengths.	113

<i>Figure 4.9 Intensity-response relationship coefficients across fly strains.</i>	<i>115</i>
<i>Figure 4.10 Intensity-response curve half maximum values across individual layers.</i>	<i>117</i>
<i>Figure 4.11 Spectral response profiles of layer groupings in the medulla</i>	<i>118</i>
<i>Figure 5.1 Receptive field mapping stimulus protocol.</i>	<i>133</i>
<i>Figure 5.2 Visual stimulus radiance.</i>	<i>134</i>
<i>Figure 5.3 Segmentation process for neuronal signal extraction.</i>	<i>136</i>
<i>Figure 5.4 Stages of the reconstruction of the spatial map.</i>	<i>139</i>
<i>Figure 5.5 Receptive field identification and measurements.</i>	<i>139</i>
<i>Figure 5.6 Temporal response profiles of spatial maps in the medulla.</i>	<i>143</i>
<i>Figure 5.7 Size properties of receptive fields in the medulla.</i>	<i>145</i>
<i>Figure 5.8 Receptive fields in the medulla exhibit an elongated structure.</i>	<i>146</i>
<i>Figure 5.9 Orientation preference of receptive fields in the medulla.</i>	<i>149</i>
<i>Figure 5.10 Receptive field properties exhibit no dependency on screen optics.</i>	<i>150</i>
<i>Figure 5.11 Example spatial maps for receptive fields.</i>	<i>151</i>
<i>Figure 6.1 Experimental setup and stereoscopic stimuli.</i>	<i>165</i>
<i>Figure 6.2 Screen and stimulus spectra.</i>	<i>166</i>
<i>Figure 6.3 Stimulus spectra, filter properties and spectral content crosstalk measurements – first generation glasses.</i>	<i>168</i>
<i>Figure 6.4 Stimulus spectra, filter properties and spectral content crosstalk measurements – second generation glasses.</i>	<i>169</i>
<i>Figure 6.5 Establishing the calculated prey location for stimuli with disparities.</i>	<i>171</i>
<i>Figure 6.6 Cuttlefish have stereoscopic vision.</i>	<i>173</i>
<i>Figure 6.7 Control data for different parameters of the hunting behaviour.</i>	<i>175</i>
<i>Figure 6.8 Binocular vision improves hunting behaviour.</i>	<i>176</i>
<i>Figure 6.9 Control analyses for monocular and binocular behaviour timings.</i>	<i>177</i>
<i>Figure 6.10 Stereopsis and luminance correlation.</i>	<i>179</i>

List of tables

<i>Table 2.1 Chemical components of Drosophila saline solution for calcium imaging from a selection of publications, as well as the saline developed for my own use.....</i>	<i>64</i>
<i>Table 3.1 Radiance values (photons/s/cm²) for 440 centre wavelength light with 25 and 30 nm slit width for a used bulb (~1500 hours) and a new bulb (~200 hours).</i>	<i>85</i>
<i>Table 4.1 Details of fly strains used and their phenotypic variations</i>	<i>105</i>
<i>Table A1 1-way ANOVA p-values from Figure 4.8</i>	<i>195</i>
<i>Table A2 1-way ANOVA p-values from Figure 4.10</i>	<i>196</i>
<i>Table A3 Fly preparation selection parameters.</i>	<i>197</i>

Chapter 1 – Introduction

1.1 STUDYING INVERTEBRATE VISION

1.1.1 Who wouldn't want to study invertebrates?

Before we stereotyped scientists as humans sporting unruly hair and an oversized lab coat accessorised with a sleek pipette, the notion of a biologist might conjure the image of a person hunched over a trail of insects with a magnifying glass. If one can get past the strong emotional reactions generally triggered by invertebrates, such as fear and disgust, one is hard pushed to refute that these critters are truly fascinating. All children are enthralled with the eponymous character in *The Very Hungry Caterpillar* who surprises us by transforming into a butterfly, and we are all awed by the organisation and discipline of a bee or ant colony, or the efficiency of a dragonfly hunt. Insects represent just a small contingency of the invertebrate realm, but the remaining members are no less intriguing. Cephalopods, for example, form an entirely spectacular group of invertebrates with such bizarre features and traits that a group of researchers has gone as far as suggesting an extra-terrestrial origin for these creatures (Steele *et al.*, 2018). Invertebrates are not just captivating because of their quirks, they are also very useful experimental subjects that have contributed much to the body of biological knowledge that has been amassed to this day.

1.1.2 The valuable contributions of invertebrate research

The fields of physiology and neuroscience are scattered with ground-breaking studies that were conducted in invertebrate organisms. My favourite example is the pioneering experimental work of the Nobel Prize laureates Hodgkin and Huxley (1952) using the squid giant axon to perform intracellular voltage-clamp recordings, which paved the way to an understanding of ion channels and their regulation of neuronal excitability and synaptic transmission. This work earned one of many Nobel Prizes awarded to invertebrate scientists. The famous work of Eric Kandel demonstrating synaptic learning mechanism in the sea slug *Aplysia* is another good example, and just recently, in 2017,

three *Drosophila* scientists - Jeffrey Hall, Michael Rosbash and Michael Young - have joined the list for their contributions towards unravelling the molecular basis of the circadian clock.

Using invertebrates for biological research presents many advantages. Firstly, it reduces the ethical controversies that can arise from using vertebrate species for experimentation purposes (the public accepts most invertebrates do not suffer pain and most people are unperturbed about using them for research with the exception, perhaps, of cephalopods). Other benefits include easier and less expensive laboratory housing (more individuals can be studied) as well as a shorter life cycle for the majority of invertebrate systems. Accordingly, generational turnover is faster which brings its own advantage where genetics are concerned. Much of invertebrate research pertains to features that have been conserved with evolution: biological concepts are teased apart by using a model with the same underlying structure or function but a lower degree of complexity. Many fundamental genetic, anatomical, physiological and behavioural traits are comparable between vertebrate and invertebrate species, thus invertebrate research has greatly contributed to our understanding of fundamental biological processes (Anton *et al.*, 2011) including advances in the biomedical arena underpinning mechanisms of health and disease (Wilson-Sanders, 2011). The vast leaps in imaging techniques in recent years (Denk *et al.*, 1990; Scanziani and Häusser, 2009), coupled to advances in optical neural sensors (e.g. genetically encoded activity indicators; Nakai *et al.*, 2001; Simpson and Looger, 2018) has shifted our approach to recording neural activity. *Drosophila melanogaster*, the fruit fly, lends itself particularly well to this research paradigm, reaffirming its value as a model organism (Seelig *et al.*, 2009).

In addition to the insights gained into general principles of animal physiology, invertebrate research can also reveal general evolutionary principles. Species-specific evolutionary adaptations to different lifestyles are interesting in themselves, but even more so when features appear in parallel through convergent evolution. Cephalopods appear as the perfect example in this context as species from this class of invertebrates exhibit surprising similarities to vertebrates, such as camera-type eyes and developed cognitive abilities. Thus, cephalopod research provides a unique opportunity to elucidate the universal selective pressures that result in convergent evolution of identical traits. Most exciting of all is the evolutionary principal driving cognition that can be examined through the comparison of two phylogenetically distant branches (O'Brien *et al.*, 2018).

1.1.3 The case for comparative neurobiology

The selection of a model organism requires a strategic choice. Important considerations include: (i) the convenience for study in a laboratory setting; (ii) the relatedness to humans, notably in the field of biomedical neuroscience; (iii) the availability of state-of-the-art research methodologies, such as advanced genetic manipulations in rodents and fruit flies; and (iv) the neuroethological relevance the suitability to studying specific behaviours (Marder, 2002; Carlson, 2012). Clear advantages exist for each of these approaches as the field of neuroscience demonstrates a rich array of organisms elected for study (i.e. mammals, birds, reptiles, amphibians, fish, invertebrates). Nonetheless, in a quest for direct medical and human applicability, 75% of neuroscience research is geared towards the study of three types of mammalian brain: mouse, rat and human (Manger *et al.*, 2008). Such a narrow selection of model organisms creates a strong bias to the design principles and features that are inherent to the species in question that may limit our understanding of general principles of brain function. Furthermore, the 80 million years elapsed since existence of the last common ancestor of the Muridae and the Hominidae calls into question the reliability of our extrapolations of human brain species from mouse studies. This argument, put forward by Manger *et al.* (2008), suggests that we might not yet know enough about brain evolution to ensure our extrapolations are pragmatic and not leaps of faith.

Comparative approaches to studying nervous systems are essential to identify broad computational principles of brain function (Hemberger *et al.*, 2016). The examination of brains of a variety of organisms allows us to consider similarities and differences not only at the mechanistical level (i.e. the variation of inherited features: genes, proteins, etc.) but less intuitively at an algorithmic level (i.e. how brains have developed different solutions to comparable neurobiological challenges). Such common computational principles reached through evolutionary convergence present a unique opportunity to study neural circuits with the same emergent functional properties but differing underlying mechanisms, hopefully leading to a better theory of neural system function (Hemberg *et al.*, 2016). Furthermore, investigations of non-model organism neural systems are likely to reveal features of brain function that are not readily discernible in our favoured mammalian critters. By choosing a comparative approach, we could even fast track the discovery process (Manger *et al.*, 2008). These arguments make a

compelling case for comparative approaches in the field of neuroscience. Invertebrate organisms, in particular, with their staggering diversity of nervous systems (Niven and Chittka, 2016), are highly relevant in this respect.

1.1.4 Key contributions to visual research from invertebrates

Vision in invertebrates is closely linked to their ecology. In other words, their visual systems specialise to meet their ecological demands and to perform tasks that are necessary to their survival. Colour vision, for example, is not universally present in all invertebrates, but has been acquired by animals such as bees that use colour information for foraging (Hempel de Ibarra *et al.*, 2014). Similarly, fiddler crabs can be counted amongst the small subset of creatures that have developed a sensitivity to polarised light, which they use for target detection on mudflats (How *et al.*, 2015). As such, invertebrates are well suited for the study of vision as they offer diverse and specialised neuroethological models. Insights from the study of invertebrate vision have been instrumental to moving the field of visual neuroscience forward and have made valuable contributions to our understanding of mammalian vision. The principle of lateral inhibition was first uncovered by Hartline *et al.* (1956) in the horseshoe crab retina, which describes the phenomenon resulting from an excited visual cell mediating inhibition of its neighbouring visual cells. The basic unit of motion detection circuitry, the elementary motion detector (EMD), was first conjectured by Reichardt (1961) following his observations of optomotor responses in the weevil beetle *Clorophanus*. Contributions extend to more sophisticated sensory computations too. The parameters of predictive coding, a theory that posits an existing internal representation of the world is used to filter and interpret incoming visual information, have been partly elucidated from research using flies (Srinivasan *et al.*, 1982).

1.1.5 Thesis outline

This thesis addresses two aspects of visual processing in two different invertebrate organisms. The following sections of this chapter aims to provide a brief introduction to *Drosophila* and cephalopod biology, as well as an overview of the target visual feature for each system. Both invertebrates studied in the coming chapters are, in their own right, useful model organisms. *Drosophila* is a classic lab companion, unrivalled in many ways through its tractability for genetic manipulations and vast array of developed

neuroscience tools. Over the past few decades, *Drosophila* has emerged as key model in vision research with detailed characterisation of photoreceptors, neural circuits and visually driven behaviours. Despite extensive characterisation of motion vision, very little is known about how flies process colour information, or how the spectral content of light affects other visual modalities. This thesis aims to address this deficit by measuring spectral response properties in the early visual system of *Drosophila*. The cuttlefish *Sepia* is a less common research subject but stands as an excellent neuroethological model with sophisticated physiological and behavioural capabilities. Specifically, the precise estimation of distance during prey capture suggests an elaborate neural strategy: stereopsis. Although these two case studies of invertebrate visual processing are not directly related, it appears that colour vision and stereopsis do not coexist in invertebrate species. It is thought that the neural circuitry underlying both of these visual processes, that rely on a comparative computation, might be an adaptation of the nervous system to repurpose the circuit for the most ecologically useful function (Nityananda and Read, 2017).

1.2 DROSOPHILA AS A MODEL FOR VISION RESEARCH

The visual world contains an extraordinarily complex combination of colours, contrast, motion and patterns. Unsurprisingly, how these differential components are assembled and integrated along the visual pathway to form an internal representation of the world still remains largely unclear. In the following section I will outline how flies, with their large, conspicuous eyes are good models for teasing apart these different modalities, not least because the prominence of this anatomical feature reflects the important role of vision as the primary source of interaction with the environment.

1.2.1 *Drosophila* holds many tools for studying neural circuitry

The fruit fly, *Drosophila melanogaster*, presents as a prime model for studying vision. Its small brain with approximately 100,000 neurons (Chiang *et al.*, 2011) and compact neural circuits can be manipulated by sophisticated genetic tools, thereby making it possible to dissect the neuronal machinery underlying vision. The traditional electrophysiological approach of neural activity recording is limited by the small diameter

of cells in the optic lobes. Recent advances in technology and genetic tools, however, make it possible to use functional imaging of neuron populations (**Figure 1.1**). The development of *in vivo* genetically-encoded neuronal activity indicators with high signal-to-noise and improved temporal sensitivity (reviewed by Simpson and Looger, 2018), as well as the ability to selectively label specific neuronal subtypes (Simpson, 2009), have opened new avenues for manipulating and monitoring neural circuits in fruit flies. Furthermore, knowledge of the anatomical substrate of the optic lobes has grown substantially over the past decade (Nern *et al.*, 2015; Takemura *et al.*, 2015). Thus, these advances provide a new framework for the investigation of the neural basis of visual processing in the optic lobes of *Drosophila*.



Figure 1.1 Imaging neural activity in *Drosophila*.

*Pan-neuronal expression of GCaMP in the *Drosophila* optic lobes reveals neural activity and can be visualised through the cuticle when a blue light source is applied.*

1.2.2 Functional imaging: visualising neural activity

The emergence of high precision imaging tools, both in terms of hardware (two-photon microscopy) and biological sensors (genetically encoded indicators of neural activity) has created a robust alternative to electrophysiology for monitoring neural activity. Although many reporters of neural activity exist, genetically encoded calcium indicators (GECIs) and genetically encoded voltage indicators (GEVIs) have been favoured amongst *Drosophila*-focused physiologists, as these allow precise labelling of specific neuron types. GEVIs enable tracking of voltage signals at a subcellular scale, providing an

excellent and direct readout of neural activity (Yang and St-Pierre, 2016). GECIs allow us to monitor calcium activity, an indirect readout of neural activity which occurs on a slower timescale to membrane voltage changes (Broussard *et al.*, 2014). However, signal-to-noise ratios in currently available GEVIs make them a less attractive option than their calcium counterparts (Panzera and Hoppa, 2019). In view of the excellent performance of the first few generations of GECIs, they have become the most popular optical probes for neural activity (Broussard *et al.*, 2014). Nonetheless, with ongoing efforts to increase indicator brightness, thus removing their primary disadvantage, GEVIs will likely be more broadly used in the neuroscience community (Yang and St-Pierre, 2016). Nakai *et al.* (2001) developed the original version of the best-known GECI: GCaMP, and efforts are ongoing to create updated versions with improved features such as increased fluorescence changes and response kinetics. GCaMP is the most popular option, however some alternatives present their own useful advantages. Ratiometric calcium sensors, for example, where the fluorescence ratio of two wavelengths is used to establish fluorescence changes, are advantageous as they can decrease sensitivity to bleaching, optical path length or illumination intensity (Thestrup *et al.*, 2014). Red-shifted GECIs have also been developed providing the option for simultaneous imaging of two differentiable neuronal populations (Dana *et al.*, 2016). In this thesis, experiments are carried out using two GECIs. The first, the green-emitting GCaMP6f (Chen *et al.*, 2013), is probably the most widely used neural activity indicator in the past half-decade, popular for its fast kinetics and good signal-to-noise ratio. The second, RGECO1 (Dana *et al.*, 2016), is a red-emitting indicator. Despite a lower overall performance by comparison to GCaMP, RGECO1 presents several advantages for functional imaging notably reduction of scattering and absorption in tissue, as well as the option for dual-colour imaging with green-emitting indicators (Dana *et al.*, 2016).

Although imaging cannot be considered a replacement method for electrophysiology (reviewed by Scanziani *et al.*, 2009), it allows *Drosophila* vision scientists to record from previously inaccessible brain regions. With optical approaches, the necessity for physical contact with the sample tissue is removed, thus overcoming a major limitation of electrophysiology. It also presents the advantage of monitoring activity in an entire population of neurons simultaneously, thus enabling scientists to readily identify the progression of response properties throughout consecutive layers of the visual circuitry. A few drawbacks must, however, also be noted. Instead of recording electrical activity with direct (or close proximity) to the membranes of neurons, functional imaging relies on a probe that translates the electrical signal into an optical readout. Calcium activity is

a suitable correlate for neural activity, however not all intracellular calcium release is necessarily a result of excitable activity in a cell. Furthermore, the indirect nature of the optical approach to neural recording reduces the signal-to-noise-ratio of neuron membrane electrical events, that can be detected with great sensitivity using electrophysiological methods. Despite evidence that GCaMP6 can trace single action potentials (Chen *et al.*, 2013), this is restricted to particular conditions and is not applicable in all recording paradigms. Many neural events are not conducive to extraction via calcium imaging. These include inhibitory responses and subthreshold events, but also responses in very small neuron terminals which can be sometimes be less than a micron in *Drosophila* and thus tricky to resolve with a two-photon microscope. It is also important to note that speed of image acquisition is also an important factor here, notably as brain movement can hamper signal extraction especially with slow acquisition that is preferential for precise tracking.

1.2.3 *Drosophila* has pioneered motion vision research

The elementary motion detector (EMD) is generally accepted as the basis for motion detection in flies (Borst *et al.*, 2010). It follows a model proposed by Hassenstein and Reichard (1956), describing how the change in luminance at two distinct locations of the visual field are sampled by independent visual channels. The comparison of temporal differences in the output of these channels then serves to detect the presence of a moving object. In practical terms, this is achieved by delayed and non-delayed lines that converge onto an output channel: motion is detected if the signals from both lines arrive simultaneously. The neuronal circuitry underlying the EMD in *Drosophila* has been carefully dissected. Two pathways work in parallel, one for the detection of light edges, and one for the detection of dark edges (Clark *et al.*, 2011; Maisak *et al.*, 2013). Neurons in the medulla are central to this computation. In the light-edge-detection circuitry, Mi1 and Tm3 medulla cells correspond to the delayed and non-delayed lines respectively. Equivalent medulla neurons in the dark-edge-detection pathway are Tm1 and Tm2 (Behnia *et al.*, 2014, Strother *et al.*, 2014). The coincidence detectors, T4 and T5 cells form the medullary output from light- and dark-edge-detection pathways (Takemura *et al.*, 2008; Shinomiya *et al.*, 2014). These pathways converge to form an output encoded by lobula plate tangential cells (LPTCs), which are selectively responsive to specific directions of motion across the visual field (Schnell *et al.*, 2012).

1.2.4 Colour vision in *Drosophila*

“Colour is one of the hobbies of the retina”. This amusing statement was made by a Midwestern physiologist, Mathew Alpern, who suggests the colour processing abilities of our visual system serve an aesthetical purpose above all. Nonetheless, my interest in fly visual processing lies with colour vision – how the visual system responds to light of different spectral compositions, and the neural mechanisms for encoding such differences. *Drosophila*’s ability to discriminate colours serves ecological purposes such as identifying food or egg-laying substrates (reviewed by Lunau, 2014), but spectral information has also been suggested to enhance feature detection by addition of a perceptual dimension that aids the discernment of objects in the visual scene, thus improving visually guided behaviour (Krauskopf and Farell, 1990; Barlow, 2001; Nishida *et al.*, 2007). The study of colour vision in flies, however, has proven itself to be a challenging task.

1.2.5 *Drosophila* *white* mutant

The steadily increasing, yet already vast, array of genetic manipulations made available to the *Drosophila* research community through years of investigations is a key factor of its success as a model organism for biological research. Specific gene identification and techniques for gene enhancement or disruption has opened unprecedented avenues towards precise manipulation of individual physiological parameters. However, modifying one genetic parameter does not cause a single isolated change across the entire organism, but can affect many, sometimes unexpected aspect of physiology or behaviour. Limitations of genetic approaches will be discussed further in the final chapter of this thesis, but in this section of the discussion I aim to elaborate a little about the white eye mutation commonly used in fruit fly research, which affects visual processing significantly.

The white eye *Drosophila* mutant, *white* (*w*), discovered over a 100 years ago (Morgan, 1910), played a fundamental role in the development of the field of fruit fly genetics, and is still the basis for many transgenic fly strains today as it is a useful tool for the selection of transformants in the process of fly line generation. Two different screening pigment molecules are found in the compound eye, drospterin, and ommochrome. They originate from the *scarlet* and *brown* genes respectively, named for the colour they appear (Nolte, 1952). The white-eye fly mutation affects the *w* gene (CG2759) necessary

for the White-Brown and White-Scarlet dimerisation essential for screening pigment synthesis (O'Hare *et al.*, 1984; Sullivan *et al.*, 1979). This is how phenotypes with a variation of screening pigment density can be achieved. However, the *w* gene mutation does not only affect pigment synthesis, but also interacts with other biosynthetic pathways such as the production of neurotransmitters serotonin, histamine and dopamine (Goodwill *et al.*, 1998). Thus, it is unsurprising that *w* mutants exhibit disrupted physiological and behavioural functions such as mobility, life span and stress tolerance (Ferreiro *et al.*, 2017), courtship behavior (Anaka *et al.*, 2008) and aggressive behavior (Hoyer *et al.*, 2008) to mention but a few. These unwanted consequences of the genetic mutation can be considered to be separate enough from the isolated aspect of visual physiology being studied in this thesis. Importantly, however, some instances of loss of visual function have been noted in previous studies in *white null* mutant flies. Borycz *et al.* (2008) report a considerable decrease in the number of synaptic vesicles at the terminals of photoreceptor cells. It has also been shown that these mutants suffer from an age-dependent, progressive neurodegenerative retinal phenotype (Ferreiro *et al.*, 2017). This manifests itself through the progressive loss of photoreceptors and smaller size of rhabdomeres in the photoreceptors that survive, thus directly impacting visual function. The authors of the study suggest 5 days of age as the cut-off point for recording visual response in flies, however Ferreiro *et al.* (2017) only assessed ERG components in 5-day old flies versus 30-day old flies so the rate of decline in visual function between these two points are unclear. Awareness of the degeneration of visual function in these flies is essential, and a conservative approach to age limits for experimental subjects should reduce the effects of the degeneration on the visual physiology.

1.3 COLOUR/SPECTRAL PROCESSING IN *DROSOPHILA*

1.3.1 Defining colour vision

In order to discriminate colour independent of intensity, comparisons between spectrally distinct photoreceptors are necessary. The *Drosophila* visual system fulfils this prerequisite with its five spectral classes of photoreceptors. Colour vision, as defined by primate visual psychophysics, refers to the weighted output of photoreceptor cells that

respond to distinct wavelengths of light in order to produce the perceptual representation we know as colour (Conway, 2009). However, not all species benefit from the developed cognitive abilities of humans, and consequently our definition of the neural processing of a stimulus's spectral composition needs to be extended beyond this conventional view. Different grades of colour vision in animals have been defined by Kelber and Osorio (2010) based on behavioural responses ranging from phototactic behaviour towards specific wavelengths of light, to the neural representation of colour, such as colour learning or colour categorisation. Although true colour vision has been demonstrated in a number of invertebrate species, it has been suggested that invertebrates also use alternate mechanisms for processing colour information. For example, the water flea visual system comprises an exceptionally large range of spectrally distinct visual pigments, but is thought to use the spectral content of light to position itself in food-rich water rather than to construct a perceptual representation of colour (Marshall and Arikawa, 2014). Spectral-specific behavioural responses have been reported in *Drosophila*, such as the positive phototactic behaviour exhibited towards short wavelengths of light (Gao *et al.*, 2008), as has true colour vision involving the neural representation of colour (Schnaitmann *et al.*, 2013). Thus, a range of downstream physiological processes and behavioural outputs rely on the ability of *Drosophila* to distinguish between spectrally distinct visual stimuli, arguing in favour of several different neural mechanisms implicated in colour processing.

Our understanding of colour vision in flies stems from two areas of focus. The first is the study of the different visual pigments present in the compound eye, their spectral characteristics/absorption properties, and their patterns of distribution throughout photoreceptive cells. The second encompasses all behavioural responses of flies relative to the spectral composition of light and its reflectance in the environment. The neural circuitry that encodes chromatic signals, however, remains relatively obscure.

1.3.2 Phototransduction and light affective parameters

In *Drosophila*, sampling of the visual world occurs via stereotyped units, ommatidia, which repeat and juxtapose in a crystalline-like lattice to form the facets of the compound eye's surface. Electromagnetic waves in the spectrum of 300 to 800 nm are converted into a biological signal by light-sensitive proteins, rhodopsins. These photopigment molecules exist in several classes – different rhodopsins will preferentially absorb photons from different wavelengths of light and can thus be characterised by a spectral

sensitivity profile (**Figure 1.2**). Absorption of light by a rhodopsin molecule causes a process called photoisomerisation that converts the molecule to its metarhodopsin state, thus shifting the spectral sensitivity of the visual pigment towards the longer wavelengths of light (Hardie, 1985). The native rhodopsin state is restored when a photon is absorbed by metarhodopsin, thus reactivating the visual pigment for another phototransduction cycle (Yau and Hardie, 2009). The 3-hydroxy-retinal chromophore of the fly rhodopsin associates with the molecule 3-hydroxy-retinol, also known as a sensitising pigment. The latter is sensitive to the ultraviolet (UV) portion of the spectrum and primes the chromophore by transferring the energy from UV photons it has absorbed (Kirschfeld *et al.*, 1983). This accounts for the high sensitivity of Rhodopsin 1 in the short wavelengths of light (**Figure 1.2 B**). Screening pigment in the eye of flies is found in cells surrounding the photoreceptors of a given ommatidia and serves as an optical screen to prevent any off-axis light reaching the photoreceptors (reviewed by Stavenga *et al.*, 2017). The spectral properties of this screening pigment have implications for the spectral properties of the photoreceptor and are discussed further in Chapter 4 (section 4.1.2). Furthermore, bright blue light flashes can result in the excessive conversion of rhodopsin into metarhodopsin. This can cause a temporary light insensitivity of the photoreceptor and is referred to as a prolonged depolarisation afterpotential (PDA, Wright & Cosens, 1977). In a case such as this, red light that shifts metarhodopsin back to rhodopsin is essential to restart the visual pigment cycle and demonstrates another spectral dependency of photoreceptor function. Thus, in addition to the spectral sensitivity of the rhodopsin expressed in the photoreceptor, many other properties of the cell can affect the spectral response.

1.3.3 Photoreceptors properties

One ommatidia of the *Drosophila* eye comprises eight photoreceptive cells (R1-R8), each expressing only one version of rhodopsin. R1-R6 constitute the 'outer photoreceptors' and express rhodopsin (Rh) 1, a broadband visual pigment that is sensitive to light across the visual spectrum with peak sensitivities (i.e. a higher probability of a photon in the peak range driving a response in the photoreceptor) at 360 nm and 480 nm (**Figure 1.2**; Salcedo *et al.*, 1999; Stavenga, 2010). 'Inner photoreceptors' R7 and R8 are positioned in the centre of the outer photoreceptor cluster, are stacked one over the other, and each express a different rhodopsin tuned to a narrow portion of wavelengths. R7-R8 cell pairs co-ordinately express a particular

rhodopsin to construct one of two types of ommatidial rhodopsin partnerships: ‘pale’ or ‘yellow’ (Franceschini *et al.*, 1981; Mazzoni *et al.*, 2008). These are stochastically distributed following a 30:70 ratio (Morante and Desplan, 2008). R7 and R8 pairs in ‘pale’ ommatidia express the UV-sensitive Rh3 in R7 and the blue-sensitive Rh5 in R8, whereas ‘yellow’ ommatidia inner photoreceptors express Rh4 in R7 and Rh6 in R8, maximally sensitive to UV and green wavelengths respectively (Figure 1.2; Chou *et al.*, 1999; Salcedo *et al.*, 1999). There are exceptions to this arrangement, however, as co-expression of Rh3 and Rh4 occurs in the same R7 cell in ommatidia of the dorsal rim of the eye (Mazzoni *et al.*, 2008). Furthermore, a specialised subset of ommatidia, present along the dorsal rim of the eye, express Rh3 in both R7 and R8 cells. These ommatidia are thought to be involved in the detection of polarised light (Wernet *et al.*, 2012).

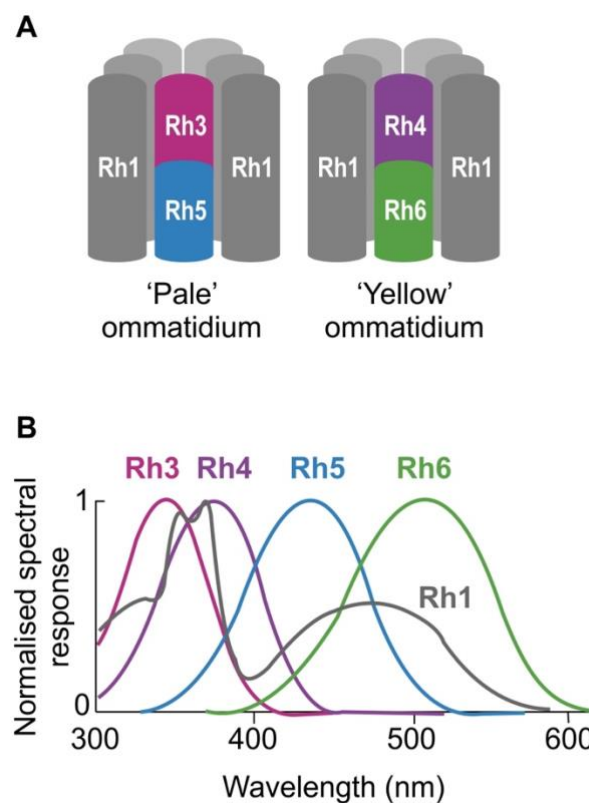


Figure 1.2 Spectral preference of rhodopsins in the *Drosophila* compound eye.

The broadly tuned Rh1 is expressed in R1-R6 photoreceptors, whereas Rh3-Rh6 found in R7 and R8 cells exhibit a narrow spectral tuning peaking in the UV, blue and green regions of the spectrum

1.3.4 Early visual processing

The cytoarchitecture of the fruit fly visual system reveals a highly structured organisation. Initial downstream processing of visual information occurs in the lamina and the medulla, the first and second neuropil respectively (**Figure 1.3**) and these process information in a modular fashion via columns called ‘cartridges’. *Drosophila* visual processing follows the principle of neuronal superposition: within an ommatidium, individual photoreceptor cells sample light from different angles. A single cartridge pools inputs from six R1-R6 of neighbouring ommatidia that collect light from the same point of the visual scene (Braitenberg, 1967). Early visual neuropil exhibit surprising complexity in the organisation of their neural circuits. The anatomy of visual circuits was first dissected by Cajal (Cajal and Sanchez, 1915) and over the last half century, this knowledge has been refined to establish not only the wiring patterns of specific subsets of neurons, but also the functional role of such cells in visual pathways. This detailed understanding of circuitry provides an excellent foundation for studies of visual network responses.

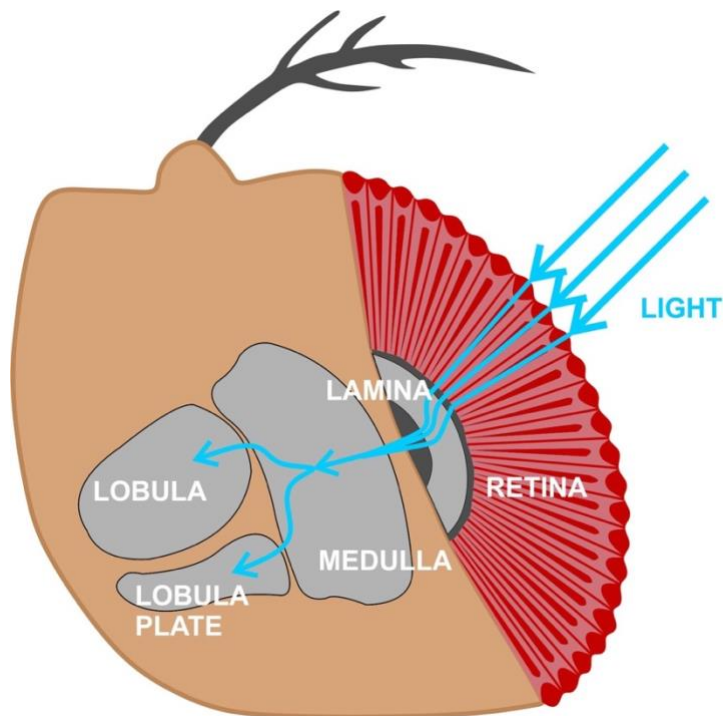


Figure 1.3 The *Drosophila* visual system.

The visual neuropil are organised into columns of cells, each processing a portion of the visual field. Light is collected by the photoreceptors and relayed through the lamina, medulla, lobula and lobula plate.

Pathways of information flow in the medulla largely remain a mystery. It has been said: “The medulla is truly a frontier and only the brave have ventured into its near impenetrable thickets. The tales brought back by these pioneers are full of promise but provide scant knowledge of commerce or currency” (Ali, 1984). Nonetheless, the identification of at least 56 types of neurons in the fly medulla (Takemura, 2015), as well as our understanding of their stereotyped organisation, provides an important scope for future investigation.

Neurons in the lamina are contacted by R1-R6 and project axons to the medulla, innervating different layers depending on cell type (**Figure 1.4**; Meinertzhagen and O’Neil, 1991). In contrast, R7/R8 cells bypass the first neuropil and project directly to the medulla (**Figure 1.4**; Morante and Desplan, 2004).

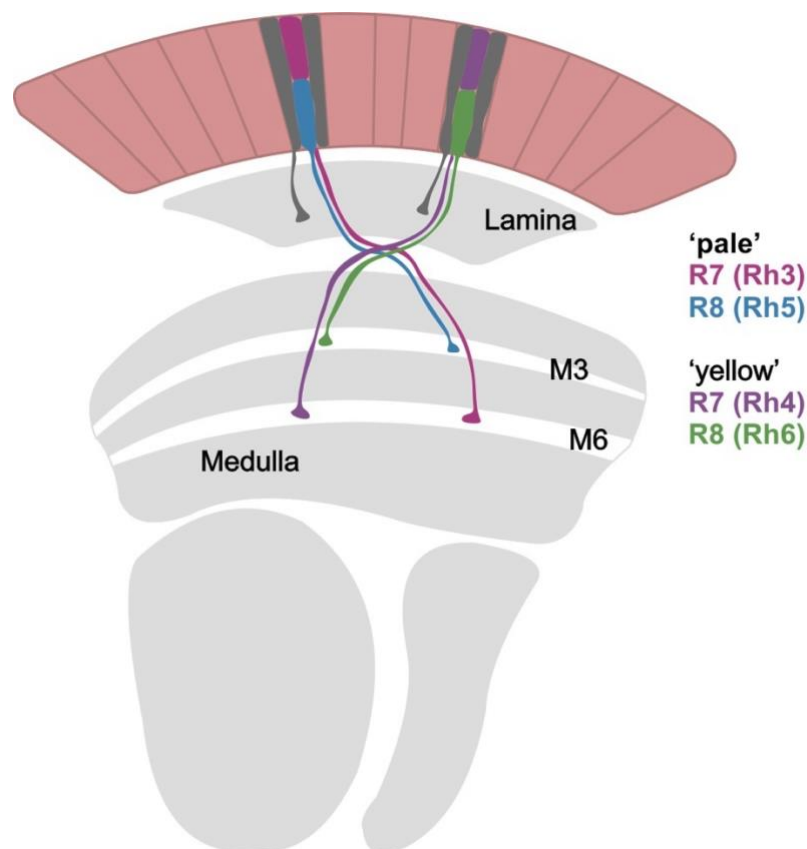


Figure 1.4 Photoreceptor terminal projections.

R1 ‘outer’ photoreceptors project to the first visual neuropil, the lamina, whereas the ‘inner’ photoreceptors project to the second neuropil, the medulla, where R7 cells terminate in layer 6 and R8 cells terminate in layer 3.

The rich array of neuron subtypes in the medulla are categorised according to their projection patterns. Intrinsic medulla (Mi) cells have dendrites spanning a single column and arborisations in several distinct layers but are confined to the neuropil. Transmedulla (Tm) cells connect discrete medulla layers but also send projections to the lobula plate, as do bushy T-cells. Y cells are similar to Tm neurons but they bifurcate to innervate both the lobula and the lobula plate. Finally, the medulla also contains cells that synapse exclusively in the lobula plate (reviewed by Borst, 2009). Despite extensive knowledge of circuit organisation, the functional properties of medulla neurons are poorly understood with the exception of pathways involved in motion detection. Medulla cell types and their role in interpreting the spatiotemporal changes in luminance from which motion can be characterised have been central to recent investigations of fly vision (Borst, 2014).

1.3.5 Circuitry underlying colour vision

Dissection of colour vision circuits in *Drosophila* has proven a challenging task thus far. The medulla presents itself as the obvious initial target within the optic lobe for the investigation of colour processing as it is the first neuropil where signals arising from all photoreceptors can be combined. Studies in other invertebrates, notably bees, have paved the way on this front, providing evidence for colour neurons in the medulla (Kien and Menzel 1977; Paulk *et al.*, 2009; Mota *et al.*, 2013). *Drosophila* scientists have attempted to build on this, employing the array of sophisticated genetic tools available to them. Behavioural experiments combined with selective ablation of visual circuitry components have revealed that colour encoding in the fruit fly medulla occurs in multiple redundant pathways. Such approaches have identified a set of candidate ‘colour’ neurons, which include Tm5a, b, and c, Tm20, Dm9 and Dm8 (Figure 1.5). These cells play a role in processing spectral information, however inactivation of individual cell types does not inhibit colour learning (Gao *et al.*, 2008; Karuppudurai *et al.*, 2014; Melnattur *et al.*, 2014). Furthermore, a recent study has established that the collection of spectral information occurs via all photoreceptors, not just R7 and R8 as previously thought (Schnaitmann *et al.*, 2013). Thus, although a ‘necessary/sufficient’ genetic approach has determined specific neurons of colour circuits, we still know very little about how colour information is actually computed and processed by visual networks. This understanding of colour circuitry pales by comparison to our knowledge of motion vision. This can be attributed, in part, to comparative ecological importance of both visual modalities to the

fly: whereas three-quarters of photoreceptors express Rh1 and are thought to provide input to the motion pathway, only the remaining quarter are considered to contribute to colour vision.

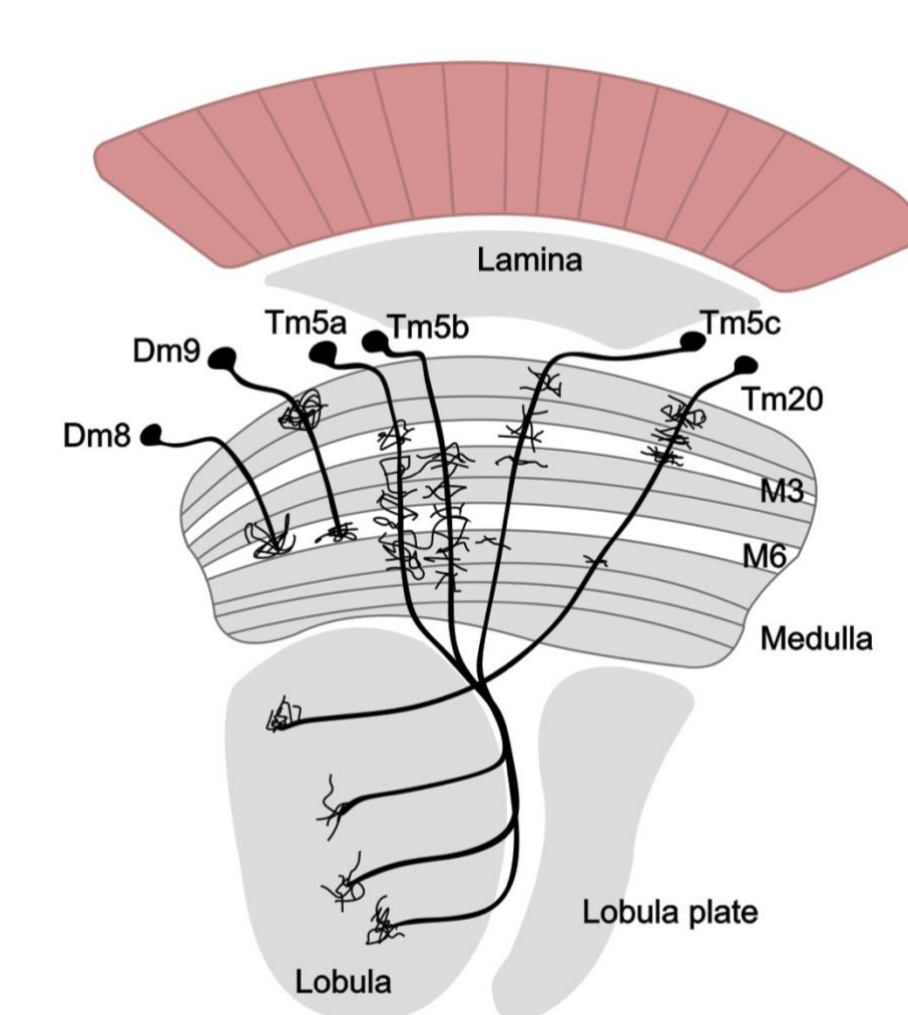


Figure 1.5 Candidate colour neurons.

Diagrammatic representation of candidate colour neurons in the medulla. Adapted from Schnaitmann et al., 2020.

1.3.6 Do flies compute colour opponency?

In mammals, colour vision is mediated via the comparison of different photoreceptor responses by combining inputs to establish the ratio of excitation from each

photoreceptor type. Specifically, this occurs via opponency mechanisms whereby signals from spectrally distinct photoreceptor classes converge onto a single neuron. The recipient cell combines the information in an opponent fashion such that the cell exhibits an excitatory response to a subset of wavelengths and inhibitory response to a different portion of the spectrum (reviewed by Jacobs, 2014). Chromatic opponency has also been found in invertebrates, specifically honeybees (Kien and Menzel 1977; Mota *et al.*, 2013), however, until recently, it remained unclear whether photoreceptor channels combine information in *Drosophila*, and if so, how relative ratios of excitation are encoded. A prior investigation shows that *Drosophila* is in fact capable of true colour vision as it can learn to distinguish between stimuli of different colours independent of intensity. The study shows that the discrimination between blue and green stimuli relies on interchangeable opsin pairs, either Rh1/Rh4 or Rh4/Rh6, suggesting that post-receptoral computations underlying colour vision may occur within an optic cartridge (Schnaitmann *et al.*, 2013). As such, chromatic opponency remains a prime candidate strongly supported by several lines of evidence. Furthermore, as a consequence of the relative positioning of R7 and R8 cells of one ommatidium, the two photoreceptors share a light pathway. Sampling light from the same point of the visual scene provides an ideal configuration for comparisons of the spectral content of light (Morante and Desplan, 2008). In addition, connectivity of cells in the medulla also points to post-receptoral comparisons in the medulla. A subset of cells, Tm3-6, are postsynaptic to both R7 and R8, thus creating the necessary neural circuitry for post-photoreceptor opponency (Morante and Desplan, 2008). Schnaitmann *et al.* (2018) have reported a form of chromatic opponency that occurs between the R7 and R8 photoreceptor terminals in the medulla. Surprisingly, the opponency arises via direct synaptic inhibition between the photoreceptor cells, a novel mechanism of photoreceptor interaction for daylight colour vision that has not been previously reported. As a result, photoreceptors exhibit a biphasic sensitivity curve maintaining their peak excitation as described above, but exhibiting an inhibitory dip matching the peak sensitivity of their counterpart R7 or R8 cell (Figure 1.6). How this form of lateral inhibition supports a downstream colour opponent circuit is not obvious, and there is an argument that the mechanism here serves the purpose of reducing signal redundancy (Longden, 2018). This offers a considerable advantage to any visual system tasked with assimilating light across a highly variable range of intensities and wavelengths. Longden delineates how this form of lateral inhibition (direct synaptic inhibition between photoreceptors) enables the implementation of a contrast-enhancing mechanism. In this way, the photoreceptors

scale their response to encode relative rather than absolute signals, thereby producing outputs that are comparable and reduce redundancies of information in the visual scene. This is an important step in the colour processing pathway, especially in the case of colour-opponency, but may also provide a filtering mechanism for more general medullary processing.

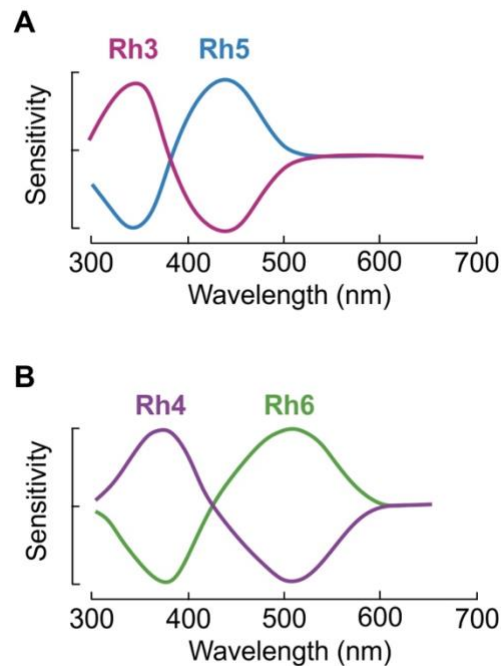


Figure 1.6 Lateral inhibition of colour photoreceptors.

The diagrammatic representation of photoreceptor sensitivities extrapolated from responses to five light emitting diodes that shows the colour opponency response profiles of R7 and R8 terminals. Photoreceptors within the same ommatidia, 'pale' (A) or 'yellow' (B), interact to influence their excitability. Through direct synaptic inhibition, excitation of the R7 photoreceptor reduces the activity of its counterpart R8 cell, and vice versa. Adapted from Schnaitmann et al. (2018).

Nonetheless, chromatic information might in fact be processed in different manners by the medulla and thus response profiles of colour sensitive neurons could be more varied than previously thought. Some alternate mechanisms for colour encoding in flies have been suggested. For example, some medulla cells are innervated by only one of the

inner photoreceptors, R7 or R8 (Morante and Desplan, 2008) and it has been a point of interest to consider how such cells might contribute to colour detection. One possibility is that these neurons span several columns and, in this way, compare R7/R8-derived information from distinct ommatidia subtypes (pale and yellow). Alternatively, these cells might not be involved in true colour vision but could instead play a role in spectral processing. For example, Dm8 cells are multicolumnar wild-field amacrine cells that are necessary for UV spectral preference. They receive input from approximately sixteen R7 cells, and it has been suggested that they pool information to detect low intensity UV light in the presence of high intensity visible light (Gao *et al.*, 2008; Karuppururai *et al.*, 2014). Another interesting theory posits that spectral discrimination does not always occur via comparison of different photoreceptor outputs. There is evidence that flies possess coloured corneal filters on a subset of ommatidia, causing different quantum catches in otherwise identical photoreceptors (Stavenga *et al.*, 2002). In other words, this is a diversification of photoreceptor types where the expression of the opsin is identical, but the spectral sensitivity is altered by the diverging corneal filter, providing a paradigm for same-opsin receptors to be involved in spectral discrimination. Of note, in addition to colour encoding, the wavelength composition of a visual stimulus is likely to influence the response of other visually-responsive neurons. Indeed, the spectral content of light might impact on other aspects of visual processing, including the enhancement of motion detection as demonstrated by Wardill *et al.* (2012). Finally, a last area of contention lies with the number and diversity of photopigments in the fruit fly eye. It is unclear why four different visual pigments might be useful. Barlow (1982) established that three spectral channels, as found in the trichromat primate, is sufficient to distinguish all colours across the visible spectrum, thus additional visual pigments would not add to the colour discrimination capabilities. This argues in favour of a system with multiple colour processing mechanisms.

1.3.7 The case for investigating fly colour vision

The existence of colour vision has been demonstrated in *Drosophila*, but the underlying neural mechanisms for colour encoding remain to be elucidated. The overall picture is being pieced together with improved knowledge of photoreceptors, candidate cells involved in circuitry, and colour-guided behaviour. Despite a recent breakthrough by Schnaitmann *et al.* (2018), much still remains unclear. Does spectral processing occur via post-receptoral comparisons? If so, which photoreceptor classes are involved, and

where in the visual neuropil do such comparisons occur? Furthermore, it is thought that spectral processing could occur in an unconventional manner, and strategies used by the fly medulla cells to encode spectral information are not fully understood. Thus, although prior studies have extensively investigated visual processing in the medulla, most have assessed the motion detection properties of the neuropil (reviewed by Borst, 2014; Yang and Clandinin, 2018). Few investigations, in contrast, have been designed with the view to understand how visual stimuli of varying spectral content might influence the response properties of cells in the medulla.

A key limiting factor in the investigation of spectral processing in *Drosophila* is the current state of visual stimulation paradigms. Commercially available visual displays are tailored to the primate retina. Their three-colour channel configuration provides an excellent experience to the trichromatic user but fall short for visual systems with different photoreceptor sensitivities. Furthermore, the high flicker-fusion frequencies in invertebrates, beyond 120 Hz in *Drosophila melanogaster* (Gonzalez-Bellido *et al.*, 2011), outpace the refresh rates of commercial displays. An array of experimental systems for visual stimulation have been developed, but many constraints still limit the investigation of combined colour and motion processing. The production of bands of monochromatic light is commonly achieved via a broadband light source coupled either to a monochromator (Salcedo *et al.*, 1999), individual colour filters (Kien and Menzel, 1977; Meinertzhagen *et al.*, 1983), LEDs (Little *et al.*, 2019), or more recently LED-based monochromator systems (Belušič *et al.*, 2016). Such monochromatic light provides full-field stimulation but lacks any spatial structure. Paradigms for spatially patterned stimuli include LCD displays, LED panels or projectors, none of which offer the option of many colours (Paulk *et al.*, 2014; Allen *et al.*, 2017; Franke *et al.*, 2019, Schnaitmann *et al.* 2018). In order to probe visual response properties to combined modalities, the integration of spectral and spatial resolution within a stimulation paradigm is essential. In addition, the spectrally broad and high detection sensitivity of two-photon imaging systems restricts the visual stimuli's spectral range and intensity: light applied within the detection range of the microscope will result in an artefact on the acquired image consequently restricting the range of wavelengths available for visual stimulation.

In order to determine the precise contribution of spectral information to visual computations, I designed a system that offers fine-wavelength resolution across a large portion of the spectrum, that can be calibrated to produce isoluminant stimuli over a biologically-relevant range of intensities and that allows the presentation of spatially- and

temporally-structured stimuli. This system presents several advantages not offered in any previous imaging-based setups for characterising physiological responses to colour. These include (1) the delivery of coloured stimuli simultaneous to the acquisition of two-photon images (previous methods rely on the scanner fly-back periods for stimulation (Franke *et al.*, 2019, Schnaitmann *et al.* 2020), (2) the ability to arbitrarily chose the centre wavelength and bandwidth), and (3) a rear projection screen which maintains isoluminant hues across the visible spectrum. Using this setup, I characterised intensity-response relationships, spectral response profiles and receptive field properties of the pan-neuronally labelled medulla in several genetically modified strains of *Drosophila*, varying in opsin functionality and screening pigment density.

1.4 STEREOPSIS

1.4.1 Depth perception

Images sampled by the retina are spatial variations in illumination collected by a two-dimensional array of photoreceptors. Nevertheless, our reconstructed percept of the world reintegrates the lost third-dimension by extrapolating depth cues through properties of the retinal images that signify variations in the depth dimension. These depth cues fall into three distinct categories (Banks *et al.*, 2016): triangulation (stereopsis, motion parallax, blur), light transport (shading, occlusion) and perspective (looming, texture gradient, relative size). The two latter groups are frequently described as pictorial cues, which broadly refers to the collection of effects present in a two-dimensional image such as shadows, shading, specular highlights and occlusion. Some species use this to their advantage, such as countershading of body colouration to avoid predation (Rowland *et al.*, 2008), but pictorial cues have also long been exploited by human artists in their endeavour to create the illusion of depth on the canvas. Triangulation depth cues are based on viewing the world from different vantage points.

Motion parallax, for example, uses the relative velocity of objects on the retina to infer depth. While the mechanisms detailed above are implemented monocularly, stereopsis relies on the comparison of disparities between left and right images acquired simultaneously to compute depth. It is thus reserved for animals that are capable of producing a significant binocular overlap (reviewed by Nityananda and Read, 2017).

1.4.2 The principle underlying stereopsis

We are all familiar with the compelling effect of a three-dimensional illusion, produced by stereograms or 3D cinematography (ironically, I am not familiar with the sensation as I lack stereoscopic vision). This reconstruction of a depth precept relies on the comparison of two retinal images that are to a larger extent identical, with minor differences arising from the physical offset of both eyes positioned at laterally symmetrical locations on the face/head ([Figure 1.7](#)). These differences in retinal images are referred to as 'binocular disparities' and can be processed by the brain to assemble a three-dimensional percept of the visual scene (Wheatstone, 1983). Interestingly, monocular stereopsis had been theorised in stomatopods where the two halves of the compound eye have overlapping visual fields and consequently the necessary prerequisite for triangulation (Schiff *et al.*, 1985), but no experimental evidence has confirmed the hypothesis.

1.4.3 Stereopsis, a remarkable feat of evolution

Stereopsis is a remarkable feat of evolution as the brain has to associate two non-identical, slightly offset images and from the paired output, needs to gauge the non-corresponding points that originate from the same point in space (Barlow *et al.*, 1967). The evolution of both binocular vision and stereopsis have occurred multiple times independently in invertebrate and vertebrate species (in insects, amphibians, birds and mammals to our current knowledge; Fox and Blake, 1971; Collett, 1977; Fox *et al.*, 1977; Rossel, 1983), though the vast majority of our knowledge and understanding of stereoscopic vision derives from the study of human stereopsis (Cumming and DeAngelis, 2001). Thus, stereopsis is a commonplace strategy; however, it is also a costly process. The requirement of a substantial binocular overlap, the field of view is dramatically reduced by comparison to the panoramic perspective of animals with laterally positioned eyes. Of note, binocular overlap yields many further non-stereopsis advantages, such as improved signal-to-noise ratio (Jones and Lee, 1981) and redundancy (Changizi and Shimojo, 2008). Furthermore, our knowledge of neural

circuitry underpinning stereopsis in primates specifies involvement of numerous cortical areas (Cumming and DeAngelis, 2001; Welchman, 2016), thus the computation of stereopsis is also costly on the neuronal architecture front.

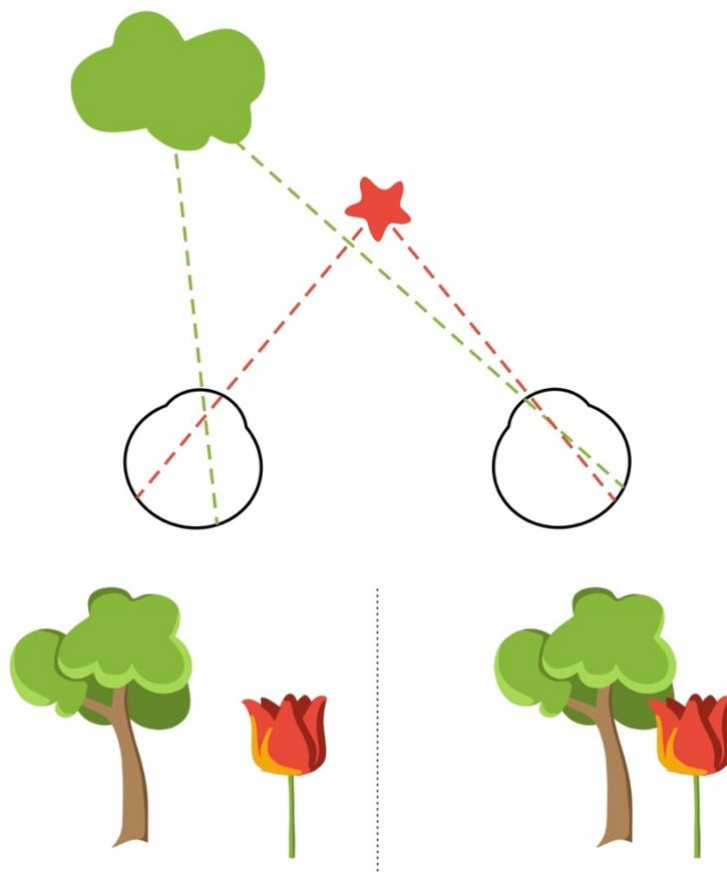


Figure 1.7 Geometry of binocular vision.

The two objects of the visual scene, the flower and tree, are fixated by both eyes. The images of each object fall on different locations of the left and right retina, thus there is a disparity between left and right retinal images. The amount of disparity depends on the depth (i.e. the difference in the distance to the two objects and the distance to the point of fixation, here the red flower), and our visual system uses this information to infer depth.

The primary functions of stereopsis (reviewed by Nityananda and Read, 2017) are range-finding and camouflage breaking. The ability to judge distances confers obvious advantages, especially for behaviours such as prey capture or predator avoidance amongst others. Praying mantids and toads are good examples of animals that lie in wait for their prey and gauge distance using stereopsis in order to know when to strike (Collet, 1977; Nityananda *et al.*, 2016). Camouflage breaking, where an object invisible to a monocular gaze is revealed through the disparity between a region of the left and right images, is equally profitable. A target can be entirely camouflaged in a monocular frame but can be identified by a shift in depth when stereopsis is employed. This strategy has been identified in falcons, sheep and owls amongst others (Clarke *et al.*, 1976; Fox *et al.*, 1977; van der Willigen *et al.*, 1998).

1.5 INVERTEBRATE MODEL ORGANISM: THE CUTTLEFISH

1.5.1 Cognition, camouflage and brain structure

Cephalopods are renowned for their advanced cognition and behavioural plasticity. The term cognition is a broad concept that eludes a consensus for its precise definition, but loosely refers to “the subset of learning phenomena that somehow involve more than basic associative processes” (reviewed by Perry *et al.*, 2013). Nonetheless, it is clearly apparent that cuttlefish possess a higher level of cognitive ability that parallels the abilities described in vertebrate species. These range from classical conditioning (Cole *et al.*, 2005) to reversal learning (Karson *et al.*, 2003) as well as varied spatial learning strategies (Alves *et al.*, 2006). A particularly fascinating behavioural output in cuttlefish is their striking camouflage ability. This highly adaptable and surprisingly speedy process permits them to express a host of patterns and colourations, as well as textures on their entire body. It has been suggested that these cephalopods can exhibit up to thirteen different pattern categories, and that in addition to concealment, the patterns also serve as a communication channel for both inter- and intra-specific interactions (Hanlon and Messenger, 1988). As this process is visually-driven (Hanlon and Messenger, 1988; Chiao *et al.*, 2015), it underlines the sophistication of visual perception and sensorimotor

transformations that occurs in the cuttlefish brain. Furthermore, the visual features that influence body pattern production are varied and complex: they range from light-dark contrast to depth cues (reviewed by Kelman *et al.*, 2008).

Taken together, these cognitive and behavioural outputs of cuttlefish argue strongly in favour of a brain structure equivalent to the mammalian cerebral cortex in cephalopods (Edelman and Seth, 2009; Roth, 2015). Although paired anatomical and functional brain mapping has been in part conducted in cephalopods, very little in the literature pertains specifically to cuttlefish. Generally speaking, the cephalopod nervous system presents itself as a centralised collection of over thirty different lobes (Young, 1971). Often described as the textbook example of convergent evolution, cephalopod brains exhibit specialised areas that can be equated to analogue regions in the vertebrate central nervous system. A full review of the current knowledge of cephalopod nervous system and its parallels to vertebrates has been compiled by Shigeno *et al.* (2018). Here, however, I will concisely highlight a few notable features. In mammals, sensory input to the cerebral cortex is generally gated by the thalamus (Swanson, 2007), but no equivalent has been uncovered in cephalopods. Candidates for other brain areas that might take on a thalamus-type role, however, have been suggested (Shigeno *et al.*, 2018). The cephalopod peduncle lobe has been identified as the counterpart to the vertebrate cerebellum and appears to play an important role in coordinating motor output, including eye movements (Young, 1976), and the frontal- and vertical lobes have been implicated in higher-level processing such as visual and tactile memory (Maldonado, 1963) and has been shown to undergo similar cellular plasticity rules as mammals (Hochner *et al.*, 2003; Shomrat *et al.*, 2008). Finally, it appears that somatotopy is not a feature of cephalopod nervous systems (Zullo *et al.*, 2009).

1.5.2 The cuttlefish visual system

The common European cuttlefish, *Sepia officinalis*, is easily recognisable by its large eyes, eight arms, and two long tentacles that extend out to capture prey, usually small crustaceans and fish. Cuttlefish can be just as easily missed, however, through behaviours of adaptive camouflage by changing the appearance of visual features on their skin (Hanlon and Messenger, 1996). Of particular interest to the community of cuttlefish researchers are their eyes, which exhibit a number of unusual features. First and foremost, the prominent size of the eyes matches their prominent role in prey capture

and predator avoidance as well as intra-specific communication (Hanlon and Messenger, 1996). Furthermore, cuttlefish have camera-type eyes bearing strong similarities to vertebrate eyes, including a cornea, a lens, an iris, a vitreous cavity and a retina, although these parallels have evolved through convergence (Packard, 1972). With the exception of a small group of mid-water squid, the majority of cephalopod species use vitamin A₁ based visual pigments for phototransduction (Chung and Marshall, 2016). The photoreceptors of the cuttlefish's retina all express the same opsin, with a peak alpha-band sensitivity at 492 nm and a peak beta-band sensitivity at 360 nm (Brown and Brown, 1958). Thus, unlike vertebrates, cuttlefish are not equipped with the ability to discriminate colours (Mäthger *et al.*, 2006; Marshall and Messenger, 1996). They are, however, thought to be sensitive to the polarisation of light as cuttlefish photoreceptors exhibit the same orthogonal structure as observed in other cephalopod species with polarisation vision (Shashar *et al.*, 1996). The two eyes are positioned on either side of the head providing lateral fields of view of approximately 177° each in the horizontal plane. The visual fields overlap to create a binocular field of 9° to 10° degrees (Messenger, 1968). The extrinsic eye muscles, described by Budelmann and Young (1993), can move each eye independently of the other. This can increase the binocular overlap to 75° and enables the occurrence of ocular convergence to position an object of interest on both retinas simultaneously (Messenger, 1968). Thus, through eye vergence, cuttlefish can markedly increase their binocular overlap when required while retaining a panoramic field of view the remainder of the time. A large portion of the central nervous system (approximately two thirds of the total brain mass) is dedicated to visual processing: the optic lobes take on the shape of kidney beans and sit behind each eye (Nixon and Young, 2003), further proving the importance of visual information for cuttlefish.

1.5.3 The cuttlefish predatory hunt

In addition to their notorious cognitive and camouflage abilities, cephalopods are visually-driven hunters. The predatory attack ([Figure 1.8](#)), first described by Messenger (1968), ranks amongst the more striking features and behaviours of the cuttlefish. Detection of the prey causes an immediate attention response including eye movements, skin colour changes, arm movements and results in the rotation of the animal to face its prey. The animal then enters the positioning phase, approaching and rotating its eyes towards the prey while maintaining its body axis directed towards the target. The

cuttlefish estimates the optimal striking distance and moves backward and forward along its anterior-posterior axis to position itself accordingly. At this stage the arms spread out and the tips of the tentacles protrude. Once the cuttlefish is ready to strike, the tentacles are propelled forward in a ballistic shoot. The prey is apprehended with suckers on the tentacle clubs and guided back to the arms and mouthparts where it is subdued with toxins (Ghiretti, 1959).

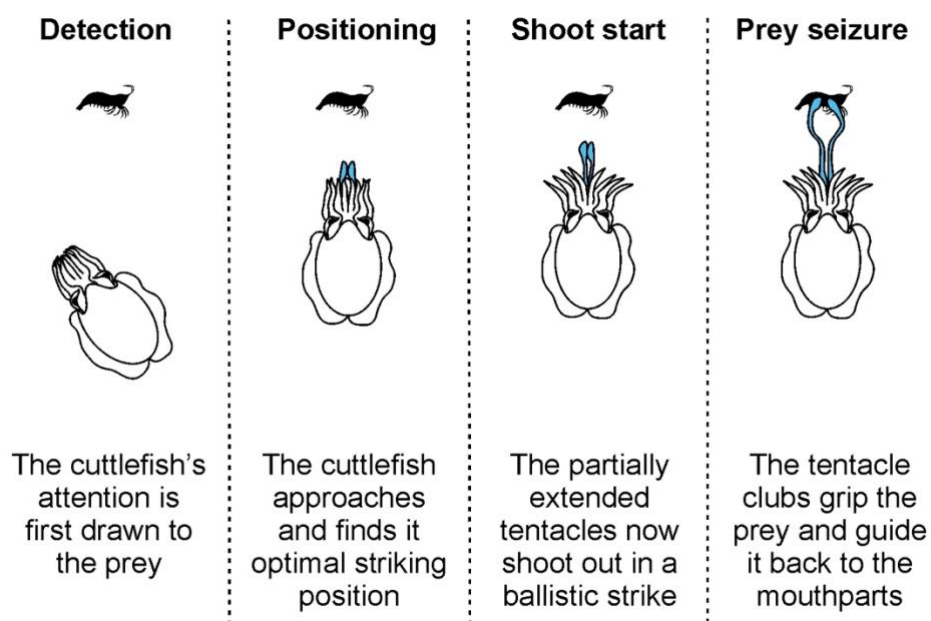


Figure 1.8 Stages of the hunt.

The predatory hunt can be segmented into four identifiable stages first described by Messenger (1968). Stage 1: detection – the target prey is noticed and identified by the cuttlefish eliciting an attention response. Stage 2: positioning – the cuttlefish moves to position itself optimally relative to the prey as the tips of tentacles appear. Stage 3: shoot start – the ballistic strike is initiated as the tentacles are propelled forward. Stage 4: prey seizure – the extended tentacles make contact with the target and the prey is gripped by the clubs to be guided back to the mouthparts.

1.5.4 Depth perception in cuttlefish

Cuttlefish depth perception has been largely investigated in the context of their exceptional camouflage skills in which they use visual information to coordinate their body patterns. Not only have they been shown to interpret an object's shape from a two-dimensional image using shading and directional illumination (Zylinski *et al.*, 2016), but they can also differentiate real pebbles from a photograph despite the strong similarity of pictorial cues (Kelman *et al.*, 2008), suggesting an alternative depth perception mechanism to these. Cuttlefish have been shown to use a saccadic movement strategy to estimate distance from translational optic flow (Helmer *et al.*, 2016). Thus, they share with humans the use of monocular cues (pictorial and motion parallax) to extrapolate three-dimensional information from images (Bruce *et al.*, 1996).

1.5.5 The case for investigating stereopsis in cuttlefish

Motion parallax and stereopsis are both good candidates in the search for mechanisms of depth perception in cuttlefish. Their hunting strategy necessitates a range estimation of their prey which could be gauged through movement of the target, but it has also been hypothesised that this distance is estimated with stereopsis on the basis of the vergence angle of the eyes (Messenger, 1968). In Chapter 6, this hypothesis is tested by manipulating the perception of depth through stereopsis-only cues. We developed a behavioural assay in which the cuttlefish wear anaglyph glasses and chase after the disparate silhouette of shrimp on a screen. This stimulus creates an illusory sense of depth to the animal, but only if it has the ability to use binocular disparity cues. Using this paradigm, we show that cuttlefish alter their position relative to the screen depending on the disparity of the stimulus. Thus, we demonstrated that cuttlefish use stereopsis while hunting prey.

1.6 REFERENCES

- Allen, A. E., R. Storch, F. P. Martial, R. A. Bedford and R. J. Lucas (2017). "Melanopsin Contributions to the Representation of Images in the Early Visual System." *Curr Biol* 27(11): 1623-1632.e1624.
- Ali, M. A. (1984). "Photoreception and Vision in Invertebrates." New York: Plenum. 858 pp.
- Alves, C., R. Chichery, J. G. Boal and L. Dickel (2007). "Orientation in the cuttlefish *Sepia officinalis*: response versus place learning." *Anim Cogn* 10(1): 29-36.
- Anaka, M., C. D. MacDonald, E. Barkova, K. Simon, R. Rostom, R. A. Godoy, A. J. Haigh, I. A. Meinertzhagen and V. Lloyd (2008). "The white gene of *Drosophila melanogaster* encodes a protein with a role in courtship behavior." *J Neurogenet* 22(4): 243-276.
- Anton, S., C. Gadenne and F. Marion-Poll (2011). "Frontiers in invertebrate physiology - grand challenge." *Front Physiol* 2: 38.
- Banks, M. S., D. M. Hoffman, J. Kim and G. Wetzstein (2016). "3D Displays." *Annu Rev Vis Sci* 2: 397-435.
- Barlow, H. (2001). "The exploitation of regularities in the environment by the brain." *Behav Brain Sci* 24(4): 602-607; discussion 652-671.
- Barlow, H. B. (1982). "What causes trichromacy? A theoretical analysis using comb-filtered spectra." *Vision Res* 22(6): 635-643.
- Barlow, H. B., C. Blakemore and J. D. Pettigrew (1967). "The neural mechanism of binocular depth discrimination." *J Physiol* 193(2): 327-342.
- Behnia, R., D. A. Clark, A. G. Carter, T. R. Clandinin and C. Desplan (2014). "Processing properties of ON and OFF pathways for *Drosophila* motion detection." *Nature* 512(7515): 427-430.
- Belušič, G., M. Ilić, A. Meglič and P. Pirih (2016). "A fast multispectral light synthesiser based on LEDs and a diffraction grating." *Sci Rep* 6: 32012.
- Borst, A. (2009). "Drosophila's view on insect vision." *Curr Biol* 19(1): R36-47.
- Borst, A. (2014). "Neural circuits for elementary motion detection." *J Neurogenet* 28(3-4): 361-373.
- Borst, A., J. Haag and D. F. Reiff (2010). "Fly motion vision." *Annu Rev Neurosci* 33: 49-70.
- Borycz, J., J. A. Borycz, A. Kubów, V. Lloyd and I. A. Meinertzhagen (2008). "Drosophila ABC transporter mutants white, brown and scarlet have altered

- contents and distribution of biogenic amines in the brain." *J Exp Biol* 211(Pt 21): 3454-3466.
- Braitenberg, V. (1967). "Patterns of projection in the visual system of the fly. I. Retina-lamina projections." *Exp Brain Res* 3(3): 271-298.
- Broussard, G. J., R. Liang and L. Tian (2014). "Monitoring activity in neural circuits with genetically encoded indicators." *Front Mol Neurosci*, 7:97.
- Brown, P. K. and P. S. Brown (1958). "Visual pigments of the octopus and cuttlefish." *Nature* 182(4645): 1288-1290.
- Bruce, V., P. R. Green and M. A. Georgeson (1996). "Visual Perception: Physiology, Psychology, and Ecology". Psychology Press
- Budelmann, B. U. and J. Z. Young (1993). "The oculomotor system of decapod cephalopods: eye muscles, eye muscle nerves, and the oculomotor neurons in the central nervous system." *Philos Trans R Soc Lond B Biol Sci* 340(1291): 93-125.
- Carlson, B. A. (2012). "Diversity matters: the importance of comparative studies and the potential for synergy between neuroscience and evolutionary biology." *Arch Neurol*, 69(8):987-993.
- Changizi, M. A. and S. Shimojo (2008). "'X-ray vision' and the evolution of forward-facing eyes." *J Theor Biol* 254(4): 756-767.
- Chen, T. W., T. J. Wardill, Y. Sun, S. R. Pulver, S. L. Renninger, A. Baohan, E. R. Schreiter, R. A. Kerr, M. B. Orger, V. Jayaraman, L. L. Looger, K. Svoboda and D. S. Kim (2013). "Ultrasensitive fluorescent proteins for imaging neuronal activity." *Nature* 499(7458): 295-300.
- Chiang, A. S., C. Y. Lin, C. C. Chuang, H. M. Chang, C. H. Hsieh, C. W. Yeh, C. T. Shih, J. J. Wu, G. T. Wang, Y. C. Chen, C. C. Wu, G. Y. Chen, Y. T. Ching, P. C. Lee, H. H. Lin, H. W. Hsu, Y. A. Huang, J. Y. Chen, H. J. Chiang, C. F. Lu, R. F. Ni, C. Y. Yeh and J. K. Hwang (2011). "Three-dimensional reconstruction of brain-wide wiring networks in *Drosophila* at single-cell resolution." *Curr Biol* 21(1): 1-11.
- Chiao, C. C., C. Chubb and R. T. Hanlon (2015). "A review of visual perception mechanisms that regulate rapid adaptive camouflage in cuttlefish." *J Comp Physiol A Neuroethol Sens Neural Behav Physiol* 201(9): 933-945.
- Chou, W. H., A. Huber, J. Bentrop, S. Schulz, K. Schwab, L. V. Chadwell, R. Paulsen and S. G. Britt (1999). "Patterning of the R7 and R8 photoreceptor cells of

- Drosophila*: evidence for induced and default cell-fate specification." *Development* 126(4): 607-616.
- Chung, W. S. and N. J. Marshall (2016). "Comparative visual ecology of cephalopods from different habitats." *Proc Biol Sci* 283(1838).
- Clark, D. A., L. Bursztyn, M. A. Horowitz, M. J. Schnitzer and T. R. Clandinin (2011). "Defining the computational structure of the motion detector in *Drosophila*." *Neuron* 70(6): 1165-1177.
- Clarke, P. G., I. M. Donaldson and D. Whitteridge (1976). "Binocular visual mechanisms in cortical areas I and II of the sheep." *J Physiol* 256(3): 509-526.
- Cole, P. D. and S. A. Adamo (2005). "Cuttlefish (*Sepia officinalis*: Cephalopoda) hunting behavior and associative learning." *Anim Cogn* 8(1): 27-30.
- Collett, T. (1977). "Stereopsis in toads." *Nature* 267(5609): 349-351.
- 'Contribution to the knowledge of the nerve centers of insects. By S. R. Cajal and Domingo Sanchez. 1915', (1983) *Trabajos del Instituto Cajal / Consejo Superior de Investigaciones Cientificas*, 74(1-4), 1-164.
- Conway, B. R. (2009). "Color vision, cones, and color-coding in the cortex." *Neuroscientist* 15(3): 274-290.
- Cumming, B. G. and G. C. DeAngelis (2001). "The physiology of stereopsis." *Annu Rev Neurosci* 24: 203-238.
- Dana, H., B. Mohar, Y. Sun, S. Narayan, A. Gordus, J. P. Hasseman, G. Tsegaye, G. T. Holt, A. Hu, D. Walpita, R. Patel, J. J. Macklin, C. I. Bargmann, M. B. Ahrens, E. R. Schreiter, V. Jayaraman, L. L. Looger, K. Svoboda and D. S. Kim (2016). "Sensitive red protein calcium indicators for imaging neural activity." *Elife* 5.
- Denk, W., J. H. Strickler and W. W. Webb (1990). "Two-photon laser scanning fluorescence microscopy." *Science*. 248(4951):73-6.
- Edelman, D. B. and A. K. Seth (2009). "Animal consciousness: a synthetic approach." *Trends Neurosci* 32(9): 476-484.
- Ferreiro, M. J., C. Pérez, M. Marchesano, S. Ruiz, A. Caputi, P. Aguilera, R. Barrio and R. Cantera (2017). "Mutant." *Front Neurosci* 11: 732.
- Fox, R. and R. R. Blake (1971). "Stereoscopic vision in the cat." *Nature* 233(5314): 55-56.
- Fox, R., S. W. Lehmkuhle and R. C. Bush (1977). "Stereopsis in the falcon." *Science* 197(4298): 79-81.
- Franceschini, N., K. Kirschfeld and B. Minke (1981). "Fluorescence of photoreceptor cells observed in vivo." *Science* 213(4513): 1264-1267.

- Franke K., A. Maia Chagas, Z. Zhao, M. J. Y. Zimmerman, P. Bartel, Y. Qiu, K. P. Szatko, T. Baden and T. Euler (2019). "An arbitrary-spectrum spatial visual stimulator for vision research." *eLife* 8: e48779.
- Gao, S., S. Y. Takemura, C. Y. Ting, S. Huang, Z. Lu, H. Luan, J. Rister, A. S. Thum, M. Yang, S. T. Hong, J. W. Wang, W. F. Odenwald, B. H. White, I. A. Meinertzhagen and C. H. Lee (2008). "The neural substrate of spectral preference in *Drosophila*." *Neuron* 60(2): 328-342.
- Ghiretti, F. (1959). "Cephalotoxin: crab-paralysing agent of the posterior salivary glands of cephalopods." *Nature* 183, 1192-1193.
- Gonzalez-Bellido, P. T., T. J. Wardill and M. Juusola (2011). "Compound eyes and retinal information processing in miniature dipteran species match their specific ecological demands." *Proc Natl Acad Sci U S A* 108(10): 4224-4229.
- Goodwill, K. E., C. Sabatier and R. C. Stevens (1998). "Crystal structure of tyrosine hydroxylase with bound cofactor analogue and iron at 2.3 Å resolution: self-hydroxylation of Phe300 and the pterin-binding site." *Biochemistry* 37(39): 13437-13445.
- Hanlon R. T., J. B. Messenger and J. Z. Young (1988). "Adaptive coloration in young cuttlefish (*Sepia officinalis* L.): the morphology and development of body patterns and their relation to behaviour." *Phil. Trans. R. Soc. Lond. B* 320: 437–487.
- Hanlon, R. T. and J. B. Messenger (1996). "Cephalopod Behaviour." Cambridge: Cambridge University Press.
- Hardie, R. C. (1985). "Functional organization of the fly retina". *Progress in Sensory Physiology*, vol. 5, ed. Ottoson D, pp. 1–79. Springer, Berlin.
- Hartline, H. K., H. G. Wagner and F. Ratliff (1956). "Inhibition in the eye of *Limulus*." *J Gen Physiol* 39(5): 651-673.
- Hassenstein, B., and W. Reichardt (1956). "Systemtheoretische analyse der zeit-, reihenfolgen- und vorzeichenauswertung bei der bewegungsperzeption des rüsselkäfers *chlorophanus*". *Z. Naturforsch.* 11b:513–24
- Helmer, D., B. R. Geurten, G. Dehnhardt and F. D. Hanke (2016). "Saccadic Movement Strategy in Common Cuttlefish." *Front Physiol* 7: 660.
- Hemberger, M., L. Pammer, L. G. Laurent (2016). "Comparative approaches to cortical microcircuits." *Curr Opin Neurobiol*, 41:24-30.

- Hempel de Ibarra, N., M. Vorobyev and R. Menzel (2014). "Mechanisms, functions and ecology of colour vision in the honeybee." *J Comp Physiol A Neuroethol Sens Neural Behav Physiol* 200(6): 411-433.
- Hochner, B., E. R. Brown, M. Langella, T. Shomrat and G. Fiorito (2003). "A learning and memory area in the octopus brain manifests a vertebrate-like long-term potentiation." *J Neurophysiol* 90(5): 3547-3554.
- Hodgkin, A. L. and A. F. Huxley (1952). "A quantitative description of membrane current and its application to conduction and excitation in nerve." *J Physiol* 117(4): 500-544.
- How, M. J., J. H. Christy, S. E. Temple, J. M. Hemmi, N. J. Marshall and N. W. Roberts (2015). "Target Detection Is Enhanced by Polarization Vision in a Fiddler Crab." *Curr Biol* 25(23): 3069-3073.
- Hoyer, S. C., A. Eckart, A. Herrel, T. Zars, S. A. Fischer, S. L. Hardie and M. Heisenberg (2008). "Octopamine in male aggression of *Drosophila*." *Curr Biol* 18(3): 159-167.
- Jacobs, G. H. (2014). "The discovery of spectral opponency in visual systems and its impact on understanding the neurobiology of color vision." *J Hist Neurosci* 23(3): 287-314.
- Jones, R. K. and D. N. Lee (1981). "Why two eyes are better than one: the two views of binocular vision." *J Exp Psychol Hum Percept Perform* 7(1): 30-40.
- Karson, M. A., G. B. Jean and R. T. Hanlon (2003). "Experimental evidence for spatial learning in cuttlefish (*Sepia officinalis*)." *J Comp Psychol* 117(2): 149-155.
- Karuppudurai, T., T. Y. Lin, C. Y. Ting, R. Pursley, K. V. Melnattur, F. Diao, B. H. White, L. J. Macpherson, M. Gallio, T. Pohida and C. H. Lee (2014). "A hard-wired glutamatergic circuit pools and relays UV signals to mediate spectral preference in *Drosophila*." *Neuron* 81(3): 603-615.
- Kelber, A. and D. Osorio (2010). "From spectral information to animal colour vision: experiments and concepts." *Proc Biol Sci* 277(1688): 1617-1625.
- Kelman, E. J., D. Osorio and R. J. Baddeley (2008). "A review of cuttlefish camouflage and object recognition and evidence for depth perception." *J Exp Biol* 211(Pt 11): 1757-1763.
- Kien, J., and R. Menzel (1977). "Chromatic properties of neurons in the optic lobes of the bee. II. Narrow band and colour opponent neurons". *J Comp Physiol* 113, 35-53.

- Kirschfeld, K., R. Feiler, R. C. Hardie, K. Vogt and N. Franceschini (1983). "The sensitizing pigment in fly photoreceptors". *Biophys Struct Mech* 10, 81–92.
- Krauskopf, J. and B. Farell (1990). "Influence of colour on the perception of coherent motion." *Nature* 348(6299): 328-331.
- Little, C. M., A. R. Rizzato, L. Charbonneau, T. Chapman and N. K. Hillier (2019). "Color preference of the spotted wing *Drosophila*, *Drosophila suzukii*." *Sci Rep* 9, 16051.
- Longden, K. D. (2018). "Colour Vision: A Fresh View of Lateral Inhibition in *Drosophila*." *Curr Biol* 28(7): R308-R311.
- Lunau, K. (2014). "Visual ecology of flies with particular reference to colour vision and colour preferences." *J Comp Physiol A Neuroethol Sens Neural Behav Physiol* 200(6): 497-512.
- Maisak, M. S., J. Haag, G. Ammer, E. Serbe, M. Meier, A. Leonhardt, T. Schilling, A. Bahl, G. M. Rubin, A. Nern, B. J. Dickson, D. F. Reiff, E. Hopp and A. Borst (2013). "A directional tuning map of *Drosophila* elementary motion detectors." *Nature* 500(7461): 212-216.
- Maldonado, H. (1963). "The visual attack learning system in *Octopus vulgaris*." *J Theor Biol* 5(3): 470-488.
- Manger, P. R., J. Cort, N. Ebrahim, A. Goodman, J. Henning, M. Karolia, S.-L. Rodrigues and G. Štrkalj (2008). "Is 21st Century Neuroscience Too Focussed on the Rat/Mouse Model of Brain Function and Dysfunction?" *Front Neuroanat*, 2:5
- Marder, E. (2002). "Non-mammalian models for studying neural development and function." *Nature*, 417:318-321.
- Marshall, J. and K. Arikawa (2014). "Unconventional colour vision." *Curr Biol* 24(24): R1150-1154.
- Mazzoni, E. O., A. Celik, M. F. Wernet, D. Vasilaitis, R. J. Johnston, T. A. Cook, F. Pichaud and C. Desplan (2008). "Iroquois complex genes induce co-expression of rhodopsins in *Drosophila*." *PLoS Biol* 6(4): e97.
- Meinertzhagen, I.A., R. Menzel and G. Kahle (1983). "The identification of spectral receptor types in the retina and lamina of the dragonfly". *Sympetrum rubicundulum*. *J Comp Physiol* 151: 295–310.
- Meinertzhagen, I. A. and S. D. O'Neil (1991). "Synaptic organization of columnar elements in the lamina of the wild type in *Drosophila melanogaster*." *J Comp Neurol* 305(2): 232-263.

- Melnattur, K. V., R. Pursley, T. Y. Lin, C. Y. Ting, P. D. Smith, T. Pohida and C. H. Lee (2014). "Multiple redundant medulla projection neurons mediate color vision in *Drosophila*." *J Neurogenet* 28(3-4): 374-388.
- Messenger, J. B. (1968). "The visual attack of the cuttlefish, *Sepia officinalis*." *Anim Behav* 16(2): 342-357.
- Morante, J. and C. Desplan (2004). "Building a projection map for photoreceptor neurons in the *Drosophila* optic lobes." *Semin Cell Dev Biol* 15(1): 137-143.
- Morante, J. and C. Desplan (2008). "The color-vision circuit in the medulla of *Drosophila*." *Curr Biol* 18(8): 553-565.
- Morgan, T. H. (1910). "Sex limited inheritance in *drosophila*." *Science* 32(812): 120-122.
- Mota, T., W. Gronenberg, M. Giurfa and J. C. Sandoz (2013). "Chromatic processing in the anterior optic tubercle of the honey bee brain." *J Neurosci* 33(1): 4-16.
- Mäthger, L. M., A. Barbosa, S. Miner and R. T. Hanlon (2006). "Color blindness and contrast perception in cuttlefish (*Sepia officinalis*) determined by a visual sensorimotor assay." *Vision Res* 46(11): 1746-1753.
- Nakai, J., M. Ohkura and K. Imoto (2001). "A high signal-to-noise Ca(2+) probe composed of a single green fluorescent protein." *Nat Biotechnol* 19(2): 137-141.
- Nern, A., B. D. Pfeiffer and G. M. Rubin (2015). "Optimized tools for multicolor stochastic labeling reveal diverse stereotyped cell arrangements in the fly visual system." *Proc Natl Acad Sci U S A* 112(22): E2967-2976.
- Nishida, S., J. Watanabe, I. Kuriki and T. Tokimoto (2007). "Human visual system integrates color signals along a motion trajectory." *Curr Biol* 17(4): 366-372.
- Nityananda, V. and J. C. A. Read (2017). "Stereopsis in animals: evolution, function and mechanisms." *J Exp Biol* 220(Pt 14): 2502-2512.
- Nityananda, V., G. Tarawneh, R. Rosner, J. Nicolas, S. Crichton and J. Read (2016). "Insect stereopsis demonstrated using a 3D insect cinema." *Sci Rep* 6: 18718.
- Niven, J. and L. Chittka (2016). "Evolving understanding of nervous system evolution." *Current Biology*, 26(20):R937-R941.
- Nixon, M. and J. Z. Young (2003). "The Brains and Lives of Cephalopods." Oxford University Press, Oxford, UK.
- Nolte, D. J. (1952). The eye pigmentary system of *Drosophila*. *Genetics* 51, 142–186.
- O'Hare, K., C. Murphy, R. Levis and G. M. Rubin (1984). "DNA sequence of the white locus of *Drosophila melanogaster*." *J Mol Biol* 180(3): 437-455.

- O'Brien, C. E., K. Roumbedakis and I. E. Winkelmann (2018). "The Current State of Cephalopod Science and Perspectives on the Most Critical Challenges Ahead From Three Early-Career Researchers." *Front Physiol* 9: 700.
- Packard, A. (1972). "Cephalopods and fish: Limits of convergence." *Biol Rev* 47, 265–273.
- Panzer, L. C. and M. B. Hoppa (2019). "Genetically Encoded Voltage Indicators Are Illuminating Subcellular Physiology of the Axon." *Front Cell Neurosci* 13: 52.
- Paulk, A. C., A. M. Dacks and W. Gronenberg (2009). "Color processing in the medulla of the bumblebee (*Apidae*: *Bombus impatiens*)." *J Comp Neural*, 13(5):441-56.
- Paulk, A. C., J. A. Stacey, T. W. J. Pearson, G. J. Taylor, R. J. D Moore, M. V. Srinivasan and B. van Swinderen (2014). "Selective attention in the honeybee optic lobes precedes behavioral choices." *PNAS*, 111(13) 5006-5011.
- Perry, C. J., A. B. Barron and K. Cheng (2013). "Invertebrate learning and cognition: relating phenomena to neural substrate." *Wiley Interdiscip Rev Cogn Sci* 4(5): 561-582.
- Reichardt, W. (1961). "Autocorrelation, a principle for the evaluation of sensory information by the central nervous system." In *Sensory Communication*, W.A. Rosenblith, ed.
- Rossel, S. (1983). "Binocular stereopsis in an insect". *Nature* 302, 821-822.
- Roth, G. (2015). "Convergent evolution of complex brains and high intelligence." *Philos Trans R Soc Lond B Biol Sci* 370(1684).
- Rowland, H. M., I. C. Cuthill, I. F. Harvey, M. P. Speed and G. D. Ruxton (2008). "Can't tell the caterpillars from the trees: countershading enhances survival in a woodland." *Proc Biol Sci* 275(1651): 2539-2545.
- Salcedo, E., A. Huber, S. Henrich, L. V. Chadwell, W. H. Chou, R. Paulsen and S. G. Britt (1999). "Blue- and green-absorbing visual pigments of *Drosophila*: ectopic expression and physiological characterization of the R8 photoreceptor cell-specific Rh5 and Rh6 rhodopsins." *J Neurosci* 19(24): 10716-10726.
- Scanziani, M. and M. Häusser (2009). "Electrophysiology in the age of light." *Nature*, 461(7266):930-9.
- Schiff, H., B. C. Abbott and R. B. Manning (1985). "Possible monocular range- finding mechanisms in stomatopods from different environmental light conditions." *Comp. Biochem. Physiol.* 80, 271-280.

- Schnaitmann, C., C. Garbers, T. Wachtler and H. Tanimoto (2013). "Color discrimination with broadband photoreceptors." *Curr Biol* 23(23): 2375-2382.
- Schnaitmann, C., V. Haikala, E. Abraham, V. Oberhauser, T. Thestrup, O. Griesbeck and D. F. Reiff (2018). "Color Processing in the Early Visual System of *Drosophila*." *Cell* 172(1-2): 318-330.e318.
- Schnaitmann, C., M. Pagni and D. F. Reiff (2020). "Color vision in insects: insights from *Drosophila*." *J Comp Physiol A Neuroethol Sens Neural Behav Physiol* 206, 183–198.
- Schnell, B., S. V. Raghu, A. Nern and A. Borst (2012). "Columnar cells necessary for motion responses of wide-field visual interneurons in *Drosophila*." *J Comp Physiol A Neuroethol Sens Neural Behav Physiol* 198(5): 389-395.
- Seelig, J. D., M. E. Chiappe, G. K. Lott, A. Dutta, J. E. Osborne, M. B. Reiser and V. Jayaraman (2010). "Two-photon calcium imaging from motion-sensitive neurons in head-fixed *Drosophila* during optomotor walking behavior." *Nat Methods*, 7(7):535-540.
- Shashar, N., P. Rutledge and T. Cronin (1996). "Polarization vision in cuttlefish in a concealed communication channel?" *J Exp Biol* 199(Pt 9): 2077-2084.
- Shigeno, S., P. L. R. Andrews, G. Ponte and G. Fiorito (2018). "Cephalopod Brains: An Overview of Current Knowledge to Facilitate Comparison With Vertebrates." *Front Physiol* 9: 952.
- Shinomiya, K., T. Karuppururai, T. Y. Lin, Z. Lu, C. H. Lee and I. A. Meinertzhagen (2014). "Candidate neural substrates for off-edge motion detection in *Drosophila*." *Curr Biol* 24(10): 1062-1070.
- Shomrat, T., I. Zarrella, G. Fiorito and B. Hochner (2008). "The octopus vertical lobe modulates short-term learning rate and uses LTP to acquire long-term memory." *Curr Biol* 18(5): 337-342.
- Simpson, J. H. (2009). "Mapping and manipulating neural circuits in the fly brain." *Adv Genet* 65: 79-143.
- Simpson, J. H. and L. L. Looger (2018). "Functional Imaging and Optogenetics in." *Genetics* 208(4): 1291-1309.
- Srinivasan, M. V., S. B. Laughlin and A. Dubs (1982). "Predictive coding: a fresh view of inhibition in the retina." *Proc R Soc Lond B Biol Sci* 216(1205): 427-459.
- Stavenga, D. G. (2002). "Colour in the eyes of insects." *J Comp Physiol A Neuroethol Sens Neural Behav Physiol* 188(5): 337-348.

- Stavenga, D. G. (2010). "On visual pigment templates and the spectral shape of invertebrate rhodopsins and metarhodopsins." *J Comp Physiol A Neuroethol Sens Neural Behav Physiol* 196(11): 869-878.
- Stavenga, D. G., M. F. Wehling and G. Belušič (2017). "Functional interplay of visual, sensitizing and screening pigments in the eyes of *Drosophila* and other red-eyed dipteran flies." *J Physiol* 595(16): 5481-5494.
- Steele, E. J., S. Al-Mufti, K. A. Augustyn, R. Chandrajith, J. P. Coghlan, S. G. Coulson, S. Ghosh, M. Gillman, R. M. Gorczynski, B. Klyce, G. Louis, K. Mahanama, K. R. Oliver, J. Padron, J. Qu, J. A. Schuster, W. E. Smith, D. P. Snyder, J. A. Steele, B. J. Stewart, R. Temple, G. Tokoro, C. A. Tout, A. Unzicker, M. Wainwright, J. Wallis, D. H. Wallis, M. K. Wallis, J. Wetherall, D. T. Wickramasinghe, J. T. Wickramasinghe, N. C. Wickramasinghe and Y. Liu (2018). "Cause of Cambrian Explosion - Terrestrial or Cosmic?" *Prog Biophys Mol Biol* 136: 3-23.
- Strother, J. A., A. Nern, M. B. Reiser (2014). "Direct observation of ON and OFF pathways in the *Drosophila* visual system." *Current Biology* 24:976–983.
- Sullivan, D. T., L. A. Bell, D. R. Paton and M. C. Sullivan (1979). "Purine transport by malpighian tubules of pteridine-deficient eye color mutants of *Drosophila melanogaster*." *Biochem Genet* 17(5-6): 565-573.
- Swanson, L. W. (2007). "Quest for the basic plan of nervous system circuitry." *Brain Res Rev* 55(2): 356-372.
- Takemura, S. Y. (2015). "Connectome of the fly visual circuitry." *Microscopy (Oxf)* 64(1): 37-44.
- Takemura, S. Y., Z. Lu and I. A. Meinertzhagen (2008). "Synaptic circuits of the *Drosophila* optic lobe: the input terminals to the medulla." *J Comp Neurol* 509(5): 493-513.
- Takemura, S. Y., C. S. Xu, Z. Lu, P. K. Rivlin, T. Parag, D. J. Olbris, S. Plaza, T. Zhao, W. T. Katz, L. Umayam, C. Weaver, H. F. Hess, J. A. Horne, J. Nunez-Iglesias, R. Aniceto, L. A. Chang, S. Lauchie, A. Nasca, O. Ogundeyi, C. Sigmund, S. Takemura, J. Tran, C. Langille, K. Le Lacheur, S. McLin, A. Shinomiya, D. B. Chklovskii, I. A. Meinertzhagen and L. K. Scheffer (2015). "Synaptic circuits and their variations within different columns in the visual system of *Drosophila*." *Proc Natl Acad Sci U S A* 112(44): 13711-13716.
- Thestrup, T., J. Litzlbauer, I. Bartholomäus, M. Mues, L. Russo, H. Dana, Y. Kovalchuk, Y. Liang, G. Kalamakis, Y. Laukat, S. Becker, G. Witte, A. Geiger,

- T. Allen, L. C. Rome, T. W. Chen, D. S. Kim, O. Garaschuk, C. Griesinger and O. Griesbeck (2014). "Optimized ratiometric calcium sensors for functional in vivo imaging of neurons and T lymphocytes." *Nat Methods* 11(2): 175-182.
- van der Willigen, R. F., B. J. Frost and H. Wagner (1998). "Stereoscopic depth perception in the owl." *Neuroreport* 9(6): 1233-1237.
- Wardill, T. J., O. List, X. Li, S. Dongre, M. McCulloch, C. Y. Ting, C. J. O'Kane, S. Tang, C. H. Lee, R. C. Hardie and M. Juusola (2012). "Multiple spectral inputs improve motion discrimination in the *Drosophila* visual system." *Science* 336(6083): 925-931.
- Welchman, A. E. (2016). "The Human Brain in Depth: How We See in 3D." *Annu Rev Vis Sci* 2: 345-376.
- Wernet, M. F., M. M. Velez, D. A. Clark, F. Baumann-Klausener, J. R. Brown, M. Klovstad, T. Labhart and T. R. Clandinin (2012). "Genetic dissection reveals two separate retinal substrates for polarization vision in *Drosophila*." *Curr Biol* 22(1): 12-20.
- Wheatstone, C. (1838). "Contribution to the physiology of vision. Part the first. On some remarkable and hitherto unobserved phenomena of binocular vision." *Philos. Trans. R. Soc. Lond. B Biol. Sci.* 128, 371-394.
- Wilson-Sanders, S. E. (2011). "Invertebrate models for biomedical research, testing, and education." *ILAR J* 52(2): 126-152.
- Wright, R. and D. Cosens (1977). "Blue-adaptation and orange-adaptation in white-eyed *Drosophila*: Evidence that the prolonged afterpotential is correlated with the amount of M580 in R1-6." *J Comp Physiol* 113, 105-128.
- Yang, H. H. and F. St-Pierre (2016). "Genetically Encoded Voltage Indicators: Opportunities and Challenges." *J. Neurosci*, 36(39): 9977-9989.
- Yang, H. H. and T. R. Clandinin (2018). "Elementary Motion Detection in *Drosophila*: Algorithms and Mechanisms." *Annu Rev Vis Sci*, 4:143-163.
- Yau, K. and R. C. Hardie (2009). "Phototransduction motifs and variations". *Cell* 139, 246-264.
- Young, J. Z. (1971). "The Anatomy of the Nervous System of *Octopus vulgaris*." Oxford: Oxford university press.
- Young, J. Z. (1976). "The 'cerebellum' and the control of eye movements in cephalopods." *Nature* 264(5586): 572-574.

- Zullo, L., G. Sumbre, C. Agnisola, T. Flash and B. Hochner (2009). "Nonsomatotopic organization of the higher motor centers in octopus." *Curr Biol* 19(19): 1632-1636.
- Zylinski, S., D. Osorio and S. Johnsen (2016). "Cuttlefish see shape from shading, fine-tuning coloration in response to pictorial depth cues and directional illumination." *Proc Biol Sci* 283(1826): 20160062.

Chapter 2 – Methodology for Drosophila visual system two-photon imaging

General experimental methodology used throughout the next few chapters is described in the following chapter.

2.1 DROSOPHILA PREPARATION METHODOLOGY

2.1.1 Fly stocks

All flies were reared at 25-27°C with approximately 60% humidity under a 12:12 light/dark cycle, and fed a standard cornmeal and molasses diet. Experiments throughout this thesis were conducted on flies expressing fluorescent activity indicators pan-neuronally throughout the optic lobes. Details of all fly stocks used are reported in the relevant experimental chapter. Flies were collected one day after eclosion using CO₂ for sedation and were transferred into fresh food vials. Flies were then selected for experiments 4-7 days after collection.

2.1.2 Fly preparation

Following cold-anesthesia (~15 min in a vial placed on ice), the fly was positioned on a sheet of aluminium foil such that the back of the head capsule protruded through a small cut-out and was tilted to form an approximate 10° angle with the foil sheet (**Figure 2.1**). This configuration allowed the back of the head to be exposed for imaging, while leaving the majority of the compound eye below the foil for visual stimulation (**Figure 2.1 B**). Using UV-curing adhesive, the fly was then secured to the sheet with special care to reduce brain movement by attaching the proboscis and legs to the upper thorax and immobilising the abdomen. A saline solution (details below) was added to create a bath over the back surface of the head. The cuticle and underlying trachea were then gently removed to expose the optic neuropil (**Figure 2.1 A**). The trachea extending from the rim of the eye outward over the medulla was removed using forceps to gently pull it away. A

gravity/suction pump was used to circulate saline over the course of the experiment to prevent build up of metabolites or other resulting from the dissection. Following the removal of the cuticle, an interval of 45 minutes, or more, was allowed to ensure stabilisation of neural activity and dark adaptation of the fly.

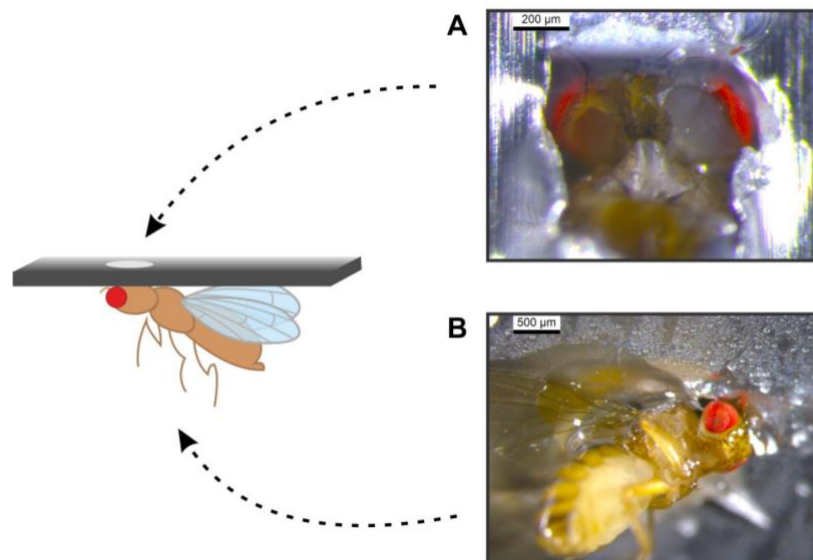


Figure 2.1 Fly preparation for visual system imaging.

The fly is positioned on an aluminium foil sheet with the back of its head protruding through a cut-out such that the cuticle can be carefully removed from a section of the fly's head to expose the visual neuropile (A), while the compound eye is positioned on the underside of the foil sheet to allow for visual stimulation (B).

2.1.3 Saline solution

I have made the decision to describe the following section of my methods in a larger amount of detail than strictly necessary as physiological stability is essential to successful experiments and in turn, appropriate saline is necessary to physiological stability. There is very little in the literature about saline and extracellular solution protocols and I was lucky enough to find some details about similar struggles and ways in which to resolve them in other theses. I hope that likewise, the following section might be of use to anyone else troubleshooting these issues.

The saline solution I initially used to bathe the optic lobes exposed through the dissected cuticle was made following a standard recipe used in other *Drosophila* functional imaging laboratories, and can be found detailed in Fujiwara *et al.* (2017). The concern of a suboptimal saline solution arose as a result of a number of issues with the physiological stability of the fly preparation, notably a prominent decrease in baseline fluorescence, but also disappearance of visual responses over the course of 1-2 hours post-dissection. The saline solution was the most likely cause of this physiological instability as fly preparations would appear perfectly healthy for the first 30 to 45 minutes after removal of the cuticle, with robust visual responsiveness, with a subsequent degradation over time.

In my quest for the ideal saline solution, four aspects were taken under consideration: chemical composition, pH, osmolarity and stability over time/storage. When investigating the pH fluctuations, I found that the solution became more basic over time (**Figure 2.2 A**). A key difference between my setup and that of other fly imaging laboratories is the absence of a carbogen “bubbling” which is thought to maintain the pH at a set value. Without actively introducing carbon dioxide to the saline bath, it is thought that the components of the buffer solution interact and breakdown causing an upward drift of the pH. Personal communications with well-established fly neurophysiology laboratories have revealed that carbogen bubbling, although helpful, does not fully eradicate the issue of pH drifts. From an exchange with Michael Dickinson, we gleaned that the current standard of carbogen bubbling was imported from vertebrate physiology methodologies and accepted as gold standard following initial success. It is his opinion, nonetheless that it is a lot of trouble to go to and doesn't really maintain the pH. His laboratory has recently switched to a HEPES based solution with increased buffer concentration which works well for imaging.

Many laboratories have been cautious about using increased buffer concentration as common belief suggests this will affect physiological properties. A recent study by de Castro *et al.* (2014) debunks this myth. The authors increased the buffer concentration up to 5-fold its usual dose (from 5 mM to 25 mM) and found no change in the physiological properties of *Drosophila* larvae neurons. By topping up the buffer concentration in my saline to 25 mM, I have gained in pH stability over the course of my experimental timeframe (**Figure 2.2 A**). I also delved into the effect of varying storage conditions on pH fluctuations and found that -80°C storage was preferable to fridge or -20°C storage (**Figure 2.2 B**).

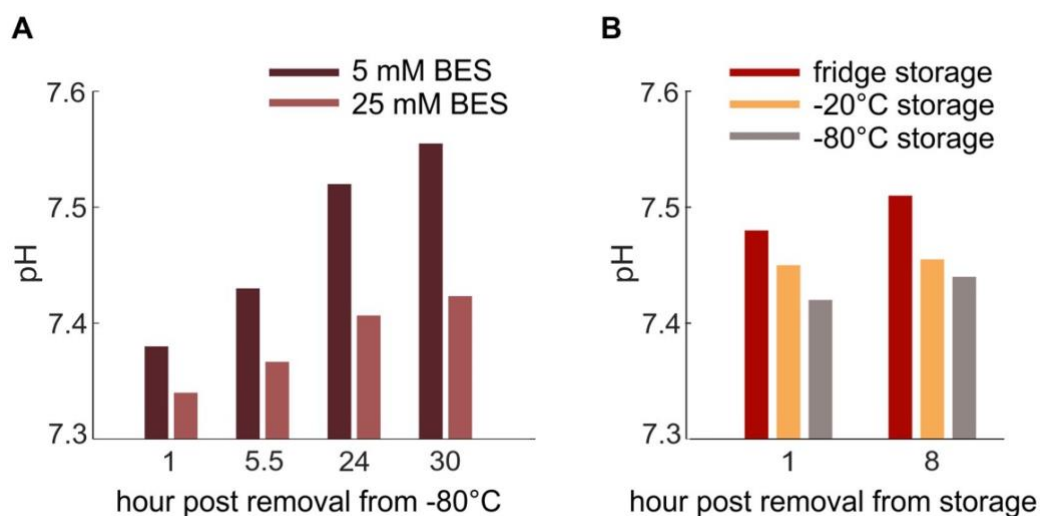


Figure 2.2 Effect of varying concentrations of buffer on saline pH stability.

In (A), the pH values of two saline solutions, identical but for their concentration in BES buffer (5 mM, 2 samples and 25 mM, 3 samples), are shown at 1h, 5.5h, 24h and 30h post pH adjustment to 7.35. In (B), a 25 mM BES saline solution has been adjusted to 7.35 and three storage conditions have been trialled, fridge storage, -20°C freezer storage and -80°C freezer storage. Measurements are taken at 1- and 8-hour time points following removal from their storage paradigm to a room temperature setting.

The main issue with such an important increase in buffer concentration is the resulting increase in osmolarity. Thus, all concentrations of chemicals had to be adjusted to lower the osmolarity. In theory, the calculation of osmolarity depends on the osmotic coefficients of all compounds present in the solution. However, such calculations are a lot more complex than expected, especially as the number of osmotes produced by a compound is not always known. Instead, I chose to approach this problem by trialling varying concentrations of saline components until I reached the appropriate proportion of each as well as the correct osmolarity. As a starting point, I compiled a list of varied extracellular solutions used for invertebrate neural preparations over the last half century, and through trial and error developed the recipe detailed in the final column ([Table 2.1](#)). The osmolarity of the adult *Drosophila* haemolymph is reported to be 251 ± 9 mOsm (Singleton and Woodruff, 1994), although many saline solutions currently used for fly brain preparations are in excess of 300 mOsm. My recipe saline recipe yields an osmolarity of 255-265 mOsm.

The finalised protocol used for making saline is as follows: (1) measure out chemicals (see Table 2.1, purchased from Sigma-Aldrich): 103 mM NaCl, 3 mM KCl, 20 mM BES, 10 mM trehalose, 20 mM sodium bicarbonate, 1 mM sodium phosphate monobasic, 2 mM CaCl_2 and 4 mM MgCl_2 (all Sigma Aldrich), and add the appropriate volume of molecular grade sterile distilled water, (2) place on magnetic stirrer and allow salts to dissolve, (3) readjust pH to 7.35 and check osmolarity (readjust if necessary), (4) filter solution with a vacuum filter system (cellulose acetate membrane, 45 μm pore size, Sigma-Aldrich) and (5) aliquot and freeze at -80°C . Of note, although many fly saline recipes will suggest adjusting the pH to 7.4, I recommend adjusting slightly lower to 7.35 to accommodate the range of the buffering agent used, BES. Doing this has solved any residual drifts in pH. This new saline recipe provides an perfectly functional and possibly improved alternative to fly neurophysiologists who do not wish to store carbogen cylinders in their laboratories.

Table 2.1 Chemical components of Drosophila saline solution for calcium imaging from a selection of publications, as well as the saline developed for my own use.

	Fiala and Spall, 2003	Yue <i>et al.</i> , 2016	Asteriti <i>et al.</i> , 2017	Fujiwara <i>et al.</i> , 2017	My saline recipe
NaCl (mM)	130	70	120	103	103
KCl (mM)	5	5	5	3	3
Buffer (mM)	5 (HEPES)	-	10 (TES)	5 (TES)	20 (BES)
Trehalose (mM)	-	5	-	8	10
Sucrose (mM)	36	115	-	10	-
NaHCO₃ (mM)	-	10	-	26	20
NaH₂PO₄ (mM)	-	-	-	1	1
CaCl₂ (mM)	2	1.5	1.5	1.5	2
MgCl₂ (mM)	2	4	4	4	4
Other	-	5 mM triethyl- silane	25 mM proline, 5 mM alanine	-	-

2.2 VISUAL STIMULATION SETUP

2.2.1 Overview of the system

A projector (DepthQ 360 DLP, WXGA resolution) coupled to a screen was modified to use an independent light source, monochromator (Cairn Research Optoscan Monochromator). This allows us to project selectable narrow bands of the spectrum to produce a range of colours to present to the fly while imaging the neural responses to the stimulus via a two-photon microscope ([Figure 2.3](#)). Details and optical properties of this setup are comprehensively described in the following chapter (Chapter 3).

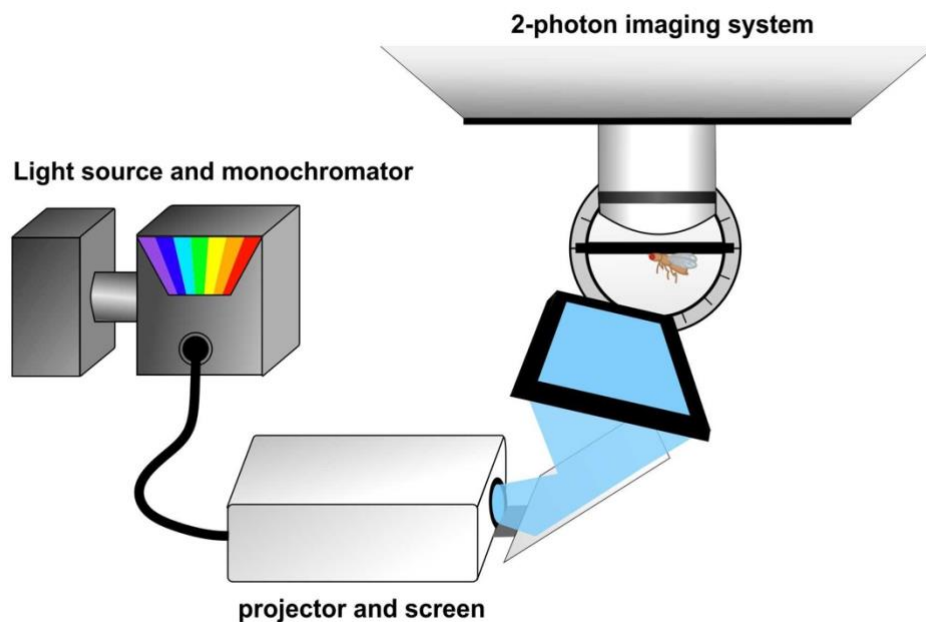


Figure 2.3 Projector/monochromator and two-photon imaging setup.

Using a monochromator as a customised light source for a projector, over 50 different narrow bands of light can be presented to the fly's eye while simultaneously imaging neuronal activity in the visual system using a 2-photon microscope.

2.2.2 Visual field coverage

Stimuli were presented to the left eye (corresponding to the left optic lobe being imaged). The screen was centralised relative to the holder such that the fly was equidistant to all four corners. The 600 x 800-pixel projected light stimulus forms a 34 x 45 mm rectangle on the screen, spanning approximately 58° of the visual field vertically and 77° horizontally. Thus 1° of visual field corresponds to approximately 10.3 pixels, providing us with ample spatial resolution.

2.2.3 Locating visual responses

Visual responses were probed using a series of full-field 1-second blue light pulses. As the light was applied, I manually scanned through the z-stack of the medulla to locate the visually-responsive region. Once identified, I progressively restricted the area of blue light on the screen to a final square of 100 x 100 pixels. I made use of the motorised tip-tilt function of the fly holder to optimise the orientation of the prep in order to ensure that the central portion of the screen covered the proximal and distal layers equally.

2.3 CALCIUM IMAGING AND DATA ACQUISITION

2.3.1 Imaging parameters

Calcium signals in neurons of the medulla were imaged using a two-photon Bruker (Prairie Technologies) In Vivo Microscope using GFP and RFP detection channels, with a 20X water immersion objective (Zeiss, W Plan-Apochromat 20x/1.0 DIC M27; Cat # 421452-9600-000). An insight DS+ laser (Newport Spectra-Physics), with 920 nm infrared excitation applied to the sample. For functional imaging of calcium responses, data was acquired at a 512 x 512-pixel resolution at a rate of approximately 30 frames per second. Visual stimuli were generated in StimGL (Howard Hughes Medical Institute) and controlled via Matlab (The MathWorks, Inc., Natick, Massachusetts, United States). The start of a visual stimulus sequence was indicated to the imaging software (PrairieView) by a trigger which subsequently initiated the acquisition of images, but also controlled the monochromator and projector.

2.3.2 Fluorescent signal extraction

Analyses were conducted using custom-made programmes in Matlab. For each recording, a reference image was created by averaging multiple frames of peak visual response. The resulting template was then used to enable manual selection of regions of interest (ROIs) on the basis of fluorescent signal (further details and exemplary images of ROI segmentation are provided in the methods section of chapters 4 and 5). A cross-correlation analysis (Guizar-Sicairos *et al.*, 2008) was implemented to compensate for motion in the x-y plane resulting from physiologically driven movement of the visual neuropil (e.g. muscular displacement), vibrations resulting from equipment, or other. With this method, images across the experiment were realigned to an initial template image in order to ensure continuity of all features, and consequently continuity of ROIs from one image to another throughout the stack. A voltage recording paired to the two-photon image stack was used to segment the experiment into individual stimulus presentations. For each segment, baseline fluorescence was averaged over a pre-stimulus darkness period (5 frames prior to stimulus onset). Baseline fluorescence was averaged for each ROI over the pre-stimulus darkness period. Calcium activity was assessed by changes in fluorescence. These were calculated as the difference between average fluorescence for a given frame and the baseline fluorescence and then divided by the baseline for each ROI:

$$\Delta F = \frac{F - F_0}{F_0}$$

where ΔF is the change in fluorescence, F is the fluorescent signal and F_0 is the baseline fluorescence. Extracted responses were then averaged across stimulus repeats. Signal-to-noise ratio is defined as ΔF divided by the standard deviation of the ΔF of the baseline frames.

2.4 REFERENCES

- Asteriti, S., C. H. Liu and R. C. Hardie (2017). "Calcium signalling in *Drosophila* photoreceptors measured with GCaMP6f." *Cell Calcium* 65: 40-51.
- de Castro, C., J. Titlow, Z. R. Majeed and R. L. Cooper (2014). "Analysis of various physiological salines for heart rate, CNS function, and synaptic transmission at neuromuscular junctions in *Drosophila melanogaster* larvae." *J Comp Physiol A Neuroethol Sens Neural Behav Physiol* 200(1): 83-92.
- Fiala, A. and T. Spall (2003). "In vivo calcium imaging of brain activity in *Drosophila* by transgenic cameleon expression." *Sci STKE* 2003(174): PL6.
- Fujiwara, T., T. L. Cruz, J. P. Bohnslav and M. E. Chiappe (2017). "A faithful internal representation of walking movements in the *Drosophila* visual system." *Nat Neurosci* 20(1): 72-81.
- Guizar-Sicairos, M., S. T. Samuel and J. R. Fienup (2008). "Efficient subpixel image registration algorithms," *Opt Lett* 33, 156-158.
- Singleton, K. and R. I. Woodruff (1994). "The osmolarity of adult *Drosophila* hemolymph and its effect on oocyte-nurse cell electrical polarity." *Dev Biol* 161(1): 154-167.
- Yue, Y., S. Ke, W. Zhou and J. Chang (2016). "In Vivo Imaging Reveals Composite Coding for Diagonal Motion in the *Drosophila* Visual System." *PLoS One* 11(10): e0164020.

Chapter 3 – Development of a novel setup for simultaneous two-photon functional imaging of neural activity indicators and precise colour visual stimulation in Drosophila.

3.1 INTRODUCTION

3.1.1 Characterising colour vision in *Drosophila*

The ability to accurately dissect the components of the *Drosophila* visual system responsible for processing colour or general spectral information relies on several crucial experimental parameters. Most important of all is the production of an adequate set of visual stimuli. The choice of approach when designing a set of visual stimuli is largely dependent on the current understanding of the visual system under scrutiny. Initial basic characterisation of the colour visual system of a species aims to determine the number of opsins and their approximate spectral tuning. *In vivo* electrophysiological recordings in dipterans generally, either measuring summed responses of photoreceptors using electroretinograms (Salcedo *et al.*, 1999) or by performing sharp electrode recordings of individual photoreceptor cells (*Musca*: Hardie and Kirschfeld, 1983) or later optic lobe cells (Honey bees: Kien and Menzel, 1977), are frequently used to determine spectral sensitivities of photoreceptors. Microspectrophotometry (MSP), a technique used to determine the absorption profile of a visual pigment by measuring the transmission of light through the pigment, can also be used (Salcedo *et al.*, 1999) but only reveals properties of a visual pigment without accounting for intraocular filtering.

3.1.2 Producing a stimulus to probe colour vision

Stimuli for such experiments require the production of bands of monochromatic light of varying wavelength within the UV to visible light spectrum. This can be achieved using a broadband light source coupled either to a monochromator (*Drosophila*: Salcedo *et al.*, 1999) or individual colour filters (Honey bees: Kien and Menzel, 1977; Dragonflies:

Meinertzhagen *et al.*, 1983). More recently, LED-based monochromator systems have been designed but are limited in spectral resolution (Belušič *et al.*, 2016). To carefully design complex multispectral light stimuli the colour visual system needs to be sufficiently quantified to establish the effect of pre-receptoral filtering, such as eye pigment screening, as well as instability and adaptation properties of visual pigments for each photoreceptor type. An example of such complex stimuli is the method known as silent substitution, in which stimuli can be designed to change the apparent light intensity for one class of photoreceptors with minimal change for other photoreceptors (Estevez and Spekreijse, 1982). This can be used to elucidate the contribution of individual photoreceptor classes to visual processing. Setups for these experiments usually require the combination of multiple LEDs to produce full-field stimuli (Mouse: Brown *et al.*, 2010), although a recent study reports a modified projector system with a five-primary light engine which allows the addition of a spatial component to the visual stimulus (Allen *et al.*, 2017). Our aim was to develop a precise spectral and spatial stimulation system that far exceeds the capabilities of those described above.

3.1.3 General experimental requirements

In basic terms, colour vision is defined as the discrimination of different wavelengths of light independent of the intensity of the stimulus. Thus, in order to determine the precise contribution of spectral information to visual computations, whether general or colour-specific, our goal was to construct a system that possessed fine-wavelength resolution across a large portion of the spectrum, that could be calibrated to produce isoluminant stimuli over a biologically-relevant range of intensities and that allowed the presentation of spatially- and temporally-structured stimuli.

Working with *Drosophila* as our model organism, however, adds a further level of technical complexity. Electrophysiological approaches to recording neural activity are limited in the early visual neuropil by the small diameter of the cells, a problem that has been overcome with recent advances in technology and genetic tools making it possible to use functional imaging methods instead. Despite the sophisticated new framework created by these advances, such as the ability to simultaneously monitor activity in many neurons, or the selective labelling of individual cell types, combining two-photon functional imaging and colour visual stimulation is not straightforward. The issue lies with the spectrally broad and extremely high detection sensitivities of a standard version of a

two-photon microscope and its inbuilt filters and optics. Indeed, the presentation of any visual stimulus of spectral content close to the detection range of the microscope will result in an artefact on the acquired image. This reduces the range of the spectrum that can be used for visual stimulation and consequently limits the wavelengths that can be used to probe spectral sensitivity of the visual system. A possible workaround method that has been developed is where the visual stimulus is only delivered during the two-photon scanner flyback period (Schnaitmann *et al.*, 2018). However, this stimulation method could introduce aliasing problems if moving patterned stimuli were to be used at certain velocities in addition to spectral stimulation.

The following report describes the system we have developed that enables us to present the fly with over 50 different wavelength bands of the visual spectrum with minimal disruption of image quality produced by the microscope. Due to the extreme sensitivity of the two-photon microscope detectors, our visual stimulation parameters in terms of spectral content and optical power have been extensively characterised to ensure the accuracy and reliability of the visual stimulus delivered to the fly while imaging. The primary components of the setup include the two-photon imaging system, for functional imaging of the fly's optic lobes, and the modified projector that uses a monochromator as its light source (see Chapter 2, section 2.2).

3.2 EXPERIMENTAL SETUP COMPONENTS

3.2.1 Microscope and monochromator modifications

Neural activity of the *Drosophila* visual system is monitored using a two-photon imaging system. The delivery of brightly coloured visual stimuli while performing optical imaging has been a long-standing problem in the field of invertebrate vision. As described above, previous studies have relied on alternating colour visual stimulation and brain imaging (i.e. the fly-back method), but this causes an aliasing effect as many invertebrates have high flicker fusion rates (five to ten times faster than vertebrates). This fly-back stimulation interlacing also reduces the microscope's photon collection time, thereby reducing the imaging sensitivity, which is especially important for calcium indicators that have slow temporal responses. It is also difficult to isolate the stimulus light from the microscope by means of an opaque holder on the fly's head as some of this light is

transmitted through the eye and cuticle. Even if effective, such a solution would be costly with the need for a perfectly fitted “hat” for the fly. An easy and efficient addition to our current fly preparation (described in Chapter 2) is the application of matte black nail polish to seal the gap between the fly’s cuticle and the aluminium foil. A key feature of our setup is the introduction of specialised bandpass optical filters (or combinations thereof) in the imaging and visual stimulation pathways. This solves the light contamination issue and allows for the presentation of a visual stimulus with minimal detection of light resulting from the stimulus by the microscope gallium arsenide phosphide (GaAsP) photomultiplier tube detectors (PMTs). One filter set consists of a combination of dichroic bandpass (Semrock) and glass absorption (Schott) filters that is integrated into the monochromator (Cairn Research Optoscan Monochromator) to block wavelengths of light within the microscope’s detection range. The other optical filter combination is integrated into the microscope to limit the wavelengths of light entering the detectors and works to reject bleed-through of detectable light wavelengths from the visual stimulus by means of an arrangement of high optical density bandpass filters. Monochromator and microscope filter positions and transmission spectra are detailed in the sections below and illustrated in [Figure 3.1](#).

3.2.2 Light source filtering

The light source filtering of stimuli consists of three filters. A fixed short pass blocking filter (Comar Optics, Schott WG280) to prevent ultralow UV stimulation (150-300 nm) from the grating 2nd harmonic. A movable short pass blocking filter (Comar Optics, Schott GG435) to prevent UV stimulation (300-400 nm) from the grating 2nd harmonic, and finally a bandpass filter to allow for green and red imaging (Semrock Custom BRU-0092) by reflecting away those bands of light.

3.2.3 Imaging pathway light filtering

The filtering of light in the imaging pathway to prevent detector artefacts from the visual stimulus consists of a number of customised filters in addition to the filter sets already present in commercially available systems. Extra high optical density versions were made (or used if available) to better divide up the visible spectrum to partition which wavelengths can be used for stimulation and those exclusively for imaging fluorescent protein emission. The filters are described in the order they are placed along the light pathway from the objective to the detectors. The first filter (Semrock Custom BRU-0092)

replaces the dichroic mirror usually present in a two-photon system and provides bandpass reflection of light to the detectors in the fluorescence turret. This allows only specific green and red wavelength bands to be reflected to the detectors (for imaging green and red fluorescent molecules), and all other wavelengths to pass (e.g. ultraviolet, yellow and infrared). Normal two-photon microscopes reflect all visible light. An IR blocking filter (Semrock Custom BRU-0093) is the next installed in detector light path. This blocks IR light but allows specific green and red wavelength bands to continue to the detectors. Normal two-photon microscopes filters at this stage let all visible light through. A dichroic filter (Chroma t550lpxr), present in most two-photon systems, divides the light into red and green bands. At this point red and green light diverge paths towards their respective detectors. First, a second set of custom IR blocking and specific red green band pass filters (Semrock Custom BRU-0093 and BRU-0094 for red and green respectively), next, a second set of custom dichroic filters to further refine wavelengths passed to detectors (Chroma t495lpxr and t600lpxr for red and green respectively), and finally, two band pass filters to refine the band of wavelengths the detectors receive (Chroma ET525/50 and ET622/36 for red and green respectively).

Finally, a filter (Semrock FF01-715LP) has been added in the optical laser path to remove any visible light reaching the fly prep from the Newport Spectra Physics Insight DS+ laser.

3.2.4 The projector/monochromator setup

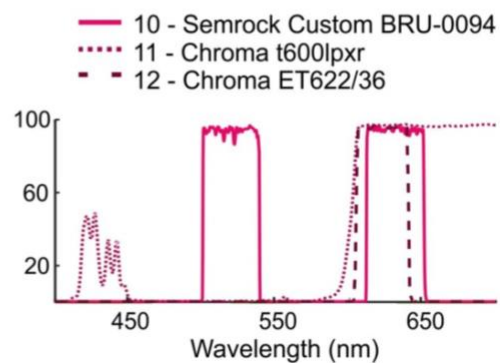
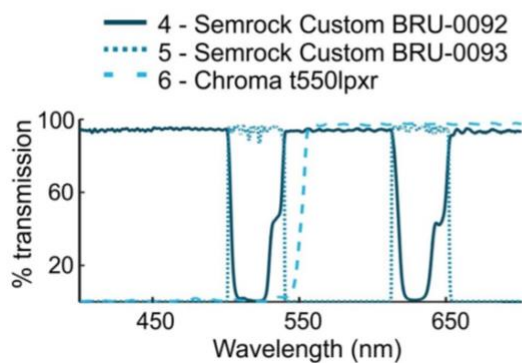
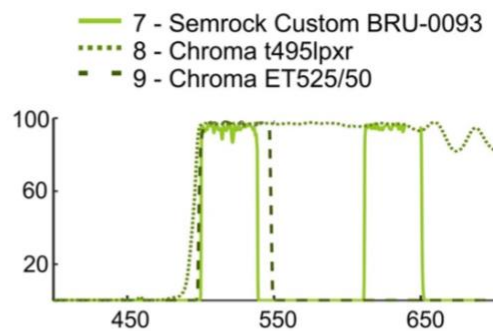
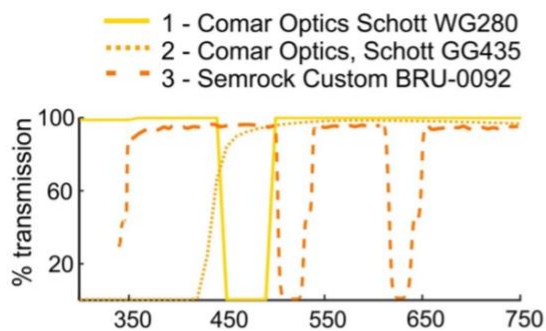
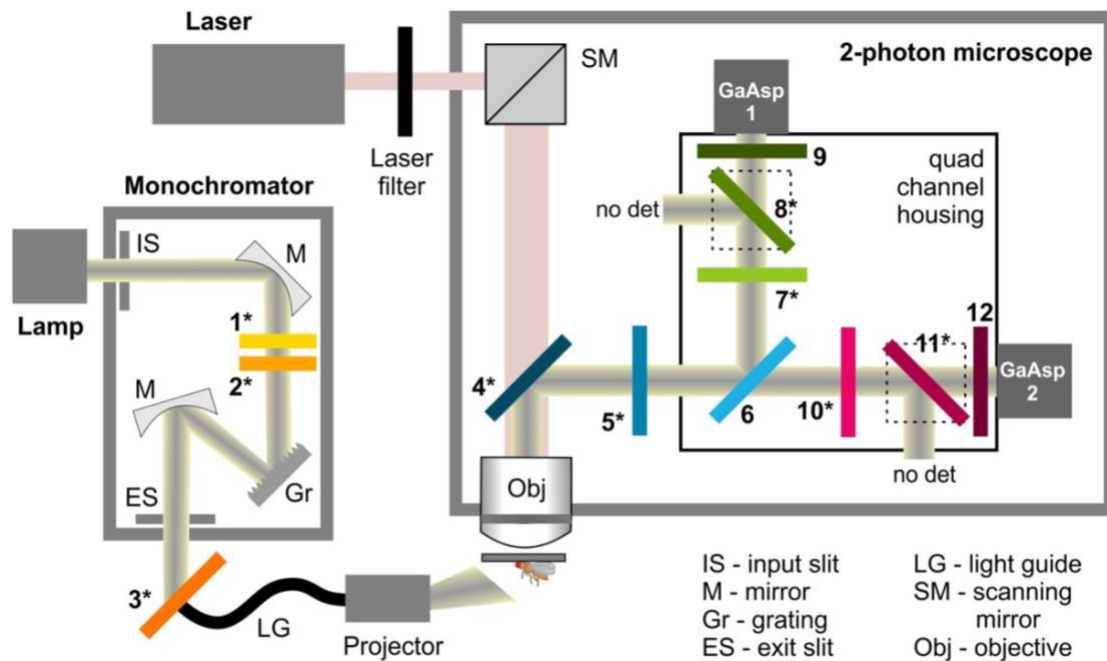
A projector (DepthQ 360 DLP, WXGA resolution) was used to project patterned stimuli at a 360 Hz frame rate as some fly species, such as *Coenosia attenuata* can see up to 300 Hz, while *Drosophila melanogaster* can see just beyond 120 Hz (Gonzalez-Bellido *et al.*, 2011). To fulfil the requirement of delivering a high precision spectral stimulus combined with a spatial pattern, we chose to install an independent light source and modified the DepthQ360 to use a liquid light guide as its source using plans kindly provided HHMI Janelia Farm. The monochromator light source is a 150W xenon bulb which is turned on 3 hours before use to ensure a stable temperature and consequently a stable light output (**Figure 3.2**). The DLP chip of the projector reaches full contrast capacity within 5 mins but is normally switched on at least 30 mins prior to starting experiments (**Figure 3.2**). The light produced by the monochromator has an approximately Gaussian waveform and can be modified for two parameters: wavelength and intensity (**Figure 3.3**). This provides ample versatility to produce stimuli across the

visible spectrum and across several log units of intensity. For each selected wavelength, the width of the monochromator slits (input and exit) can be specified to produce slit widths ranging from 1 to 30 nm using the selected wavelength as the centre wavelength. The optical power increases with slit width, and as such, can be calibrated to produce equal optical power for each centre wavelength. This allows me to calibrate the different colour stimuli to be of equal optical intensity across the spectrum, thus fulfilling a prerequisite for the study of colour vision, which relies on the ability to discriminate wavelength independent of intensity. I chose centre wavelengths ranging from 385 nm and 720 nm. Successive 5 nm increments between centre wavelengths allows for high precision of spectral sensitivity mapping.

Our system uses narrow bands of monochromatic light well suited to our investigation into spectral response properties. Nonetheless it is entirely possible to modify the light source to produce multispectral light using a system such as the LED-based monochromator (Belušič *et al.*, 2016), with the minor drawback of reduced spectral resolution.

Figure 3.1 Customised filter system for the monochromator/projector setup.

Light from a broadband tungsten 150W bulb (lamp) is selectively transmitted through the monochromator via an input slit (IS), several mirrors (M), a grating (Gr) and an exit slit (ES). Three custom filters are added along this pathway. Filters 1 and 2 are longpass filters that prevent the transmission of harmonics in the UV range. Filter 1 is moveable and is only used for light above 460 nm. Filter 3 prevents the transmission of the bands of red and green light that are detected by the microscope. A custom filter (4) replaces the dichroic mirror at the start of the imaging pathway, and combined with 5 and 6, these three filters serve to block the transmission of any light beyond the narrow bands of red and green detected by the microscope. A further three filters are combined for each GaAsp detector. Filters 7 and 10 block light that falls outside the red and green band ranges. Filters 8 and 11 are long pass filters. And finally filters 9 and 12 selectively transmit only specific red and green band of light for GaAsp detectors 1 and 2 respectively. Unlike classic quad housing designs, there are only two detectors instead of four and all 200-500 nm and 550-600 nm light along the GaAsp1 and GaAsp2 detector pathways respectively is discarded. Filters denoted with asterisks () are a custom addition to the commercially available version of the system.*



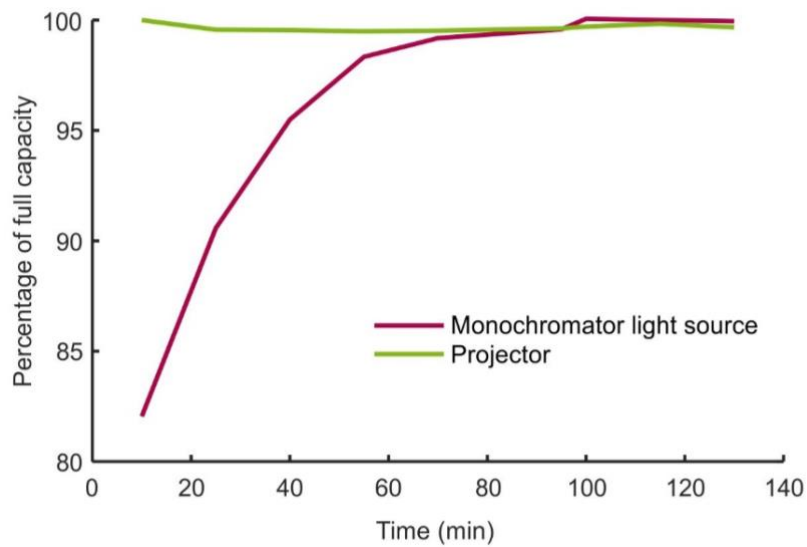


Figure 3.2 Optical equipment warm up time.

The monochromator light source takes approximately 90 minutes to reach full intensity following switch on, whereas the projector is ready for use within 5 minutes following switch on.

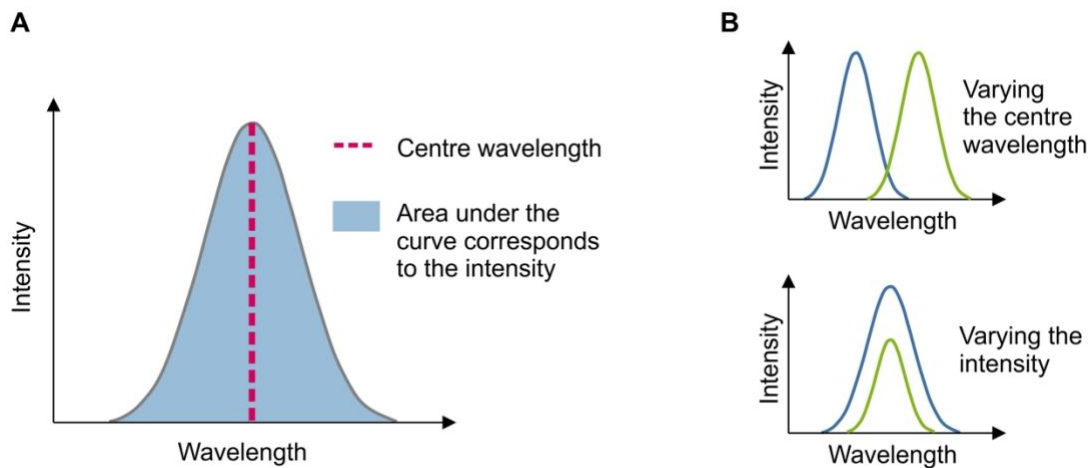


Figure 3.3 Versatility of monochromator produced light.

(A) The light produced by the monochromator is plotted along two axes: wavelength and intensity as an approximate Gaussian curve represented as a diagramme here. The centre wavelength corresponds to the peak of the Gaussian curve and the overall intensity of the light can be derived by integrating the area under the curve. (B) The light output can be modified for both parameters by modifying the monochromator grating position for wavelength and varying the input and output slits widths for intensity.

3.3 VISUAL STIMULUS PARAMETERS

3.3.1 Light measurement methodology

To ascertain the precision and reliability of the setup, I characterised the optical parameters of the projected visual stimulus. All measurements are taken using a NIST calibrated spectrometer Avantes AvaSpec 2048 Single Channel spectrometer coupled to an Avantes UV-VIS 600 μm fibre (numerical aperture $\text{NA} = 0.22$, acceptance angle $\text{AA} = 25.4$ and solid angle $\text{SA} = 0.1521$) with the detector positioned in a holder in such a manner to receive light exactly as the fly would ([Figure 3.4](#)). Unless otherwise specified, all measurements are taken with the spectrometer pointing at the screen centre (this careful positioning can be achieved by back-projecting light through the spectrometer fibre). The spectrometer is controlled via Matlab, allowing me to automate the acquisition of measurements. A fresh dark reference spectrum is collected prior to each measurement for optimal accuracy of radiance measurements and the integration time of the spectrometer was adjusted to maximise light detection without causing saturation. Radiance values provided by the spectrometer in $\mu\text{W}/\text{cm}^2$ were converted to $\text{photons}/\text{s}/\text{cm}^2$, and the integral value corresponding to the area under the curve was extracted to provide a measure of optical intensity for each spectrum. To avoid a large margin of variation in the measure of radiance, the area under the curve was calculated for 40 nm either side of the centre wavelength. This reduces the variability in the summed power value resulting from small wobbles in the far ends of the spectrum. In order to elucidate the area of the screen detected by the spectrometer, light circles of increasing diameter were projected and integral values for each were recorded to produce a size response curve ([Figure 3.5 A](#)). Accordingly, a diameter of approximately 120 pixels is determined as the spectrometer detection area. Of note, to account for the increasing ellipsoid shape of the area detected by the spectrometer as it tilts, a larger margin than the diameter of pixels determined is accounted for to avoid including areas beyond the projection edges. Next, as the optical fibre with the detector is removed between measurement series (to back-project light for accurate positioning of the spectrometer detector), I assessed the reliability of the connection by taking repeat measurements of an identical light stimulus while detaching and reconnecting the fibre between each measurement ([Figure 3.5 Bi](#)). The maximum percentage variance of the integral value from the mean is $\pm 1.7\%$ ([Figure 3.5 Bii](#)), indicating a strong reliability of the connection.

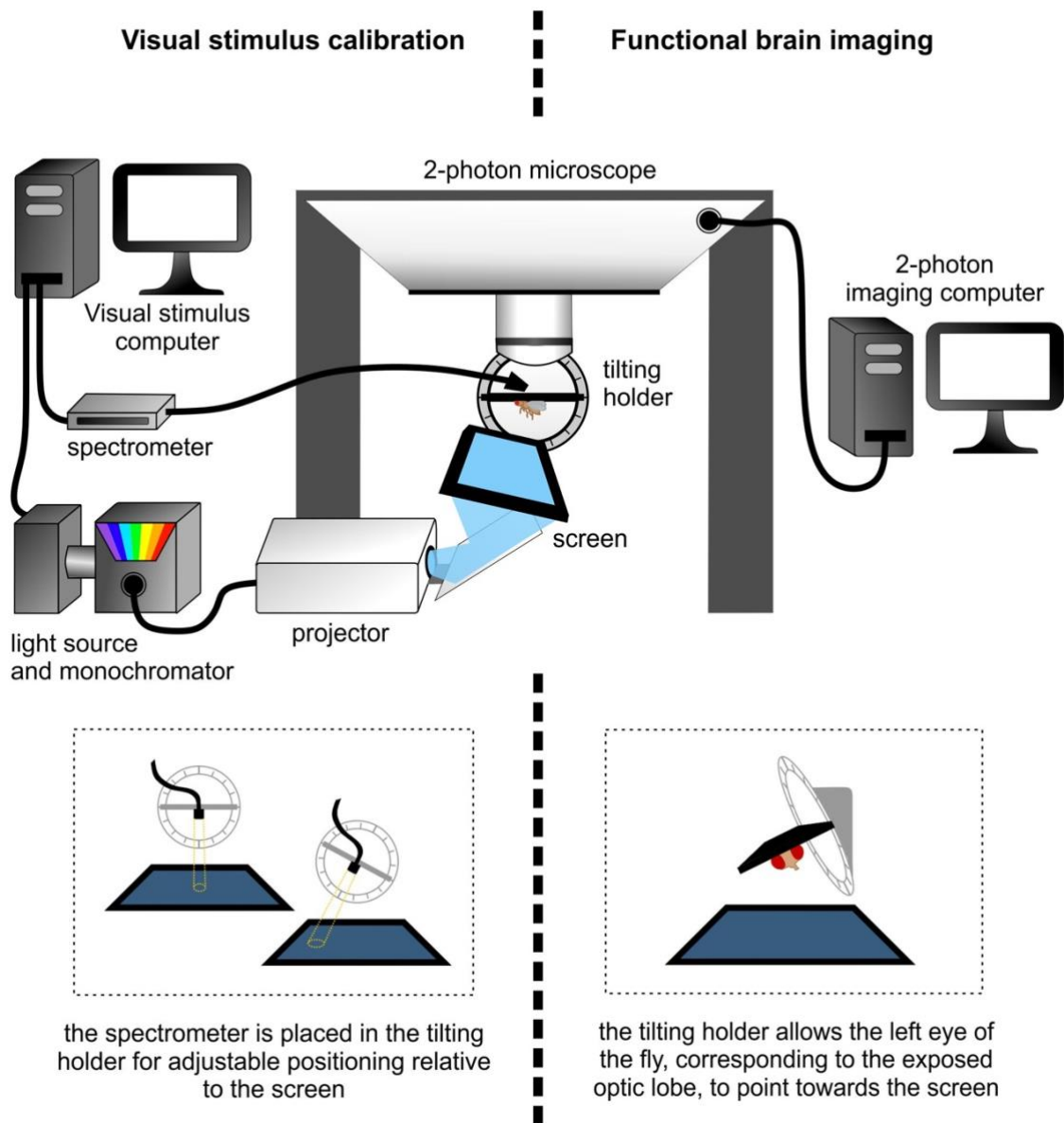


Figure 3.4 Experimental setup for simultaneous precise colour stimulation and two-photon functional imaging.

Left – A modified projector with a monochromator light source projects over 50 different bands of the visual spectrum onto a screen. These colour bands are precisely calibrated using a spectrometer to measure the radiance value of the visual stimulus. Both the monochromator and the spectrometer are controlled by a Matlab script which allows for an automated system using a feedback loop to calibrate the monochromator to produce light of the required intensity. A tilted holder allows the spectrometer position to be adjusted for measurements of specific points of the screen. **Right** – Placement of the fly in the holder with its cuticle removed to expose the optic lobes allows simultaneous brain activity imaging and visual stimulation. The tilting holder is used to position the right eye of the fly (corresponding to the dissected optic lobe) to ensure maximal coverage of the visual field by the screen.

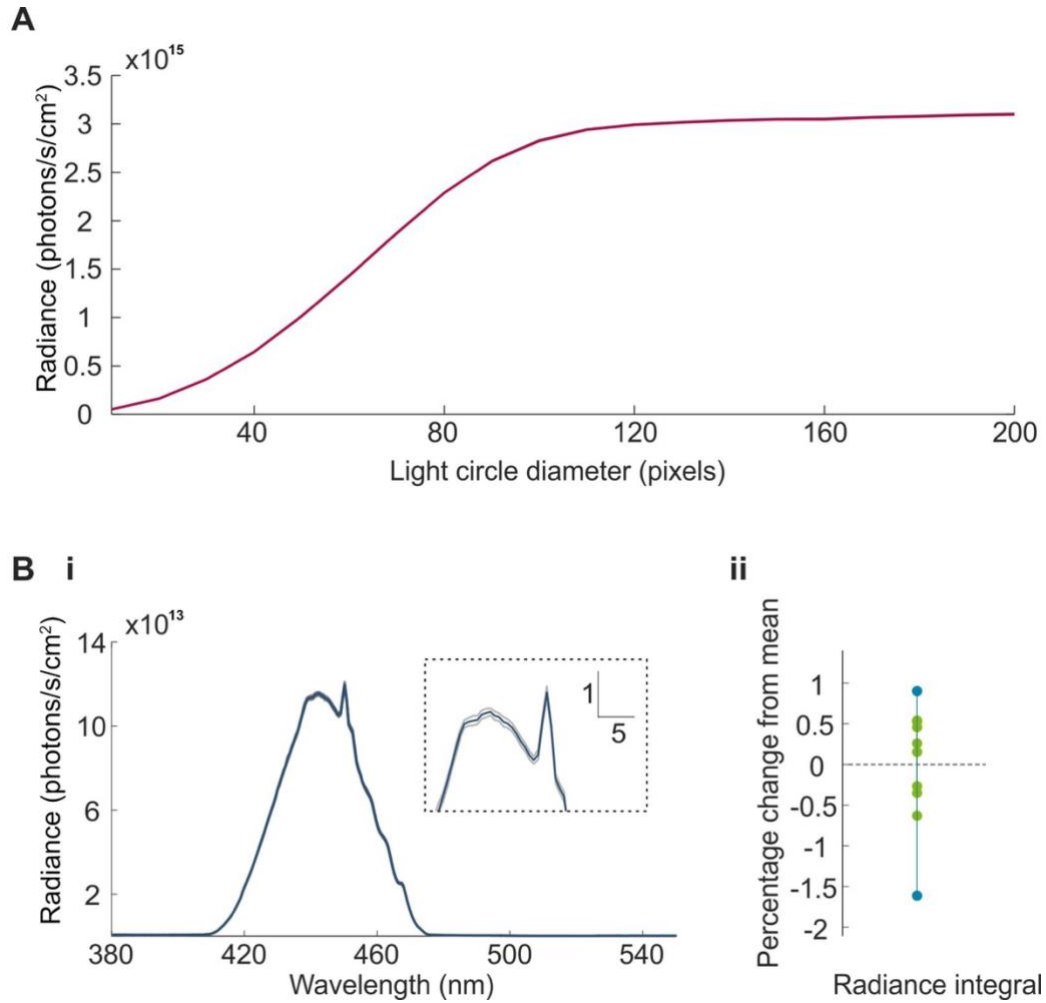


Figure 3.5 Spectrometer measurement parameters.

(A) The screen area sampled by the spectrometer was determined by increasing the diameter of the light stimulus presented (440 nm centre wavelength with 30 nm input and exit slits) and measuring the mean radiance integral value ($n=5$). Means are reported with standard deviations. (B) The reliability of the connection between the spectrometer and the optical fibre was assessed spectrally and quantitatively by repeatedly disconnecting and reconnecting the FC/PC connector. By back projecting light through the fibre the spectrometer fibre could be precisely positioned to sample a specific location of the screen (aligning to a projected dot on the screen). (i) The mean radiance curve \pm SD ($n=10$) of a light stimulus (440 nm centre wavelength with 30 nm input and exit slits) when repeatedly reconnected. (ii) The percentage variance between repeated integral measurements for each radiance curve from the mean of all integrals.

3.3.2 Transmission properties along the optical path

The optical path, from the light source to the projection on the screen, is constituted of several components. Light from the bulb feeds into the monochromator which uses a 1200 l/mm ruled diffraction grating to spatially separate different wavelengths of light. The chosen bandwidth of light then passes through a light guide, the extremity of which is positioned inside the projector to replace the original light source. The projector serves to add a spatial structure to the monochromator light (i.e. for gratings, bars, ellipses), and finally the stimulus is rear-projected onto a screen which serves to focus and align the finalised visual stimulus. Until the screen is reached, the primary concern lies with transmission (defined as the passage of electromagnetic waves through a medium). In order for our experimental paradigm to enable us to study colour vision, the bands of light used for visual stimulation need to cover a maximal range of the spectrum visible to the fly's eye. Visual pigments expressed in *Drosophila* photoreceptors sample light between approximately 300 and 650 nm, in other words from UV to red wavelengths of light. Thus, our optical equipment needs good light transmission across a large portion of the spectrum. The further requirement of appropriate UV transmission adds to the complexity. A general issue with transmittance arises as a basic energy problem. When photons interact with the material they are passing through, the energy of the new photon resulting from the interaction does not match the energy of the old one and is generally lower. A lower energy photon results in a longer wavelength of light, thus as light progresses through the optical pathway higher energy photons (shorter wavelengths) get lost. Finally, not only is UV light outside of the visible spectrum of light for humans, it also causes damage to our skin and retinas. As a result, most optical equipment is designed to reduce the transmittance of UV wavelengths of light. In particular, the DLP chip in the projector drastically reduces the UV content of light. Consequently, my chosen centre wavelength at the UV extremity is 385 nm as beyond this wavelength the optical power decreases drastically and the spectra lose their Gaussian shape. An ideal spectral stimulation range would extend further into the UV portion of the spectrum to match the known spectral sensitivities of Rh1, Rh3 and Rh5. The ongoing progress in the development of UV transmitting projectors (e.g. Texas Instruments) and optics might soon provide an adequate and affordable solution and extend the capabilities of our system to include UV visual stimulation.

3.3.3 Setup geometry and alignment

The light guide, the projector, the screen and the stage/holder were adjusted to ensure an ideal alignment of the optical pathway and visual field of the fly. A first adjustment was made to the light guide and projector mirror position to place the maximal brightness at the screen projection centre with an even drop in optical power towards the edges of the screen in all directions (see [Figure 3.11](#)). Next, the holder was positioned in relation to the screen such that the holder centre is perpendicular to the projection centre and equidistant to all four corners. Furthermore, the holder and screen/projector are adjusted such that when the holder is positioned to be parallel to the screen, the spectrometer samples light directly at the centre of the screen. A motorised tip/tilt system allows me to precisely tilt the holder in any direction such that the central point of the holder where the spectrometer detector (or fly's eye) is positioned remains in the same point of space but the angle of the detector varies such that it samples light from a different location of the screen. Using this system, I characterised optical stimulus parameters across the screen as perceived by the fly ([Figure 3.4](#)).

3.4 SPECTRAL CHARACTERISATION OF THE STIMULATION SETUP

3.4.1 Radiance properties of the visual stimulus

To determine the maximum optical power at each centre wavelength, radiance was measured using maximum slit width settings of the monochromator ([Figure 3.6 A](#)) and then integrated to produce a summed power value for each centre wavelength ([Figure 3.6 B](#)). There is no apparent difference between the power at the start and the end of the experimental day, once the equipment has warmed up to its peak capacity (1.5 h is needed for the monochromator lamp, [Figure 3.2](#)). The gaps in the spectra between 500-540 nm and 610-650 nm ([Figure 3.6 A](#)) correspond to the dichroic filters that are present in the monochromator to block wavelengths of light that will be detected by the microscope. The change in the power between 455 and 460 ([Figure 3.6 B](#)) results from the insertion of a glass filter in the monochromator necessary to prevent harmonics that occur for the longer wavelengths of light. The monochromator bulbs have a life span of approximately 3000 hours. To characterise the evolution of the bulb over its lifespan, I assessed the maximal power for each centre wavelength in a new bulb (which had been burnt in for 200 hours first) and a bulb half way through its lifespan (~1500 hours). My

aim is to determine a reference radiance value to use for my calibration that will provide a visual stimulus of adequate brightness whilst not exceeding the optical power capability of an older bulb as the bulb brightness decays slowly over its lifetime. Although there was an apparent drop in power with the latter, the radiance integral curves from both maintained the same shape (data not shown). Next, I measured the optical power of both bulbs using 25 nm input and exit slits for all centre wavelengths. As 385 nm centre wavelength remains the minimal radiance value throughout, I compared the integral value for this wavelength at 25 and 30 nm slits for the old and the new bulb ([Table 3.1](#)). A small drop in power is observed over the bulb's lifetime, consequently a reference radiance value, 2.63×10^{13} photons/s/cm², was chosen. This value lies within the power bracket of the 25 nm slit radiance value for the new bulb and the 30 nm slit radiance value for the old bulb was chosen to ensure consistent optical power for all experiments with minimal slit width variation for any given band of the spectrum over time.

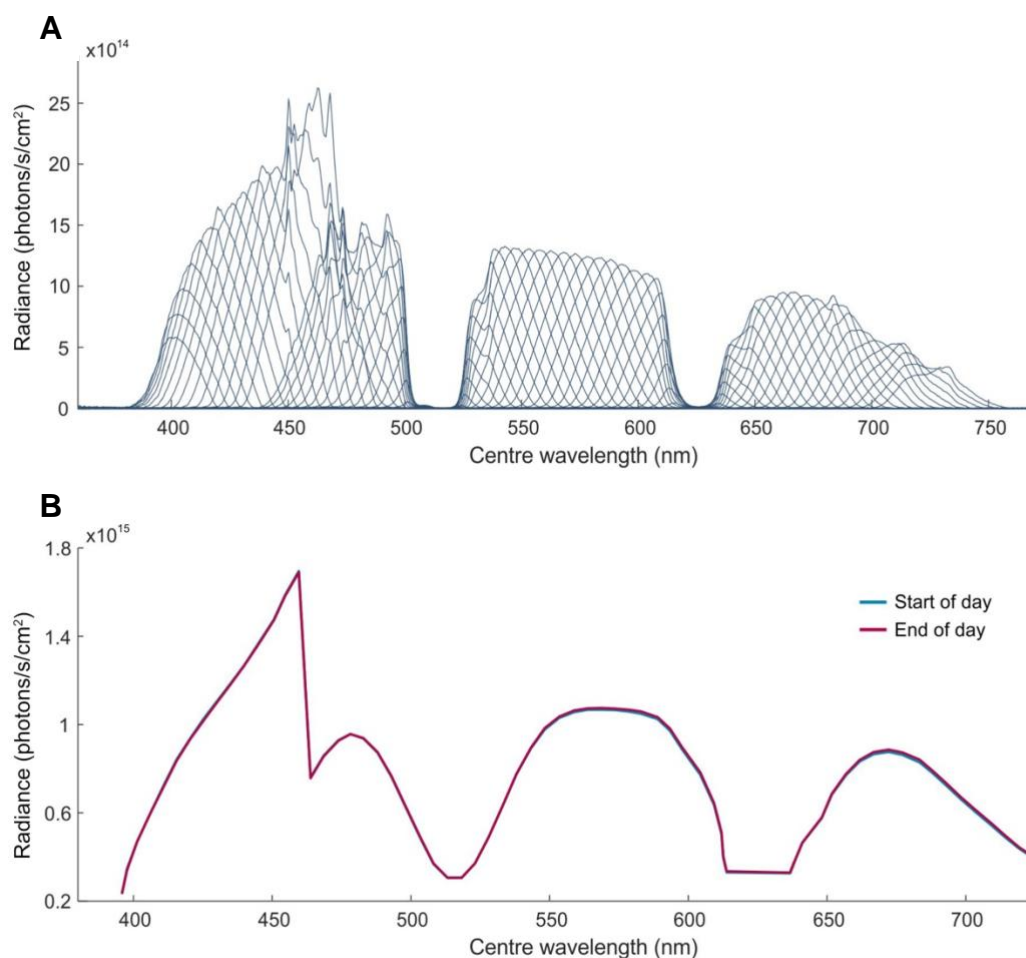


Figure 3.6 Maximal optical power capacity of the monochromator/projector system.

(A) Radiance curves for each centre wavelength (385 to 720 nm in 5 nm increments) for 30 nm input and exit slits (maximum slit width) (B) Area under the curve for each radiance curve of (A) as a measure of optical power in photons/s/cm², measured at the start and end of the experimental day (approx. 9:00 and 18:00 respectively).

Table 3.1 Radiance values (photons/s/cm²) for 440 centre wavelength light with 25 and 30 nm slit width for a used bulb (~1500 hours) and a new bulb (~200 hours).

	Old bulb	New bulb
25 nm slits	1.38 x 10 ¹⁴	1.58 x 10 ¹⁴
30 nm slits	2.10 x 10 ¹⁴	2.30 x 10 ¹⁴

3.4.2 Stimulus calibration process

My aim is to produce a visual stimulus set where each band of light produces the same intensity. Using Matlab to control both the monochromator hardware and the spectrometer hardware, I developed a programme for automated calibration of slit widths. This involves a loop system consisting of an initial command sent to the monochromator specifying slit voltages and consequently slit width and a measurement of the resulting projected light by the spectrometer which is fed back into the Matlab programme. Using a set reference radiance, all bands of the spectrum can be calibrated to equal the reference value. Although the reference value for experimental purposes had not yet been determined by means of an intensity-response relationship assessment, I chose to use 25 and 30 nm slits for the dimmest centre wavelength (385 nm) to test for any potential differences that might occur across different intensities. By ensuring the setup exhibits the same optical properties for both the high and the low power, I can confirm consistency of the visual stimulus. Using either the 25 or 30 nm slit, 385 nm centre wavelength light as the starting point of my calibration, I determine the reference radiance value by averaging five measurements of the projected light. For all subsequent centre wavelengths, the voltages of associated input and exit slits start at their half maximum value, and are modified (stepped up or down), with the steps getting smaller on each iteration, until the reference radiance value is reached within 0.3% (**Figure 3.7**). To ensure that both input and exit slits are the same width at all times, the voltages for both slits are modified in an identical manner. Keeping the variance between both slit widths to a minimum results in greater stability of the stimulus radiance from one iteration to another (**Figure 3.8**).

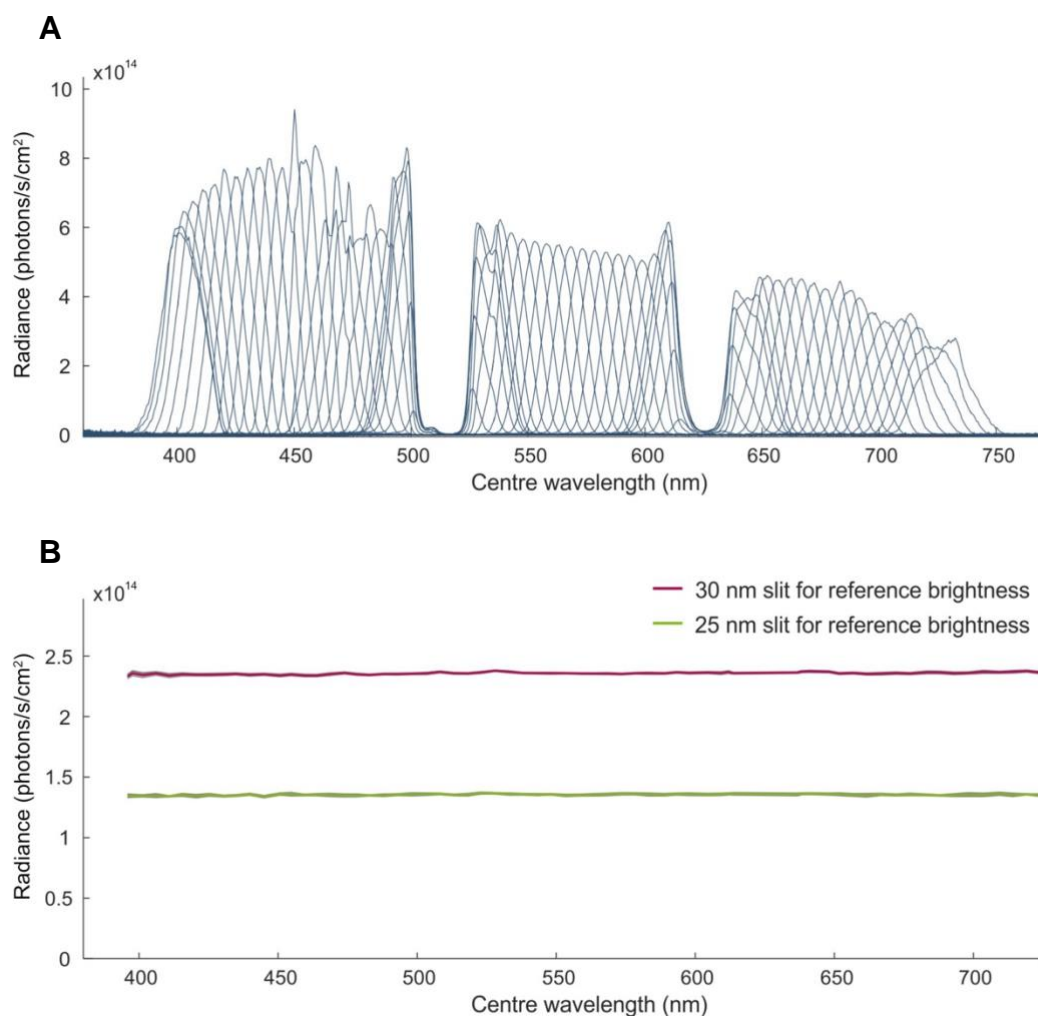


Figure 3.7 Calibrated optical power capacity of the monochromator/projector system.

(A) Radiance curves for each centre wavelength (385 to 720 nm in 5 nm increments) for monochromator input and exit slits calibrated to produce equal optical power corresponding to the radiance of the dimmest band of light (385 nm centre wavelength) for a 30 nm slit width. (B) Calibrated radiance values determined by area under the curve of radiance spectra (shown in A) in photons/s/cm² for a 30 nm slit, 385 nm centre wavelength reference value (pink) and a 25 nm slit, 385 nm centre wavelength reference value (green). Curves are a mean of measurements (30 nm slits: $n=15$ and 25 nm slits: $n=3$) taken at different time points over the course of the experimental day and are reported with their standard deviation.

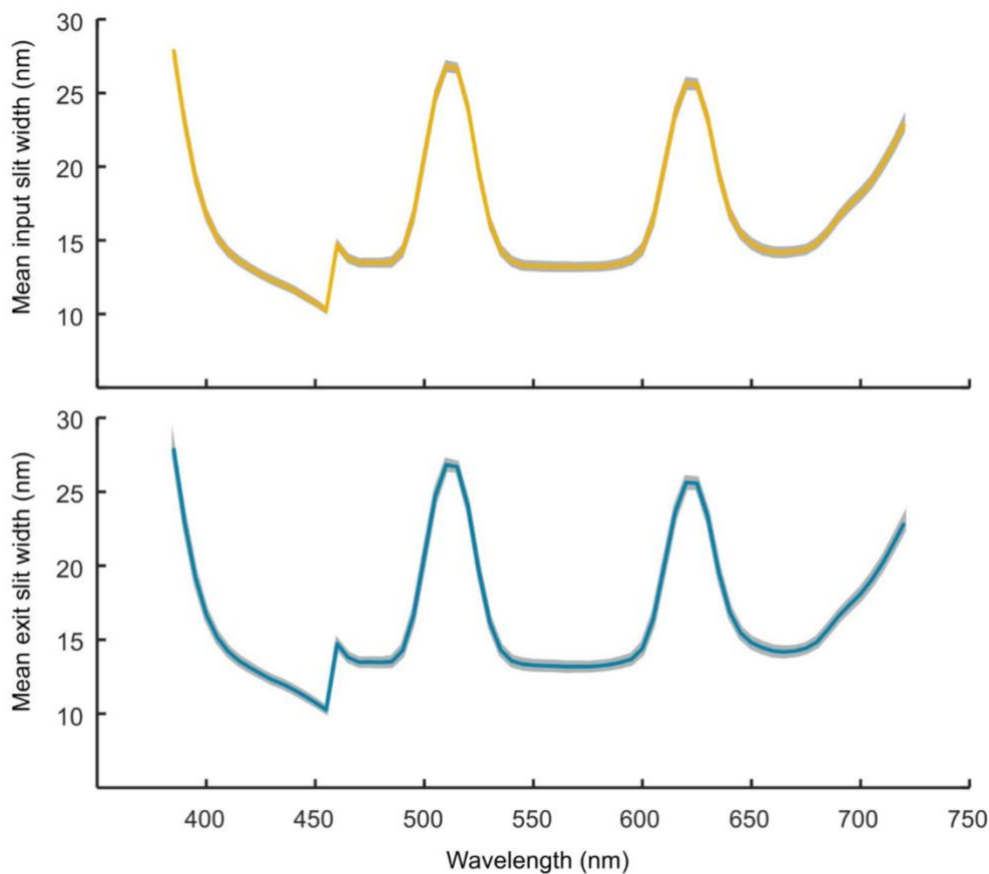


Figure 3.8 Variation in monochromator slit widths across daily calibrations.

The mean slit widths for input (yellow) and exit (blue) slits of the monochromator for a flat calibration across the spectrum for 18 subsequent days are reported with standard deviations (grey area), showing minimal variation.

3.4.3 Visual stimulus stability

A 150W light bulb was used to achieve sufficient brightness of the projected visual stimulus, however the temperature-dependent performance of the light bulb necessitates implementation of an efficient temperature control system. In addition to an initial three-hour warm-up period for the bulb to reach maximal brightness, an array of heat sinks and fans were used to ensure temperature stability across the day, and consequently consistency of the visual stimulus. Following the calibration of the monochromator slit widths, radiance measurements were then taken at half hour intervals across the day, demonstrating that the calibration curve remains flat across the spectrum over time (Figure 3.9 A). Despite a larger variation in the radiance integrals at either end of the spectrum relative to the middle wavelengths, there is no significant drift in the power

values, both within a given calibration curve and across all calibration checks in a day (Figure 3.9 B).

I next set out to assess the fluctuations of the light source over a short timescale corresponding to a set of visual stimuli. By repeating measurements of radiance for a given centre wavelength over the course of several minutes, I was able to assess the degree of fluctuation in optical power between supposedly identical stimuli. This was conducted for seven centre wavelengths spanning the spectrum, both for maximum monochromator slit width as well as calibrated slit widths (Figure 3.9 C). The percentage variation in power is expressed as the percentage change between the maximum or minimum radiance value and the mean of all radiance values for a given stimulus. These data demonstrate that fluctuations in power are minimal across the spectrum, with the maximum variance less than 3% (Figure 3.9 C). The apparent difference between short-term brightness fluctuations for max slit width and calibrated slit width stems from the difference in the area under the curve. An integral value from the calibrated slit spectra will result in more variability as the power is less. To minimise the influence of micro power fluctuations on the calibration process, multiple spectra were acquired over the course of several seconds to produce an averaged radiance value. Furthermore, a fail-safe loop in the calibration warrants that the reference value must be reached twice in a row before the monochromator slit widths are finalised.

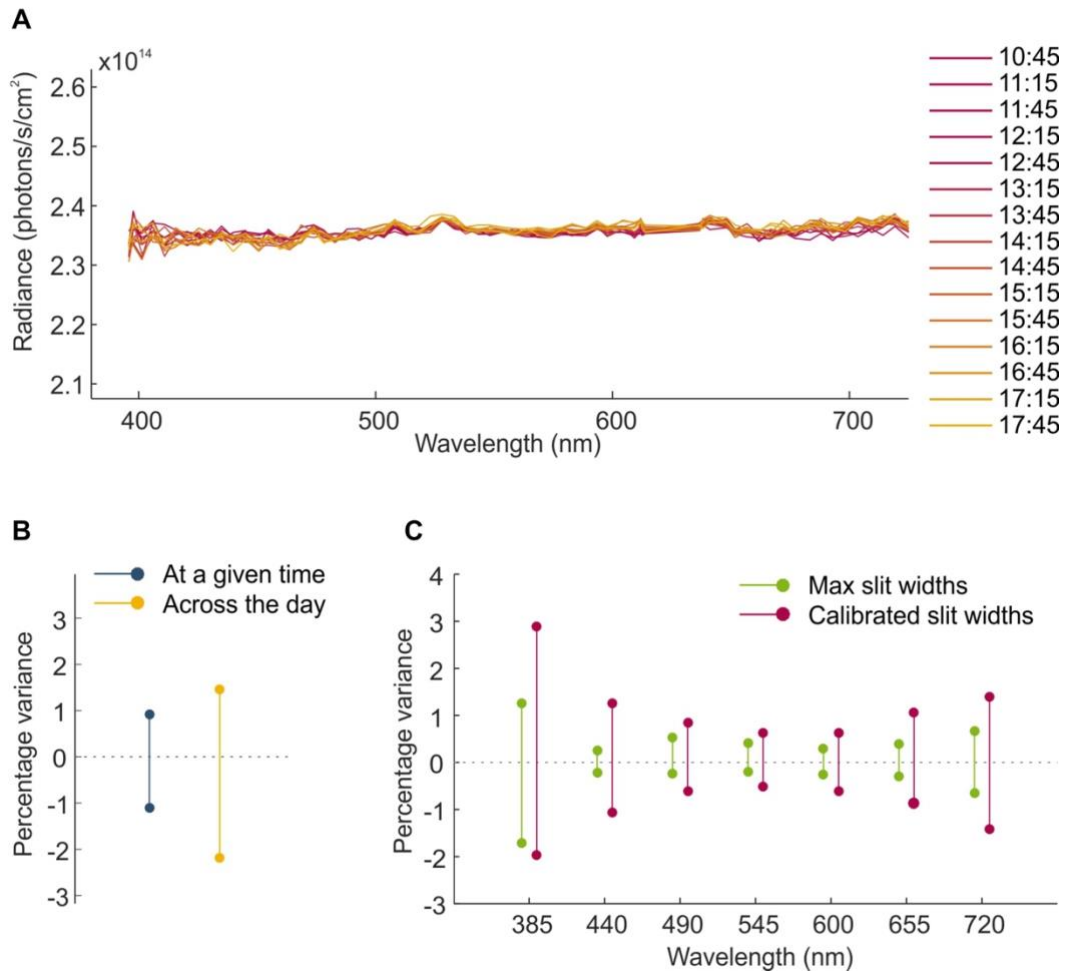


Figure 3.9 Assessment of optical power stability.

(A) Calibrated radiance values determined from the area under the curve for each radiance curve of radiance spectra, measured at half hour intervals across the experimental day. (B) Power fluctuation of calibrated light across the spectrum reported as the maximum and minimum percentage variance from the mean at any given time (see A), and over the course of the entire day. (C) Power fluctuations for individual centre wavelengths at maximum slit width and calibrated slit widths over the course of 5 minutes. Percentage change corresponds to maximum and minimum change from the mean of measurements taken every second over the course of five minutes.

3.5 SPATIAL CHARACTERISATION OF THE STIMULATION SETUP

3.5.1 Light scattering is a function of wavelength

All measurements described above were taken with the light guide assessing the central point of the screen. The screen, however, consists of a two-dimensional plane, all points of which will be sampled by a single, small spherical point in space: the fly's eye. The inverse-square law states that the intensity of light as a function of the distance from the light source follows an inverse square relationship. Thus, as the distance between the fly's eye and the screen increases towards the outer edges of the screen, the optical power diminishes accordingly (Figure 3.10). The transmission of a unidirectional beam of light through the screen is accompanied by scattering, which is the process of deflection of the unidirectional beam into many directions. Scattering is an inherent and necessary property of the screen material used in my setup. Without scattering, the light transmitted through the screen would not diffuse over the array of angles required to reach the fly's eye (Figure 3.10).

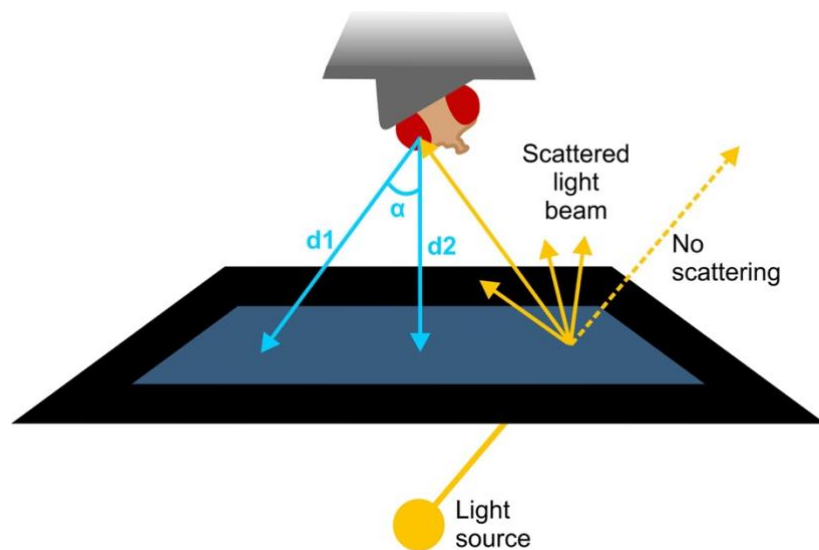


Figure 3.10 Optical properties for consideration when selecting a screen material.

At all points of the screen, the distance (e.g. $d1$ and $d2$) and the angle (e.g. α) of the light pathway between the fly's eye and the screen varies. As the distance increases, the light intensity inevitably drops. Scattering is a necessary property of the screen material to ensure light reaches the fly's eye despite its angle variance to the screen.

Furthermore, scattering properties of a material are coupled to the wavelength of the light. Thus, the particles, which make up the screen, will scatter light differentially relative to its wavelength as it hits these particles. Consequently, my quest was to find a screen material that scatters light in an equivalent manner between 385 and 720 nm to ensure that calibrated isoluminant bands of light at the screen centre retain their flat isoluminant calibration across the screen.

3.5.2 Intensity distribution across the screen

I first set out to assess the variation of optical power across the screen. This was done using a maximum slit width (input and exit) at 440 nm centre wavelength. The holder containing the spectrometer was tilted to sample three points of the screen at regular intervals along each of the orthogonal and diagonal axes, thus enabling me to estimate the decrease in power between the screen centre and the edges of the screen by plotting radiance values at each location ([Figure 3.11 A](#)). Using the maximal power value, corresponding to the central point of the screen (positioning as described above), I determined the percentage decrease of radiance values as a function of distance from the centre of the screen, and fitted a linear regression to the data ([Figure 3.11 B](#)). The radiance value for the bottom left corner is missing as the screen/stage motor configuration does not allow the holder to be tilted as far as that particular position. This shows that the decay in power is even from the centre of the screen outward. Although for the most part, points fit along the regression line, the obvious outliers result from the fact that although the radiance value for the screen centre point is the highest, the actual highest point of optical brightness is slightly off-centre. The drop in the power away from the centre is likely caused by a combination of the increasing distance from the spectrometer detector as the distance from the screen centre increases, and the spatial distribution properties of the light guide from the monochromator to the projector where the output is circular with more light concentrated at the centre than the edges.

3.5.3 Spectral constancy across the screen

When hunting for a screen material that fit the required optical properties, specifically the ability to maintain a flat calibration curve at all points of the screen, I trialled a variety of screen materials. Data from unsuccessful screen material trials is not reported here, only data from the screen best fitting our requirements (Da-Lite, Polacoat® Flex Plex Video Vision) is presented below.

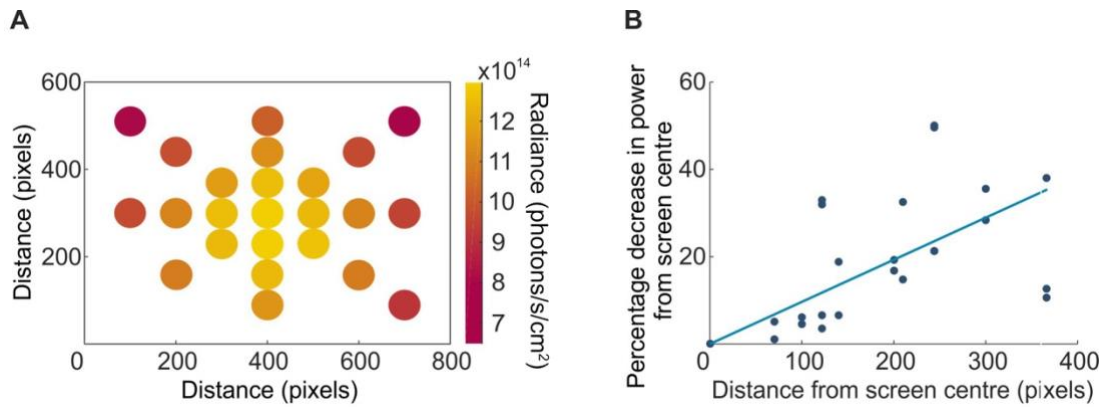


Figure 3.11 Optical power variation across the screen surface.

(A) The integral value of the radiance curve in photons/s/cm² for 440 nm centre wavelength light with 30 nm input and exit slits for is plotted for 24 different screen locations along the orthogonal and diagonal axes of the screen. (B) The percentage decrease in power from the screen centre is plotted as a function of distance. A linear regression is fitted to the data.

In order to characterise any change to the calibrated flat radiance curve, I calibrated the monochromator voltages for the central point of the screen and subsequently checked the radiance values for the calibrated voltages across the spectrum along the orthogonal and diagonal axes as described above (Figure 3.11). I then fitted a regression line to each of the of the calibration check curves at different screen locations, and used the values of the regression at either end of the spectrum (385 and 720 nm) to determine the percentage change in the power from UV light to red light. Furthermore, I verified the stability of a central flat calibration across the screen for an initial dim reference value (385 nm centre wavelength) with both 30 and 25 nm slits (Figure 3.12 A and 3.12 B respectively), and these exhibit very little difference. This was to reassure that these characterised optical properties do not vary within the range of monochromator bandwidths used (these vary from day to day as the bulb brightness can fluctuate over time). In order to minimise the spectral variance and optical power variance of the visual stimulus presented to the fly, I decide to exclude the less optimal portions of the screen by presenting a circle of light covering two thirds of the screen along the vertical axis and half the screen along the horizontal axis (400 and 400 pixels respectively). As the calibrated curve slopes decrease faster in some directions than others, I chose to realign

the centre of my circle on the point of the screen corresponding to the centre of spectral power variance. To do this, I fitted Gaussian curves the spectral power variance values of each of the cardinal axes, extracted the Cartesian coordinates for the maximal value of each fitted Gaussian and used a weighted mean of those four peak values to determine the centre of the circle (shown in blue in [Figure 12 A](#) and [12 B](#)). Using an average of the coordinates for the screen centre for the 25 and 30 nm slit calibration, I then plotted the spectral variance values as a function of distance from the average circle centre and fitted a regression line to the data ([Figure 12 C](#)). An example of the curves along one diagonal of the screen is shown in [Figure 12 D](#).

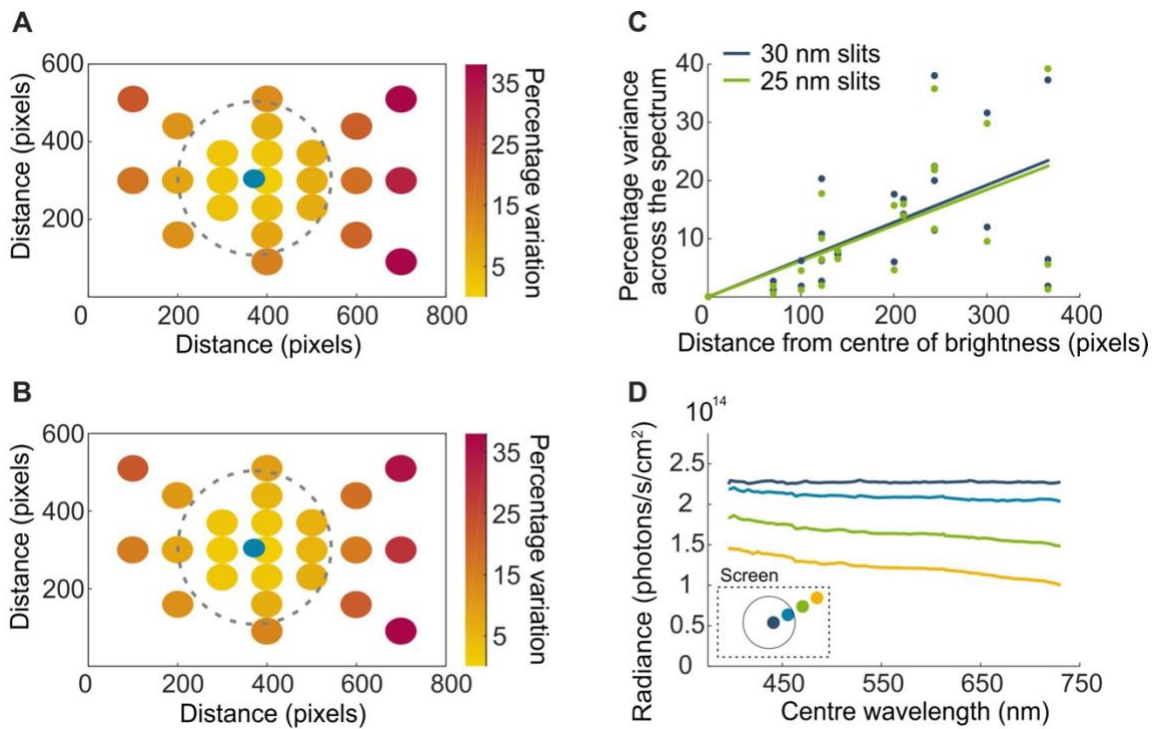


Figure 3.12 Variation in spectral constancy across the screen surface.

(A) The integral value of the radiance curve in photons/s/cm² for 440 nm centre wavelength light with 30 nm input and exit slits for 24 different screen locations along the orthogonal and diagonal axes of the screen. (B) The same data as shown in (A) using 25 nm slits instead of 30 nm slits. (C) The percentage decrease in power from the screen centre plotted as a function of distance. A linear regression fitted to the data shows the two slit widths have similar trends for variance across the spectrum. (D) Example traces of calibrated monochromator slits for one diagonal of the screen.

3.6 REFERENCES

- Allen, A. E., R. Storch, F. P. Martial, R. A. Bedford and R. J. Lucas (2017). "Melanopsin Contributions to the Representation of Images in the Early Visual System." *Curr Biol* 27(11): 1623-1632.e1624.
- Belušič, G., M. Ilić, A. Meglič and P. Pirih (2016). "A fast multispectral light synthesiser based on LEDs and a diffraction grating." *Sci Rep* 6: 32012.
- Brown, T. M., C. Gias, M. Hatori, S. R. Keding, M. Semo, P. J. Coffey, J. Gigg, H. D. Piggins, S. Panda and R. J. Lucas (2010). "Melanopsin contributions to irradiance coding in the thalamo-cortical visual system." *PLoS Biol* 8(12): e1000558.
- Estévez, O. and H. Spekreijse (1982). "The "silent substitution" method in visual research." *Vision Res* 22(6): 681-691.
- Hardie, R. C. and K. Kirschfeld (1983). "Ultraviolet sensitivity of fly photoreceptors R7 and R8: evidence for a sensitizing function". *Biophys. Struct. Mech.* 9, 171–180
- Kien, J. and R. Menzel (1977). "Chromatic properties of interneurons in the optic lobe of the bee. II. Narrow band and colour opponent neurons". *J. Comp. Physiol. A* 113: 35-53.
- Meinertzhagen, I.A., R. Menzel and G. Kahle (1983). "The identification of spectral receptor types in the retina and lamina of the dragonfly". *Sympetrum rubicundulum*. *J Comp Physiol* 151: 295–310.
- Salcedo, E., A. Huber, S. Henrich, L. V. Chadwell, W. H. Chou, R. Paulsen and S. G. Britt (1999). "Blue- and green-absorbing visual pigments of *Drosophila*: ectopic expression and physiological characterization of the R8 photoreceptor cell-specific Rh5 and Rh6 rhodopsins." *J Neurosci* 19(24): 10716-10726.
- Schnaitmann, C., V. Haikala, E. Abraham, V. Oberhauser, T. Thestrup, O. Griesbeck and D. F. Reiff (2018). "Color Processing in the Early Visual System of *Drosophila*." *Cell* 172(1-2): 318-330.e318.

Chapter 4 – Spectral Response Properties in the *Drosophila Medulla*

4.1 INTRODUCTION

4.1.1 Detecting the spectral quality of light

The efficiency with which a photon of light is absorbed by the fly's eye has everything to do with the energy it carries, a property directly related to its electromagnetic frequency, and consequently, to its wavelength. In other words, photons that fall into different ranges of the visible spectrum, from UV to red, will be caught more or less efficiently by the light-sensitive opsins present in the photoreceptor cells in order to generate an electrochemical signal interpretable by the brain. The spectral sensitivity curve of an opsin defines the probability of absorption of a photon of light as a function of its wavelength. Previous studies have generated this curve for the opsins expressed in different photoreceptor cells in the eye (Salcedo *et al.*, 1999; Stavenga, 2010), providing us with some understanding of the transformation of an electromagnetic wave, light, into an electrochemical signal. It is important to note, however, that these studies of *Drosophila* opsin spectral sensitivity have used paradigms such as the transgenic expression of inner R7-R8 rhodopsins in outer R1-R6 photoreceptors combined with microspectrophotometry to determine absorbance. These efforts, while improving our understanding, do not take into account the interactions of opsins with sensitising pigments and screening pigments (reviewed by Stavenga, 2002; Stavenga *et al.*, 2017, see Chapter 1, section 1.3.2) or the interaction between receptors (Schnaitmann *et al.*, 2018, see Chapter 1, section 1.3.6). There are no sharp electrode recordings from the inner colour receptors of *Drosophila* as the cells are considered too small. There are also no imaging studies published that precisely characterised the spectral sensitivity of the Rh3-6 in their native inner photoreceptors. How the spectral properties of light are encoded by the receptors containing rhodopsins Rh3-6, are conserved or transformed throughout the visual pathway, or how they might serve to enhance visual processing, however, remains largely the object of conjecture.

4.1.2 The functional role of screening pigment

Screening pigments are found in many insect eyes. These vary between species and usually determine the eye colour. Most common are black screening pigment expressing compound eyes, but red eyes are not uncommon, for example in higher dipterans, and tabenid fly eyes are marked by metallic colours (reviewed by Stavenga, 2002). Each ommatidia in the fly's eye is encircled by cells containing a strongly light-absorbing screening pigment. These serve to restrict the direction from which light enters the ommatidia, thus ensuring that any off-axis light cannot reach the photoreceptors (reviewed by Stavenga *et al.*, 2017). In addition to the screening pigment cells, yellow-coloured pigment granules are found in R1-R6 photoreceptors. These granules exhibit a dynamic and light-dependent migratory pattern: when the photoreceptor cell is strongly illuminated, the granules move from the cell soma to the centre of the rhabdomere, thus creating an optical screen (Kirschfeld and Franceschini, 1969). These mechanisms are not dissimilar to the vertebrate pupil expansion constriction to control the amount of light entering the eye to expand the intensity working range of the photoreceptor (Howard *et al.*, 1987). The migration of pigment granules is triggered by the absorption of light by the visual pigment in the photoreceptor and consequently is dependent on the expressed opsin's spectral sensitivity. Surrounding screening pigment cells, however, exert a notable influence on the spectral tuning of the photoreceptor through its own intrinsic spectral properties. The red screening pigment observed in the eye of *Drosophila* is atypical among dipterans. The near-black colouring of the eye more commonly seen in fly eyes results from dense packing of the screening pigment around the ommatidia which provides a highly effective light block. As the hue of the fruit fly's eye suggests, red wavelengths are reflected, not absorbed, by the screening pigments, resulting in off-axis sampling of longer wavelengths of light for photoreceptors (Stavenga *et al.*, 2017). Of course, this only affects photoreceptors that exhibit a sensitivity to longer wavelengths, however it does have implications for both spectral sensitivity by creating a bias in favour of longer wavelengths of light, but also the interaction of spectral sensitivity and spatial acuity as the off-axis light sampling in the longer wavelengths will increase the receptive field sizes of visual cells for that portion of the spectrum.

4.1.3 The advantages spectral information brings to visual processing

The broadband Rh1-expressing photoreceptors have long been shown to provide the input to the motion detection pathway (Rister *et al.*, 2007; Gao *et al.*, 2008; Yamaguchi

et al., 2008; Joesch *et al.*, 2010), while the Rh3-Rh6 photoreceptors with narrower sensitivities peaking in the UV, blue and green ranges are thought to provide the input to the colour vision pathway. This fits with many studies that show that motion vision is dependent on luminance contrast and insensitive to colour contrast, for example in the fleshfly (Kaiser, 1968), bees (Kaiser and Liske, 1968) and fruit flies (Yamaguchi *et al.*, 2008). Although this neatly separates the different visual processing streams, delineating a specific processing stream reserved for the perception of colour information, it might be an oversimplification of matters. Combining individual visual modalities at an early stage has been suggested as a strategic mechanism for retaining the more salient and useful aspects of the visual field (Gollisch and Meister, 2010). Furthermore, studies in vertebrates suggest that the integration of colour and motion signals improves perceptual discrimination (Takeuchi *et al.*, 2003; Nishida *et al.*, 2007). More recent experimental evidence in *Drosophila* demonstrates that colour signals improve motion processing behaviourally and calcium imaging resolved that R7-R8 colour receptor information is pooled with signals originating from outer R1-R6 receptors prior to the lobula plate (Wardill *et al.*, 2012). It was also shown that information from R7-R8 cells is pooled between receptor axons via gap junctions when exiting the retina prior to the lamina (Wardill *et al.*, 2012). These findings changed 30 years of dogma suggesting the channels were entirely separate.

4.1.4 Chapter aims

The aim of this chapter was to delve into the impact of the spectral composition of light on the visual response properties recorded from the early visual neuropil. Specifically, I aimed to address two main questions: (1) How does each of the photoreceptor types contribute towards visual processing? And can we see colour photoreceptor-driven responses in general medullary processing? (2) Does screening pigment density have an important influence on spectral sensitivity? R1-R6 cells project to the lamina, but this neuropil is bypassed by R7 and R8 cells which project directly to the medulla. Thus, this latter neuropil is where I chose to start my investigation as it presents the first opportunity in the visual pathway for signals from all five photoreceptor types to be integrated. As an initial foray into medullary spectral processing and in the absence of any obvious target neurons to record, the flies used in this chapter express neuronal activity indicators pan-neuronally. In order to probe spectral response properties, I sampled the summed activity of neurons across the ten layers of the medulla to gain an insight into general

response properties for each of these layers. I also aimed to investigate the contribution of photoreceptor types and screening pigment to these recorded response properties. To this end, I chose a genetic approach using fly strains expressing either all or a subset of functional photoreceptors as well as flies with normal or low levels of screening pigment density. Lastly, the dataset presented in this chapter was the first to be collected on the setup for simultaneous spectral stimulation and two-photon imaging described in the previous chapter. Thus, the final aim of this chapter is to confirm the precision and reliability of this system through the production of quality biological data.

4.2 METHODS

4.2.1 Fly stocks

Expression of the fluorescent calcium indicators GCaMP6f (Chen *et al.*, 2013) and RGECO (Dana *et al.*, 2016) was achieved using the GAL4/UAS expression systems (Brand and Perrimon, 1993) using the pan-neuronal promoter *nSyb* (Bloomington Stock Center, 39171) and the following stocks for the red eye *norpA*³⁶ X chromosome mutant (Wardill *et al.*, 2012), white eye *norpA*³⁶ mutant (Bloomington Stock Center, 52276) and rhodopsin 1 rescue construct for *norpA* (Bloomington Stock Center, 9048).

Four different fly stocks were used in this study:

- (1) w[+]; P{yw [20XUAS-IVS-GCaMP6f]attP40/+; P{yw [GMR57C10-GAL4]attP2/+
- (2) w[+]; +; P{yw [GMR57C10-GAL4]attP2, PBac{w, 20xUAS-jRGECO1a-p10}VK5
- (3) w[+] *norpA*[36]; UAS-GCaMP6f / P{w[+mC]=ninaE-*norpA*.W}2; 39171-Gal4/+
- (4) w[-] *norpA*[36]; UAS-GCaMP6f / P{w[+mC]=ninaE-*norpA*.W}2; 39171-Gal4/+

Stock1: n = 5; stock 2: n = 5; stock 3: n = 4; stock 4: n = 5

Fly stocks were made using standard fly crossing techniques using balancer chromosomes and in the case of stock 2, recombination was used to bring two insertions onto the same chromosome. Note that P{yw [20XUAS-IVS-GCaMP6f]attP40 is abbreviated as UAS-GCaMP6f, P{yw [GMR57C10-GAL4]attP2 is abbreviated as 39171-Gal4. Stock 1 is referred to throughout as red eye/ wild type photoreceptor function/ GCaMP, Stock 2 is referred to throughout as red eye/ wild type photoreceptor function/ RGECO, Stock 3 is referred to throughout as red eye/ Rh1 photoreceptors only/ GCaMP,

and Stock 4 is referred to throughout as orange eye/ Rh1 photoreceptors only/ GCaMP. Females were used for stocks 1 and 2 and males for stocks 3 and 4.

Fly care and physiological preparations were carried out as detailed in the methodology chapter (section 2.1). As Ferreiro *et al.* (2017) caution against using flies aged beyond 4-5 days if they carry the w^{1118} mutation for reasons of retinal degeneration, my recordings were carried out in 4 to 7-day old flies. Slightly older flies were used due to ease of making the imaging preparation and did not show different results across this age range.

4.2.2 Two-photon imaging

Two-photon imaging was carried out as described in the methodology chapter (section 2.3). Images were acquired using the green channel (GaAsP detector 1) for flies expressing GCaMP and the red channel (GaAsP detector 2) for flies expressing RGEKO. A 200X zoom (20X on the objective and 10X on the software) was used to visualise the fly medulla. This allowed me to image all layers of the neuropil from proximal to distal across a number of cartridges (ranging from a half a dozen to a dozen in different experiments, 0.104 to 0.115 $\mu\text{m}/\text{pixel}$ with a field of view of 53 to 59 μm). The response of medullary neurons, not photoreceptors, are measured in this study.

4.2.3 Visual stimulation

The combined monochromator-screen stimulation setup described in previous chapters was used for the following experiments. Stimuli applied here were full-field stimuli (i.e. they have no spatial structure) and were designed to investigate intensity and spectral response properties independent of other visual modalities. As outlined in the previous chapter, only the central portion of the screen was used, segmented by a circular ellipse of 400 pixels in diameter corresponding to 38.8 degrees of visual field. By removing the corners and edges, spectral variation resulting from light scattering is reduced (see [Figure 3.12](#) in Chapter 3).

Intensity-Response Relationship

The first set of visual stimuli applied to the fly were used to establish intensity-response relationships of medulla neurons. The stimulation protocol consisted of three repeated 1

second light flashes intercalated with 3 seconds of darkness. This motif was repeated for a range of twenty incremental intensities spanning four log units of light (from 10^{12} to 10^{15} photons/s/cm²) to establish the dynamic range of the visual response. Intensity-response relationships were probed for three different bands of the spectrum defined by the following centre wavelengths: 385 nm (UV), 440 nm (blue) and 565 nm (green). These colours were chosen with the intent to match the known spectral sensitivity peaks of the fruit fly opsins within the limitations of the system, such as the lack of UV light transmission through the projector and the restriction of most green wavelengths by the filters to prevent sampling by the GaAsP detectors.

Spectral Response

Next, in order to probe spectral response properties, the fly was presented with a spectral sweep of randomised light flashes of varying centre wavelengths ranging from 390 to 720 nm, all calibrated to produce the same radiance of 2.63×10^{13} photons/s/cm². This intensity was chosen as it sits in the middle of the intensity-response range across all tested wavelengths and all tested fly genotypes. A gap in the spectral sweep was introduced spanning 490 to 565 nm and 595 to 700 for the green-emitting GCaMP and the red-emitting RGECO, respectively, to accommodate the red and green GaAsP detector sensitivities. Flashes of light were applied for 1 second with a 3 second interval between each pulse, and the entire spectral sweep was repeated five times with a different colour randomisation for each repetition. Spacing between centre wavelengths was originally set to be 5 nm increments, as specified by the voltages supplied by the monochromator software. However, an assessment of the Gaussian curve describing the band of light revealed that the peak of each curve is, in fact, not aligned with the expected centre wavelength, but shifted in either direction by a negligible amount. Nonetheless, in the interest of precision, centre wavelengths have been adjusted in graphs throughout.

Further visual stimulus considerations

Each experiment consisted of all stimuli types and these were always presented in the following order: spectral sweep, green-, UV- and blue intensity-response stimuli. A ten-minute dark adaptation period preceded the five repetitions of the spectral sweep and preceded each presentation of the intensity-response stimulus.

Stimulus calibration

Daily calibrations were carried out for all stimuli, and a post-calibration check was conducted to ensure precision of the stimuli. This data also provides information on the stimulus bandwidth at the half maximum of the Gaussian curve, which we compared across the spectral sweep to assess the uniformity of the light across all centre wavelengths. The larger spread in width variation between the stimuli for the GCaMP expressing flies (**Figure 4.1 A**) than the RGECO expressing flies (**Figure 4.1 B**), as seen by a bigger variation of the standard deviation, can be attributed to the timescale across which the experiments were carried out, 6 months and 2 months respectively. As bulb shifts can occur over time, the larger standard deviation is expected in (**Figure 4.1 A**). Of note, stimulus bandwidths vary from 5 to 11 nm (**Figure 4.1 C**), in part because of the spectrum of the xenon bulb which peaks in the range of 470 nm, but also as a result of the complex interplay of filters involved in the monochromator/2P system.

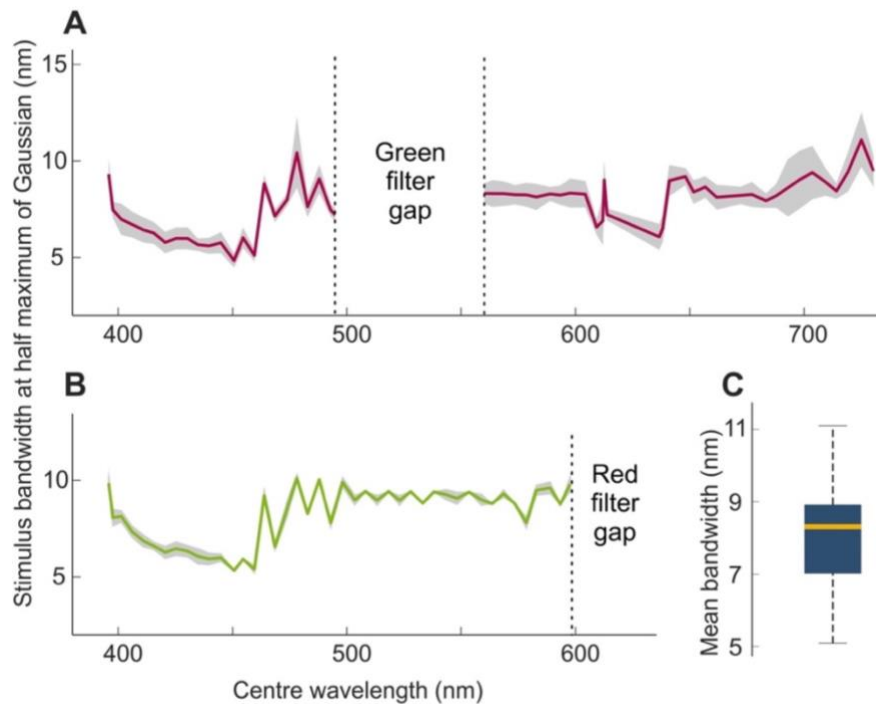


Figure 4.1 Spectral sweep stimuli bandwidths.

The width at half max of the Gaussian peak is plotted against its respective centre wavelength for the bands of light used in the spectral sweep, in (A) the spectral sweep stimuli for flies expressing GCaMP with the filter gap between 495 and 560 nm in the range of the green GaAsP detector, and (B) the spectral sweep stimuli applied to RGECO flies terminating at 595 nm, the start of the red GaAsP detector range. (C) Boxplot of the spread of stimuli bandwidths.

4.2.4 Analysis

ROI selection

For region of interest (ROI) selection, a reference image was used corresponding to averaged frames across the response period for a blue light pulse. Circular ROIs 12 pixels in diameter were manually positioned to tile the sections of the 512 x 512-pixel image containing the medulla that are visually distinguishable from their fluorescence (both baseline and light response, example ROI segmentation in [Figure 4.2](#)). The aim of this selection process was to assess responses in a given discernible layer without making the assumption of response uniformity across the layer. Each ROI covers a sufficient number of pixels to ensure a good response can be extracted whilst limiting noise issues that may arise in larger ROIs. Each imaging sequence from a fly medulla averaged approximately 150 ROIs that were extracted for analysis.

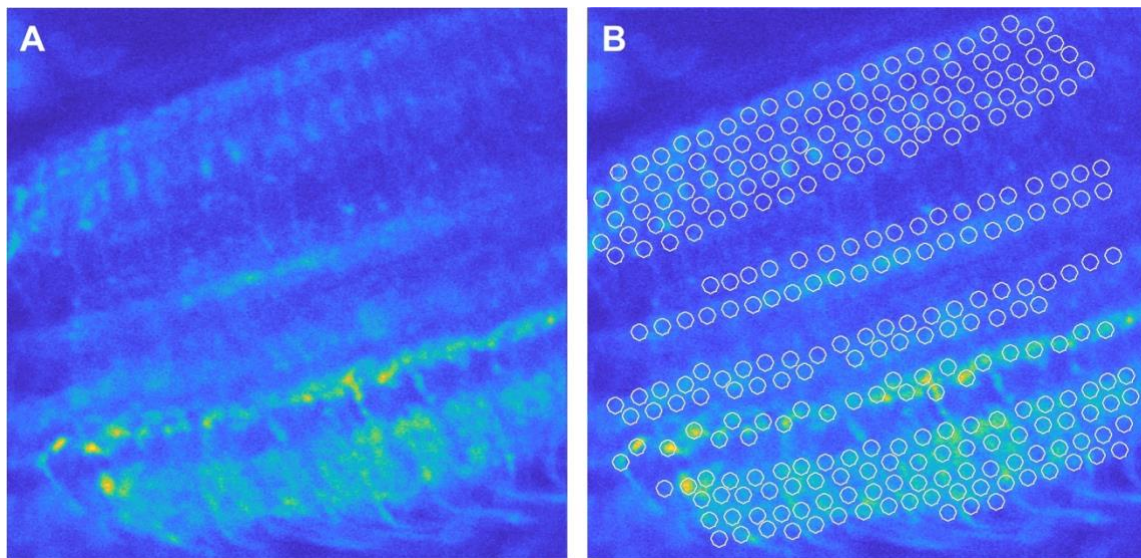


Figure 4.2 Segmentation process for neuronal signal extraction.

Layers and structures of the medulla are readily discernible under the two-photon microscope. (A) Baseline fluorescence of the calcium indicator provides a solid outline of the neuropil, but visually responsive segments can be evidenced further by averaging images of the response to a flash of blue light. (B) 12-pixel circular ROIs are manually tiled across the visible layers that exhibit visually distinguishable fluorescence.

Fluorescent data extraction, curve fitting parameters and data selection

Changes in fluorescence (DeltaF) traces were extracted (see Chapter 2, section 2.3 for details) for individual ROIs and averaged across repetitions of identical stimuli. In the case of data resulting from the spectral sweep, only three of the five repetitions were retained via a selection method whereby the two responses furthest from the mean of all five responses for a stimulus were removed. This methodology was introduced in an effort to reduce noise in the data. Next, a stimulus response value was calculated by integrating the response over time. The time segment for response integration was matched to the excitatory phase of the response profile observed to ensure maximal signal. In practical terms, integral values of the trace were calculated either over the one second duration of the stimulus, over the one second duration post stimulus or over the time course of both. Sigmoid curves were fitted to the intensity-response data using the Naka-Rushton equation classically used for electroretinogram data (Naka and Rushton, 1966):

$$\frac{V}{V_{max}} = \frac{I^n}{I^n + K^n}$$

V is the response and V_{max} the maximum amplitude of the response, I is the stimulus intensity, K is the intensity at the half maximum response and n is the exponential slope measured at the half maximum response. The curves were fitted in a two-step process. First the intensity-response data was transformed for each stimulus intensity: $\log \left[\left(\frac{V_{max}}{V} \right) - 1 \right]$. Then a linear regression was fitted to the transformed data to determine an initial approximation of K and n (Evans *et al.*, 1993; McCulloch *et al.*, 2016). Next, the estimated K and n values were used to fit the curve with the above equation. The goodness-of-fit of the curve was evaluated by means of the mean square error value (MSE) and curves presenting MSE values superior to 0.01 were discarded. Furthermore, data was retained only if a curve could be fitted to all three intensity-response stimuli colours (UV, blue and green) within the set MSE parameter threshold.

A selection process was also applied to spectral sweep data, spectral response curves were only retained for a given ROI if the following conditions were fulfilled: (1) all three intensity-response curves were fit as per the above criteria and (2) the light intensity used for the spectral sweep sits at least 1/5 below the maximal value of the intensity-response curve for all three colours (to ensure saturation was not reached at any point of the spectral sweep).





Statistics

All stages of data analysis (image analysis, curve fitting, data representation and statistical analyses) were conducted using custom scripts which used statistical packages available in Matlab (Mathworks, MA, USA). Individual statistical tests are reported in figure legends and the results of post hoc tests, original data points, mean, standard deviation, and standard error of the mean are reported throughout using notBoxPlot Matlab function (version 1.31.0.0, Rob Cambell).

4.3 RESULTS

This investigation set out to probe spectral response properties of neurons in the medulla of *Drosophila*. Specifically, I aimed to uncover the role for different photoreceptor types (outer versus inner), as well as the role for screening pigment in general medullary information processing. To this end, I applied intensity-response stimuli and spectral sweep stimuli to four different *Drosophila* transgenic strains and monitored the responses of medulla cells by means of calcium activity indicator imaging. The fly strains used differed from each other for one or more of the following parameters: (1) screening pigment was either expressed at wild type densities to produce a red eye phenotype, or at a lower density to yield an orange eye phenotype; (2) photoreceptor function was either left intact (all five photoreceptors functional) or depleted with only photoreceptors expression Rh1 as fully functional; and (3) one of two calcium activity indicators with different spectral emission properties (GCaMP6f: green and RGEKO: red) was expressed ([Table 4.1](#)). I chose pan-neuronally labelled fly lines to gain an initial insight into possible variations in spectral response properties across the medulla. Candidate colour neurons have been identified (Chapter 1, 1.3.5), however generation of fly lines with neuron-specific calcium activity indicators is a lengthy process and could not be completed within the time frame allocated to this project. These fly lines were chosen from a larger selection of opsin mutants which did not all present discernible visual responses. I expand on this in the discussion (4.4.2).

Table 4.1 Details of fly strains used and their phenotypic variations

Genotype icon	Screening pigment density	Functional rhodopsins	Calcium activity indicator
	High (red eye)	Rh1, Rh3, Rh4, Rh5, Rh6	GCaMP6f
	High (red eye)	Rh1, Rh3, Rh4, Rh5, Rh6	RGECO
	High (red eye)	Rh1	GCaMP6f
	Low (orange eye)	Rh1	GCaMP6f

4.3.1 Response profiling across medulla layers

The fly preparation enabled image acquisition from all the layers of the medulla. In addition to a discernible cartridge structure, the neuropil exhibits distinct features along the proximal-distal axis such that although every individual layer is not distinguishable, layer groupings are recognisable. For the purpose of this study, I have categorised layer structures into six groups as follows: medulla layers M1, M2, M3, M5, M6-M7 and M8-M10 (**Figure 4.3 A-C**, Gao *et al.*, 2008). The response to a light pulse delivered to the fly's eye is stereotyped within a group, with M1, M5, M6-M7 and M8-M10 exhibiting an excitatory response when the light is on, M3 also presenting a small excitatory response to the light pulse followed by a larger excitatory phase when the light turns off, and finally, M2, exhibiting an inhibitory response to lights on and excitatory response to the light turning off (**Figure 4.3 D**).

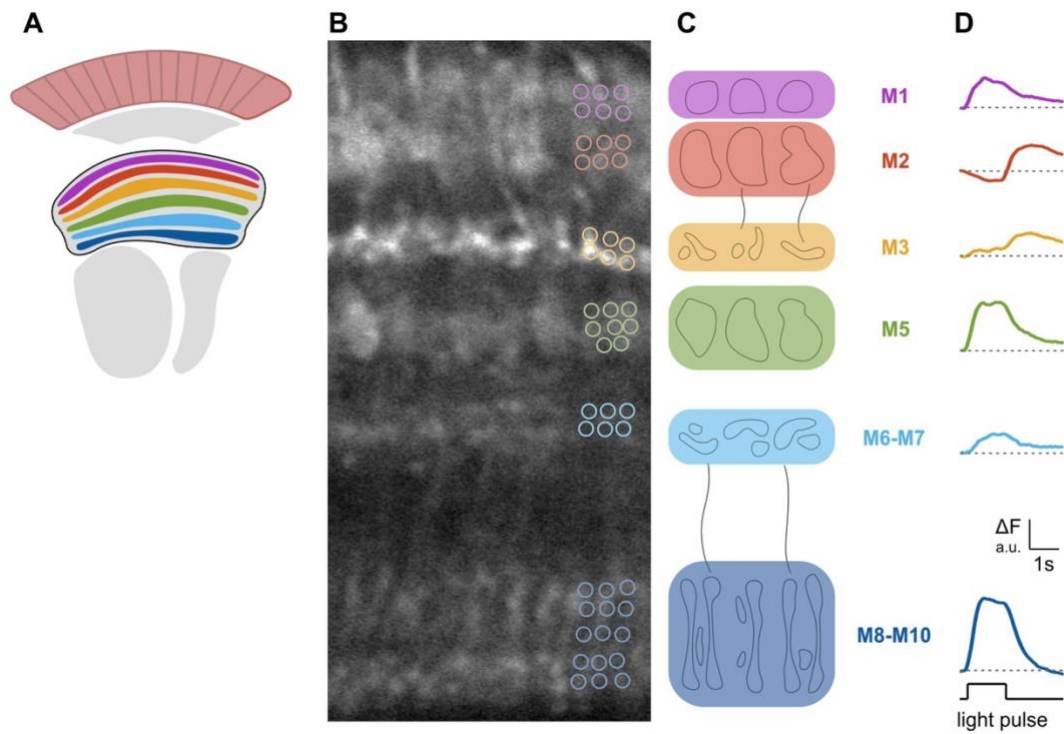


Figure 4.3 Layer specific response profiles of summed neural activity.

Pan-neuronal GCaMP labelling of the medulla reveals six distinguishable layer structures (**A**, schematic; **B**, 2-photon image of baseline fluorescence), each exhibiting discernable cartridge-width substructures. Example ROI segmentation is superimposed. (**C**). Example response from a single ROI to a blue (440 nm) light pulse are stereotyped within a layer structure. These vary in temporal profile and size of response across layers M1, M2, M3, M5, M6-M7 and M8-M10 (**D**).

4.3.2 General medulla processing

A set of full-field light pulses of increasing intensity were applied to the fly eye to establish intensity-response relationships (**Figure 4.4**). I measured and fitted curves to the intensity-response relationship of ROIs across all layer groupings of the medulla for three distinct monochromatic bands of light in the UV, blue and green portions of the spectrum. Of note, individual data points in **Figures 4.5** and **4.8** correspond to data averaged across all ROIs within a layer grouping. I observed a left shift of the green intensity-response curve and half-maximum values in orange-eye flies by comparison with their red counterparts (**Figure 4.5A and 4.5B**), indicative of increased sensitivity to longer wavelengths of light.

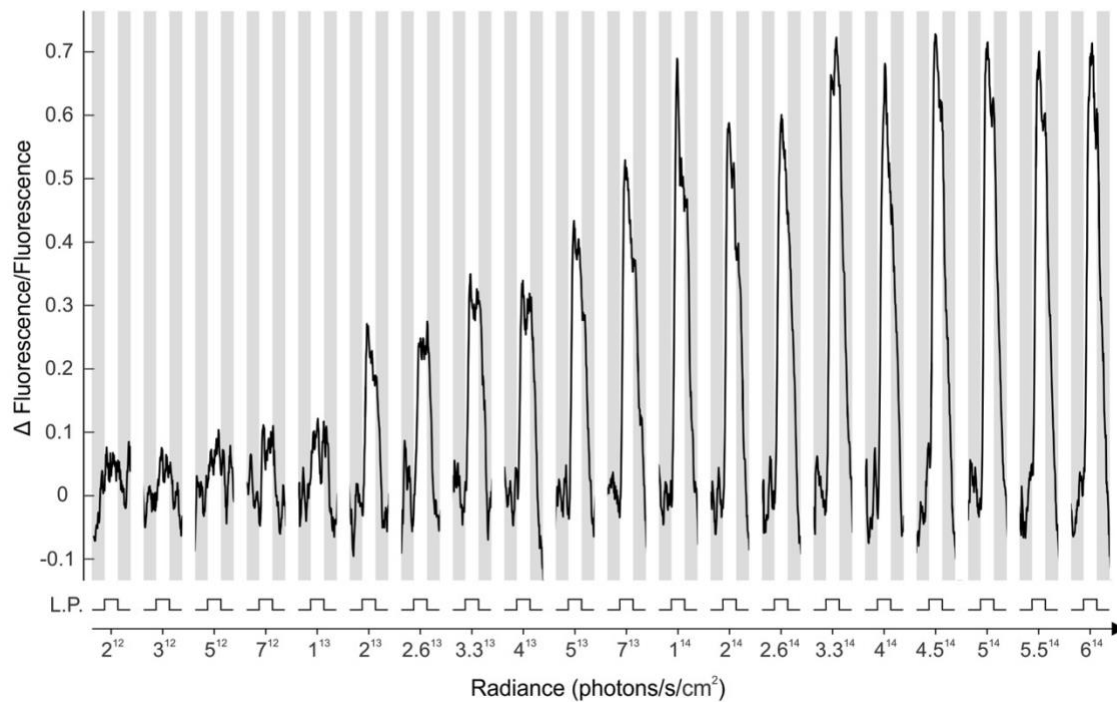


Figure 4.4 Intensity-response stimulus: example responses.

Example fluorescence responses of an ROI to the intensity-response stimulus protocol consisting of light pulses (L.P.) of increasing intensity. Traces for a given intensity represent the mean of the response from all three stimulus repeats.

Characterising intensity-response relationships provides us with the dynamic range of the ROI responses. I used this to determine a light intensity value that sits within the middle range of the curve for all fly genotypes from shorter to longer wavelengths of light. This light intensity could then be used for the spectral sweep to elicit a sizeable response without nearing saturation levels. Thus, I probed the ROI responses to a series of light pulses ranging from UV light through to red light set at approximately 5 nm centre wavelength intervals ([Figure 4.6](#)).

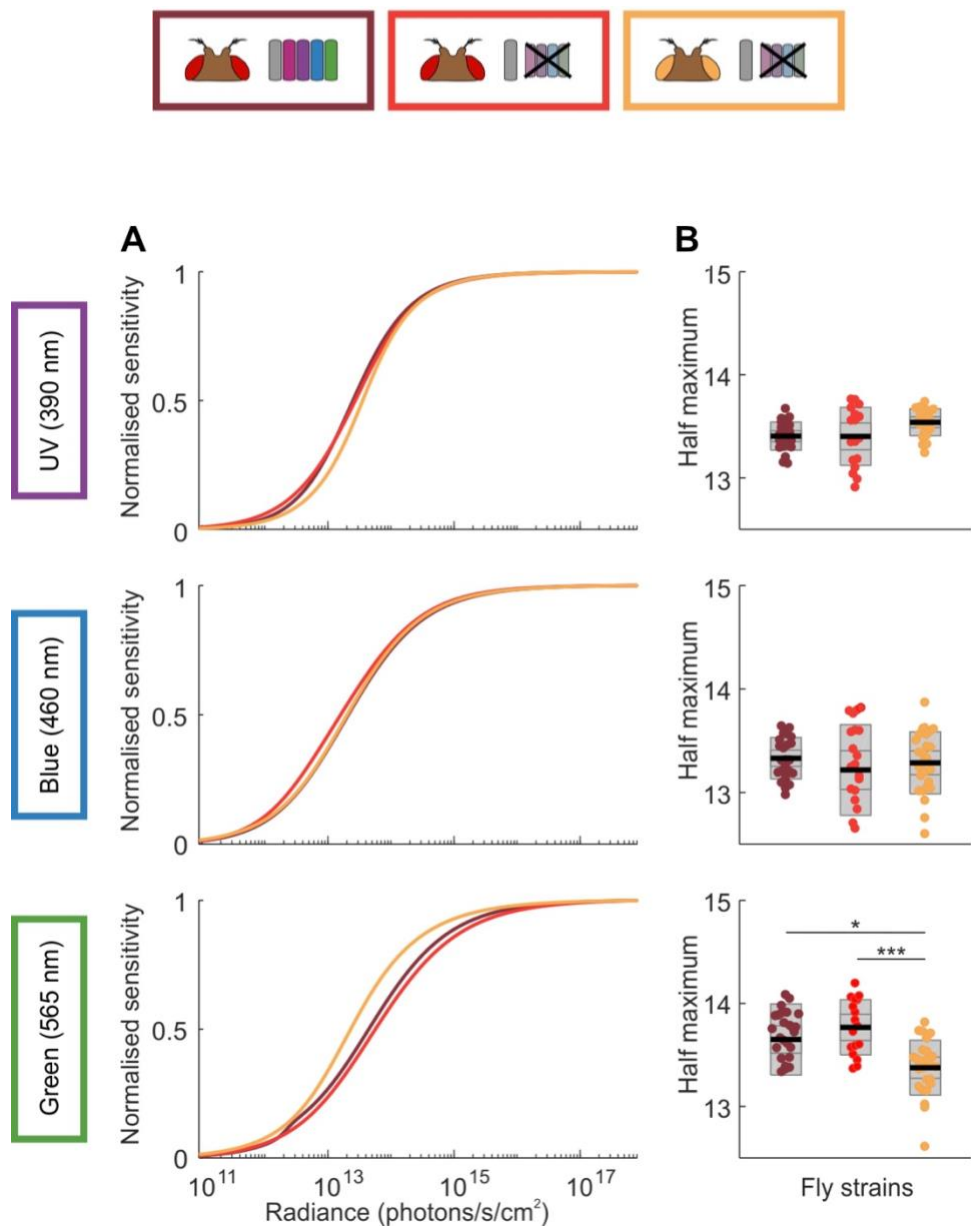


Figure 4.5 Intensity-response relationship comparison across fly strains.

*Intensity-response relationship curves (A) for three different bands of monochromatic light (UV, blue and green; centre wavelengths 390, 460 and 565 nm respectively) collected for three different fly strains- red eye, wildtype photoreceptors and GCaMP6f (bordeaux); red eye, Rh1 only and GCaMP6f (red) and orange eye, Rh1 only and GCaMP6f (orange). Coefficient values extracted from the fitted curves represent the half maximum (B) of the intensity-response relationship. Individual data points correspond to the average of ROI responses across a given layer structure (see methods) for a given fly preparation. Significant differences are noted with star values, with the P values from left to right: *P = 0.0105 and ***P = 0.0002 (one-way ANOVA). Black, solid lines represent the mean value. From the mean outwards, the first grey line of the background box shows the 95% confidence interval (or 1.96 standard error of the mean) and the second grey line represents 1 standard deviation from the mean. The curves in (A) are a mean of the fitted curves of individual data points.*

Our data indicates that normalised spectral response curves exhibit variation in the shorter wavelengths (395-450 nm range) as well as in the longer wavelengths (570-600 nm range) (**Figures 4.7** and **4.8**). For the first few wavelengths of light at the UV end of the spectral sweep, standard deviations are more pronounced suggesting a variability in the response data that needs to be taken into consideration when interpreting the results (**Figure 4.7A**, lower panel). In the UV-blue range approximating 395 to 450 nm, however, a trend appears revealing a lower sensitivity of orange eye/ Rh1 photoreceptors only/ GCaMP flies versus red-eye flies. This pattern is reversed in the green-yellow portion of the spectrum where orange eye/ Rh1 photoreceptors only/ GCaMP flies exhibit a markedly stronger response than other fly strains although the responsiveness in the orange-eye flies does not appear to continue any further into the longer wavelengths with all curves decaying to a near-absent response by 600 nm (**Figures 4.7** and **4.8**).

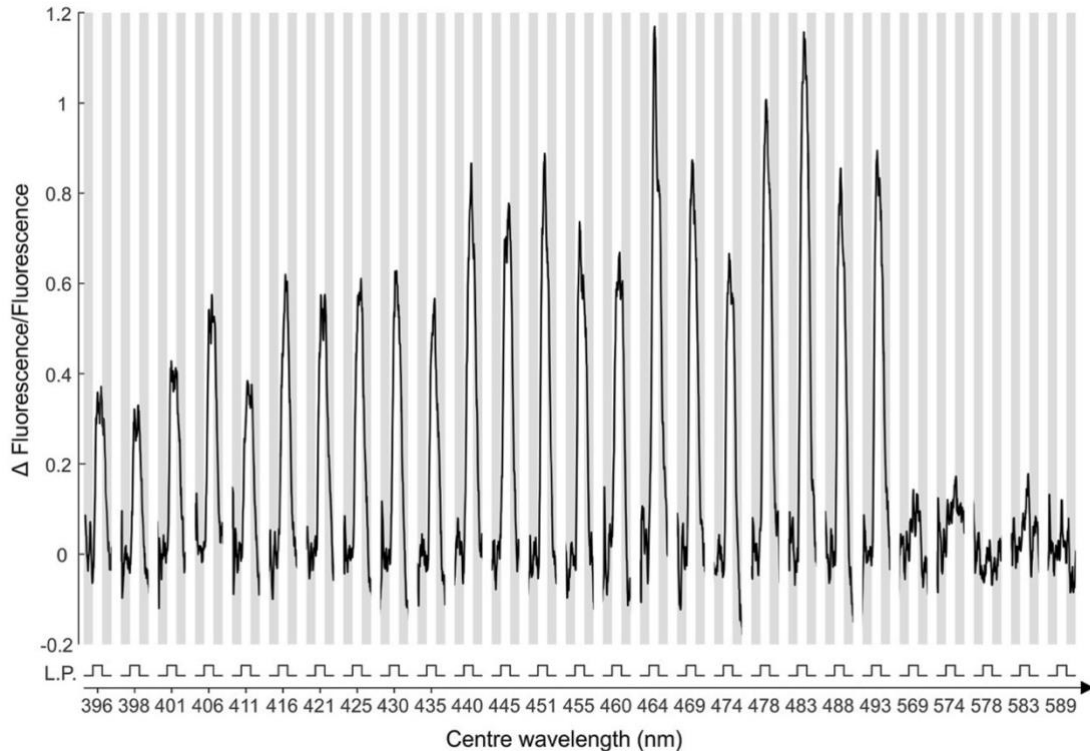
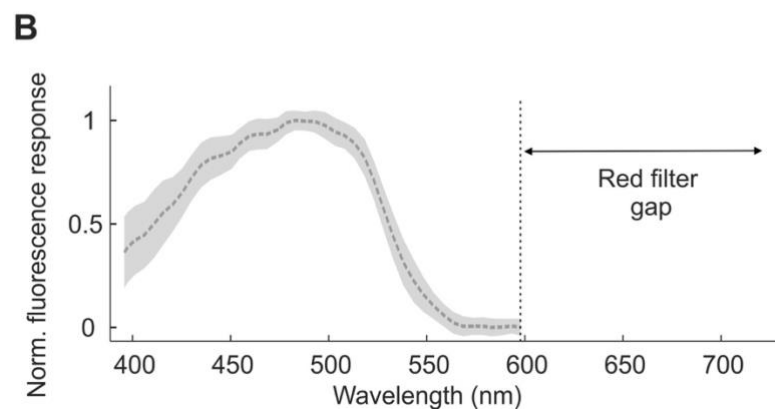
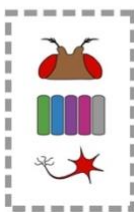
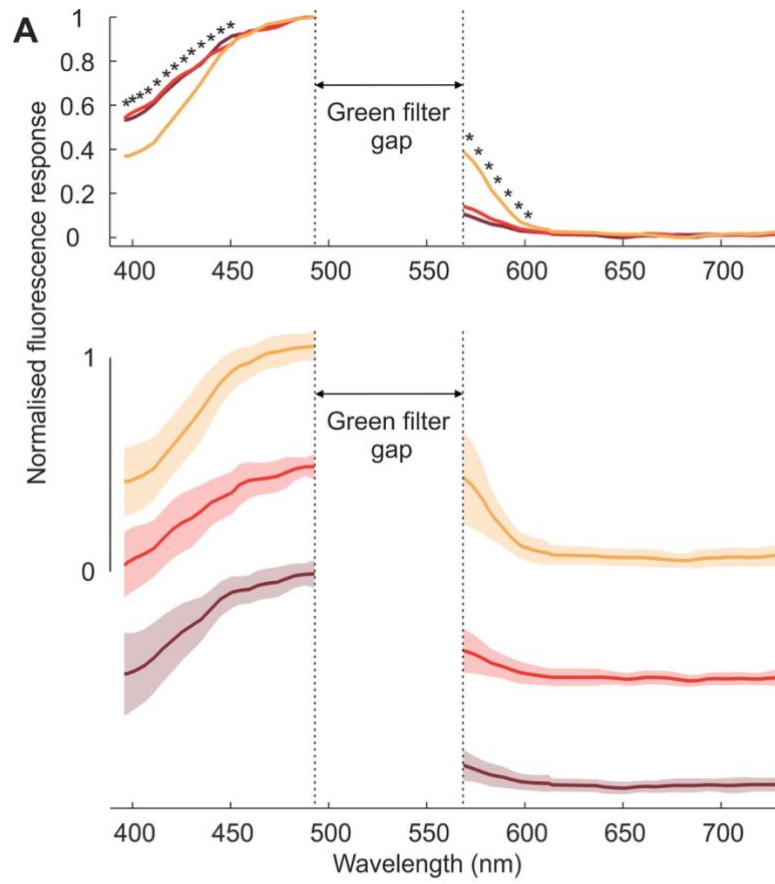
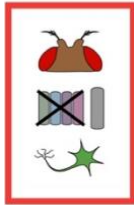
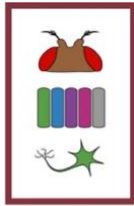


Figure 4.6 Spectral sweep stimulus: example responses.

Example fluorescence responses of an ROI to the spectral sweep stimulus protocol consisting of light pulses (L.P.) of varying centre wavelengths. Traces for a given intensity represent the mean of the response from all three stimulus repeats. Response traces are not represented beyond 590 nm for the sake of clarity as no discernible change in fluorescence is detected beyond this point. Note that pulses were presented randomly but have been reordered here in ascending wavelength.

Figure 4.7 Spectral response profiling.

Normalised spectral response profiles, determined by a sweep of equal intensity light pulses across the spectrum, are plotted for four different fly strains. In (A), red eye, wildtype photoreceptors and GCaMP6f (bordeaux); red eye, Rh1 only and GCaMP6f (red) and orange eye, Rh1 only and GCaMP6f (orange). In (B), red eye, wildtype photoreceptors and RGEEO (grey). For GCaMP-expressing flies, a gap in the spectral sweep is necessary in the green wavelengths of light corresponding to the microscope's green detection range. The spectral sweep gap for RGEEO-expressing flies sits at the red end of the spectrum. Superimposed means-only traces are represented in the upper panel and the same mean traces are depicted staggered with the addition of standard deviations in the lower panel. Stars indicate significant differences between fly strains for a given centre wavelength. Further statistical information is reported in Figure 4.8.



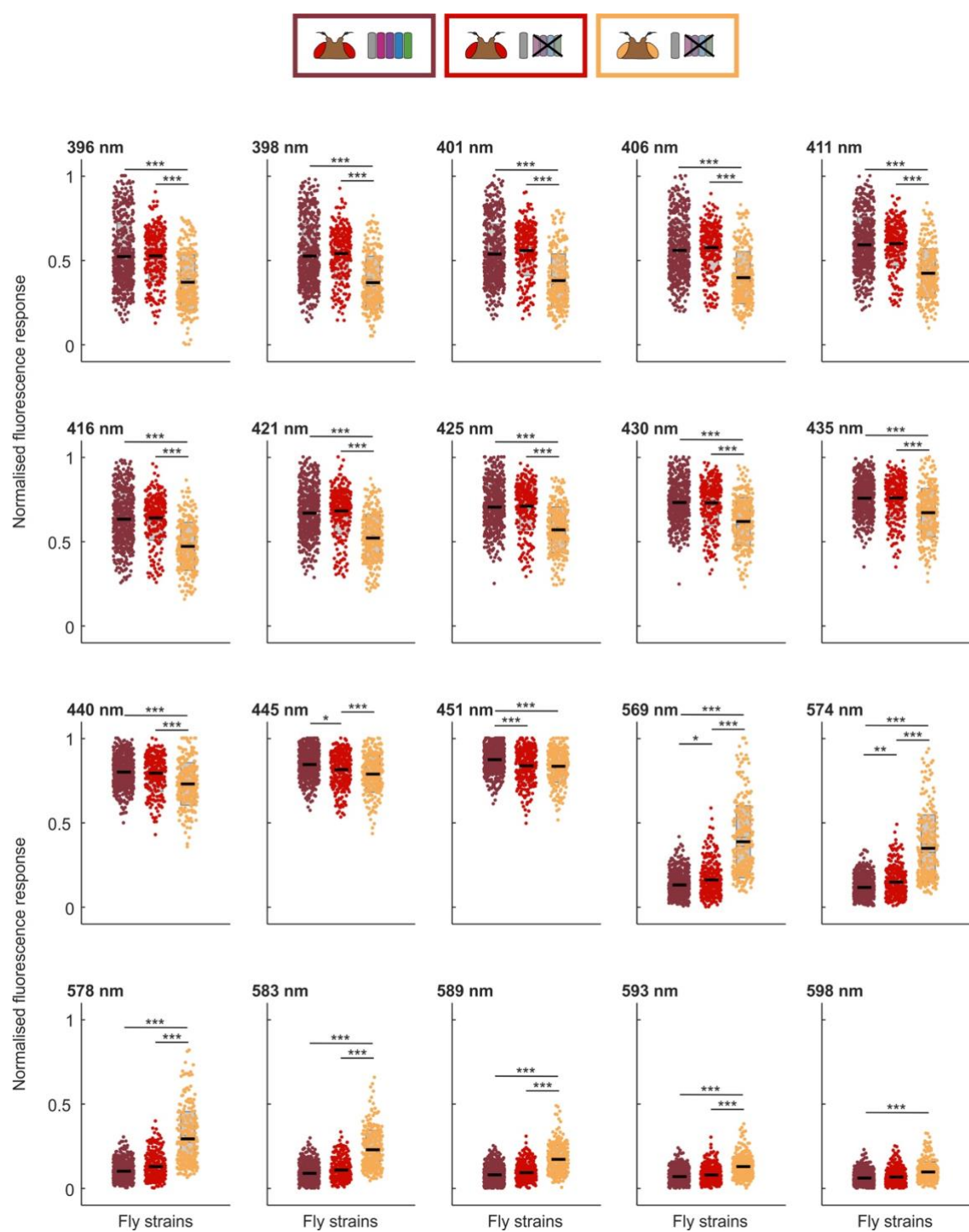


Figure 4.8 Spectral response profiling – breakdown for individual wavelengths.

Responses to the individual wavelengths of the spectral sweep (Figure 4.10) that exhibit significant differences for three different fly strains- red eye, wildtype photoreceptors and GCaMP6f (bordeaux); red eye, Rh1 only and GCaMP6f (red) and orange eye, Rh1 only and GCaMP6f (orange). Black, solid lines represent the mean value. From the mean outwards, the first grey line of the background box shows the 95% confidence interval (or 1.96 standard error of the mean) and the second grey line represents 1 standard deviation from the mean. 1-way ANOVA p-values are reported in Appendix 1, table A1.

Coefficient values extracted from fitted intensity response curves (slope and half maximum, [Figure 4.9](#)) suggest minor response property discrepancies between flies expressing GCaMP6f and RGECO ([Figure 4.9B](#)), attributable to differences in amplitude and decay times (Dana *et al.*, 2016). Consequently, I did not pool data from RGECO-expressing flies with GCaMP6f data for statistical analyses. Nonetheless, this red-emitting indicator serves the valuable purpose of completing the spectral profile as the red GaAsP is used to record RGECO signals, thus allowing the GCaMP-restricted green wavelengths of the spectral sweep to be filled in ([Figure 4.7B](#)).

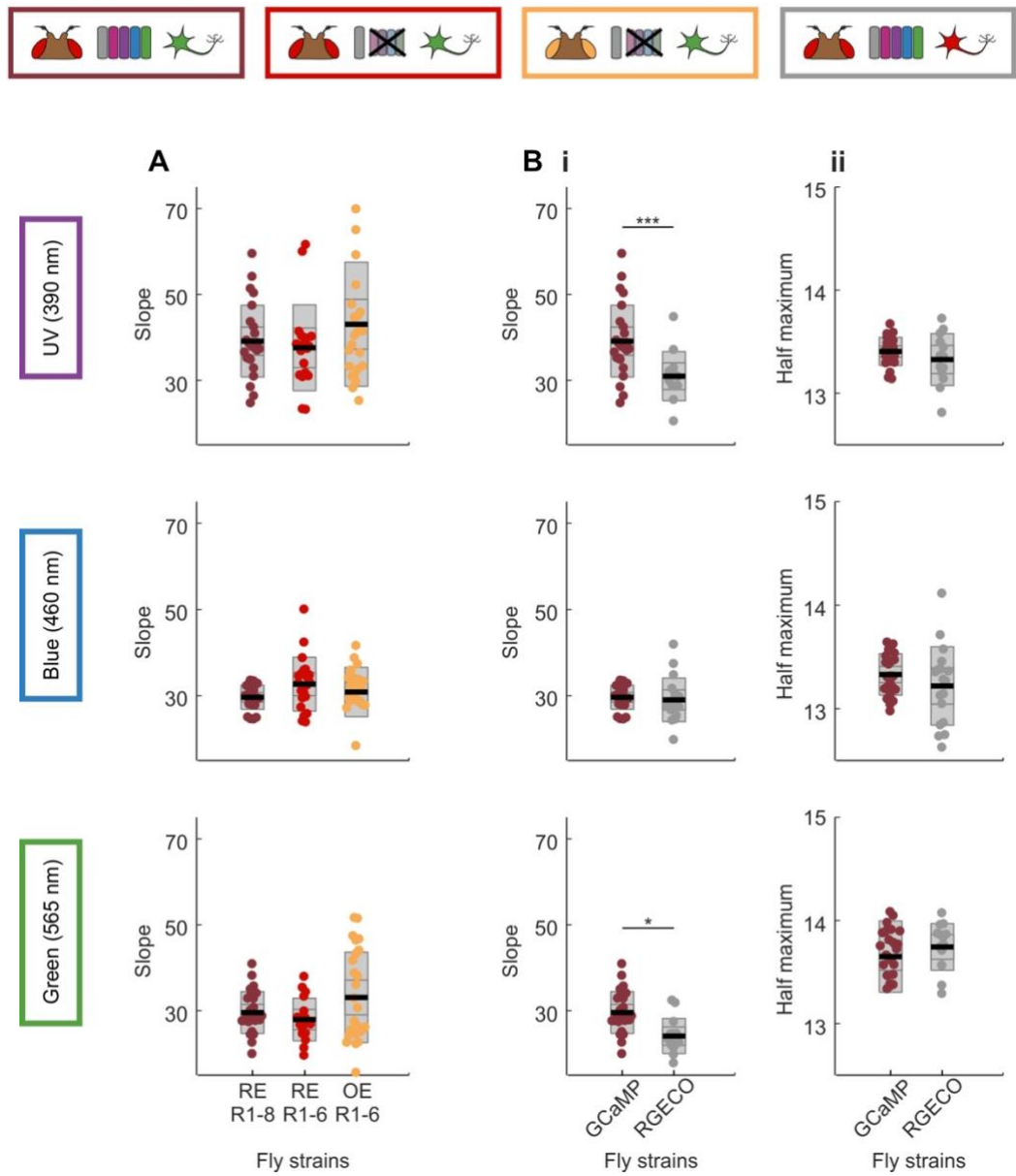


Figure 4.9 Intensity-response relationship coefficients across fly strains.

Experiments were performed in four different fly strains expressing pan-neuronal calcium activity indicators— red eye, wild type photoreceptors and GCaMP6f (bordeaux); red eye, Rh1 only and GCaMP6f (red); orange eye, Rh1 only and GCaMP6f (orange) and red eye, wild type photoreceptors and RGECO (grey). (A) Slope values extracted from intensity-response relationship curves for three different bands of monochromatic light (UV, blue and green; centre wavelengths 390, 460 and 565 nm respectively) for GCaMP-expressing fly strains. (B) Slope (i) and half maximum (ii) values extracted as in (A) comparing responses in red eye/wild type photoreceptors flies expressing either GCaMP6f or RGECO. Individual data points correspond to the average of ROI responses across a given layer structure (see methods) for a given fly preparation. The curves in (A) are a mean of the fitted curves of individual data points. Black line = mean, inner grey box = SEM, outer grey box = SD. Significant differences are noted with star values, with the *P* values from top to bottom: ****P* = 0.0005 and **P* = 0.0415 (one-way ANOVA).

4.3.3 Inter-layer variability of intensity-response curve coefficients

Next, I chose to investigate how intensity-response curve properties might vary across the different layer groupings of the medulla. Pan neuronal labelling of the medulla reveals clearly discernible and identifiable layer structures ([Figure 4.3](#)) allowing us to delve into layer-specific responses for the intensity-response relationships and spectral response curves as above ([Figures 4.10](#) and [Figure 4.11](#)). In bees, medullary neurons exhibit increasing complexity in their colour responses from the first layers, proximal to the eye, to the later layers, proximal to the brain (Paulk *et al.*, 2009). I thus predicted that layers of the medulla in *Drosophila* would also display variations in their spectral responses. A bias towards UV light might be expected in M6 where R7 cells project, whereas responses to blue or green light would be expected at the termination of R8 photoreceptors in M3. Neurons that arborize in both layers might exhibit responses tuned to both R7 and R8 spectral sensitivities, or a different response derived from the combination of R7 and R8 inputs.

My results demonstrate that half maximum values for UV, blue and green light exhibit layer-specific variability between fly strains ([Figure 4.10](#)). Although most layer groupings retain the higher sensitivity of orange-eye flies to green light, this difference disappears in layers M2 and layers M6-M7. The decreased sensitivity of orange-eye/Rh1-rescue

flies relative to the red eye/wildtype photoreceptor flies in the UV-blue range of the spectral response curve (Figure 4.7) is only apparent in layers M6-M7 and M9-M10. Strikingly, the red eye/Rh1-rescue flies exhibit increased sensitivity to UV, blue and green light in M2, but this increased sensitivity does not occur in the orange eye/Rh1 rescue flies. We also see this trend in layer M3, and we attribute the absence of statistical significance to the lower number of ROIs with successfully fitted intensity-response curves as response size is smaller than other layers.

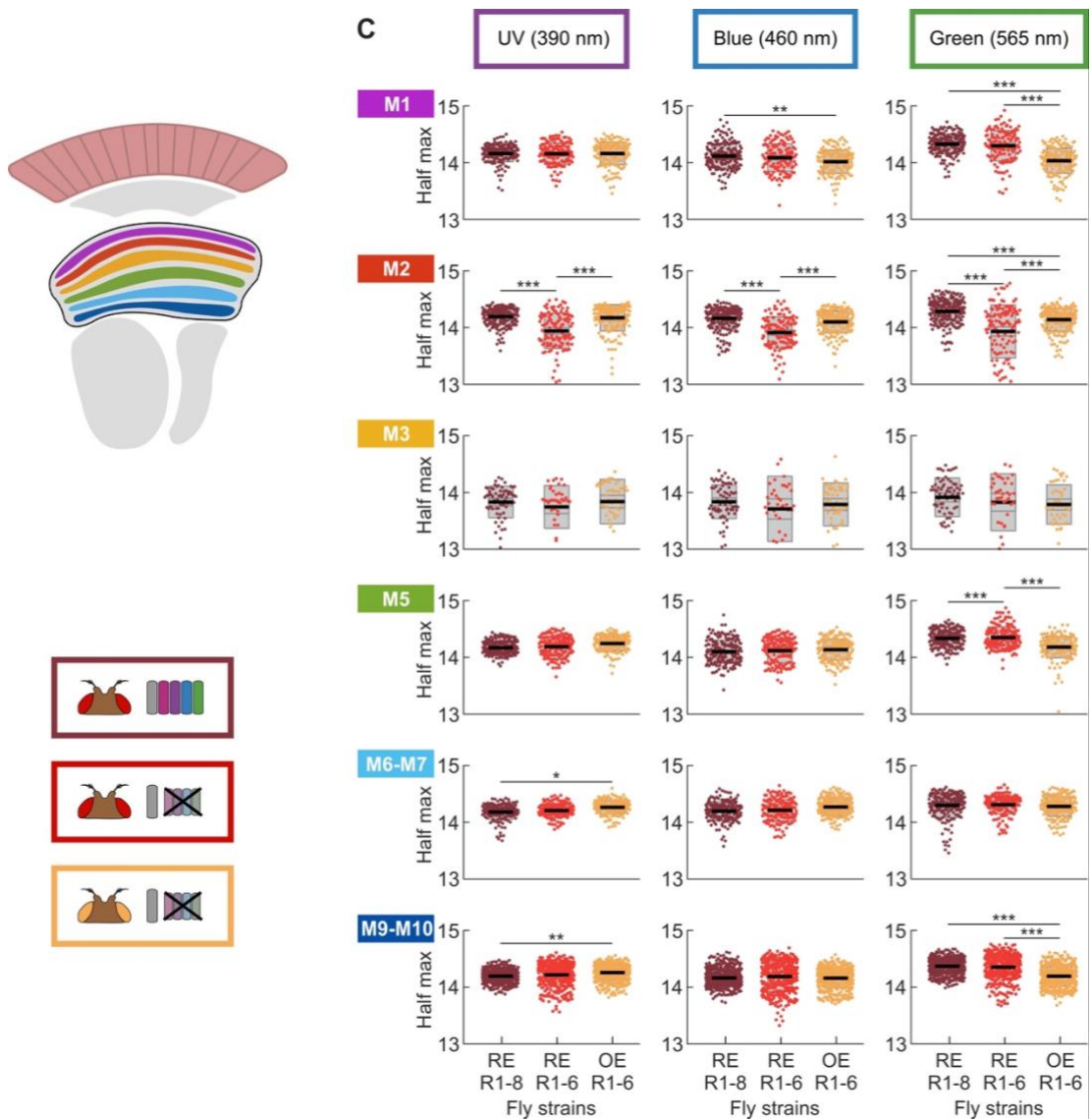


Figure 4.10 Intensity-response curve half maximum values across individual layers.

Half maximum values extracted from intensity-response curves fitted to individual ROIs and plotted for discrete layer structures for three different bands of monochromatic light UV, blue and green (centre wavelengths 390, 460 and 565 nm respectively) for three different fly strains- red eye, wildtype photoreceptors and GCaMP6f (bordeaux); red eye, wildtype photoreceptors and RGECO (grey); red eye, Rh1 only and GCaMP6f (red) and orange eye, Rh1 only and GCaMP6f (orange). Black, solid lines represent the mean value. From the mean outwards, the first grey line of the background box shows the 95% confidence interval (or 1.96 standard error of the mean) and the second grey line represents 1 standard deviation from the mean. 1-way ANOVA p-values are reported in Appendix 1, table A2.

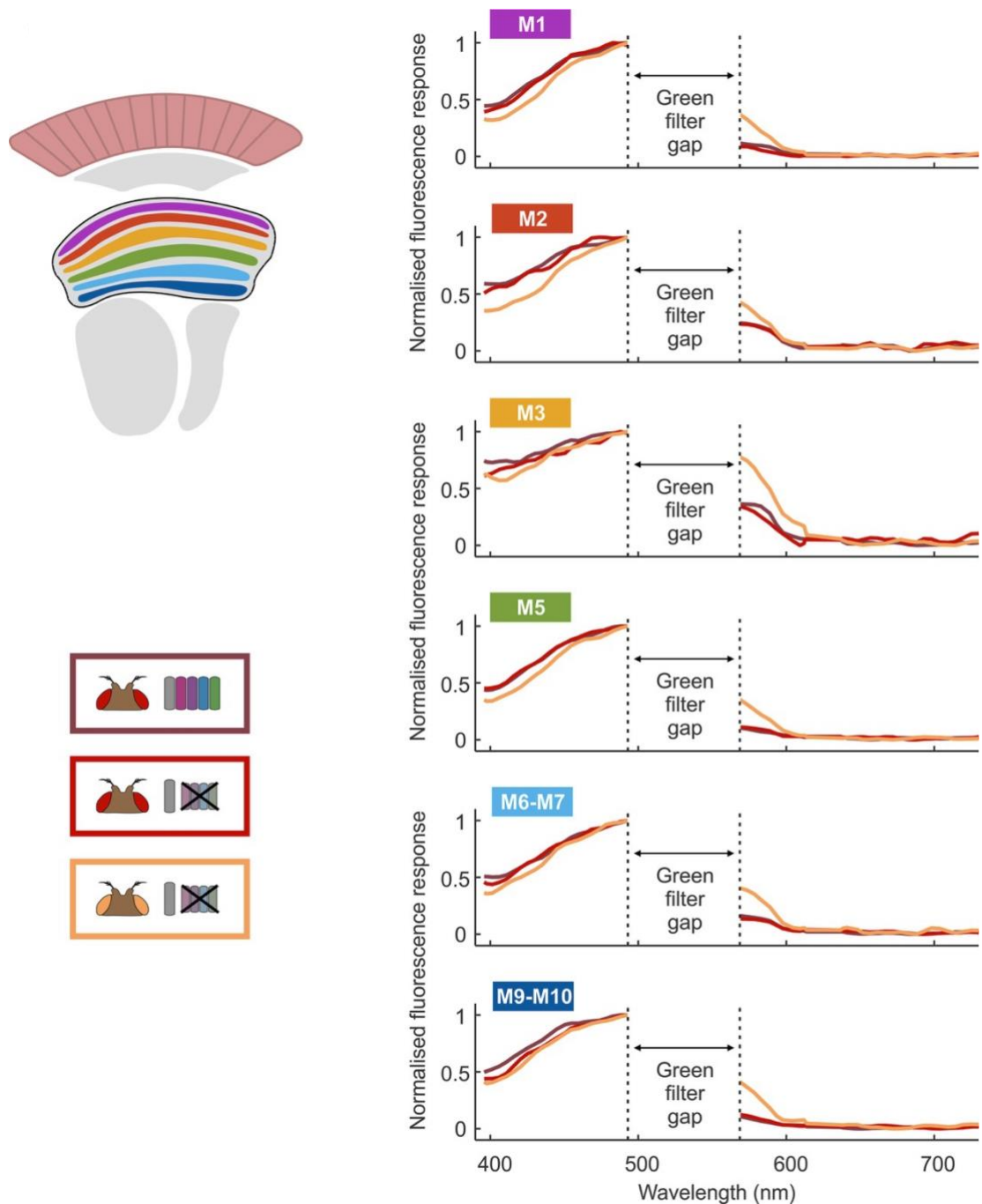


Figure 4.11 Spectral response profiles of layer groupings in the medulla

Normalised spectral response profiles, determined by a sweep of equal intensity light pulses across the spectrum, are plotted for discreet layer structures for three different fly strains: red eye, wildtype photoreceptors and GCaMP6f (bordeaux); red eye, Rh1 only and GCaMP6f (red) and orange eye, Rh1 only and GCaMP6f (orange).

4.4 DISCUSSION

My experimental setup enabled us to record the responses to a range of narrow bands of light across the spectrum, over a range of intensities spanning several log units of light, thus establishing intensity-response relationship and spectral profiles in the medulla. The pan-neuronal labelling of medulla neurons with neuronal activity indicators allowed for an investigation of response properties across all cells simultaneously. Despite the absence of cell-specific responses, I was able to generate a map of spectral responses across medulla layers. In addition, by using two reporters, GCaMP6f and RGECO, with different emission spectra detected by alternate PMT detectors, the issue of a gap in the visual stimulation spectrum could be overcome. I find that visual responses extracted from the summed activity of neurons in specific layer structures of the medulla exhibit stereotyped temporal response profiles within a layer structure which vary from one layer grouping to another. Furthermore, I find several modifications of spectral response properties in the summed activity of the pan-neuronally labelled neuropil between transgenic fly strains, demonstrating the precision, reliability and sensitivity of our setup. Finally, I found that lower screening pigment density biases the medullary responses in favour of longer wavelengths of light.

4.4.1 Inner photoreceptor-driven responses

Assessment of inter-layer variability revealed a diversity of responses. Most intriguing is the increased sensitivity of layers M2 and M3 in red eye flies that have lost R7 and R8 function, suggestive of inhibitory control of postsynaptic neurons in wild type flies by the R8 cells that terminate in M3 (Takemura *et al.*, 2008). Several reasons may explain why orange eye flies lacking functional photoreceptors do not also exhibit increased sensitivity in M2 and M3. Flies homozygous for the white null allele 1118 are known to have retinal degeneration (Ferreiro *et al.*, 2017) and this may not be rescued with the mini-white vector expression. This effect could also be attributed to prolonged depolarisation afterpotential (PDA, Wright and Cosens, 1977), more common in white-eye flies (Belušič, 2011) where the temporary light insensitivity of the photoreceptor requires red to shift metarhodopsin back to rhodopsin. This could also explain the decreased responsiveness to short wavelengths observed in the spectral response profile of this strain. The decreased sensitivity in the orange-eye flies to UV light in layers M6-M7 could be attributable to the lack of input from UV-sensitive R7 photoreceptors that project to this layer (Takemura *et al.*, 2008; Takemura *et al.*, 2013). It is less clear,

however, why these flies lose their increased sensitivity to green light uniquely in this layer structure. If the shift in response properties is caused by the photoreceptor terminals, green light should inhibit R7 activity (Schnaitmann *et al.*, 2018), resulting in decreased sensitivity in the red-eye flies expressing all functional opsins while maintaining unaffected high sensitivity in the orange-eye strain. Our data appears to suggest layer-specific shifts in spectral response properties in the medulla corresponding to projection regions of photoreceptor terminals. We did not detect summation of R7-R8 with R1-R6 signals proposed to drive lobular plate responses reported previously (Wardill *et al.*, 2012) as we found no difference between wild type and Rh1-only red-eye flies in most layers, however further investigation is required to establish this with certainty.

In this initial attempt to reveal clues as to the mechanism of spectral signals in the medulla, we uncovered some interlayer variability of spectral response profiles. The specifics of a neural circuit underlying the processing of colour information, however, remains elusive at this stage. A more targeted approach would likely prove more fruitful, but such a method requires pre-existing knowledge of candidate cells for the colour vision circuitry. As discussed in the introductory chapter, such candidate neurons have been identified through behavioural experiments combined with selective ablation of cells via a genetic approach. These include Tm5a, b and c, Tm20, Tm9 and Dm8, however ablation of any of these cells individually does not impede colour learning and discrimination tasks (Gao *et al.*, 2008; Karuppururai *et al.*, 2014; Melnattur *et al.*, 2014). Establishing spectral response properties for these neurons would be an excellent first step towards understanding the functional circuitry. It would also be interesting to consider whether characterised neurons from the motion vision pathway exhibit a spectral bias. Motion visual responses are classically probed with blue light, primarily as this corresponds to the peak range of Rh1 sensitivity, but also to bypass the technical issue of detection of the visual stimulus by the microscope. With our setup, we no longer encounter this problem. In light of the study by Wardill *et al.* (2012) suggesting the pooling of spectral information from R7-R8 cells into R1-6 cells, it would be interesting to verify whether individual cells within the motion circuitry are in fact all driven only by Rh1-expressing photoreceptors, or whether they receive any contribution from the 'colour' photoreceptors.

4.4.2 Unreported trials of alternative mutant strains

Of note, a number of genetic variants other than the fly strains reported above have been trialled with little success. We originally aimed to dissect the contribution of R7 and R8 photoreceptors with a fly expressing Rh3-Rh6 in relevant photoreceptors but not Rh1, thus creating a mutant with loss-of-function outer photoreceptors. I was faced, however, with the unexpected complication of not being able to locate any visual responses in the medulla of these flies. I assumed that the visual responses arising from inner photoreceptors might be too small to detect by eye, so I next trialled a fly strain where Rh1 photoreceptors expressed Rh3 instead. In this way, the outer photoreceptors retained their functionality, but their spectral sensitivity was no longer broadband thus removing the extensive overlap with inner photoreceptors. Instead, the far-UV Rh3 spectral sensitivity could be used to locate the strong R1-R6 driven response thus establishing the correct imaging location within the medulla. This endeavour, however, proved no more successful than the latter and I was still unable to detect any responses originating from Rh5- and Rh6-expressing photoreceptors. This raises several possible interpretations. It is highly likely that the pan-neuronal labelling causes 'colour' responses to be masked, either by stronger Rh1-driven signals (this theoretically account for 75% of the visual input to the medulla) or simply by the permanently present baseline fluorescence that could make it harder to detect subtle changes in small, sparse dendrites. It is not clear what proportion of cells in the medulla might be dedicated to the colour circuitry, nor if much colour processing occurs in this neuropil at all. Furthermore, it has become apparent that the classic Gal4/UAS system can cause significant abnormalities in cell function. This has been demonstrated, for example, in *Drosophila* photoreceptors where the GMR-Gal4 driver is used to express GCaMP6f as severe modifications to structure and physiology are observed (Asteriti *et al.*, 2017). The authors of this study also expose a near 7-fold increase in the maximum $\Delta F/F_0$ change in the cells of flies that use a fused promoter to express GCaMP6f instead of the Gal4/UAS system. Needless to say, it is highly probable that the Gal4/UAS system used to create the fly lines in this study are also affected in this way. What this means for our findings is not clear cut, however it is interesting to consider that not all medulla cells are functioning optimally under these conditions. In an attempt to assess the impact of Gal4 driven promoters on the visual responses we recorded, my colleague Jorge created a new fly line where the pan-neuronal promoter *nSyb* was directly fused to GCaMP. Interestingly, not only did cells in the medulla of these flies exhibited surprisingly low baseline fluorescence, but visual responses were also largely reduced and barely

detectable by eye, probably due to low GCaMP expression. Consequently, I was not able to include any of the strains described above in the results section of this chapter.

4.4.3 The effect of screening pigment on spectral processing

In agreement with previous studies, we find that a modification in the density of screening pigment in the fly's eye causes a shift in the spectral response properties of cells in the visual system. This is the first study to assess such responses in a visual neuropil, with previous investigations measuring this effect at the level of photoreceptor cells in the fly retina. The most prominent shift observed with a decrease in screening pigment density is the increased sensitivity to longer wavelengths of light in medulla neurons, depicted by lower half maximum values in the intensity-response relationship matched by the spectral response curves. Furthermore, we observe an increase, although non-significant, in the slope of the intensity-response curve of flies with lower screening pigment density. These results are consistent with reports from electroretinogram data (Goldsmith, 1965; Stark and Wasserman, 1972; Stark and Wasserman, 1974). Stark and Wasserman's 1974 paper, in particular, compares ERG responses from white-eye and red-eye flies and their findings support ours. Goldsmith's (1965) recruitment process hypothesis stipulates that absorption of light by screening pigment located in cells surrounding the photoreceptors of an ommatidium decreases any light contribution from neighbouring photoreceptors to the visual response in that ommatidium. In other words, the screening pigment serves to shield photoreceptors sharing ommatidium facets thus ensuring that only on-axis light reaches the photoreceptor cells. It follows that the degree of efficiency of this process is directly related to the density of the screening pigment present in the pigment cells. Furthermore, it has been shown that the acceptance angle of a photoreceptor cell, defined as the half-width of the Gaussian approximation to the angular sensitivity characteristic, is larger for long wavelengths of light than it is for short wavelengths. A study by Streck (1972) demonstrates that in blowflies, the acceptance angle of a photoreceptor increases from 2.8 degrees measured at 360 and 495 nm to 4 degrees, measured at 625 nm. Although not of direct relevance here, Streck's study confirms the importance of screening pigment for spatial acuity, but more importantly, it underlines the fact that visual response properties are altered in the red portion of the spectrum as the screening pigment does not absorb these wavelengths so efficiently. Thus, we understand the increased sensitivity of orange-eye flies to longer wavelengths to derive from the decrease in screening pigment density coupled to the intrinsic

properties of the pigment favouring the reflectance of wavelengths in the red portion of the spectrum.

The red-eye phenotype in *Drosophila* has adapted as a way to optimise the reconversion of metarhodopsin back to the native rhodopsin: long-wavelength light is necessary for this process to occur and the reflectance of red by the screening pigments increases the amount of red light available for the task (Stavenga *et al.*, 2017). It is interesting to consider the overall shift in the shape of the spectral response curve for orange-eye flies which exhibit a lowered short-wavelength sensitivity and an increased long-wavelength sensitivity compared to red-eye flies. This shift is most striking when comparing the relationship between intensity-response half maximum values for the UV, blue and green portions of the spectrum. The implications of this finding are minimal when considering Rh1-driven visual processing: although we do observe a modification in the spectral content of light visual cells respond to, with longer wavelength light now playing a more important role, the more significant impact will occur in the case of visual processing involving photoreceptor output comparisons. Indeed, if a colour vision system based on chromatic opponency does exist in *Drosophila*, already partially confirmed by Schnaitmann *et al.* (2018), the evolutionary considerations of screening pigment colour and density are remarkable. The chromatic opponency system in vertebrates relies on the precise relative excitation ratios from all three cones to form a specific colour percept distinguishable from an infinite other possible colour percepts. Here, we have demonstrated that variations in screening pigment significantly affects spectral response properties of visual cells – does this imply that dipterans with varying eye colours (black, red or other) have undergone an individual adaptation process to optimise their colour processing visual system?

Orange-eye flies show a more pronounced inter-layer variability of their intensity-response half maximum values for blue and green light than red-eye strains. If sensitivity of individual photoreceptors is boosted by the bleed through of stray light from neighbouring ommatidia, the limited portion of the visual field covered by the stimulus is likely to affect these flies more than their red counterparts. Indeed, light sampled by an ommatidium at the edge of the circular patch of light will only receive stray light input from the neighbouring ommatidia within range of the visual stimulus, but not those ommatidia sampling the dark periphery of the stimulus. In summary, the wider acceptance angle of a given ommatidium resulting from the decreased pigment density

could be causing the high inter-layer variability observed. Prior investigations have reported enlarged receptor potential in *white null* mutant, i.e. lower screening pigment density flies (Belušič, 2011, Ferreiro *et al.*, 2017). The nature of the calcium activity indicators makes it difficult to establish this in our own dataset as a direct comparison of individual responses is not an accessible option. The fluorescent response extracted from our recordings is dependent on a number of parameters including levels of expression of the indicator and laser power applied to the fly preparation. Recorded response data must be normalised to the minimum and maximum of the intensity-response and spectral response curves respectively in order to scale individual responses to produce comparable entities from one ROI to another within and between fly preparations. Consequently, absolute response sizes are not comparable.

Of note, Autrum and Stumpf (1953) reported an unexpected peak in the red portion of the spectrum when measuring blowfly electroretinograms. They attributed this peak to a red-sensitive photoreceptor class but it was later demonstrated (in the housefly) to arise from the increased transparency of screening pigment in those wavelengths by Goldsmith (1965). We see no such peak in our data, either in red- or orange-eye flies, however this could be due to the small number of ommatidia that receive input from the visual stimulus. Goldsmith (1965) suggests that variations in the numbers of photoreceptors stimulated occur for different experimental paradigms. If an extensive group of ommatidia in the fly's eye are receptive to a full-field red light stimulus, widespread leakage of long-wavelength light through the screening pigment causes a response in the red. If, however, visual stimulation is localised to a specific portion of the eye, as with our paradigm, this peak in sensitivity is significantly reduced.

4.4.4 Genetically encoded calcium activity indicators

Finally, this study reveals some interesting insights into performance variability between different calcium activity indicators. We find here some discrepancies between flies varying only in their expression of either GCaMP or RGECHO. Whereas the GCaMP recordings in this chapter exhibit signal-to-noise ratios and response sizes spread across an extensive range, these same measurements for RGECHO are consistently clustered in the lower portion of this range. It is well established that red shifted indicators underperform in comparison to their green counterparts (Dana *et al.*, 2016). Our data

reveals a discrepancy in slope values of intensity-response relationships for both indicators, GCaMP and RGECO, but not for half maximum values. Slope measurements from the Naka-Rushton fit are challenging to interpret in the context of visual function. In *Drosophila* ERG's, it is used to describe the dynamic working range of a photoreceptor cell (Belušič, 2011). It is entirely plausible, however, that the kinetics of the calcium activity indicators also affect the response measured in medulla neurons, and thus the slope of the intensity-response curve. Differences in calcium affinity exist between indicators which affect rise and decay kinetics of the fluorescence. A slower rise of the fluorescence leads to a smaller measured response from the area under the curve of the fluorescent trace. As we see comparable half maximum responses for both GCaMP and RGECO, it seems that the responses elicited by an identical pulse of light are, in fact, very similar for both indicators. Caution must be applied to the comparison of slope values where variability is attributable to indicator kinetics, however spectral sweep measurements were conducted at the mid-range of the intensity-response curve, and are consequently unlikely to be affected by the small shift in slope values. In conclusion, switching between neural activity indicators with different emission spectra detected by alternate PMT detectors to overcome the gap in the spectrum corresponding to each PMT's detection range is a useful and sound strategy.

4.5 REFERENCES

- Asteriti, S., C. H. Liu and R. C. Hardie (2017). "Calcium signalling in *Drosophila* photoreceptors measured with GCaMP6f." *Cell Calcium* 65: 40-51.
- Autrum, H. (1953). "[Electrobiology of the eye]." *Klin Wochenschr* 31(9-10): 241-245.
- Autrum, H. and H. Stumpf (1953). "Elektrophysiologische Untersuchungen über das Farbensehen von *Calliphora*". *Zeitschrift für Vergleichende Physiologie* 35(1-2): 71-104.
- Belusic, G. (2011). "ERG in *Drosophila*, Electoretinograms" (Ed.), ISBN: 978-953-307-383-5
- Brand, A.H., and N. Perrimon (1993). "Targeted gene expression as a means of altering cell fates and generating dominant phenotypes". *Development* 118, 401-415.
- Chen, T. W., T. J. Wardill, Y. Sun, S. R. Pulver, S. L. Renninger, A. Baohan, E. R. Schreiter, R. A. Kerr, M. B. Orger, V. Jayaraman, L. L. Looger, K. Svoboda and D. S. Kim (2013). "Ultrasensitive fluorescent proteins for imaging neuronal activity." *Nature* 499(7458): 295-300.
- Dana, H., B. Mohar, Y. Sun, S. Narayan, A. Gordus, J. P. Hasseman, G. Tsegaye, G. T. Holt, A. Hu, D. Walpita, R. Patel, J. J. Macklin, C. I. Bargmann, M. B. Ahrens, E. R. Schreiter, V. Jayaraman, L. L. Looger, K. Svoboda and D. S. Kim (2016). "Sensitive red protein calcium indicators for imaging neural activity." *Elife* 5.
- Evans, L. S., N. S. Peachey and A. L. Marchese (1993). "Comparison of three methods of estimating the parameters of the Naka-Rushton equation." *Doc Ophthalmol* 84(1): 19-30.
- Gao, S., S. Y. Takemura, C. Y. Ting, S. Huang, Z. Lu, H. Luan, J. Rister, A. S. Thum, M. Yang, S. T. Hong, J. W. Wang, W. F. Odenwald, B. H. White, I. A. Meinertzhagen and C. H. Lee (2008). "The neural substrate of spectral preference in *Drosophila*." *Neuron* 60(2): 328-342.
- Goldsmith, T. H. (1965). "Do Flies Have A Red Receptor?" *J Gen Physiol* 49(2): 265-287.
- Gollisch, T. and M. Meister (2010). "Eye smarter than scientists believed: neural computations in circuits of the retina." *Neuron* 65(2): 150-164.
- Joesch, M., B. Schnell, S. V. Raghu, D. F. Reiff and A. Borst (2010). "ON and OFF pathways in *Drosophila* motion vision". *Nature* 468(7321):300-4.

- Kaiser, W. (1968). "Towards the Question of the Ability to Distinguish Spectral Colours: An Investigation of an Optomotor Response in the Flesh Fly, *Phormia regina* MEIG." *J Comp Physiol* 61:71–102.
- Kaiser, W. and E. Liske (1974). "Optomotor Reactions of Stationary Flying Bees during Stimulation with Spectral Lights." *J Comp Physiol* 89:391–408.
- Karuppudurai, T., T. Y. Lin, C. Y. Ting, R. Pursley, K. V. Melnattur, F. Diao, B. H. White, L. J. Macpherson, M. Gallio, T. Pohida and C. H. Lee (2014). "A hard-wired glutamatergic circuit pools and relays UV signals to mediate spectral preference in *Drosophila*." *Neuron* 81(3): 603-615.
- McCulloch, K. J., D. Osorio and A. D. Briscoe (2016). "Determination of Photoreceptor Cell Spectral Sensitivity in an Insect Model from In Vivo Intracellular Recordings." *J Vis Exp*(108): 53829.
- Melnattur, K. V., R. Pursley, T. Y. Lin, C. Y. Ting, P. D. Smith, T. Pohida and C. H. Lee (2014). "Multiple redundant medulla projection neurons mediate color vision in *Drosophila*." *J Neurogenet* 28(3-4): 374-388.
- Naka, K. I. and W. A. Rushton (1966). "An attempt to analyse colour reception by electrophysiology." *J Physiol* 185(3): 556-586.
- Nishida, S., J. Watanabe, I. Kuriki and T. Tokimoto (2007). "Human visual system integrates color signals along a motion trajectory." *Curr Biol* 17(4): 366-372.
- Paulk, A. C., A. M. Dacks and W. Gronenberg (2009). "Color processing in the medulla of the bumblebee (*Apidae*: *Bombus impatiens*)." *J Comp Neural*, 13(5):441-56.
- Rister, J., D. Pauls, B. Schnell, C. Y. Ting, C. H. Lee, I. Sinakevitch, J. Morante, N. J. Strausfeld, K. Ito, M., Heisenberg (2007). "Dissection of the peripheral motion channel in the visual system of *Drosophila melanogaster*". *Neuron* 56(1):155-70.
- Salcedo, E., A. Huber, S. Henrich, L. V. Chadwell, W. H. Chou, R. Paulsen and S. G. Britt (1999). "Blue- and green-absorbing visual pigments of *Drosophila*: ectopic expression and physiological characterization of the R8 photoreceptor cell-specific Rh5 and Rh6 rhodopsins." *J Neurosci* 19(24): 10716-10726.
- Schnaitmann, C., V. Haikala, E. Abraham, V. Oberhauser, T. Thestrup, O. Griesbeck and D. F. Reiff (2018). "Color Processing in the Early Visual System of *Drosophila*." *Cell* 172(1-2): 318-330.e318.
- Stark, W. S. and G. S. Wasserman (1972). "Transient and receptor potentials in the electroretinogram of *Drosophila*." *Vision Res* 12(10): 1771-1775.
- Stark, W. S. and G. S. Wasserman (1974). Wavelength-specific ERG Characteristics

- of Pigmented- and White-eyed Strains of *Drosophila*.
- Stavenga, D. G. (2002). "Colour in the eyes of insects." *J Comp Physiol A* 188:337-348
- Stavenga, D. G. (2010). "On visual pigment templates and the spectral shape of invertebrate rhodopsins and metarhodopsins." *J Comp Physiol A Neuroethol Sens Neural Behav Physiol* 196(11): 869-878.
- Stavenga, D. G., M. F. Wehling and G. Belušič (2017). "Functional interplay of visual, sensitizing and screening pigments in the eyes of *Drosophila* and other red-eyed dipteran flies." *J Physiol* 595(16): 5481-5494.
- Streck, P. (1972). Der Einfluss des Schirmpigmentes auf das Sehfeld einzelner Sehzellen der Fliege *Calliphora erythrocephala* Meig. *Z. Verg. Physiol.* 76, 372-402.
- Takemura, S. Y., Z. Lu and I. A. Meinertzhagen (2008). "Synaptic circuits of the *Drosophila* optic lobe: the input terminals to the medulla." *J Comp Neurol* 509(5): 493-513.
- Takemura, S. Y., A. Bharioke, Z. Lu, A. Nern, S. Vitaladevuni, P. K. Rivlin, W. T. Katz, D. J. Olbris, S. M. Plaza, P. Winston, T. Zhao, J. A. Horne, R. D. Fetter, S. Takemura, K. Blazek, L. A. Chang, O. Ogundeyi, M. A. Saunders, V. Shapiro, C. Sigmund, G. M. Rubin, L. K. Scheffer, I. A. Meinertzhagen and D. B. Chklovskii (2013). "A visual motion detection circuit suggested by *Drosophila* connectomics." *Nature* 500(7461): 175-181.
- Takeuchi, T., K. K. De Valois and J. L. Hardy (2003). "The influence of color on the perception of luminance motion." *Vision Res* 43(10): 1159-1175.
- Wardill, T. J., O. List, X. Li, S. Dongre, M. McCulloch, C. Y. Ting, C. J. O'Kane, S. Tang, C. H. Lee, R. C. Hardie and M. Juusola (2012). "Multiple spectral inputs improve motion discrimination in the *Drosophila* visual system." *Science* 336(6083): 925-931.
- Wright, R. and D. Cosens (1977). "Blue-adaptation and Orange-adaptation in white-eyed *Drosophila*: Evidence that the prolonged afterpotential is correlated with the amount of M580 in R1-6". *J Comp Physiol* 113:105–127
- Yamaguchi, S., R. Wolf, C. Desplan and M. Heisenberg (2008). "Motion vision is independent of color in *Drosophila*." *Proc Natl Acad Sci U S A* 105(12): 4910-4915.

Chapter 5 – Receptive Field Mapping in the *Drosophila Medulla*

5.1 INTRODUCTION

5.1.1 Why study receptive fields?

The term ‘receptive field’ was coined by Sherrington (1906) over a century ago. A receptive field corresponds to a portion of sensory space that can elicit neuronal responses when stimulated, and exist for all sensory modalities (e.g. visual, somatosensory, auditory or olfactory receptive fields). Studies exploring the characteristics of visual receptive fields do not appear in the literature until the 1940s when Hartline (1940) found that an isolated optic nerve fibre in the frog could be excited by light falling on a small circular area of the retina. The antagonist centre-surround organisation of receptive fields in cats was described by Barlow *et al.* (1957), followed by the iconic paper the iconic paper ‘What the frog's eye tells the frog's brain’ was published by Lettvin *et al.* (1959). A few years later, Hubel and Wiesel’s (1962) published a depiction of simple and complex cells in the primate visual system. Kuffler (1973) argues that delineating receptive field properties provides an excellent methodology to understand the functional organisation of the brain: the activity of individual neurons along the visual pathway reflect the progressive refinement of visual information. Thus, the evolution of receptive fields throughout the neural circuitry underpinning visual processing can provide information about how the visual world is being computed and processed. A neuron’s receptive field can be described by two primary characteristics, its spatial component that describes the area of the visual field in which the presentation of a stimulus elicits a change in that cell’s activity, and its temporal component that constitutes the neuron’s response to a given stimulus over the duration of the stimulus presentation. Prior studies have demonstrated how both of these components provide key insights into visual processing mechanisms (Berry *et al.*, 1999; Sher and Devries, 2012), and that a combined spatiotemporal filter is essential to motion vision (Adelson and Bergen, 1985).

5.1.2 Receptive fields of medulla cells

Reports of functional receptive fields in the *Drosophila* medulla are rare. Nonetheless, anatomical studies offer some insight into connectivity properties in the early visual system, from which receptive field properties can be conjectured. The medulla is organised into columnar units, known as cartridges, which receive direct input from the inner photoreceptors and indirect input from the outer photoreceptors via relay laminar neurons. Developmental studies suggest that synaptic connections from all photoreceptors are confined to their respective columns, however neurons with dendrites spanning multiple cartridges, thus interconnecting columns, exist in the medulla (reviewed by Melnattur and Lee, 2011). Accordingly, we can expect receptive field sizes to fall anywhere between the acceptance angle of the photoreceptors, estimated at 5°-8° of visual field (Fischbach and Dittrich, 1989; Gonzalez-Bellido *et al.*, 2011), up to much larger portions of visual space. A connectivity study by Takemura *et al.* (2013) suggests that the medullary cells Mi1 and Tm3, that supposedly make up the two channels of the ON component of the elementary motion detector, retain their cartridge confinement until they project unto T4 cells, the direction-selective ON motion cells, where their receptive fields exhibit some overlap. The size of spatial receptive fields for Mi1 and Tm3 as well as for Mi4 and Mi9, two other neurons providing input to T4 cells, have been roughly gauged by assessing their responses to a small 5° spot of light versus a much wider 30° spot. Mi4 and Mi9 cells exhibit much bigger responses to the smaller disc over the larger one, suggestive of a receptive field comprising a strong inhibitory surround (Strother *et al.*, 2017). In contrast, Mi1 and Tm3 neurons appeared to respond to the different stimulus sizes equally well, thus probably have small receptive fields with no antagonistic structure properties (Strother *et al.*, 2017). The primary focus of work pertaining to medullary visual processing is motion vision, however some investigations have also centred around motion-independent feature detection. Neurons downstream of the medulla in the lobula retain retinotopy in their dendrites but also display the ability to show robust responses to small 2.2° objects (Keles and Frye, 2011). Further receptive field properties of medulla cells remain to be elucidated.

5.1.3 Project aims

Here we aim to address this deficit by mapping receptive fields from regions of interest across the medulla in a fly where the calcium indicator GCaMP6f is pan-neuronally labelled. We chose to use a novel method developed by Johnston *et al.* (2014) which

uses a filtered back projection algorithm akin to computed tomography (CT). Projected bars of light serve to reconstruct the neural response in the same way that parallel beams of radiation are used to reconstruct the density of an object in CT. This technique boasts several advantages, such as rapid mapping of receptive fields, but also delineation of spatial and temporal properties, and receptive field substructure information including tuning of orientation selective neurons and ON/OFF components. We present here these receptive field properties across different layers of the medulla.

5.2 METHODS

5.2.1 Fly stocks

Experiments were conducted on *w[+]; UAS-GCaMP6f/+; 39171-Gal4/+* flies, which express the fluorescent calcium indicator GCaMP6f (Chen *et al.*, 2013) in all neurons of the optic lobes using the GAL4/UAS expression systems (Brand and Perrimon, 1993) and the pan-neuronal promoter *nSyb* (Bloomington Stock Center, 39171). Flies were aged 6-7 days in the following experiments ($n = 10$). Fly care was carried out as detailed in the methodology chapter (Chapter 2, section 2.1).

5.2.2 Two-photon imaging

Two-photon imaging was carried out as described in the methodology chapter (section 2.3). Images were acquired using the green channel (GaAsP detector 1) as flies expressed the green calcium activity indicator: GCaMP. A 200X zoom (20X on the objective and 10X on the software) was used to visualise the fly medulla. This allowed me to image all layers of the neuropil from proximal to distal across a number of cartridges (ranging from a half a dozen to a dozen in different experiments, 0.104 to 0.115 $\mu\text{m}/\text{pixel}$ with a field of view of 53 to 59 μm). The response of medullary neurons, not photoreceptors, are measured in this study.

5.2.3 Visual stimulation

The combined monochromator-screen stimulation setup described in previous chapters was used for the following experiments. In contrast to the full-field light stimulation

applied in the previous chapter, the stimuli used for the following study exploits the combined high precision spatial and spectral properties of the screen to investigate receptive field properties. In a trade-off between increased visual field coverage and perfect spectral constancy, I deemed the former more important. Thus, the visual stimulus was not restricted to the central portion of the screen as described in the previous chapter, but instead covered the totality of the available surface.

Receptive field mapping stimulus protocol

The stimulus protocol I used to probe receptive fields follows a method depicted by Johnston *et al.* (2014). This approach uses similar visual parameters as classic receptive field mapping, with long bars (covering the entire width of the screen) of varying orientations flashing across the visual field (**Figure 5.1 A**). Bars were presented for a duration of 500 ms interspersed with a 1 second period of darkness. Following trials for different bar sizes, I elected to use 30-pixel wide bars corresponding to approximately 3 degrees of visual field as this bar size provided me with good visual responses combined with maximal spatial resolution. The 26 non-overlapping 30-pixels bars covered a 780-pixel range and were presented in a pseudorandomized order such that two bars were never presented sequentially in neighbouring locations. This stimulus set was repeated for six different, equally-spaced orientations of 30-degree increments (**Figure 5.1 B**). This creates a circular portion of the screen covered by all presented bars. The 551.5 x 551.5-pixel square (corresponding to 53.3 x 53.3 degrees of visual field) inscribed in this circle (**Figure 5.1 C**) is the resulting output of the spatial response mapping (see analysis section for further details).

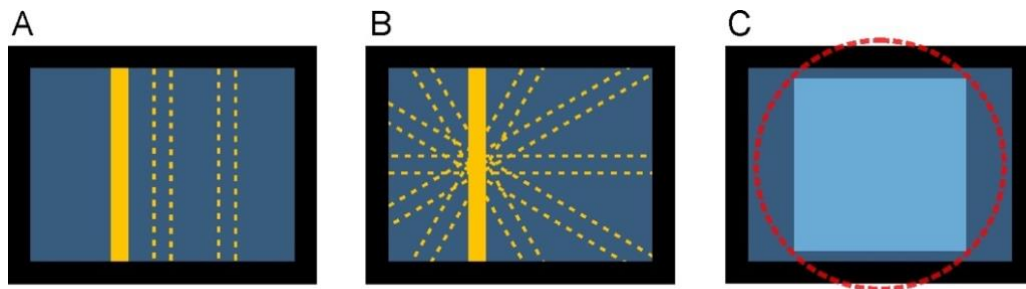


Figure 5.1 Receptive field mapping stimulus protocol.

(A) The stimulus protocol for receptive field mapping consisted of non-overlapping flashing bars covering 3 degrees of visual field presented sequentially in a pseudorandom order. (B) This flashing bar sequence is repeated at six different orientations. (C) The scope of the visual stimuli that are used by the algorithm for spatial reconstruction is delineated by the red circle. The output consists of a spatial map of visual responses corresponding to the blue square inscribed in the circle. This methodology is adapted after Johnston et al. (2014).

I chose a radiance of 3.3×10^{13} photons/s/cm² for the bar presented as 460 nm centre wavelength light, based on the intensity-response relationship established for cells in the medulla in the previous chapter. The light intensity of the bar was measured by placing the end of the spectrometer fibre in the tilting holder to establish the radiance of the bar but also the unlit portion of the screen adjoining the bar (Figure 5.2 A). This ensured that the intensity of the bar was sufficient to elicit a physiological response without saturating the photoreceptors, but also confirmed that any light scattering from the projected bar stimulus was minimal and below visual detection levels (Figure 5.2 B).

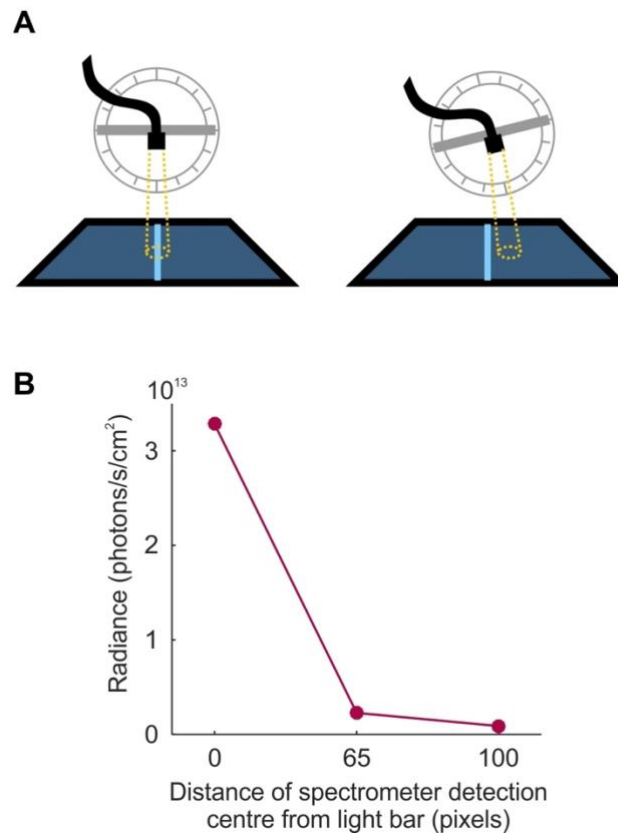


Figure 5.2 Visual stimulus radiance.

(A) Placing the spectrometer fibre in a tilting holder enables accurate measurements of the light reaching the fly's eye while allowing for measurements to be made at specific screen locations. (B) This methodology was used to ensure the radiance of the light bar was sufficient to elicit a visual response but not high enough to create physiologically detectable scattered light on the adjacent dark screen (data points average five measurements and standard deviations are too small to be shown). The 65-pixel distance was chosen as Figure 3.5 specifies that the screen detection area of the spectrometer is approximately 60 pixels in diameter.

5.2.4 Analysis

Fly preparation selection

In order to ensure maximal accuracy of receptive field properties, a further step was introduced in addition to realignment of all the images to compensate for movement in the x-y axes. Two criteria had to be matched in order for an experiment to be included in the dataset, and these were applied to a reference image corresponding to averaged frames across the response period for all bars of a given orientation. This image was compared for the first and the last stimulus set repetition of an experiment. In order to be retained, the average fluorescence of both images had to be within 10% of each other, and the mean cross-correlation value of pixels of the normalised images had to be above 0.94 (see Appendix 2, [Table A3](#)). This latter parameter was particularly important to satisfy no z-axis motion had occurred over the course of the recording.

ROI selection

For region of interest (ROI) selection, the reference image of the medulla described in the above paragraph was used. Circular ROIs 12 pixels in diameter were manually positioned over segments of the 512 x 512-pixel image that exhibited high levels of fluorescence (example ROI segmentation in [Figure 5.3](#)). Each ROI covers a sufficient number of pixels to ensure a good response can be extracted whilst limiting noise issues that may arise in larger ROIs.

Visual response spatial map reconstruction

DeltaF traces were extracted for individual ROIs and three of the five repetitions of each identical bar presentation were retained via a selection method whereby the two responses furthest from the mean of all five responses for a stimulus were removed. This methodology was introduced in an effort to reduce noise in the data. The selected DeltaF traces were then averaged across repetitions and peristimulus time histograms (PSTHs) were generated where each bin corresponds to an image frame. PSTHs were reshuffled to show the ordered responses to bar presentations across the screen (as opposed to the pseudorandomised presentation order) and plotted for each angle of bar presentation ([Figure 5.4 A](#)). For each PSTH, values were summed over a specified time period to produce a radon transform of the spatial map to characterise the strength of the response

for each bar location and orientation (**Figure 5.4 B**). This was done for six time periods corresponding to (1) the 5 frames prior to the light bar appearing, (2) frames 1-5 of the bar stimulus, (3) frames 6-10 of the bar stimulus, (4) frames 11-15 of the bar stimulus, (5) frames 1-5 post bar stimulus, (6) frames 6-10 post bar stimulus. Finally, the projection data (radon transform) was used to reconstruct the spatial map by means of a filtered back projection algorithm (Matlab function *iradon*, 'Hamming' filter) for all six time periods (**Figure 5.4 C**). To increase the resolution of the maps, I interpolated the 18 x 18-pixel maps to 54 x 54-pixel maps using the Matlab function *imresize* (**Figure 5.4 D**). Of note, all spatial maps generated for a given ROI were normalised to the minimum and maximum response of that ROI.

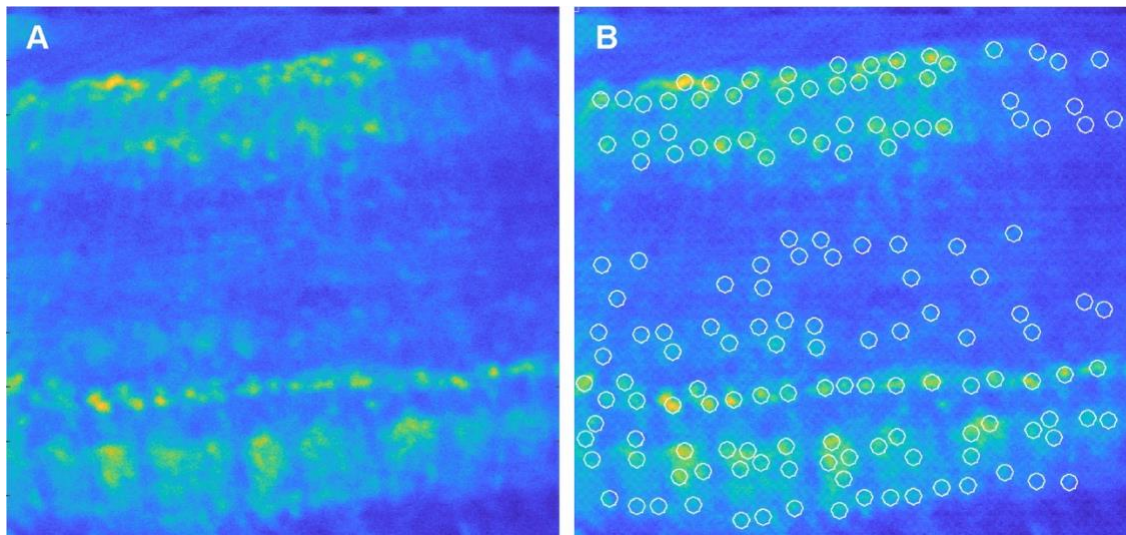


Figure 5.3 Segmentation process for neuronal signal extraction.

Layers and structures of the medulla are readily discernible under the two-photon microscope. (A) Baseline fluorescence of the calcium indicator provides a solid outline of the neuropil, but visually responsive segments can be evidenced further by averaging images of the response to each individual bar for a given orientation. (B) Circular ROIs, 12-pixels in diameter, are manually positioned on segments of the visible layers that exhibit distinguishable fluorescence.

Receptive field extraction

The filtered back projection method reconstructs a spatial map of the visual response of the ROI. Receptive fields were identified within the spatial map if a group of pixels exhibited a suprathreshold response (80% above or below baseline). In order for these pixels to qualify as a receptive field, several conditions were set: (1) more than 3.4% of pixels across the map exhibited a response below 70% above baseline and less than 51.4% of pixels exhibited a response above 30%, (2) no more than 8 pixel groupings of more than 6 pixels above 40% were detected and (3) no more than 2 pixel groupings of more than 6 pixels above 80% were detected. Of note, in the case of an inhibitory response, all outlined conditions were applied as a percentage of the minimum response instead of maximum response. If all conditions were fulfilled, an ellipse was fitted to the designated group of pixels (**Figure 5.5 A**) (`fit_ellipse` Matlab function, Ohad Gal) in order to determine the preliminary receptive field properties including axis of orientation and centre of mass. A subset of the spatial map restricted to the identified receptive field (dimensions of this out-take varied according to the size of the fitted ellipse). A Gaussian curve was then fitted along the short and the long axis of the receptive field as demarcated by the ellipse using the Matlab 'fit' function ('gauss 1', one term Gaussian model). The full width at half max (FWHM) of the curve was determined and used as the measurement of the receptive field size (**Figure 5.5 B**). If the mean square error of the fit was above 0.01 or the tails of the Gaussian did not reach a similar value (within 0.2 of each other), the FWHM value was discarded for the receptive field.

Statistics

All stages of data analysis (image analysis, curve fitting, data representation and statistical analyses) were conducted using custom-made scripts utilising statistical packages available in Matlab (Mathworks, MA, USA). Individual statistical tests are reported in figure legends and the results of post hoc tests, original data points, mean, standard deviation, and standard error of the mean are reported throughout using `notBoxPlot` Matlab function (version 1.31.0.0, Rob Cambell).

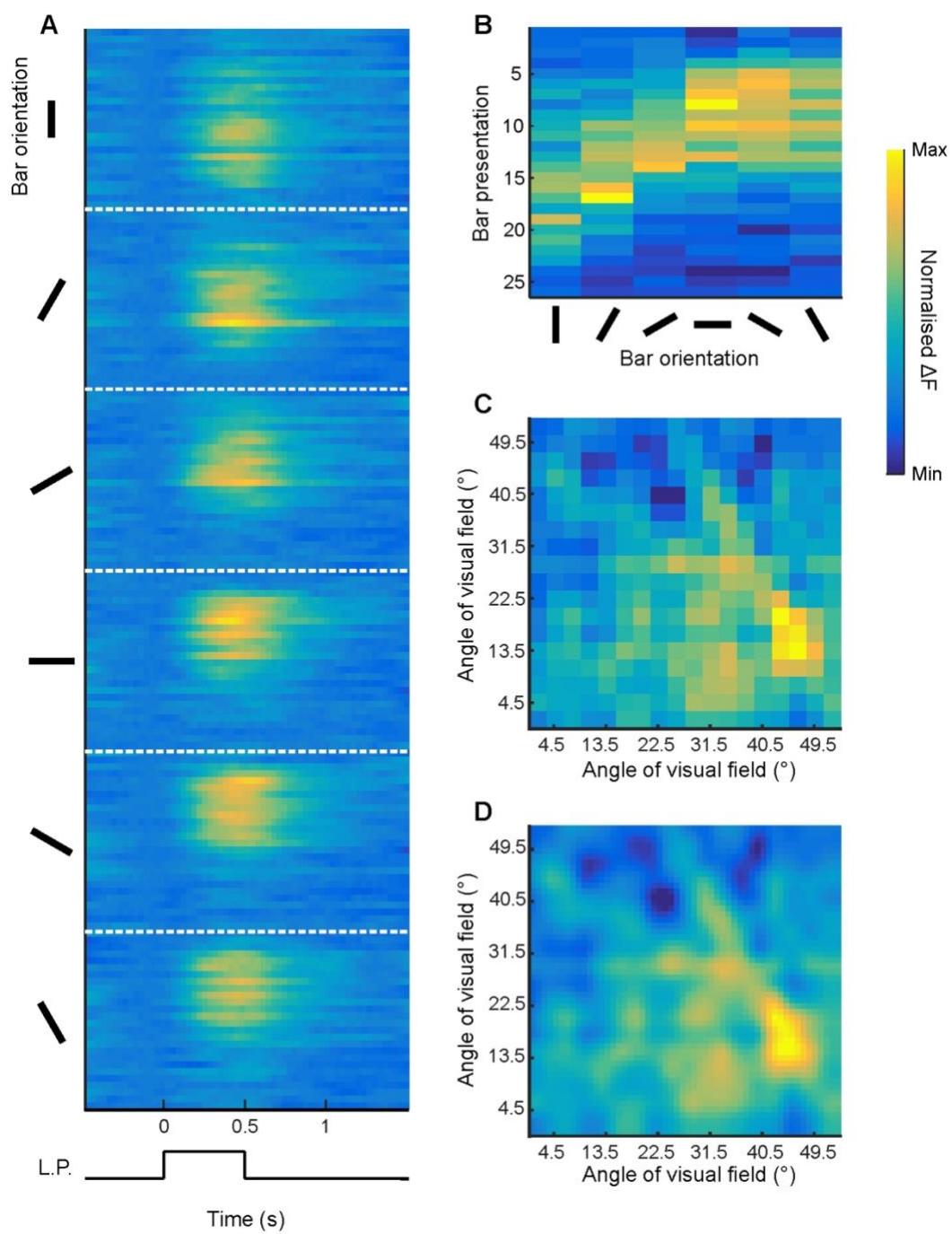


Figure 5.4 Stages of the reconstruction of the spatial map.

(A) Peri-stimulus time histograms (PSTHs) show the response to a flashing light bar (L.P. = light pulse) at successive locations moving across the non-elongated axis of the bar (randomised data has been reordered in this figure) for six different bar orientations. The 500 ms bar presentation starts at 0 seconds, the response delay is due to the slow temporal response time of the calcium indicator. PSTH responses are summed across a chosen time period, here 166 ms, to generate a radon transform. (B) Magnitude of the response at each bar location and orientation. (C) This projection image was reconstructed as a receptive field via filtered back projection algorithm. (D) Interpolation of (C) was performed to improve resolution.

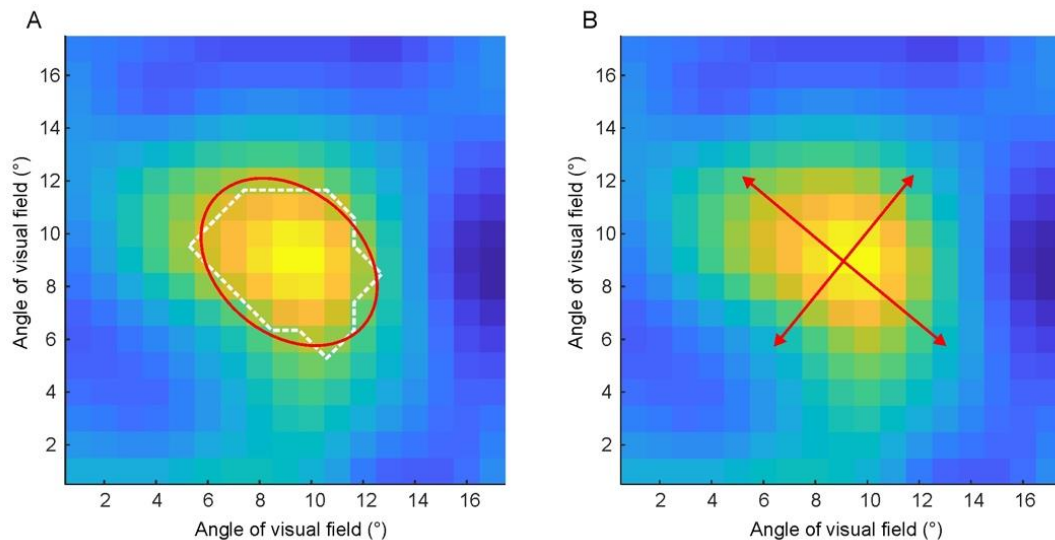


Figure 5.5 Receptive field identification and measurements.

(A) An ellipse (red line) is fitted to suprathreshold pixel clusters (outlined by the white dotted line) exhibiting responses 80% above, if excitatory, or below, if inhibitory, the baseline in order to determine the centroid and short and long axis orientations. (B) A Gaussian curve can then be fitted along both axes, and the full width at half max of the curve measured (red arrows) to establish the size of the receptive field.

5.3 RESULTS

This investigation set out to probe receptive fields of neurons in the medulla of *Drosophila*. Specifically, I aimed to uncover size and orientation sensitivity properties of medullary neurons and how these might vary from distal to proximal layers, as well as over time. To produce spatial maps, I applied a light bar stimulus (blue light) that canvases the screen, repeated for several orientations. The intersection of responsive regions elicited from different bar orientations provides a map of the responsive regions of visual space of an ROI. The novelty of this method, developed by Johnston *et al.* (2014) lies with the analysis paradigm based on ‘filtered back projection’, an algorithm that takes the strength of the neural response into account.

5.3.1 Spatial and temporal response profiles

An important advantage of this mapping methodology is that it allows for the reconstruction of the temporal component of the map, thus enabling me to evaluate the evolution of the spatial response over time. I chose to bin my data such that I produced six spatial maps over the time course of one second, including a baseline response map, three phases of the response to the light bar and two phases of the response after the bar presentation (**Figure 5.6 A**). ROI response profiles varied, but for the most part, could be classified into one of the three following categories: (1) ROIs that exhibited a detectable excitatory response during the ON component (i.e. light bar ON) of the stimulus (**Figure 5.6 Bi** and **Bii**), (2) ROIs that exhibited a detectable excitatory response during the OFF component (i.e. light bar OFF) of the stimulus (**Figure 5.6 Biii**) and (3) ROIs that showed very little variation in their neural activity over all time frames and were thus discarded as non-respondent (examples not shown). If ROIs in categories (1) and (2) exhibited a group of strongly responding pixels, easily distinguishable from other neighbouring pixels, and to which an ellipse could be fitted (see methods section 5.2.4 ‘*Receptive field extraction*’ for more details on the selection process), the pixel grouping was recognised as a receptive field (**Figure 5.6 Bii** – T3 and **Figure 5.6 Biii** – T5).

If a receptive field was not identified, the spatial response of that ROI was not characterised as no readily accessible method or quantification tool is available for such data. Every ROI that falls within the second category (**Figure 5.6 Biii**) is located to the medulla layer M2, and a large proportion of these ROIs appear to exhibit an inhibitory response during the ON component of the stimulus prior to the excitatory OFF phase.

This is reminiscent of the response profile observed for full-field stimulation of that layer (see chapter 4). Despite some temporary excitement I experienced when considering the complementary spatial patterns of the inhibitory and excitatory responses, suggestive of a potential centre-surround configuration, it seems a lot more likely that the supposed inhibitory responses are in fact just a continued decay of the fluorescent response to a previous bar presentation. The 1 second dark interval between 500 ms bar presentations is not sufficient for GCaMP fluorescence to return to baseline if the response occurs during the OFF component.

5.3.2 Receptive field dimensions

The FWHM of a Gaussian fit was used to determine the size of identified receptive fields, for both the width and the length, following detection via the ellipse-fitting method. For ON-component responses, the majority of ellipses were fit at T3 and T4, T2 being too early in the calcium rise phase to present a strong response. Likewise, a greater number of ellipses were fit at T6 than T5 for OFF-component responses. We see no significant variation between layers of the medulla for all widths and lengths across all layers (**Figure 5.7**, 1-way ANOVA, all p-values > 0.05), with all ten layer-structures averaging just over 10° of visual field for the ON-component (**Figure 5.7 A**, all layers combined: 10.48 ± 1.66 , mean \pm SD) for the width measurement and a couple degrees increase for width at approximately 11° of visual field (**Figure 5.7 B**, all layers combined: 10.96 ± 2.34 , mean \pm SD). OFF-component responses are marginally higher with around 11.5° of visual field for both width and length (**Figure 5.7 C** and **D**, all layers combined: 11.30 ± 2.00 and 11.38 ± 2.38 respectively, mean \pm SD). We observe matching layer-specific temporal response profiles between the full-field stimulation of the previous chapter and the receptive field data presented here. The ON-component generated receptive fields primarily for layers M1, M6-M7, M8 and M9-M10, as well as a few for layers M3-M5. The reverse is true for the OFF-component, with a large number of receptive fields in layers M2 and M3-M5, and a smaller proportion for other layers. The latter are possibly a result of slow fluorescence decay, rather than excitatory responses in the Off-phase *per se*. Of note, ROIs from M3-5 were discarded in the previous chapter because of poor signal-to-noise ratio, but here we have no evidence that suggests the data from this layer grouping should be removed.

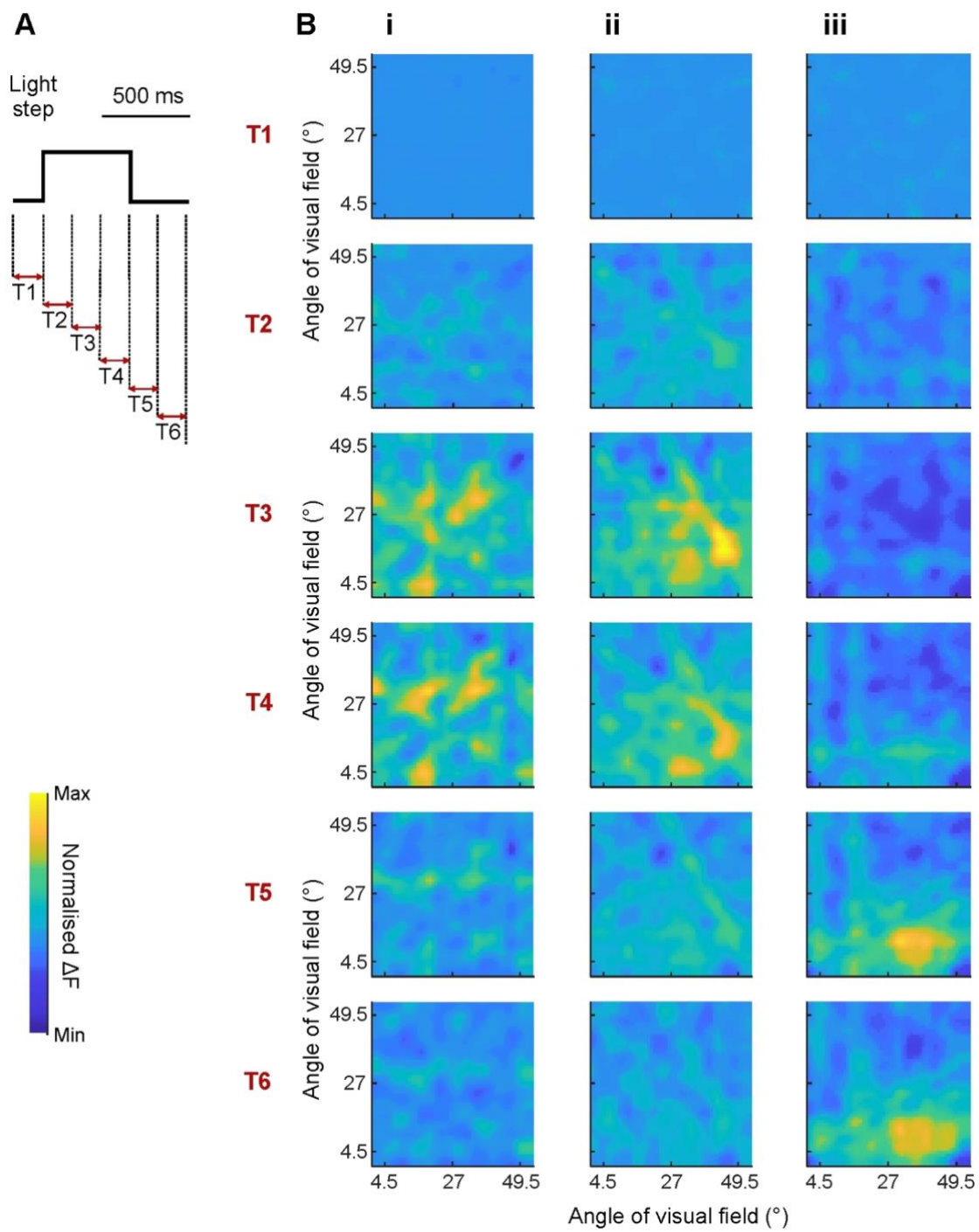


Figure 5.6 Temporal response profiles of spatial maps in the medulla.

The spatial map of an ROI was established for successive time segments (**A**) encompassing pre-stimulus baseline, response to the light bar presentation, and response post light bar. In (**B**), examples of the three types of temporal response profiles observed in the data set: (**i**) an ROI exhibiting an excitatory response during the bar phase presentation followed by a decay in the response when the bar disappears, (**ii**) as in (**i**) but with a pixel grouping clearly identifiable as a receptive field (at T3 in this example), and (**iii**) an ROI exhibiting an apparent lack of excitation during the light bar phase followed by an excitatory response to the disappearance of the bar. As in (**ii**), the response is restricted to a small subset of pixels suggestive of a receptive field (at T5 and T6).

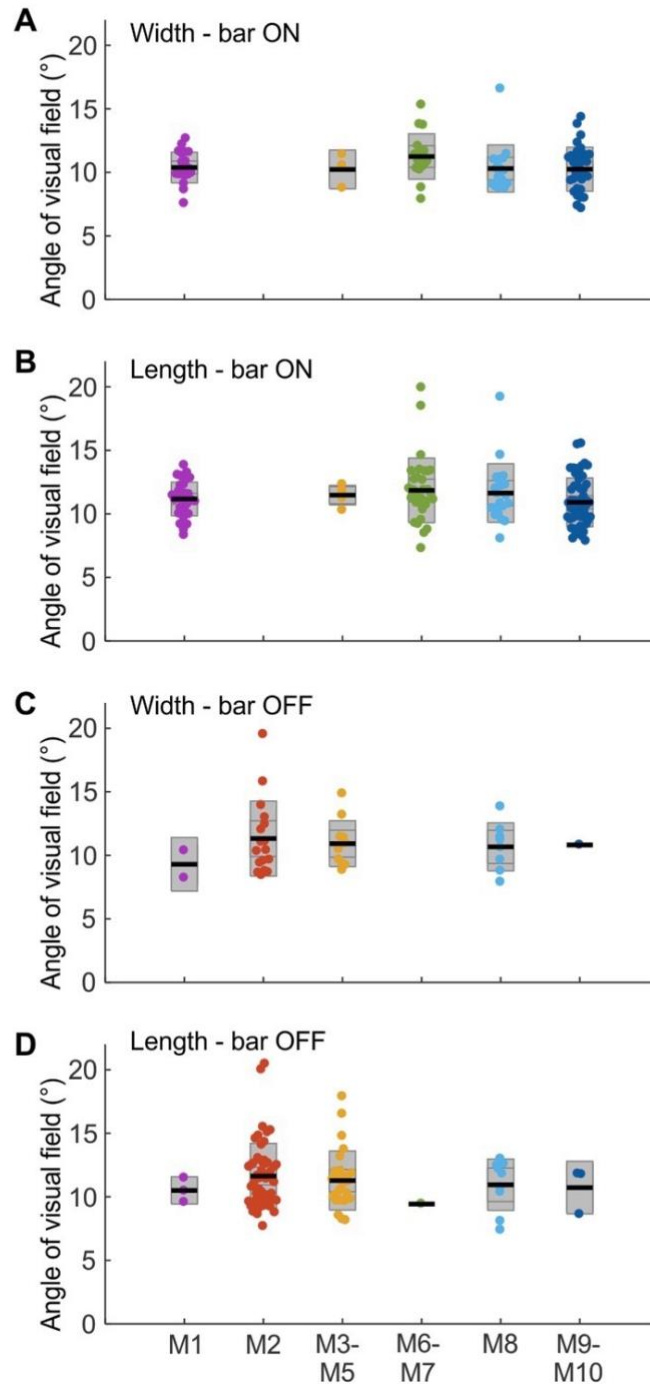


Figure 5.7 Size properties of receptive fields in the medulla.

Dimensions of receptive fields extracted during T2, T3 and T4 time frames corresponding to the light bar presentation phase (measurements of width (A) and length (B)), as well as dimensions of receptive fields extracted for time segments T5 and T6 post bar presentation (measurements of width (C) and length (D)). Data is categorised according to layer groupings in the medulla: M1 (magenta), M2 (red), M3-M5 (yellow), M6-M7 (green), M8 (cyan) and M9-M10 (blue), and each dot represents a receptive field measurement that could be determined from a Gaussian fit. Black, solid lines represent the mean value. From the mean outwards, the first grey line of the background box shows the 95% confidence interval (or 1.96 standard error of the mean) and the second grey line represents 1 standard deviation from the mean. Data was collected from 10 flies.

5.3.3 Receptive field orientation preference

As a result of noise in the spatial maps, and stringency with Gaussian curve fitting, not all identified receptive fields have measures of both width and length. When both dimensions of the receptive field were recorded, however, they were paired to produce a length to width ratio. I find that ratios vary between 1 (indicating no orientation preference) and 1.5, with a continuity of data points between both extremes, suggesting the strength of orientation selectivity is a sliding scale ([Figure 5.8](#)). Again, no differences are observed between layers.

The radon transform, the intermediate stage of the spatial map reconstruction, can be used to extract orientation selectivity by summing the responses across a given orientation and comparing the total response strength between orientations. I chose, however, to specify orientation of the receptive field from the fitted ellipse. This is advantageous as it confers more precision to the measure than a categorical determination of just one of six possible orientations (as defined by the number of light

bar orientations, see [Figure 5.4](#)). Furthermore, our spatial maps often contain excitatory pixel cluster that do not belong to the receptive field ([Figure 5.6 Bi](#)) and in some cases more than one receptive field. Thus, radon transforms will not relate signals pertaining solely to the receptive field.

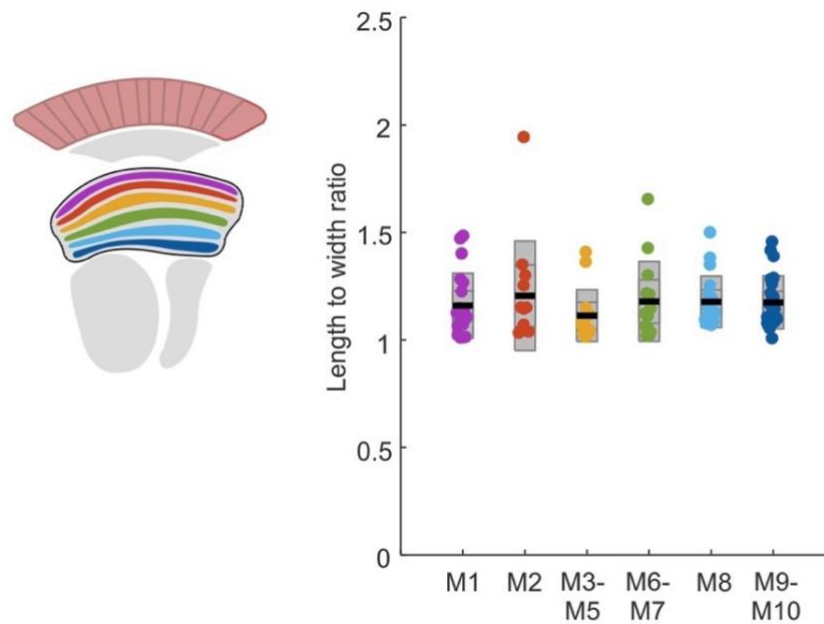


Figure 5.8 Receptive fields in the medulla exhibit an elongated structure.

Length to width ratio of receptive fields where both dimensions could be measured, categorised according to layer groupings in the medulla: M1 (magenta), M2 (red), M3-M5 (yellow), M6-M7 (green), M8 (cyan) and M9-M10 (blue), and each dot represents a receptive field measurement that could be determined from a Gaussian fit. Black, solid lines represent the mean value. From the mean outwards, the first grey line of the background box shows the 95% confidence interval (or 1.96 standard error of the mean) and the second grey line represents 1 standard deviation from the mean. Data was collected from 10 flies.

In order to relate any uncovered orientation selectivity to general visual ecology properties in the fly, I first established how the region of the eye sampling the light stimulus (**Figure 5.9 Ai**) related both to the dorso-ventral and temporo-nasal axes of the fly eye (**Figure 5.9 Aii**) and to the cardinal axes on the screen (**Figure 5.9 Aiii** and **Aiv**). The dorso-ventral axis of the fly does not align with the vertical axis of the screen, but instead is rotated approximately 45° to the right-hand side of the screen. Orientation properties of receptive fields were delineated by two measures, the strength of the orientation selectivity, as described in the above paragraph, and the angle of tilt from the perpendicular axis. I found that preferred orientations were spread across all possible directions, with no evidence of layer-specific responses (**Figure 5.9 B**, 1-way ANOVA, all p-values < 0.05). Nonetheless, visual inspection of the polar plot reveals a noticeable gap in the density of orientation vectors between 50° and 100° , suggestive of division of orientation selectivity into two groups. Despite careful positioning of the fly preparation within the holder, it is impossible to ensure that alignment between the fly and the screen is identical from one experiment to the next, and some variability will occur. Thus, I decided to investigate orientation properties within each individual fly preparation. As expected, the gap between 50° and 100° was maintained and I summed the response from vectors on either side of the divide to create two summary vectors (examples from three experiments in **Figure 5.9 Ci**, **Cii** and **Ciii**). The angle of one summary vector to the other was found to average approximately 115° across experiments (**Figure 5.9 Civ**; 116.85 ± 20.59 , mean \pm SD). As a control, I ascertained that this spread of orientation preferences and elongation measurements was not a result of screen optics where distortion of the bars might occur in the fly visual system towards the outer edges of the screen. Indeed, we see no trend in the spatial distribution of the receptive fields across the screen (**Figure 5.10 A** and **5.10 B**). A randomly generated subset of example spatial maps containing identified receptive fields are depicted in **Figure 5.11**.

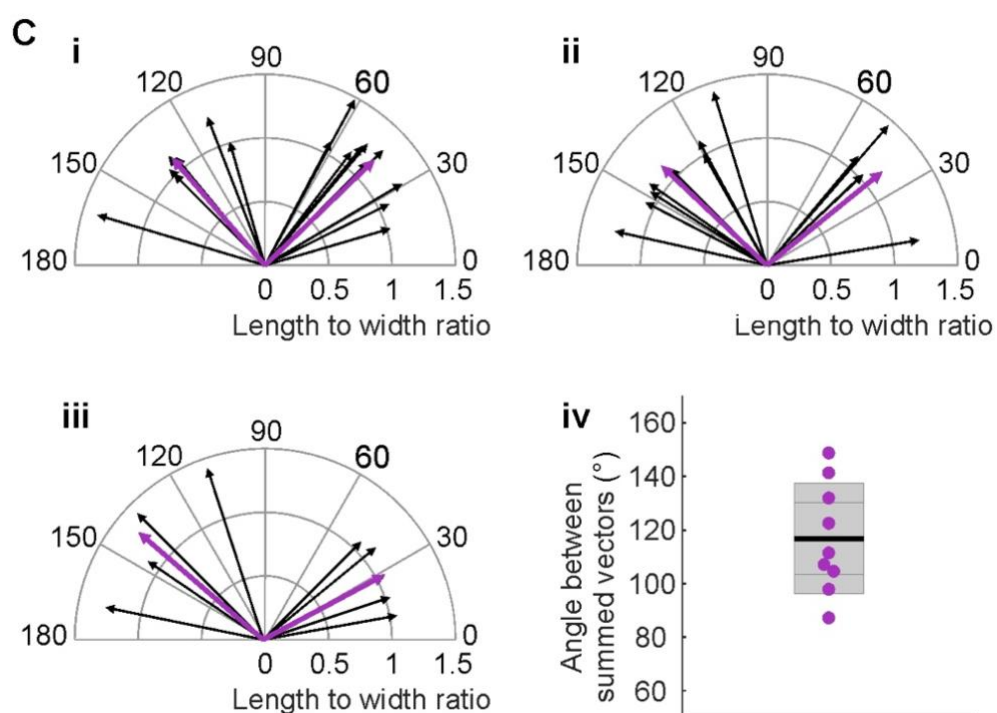
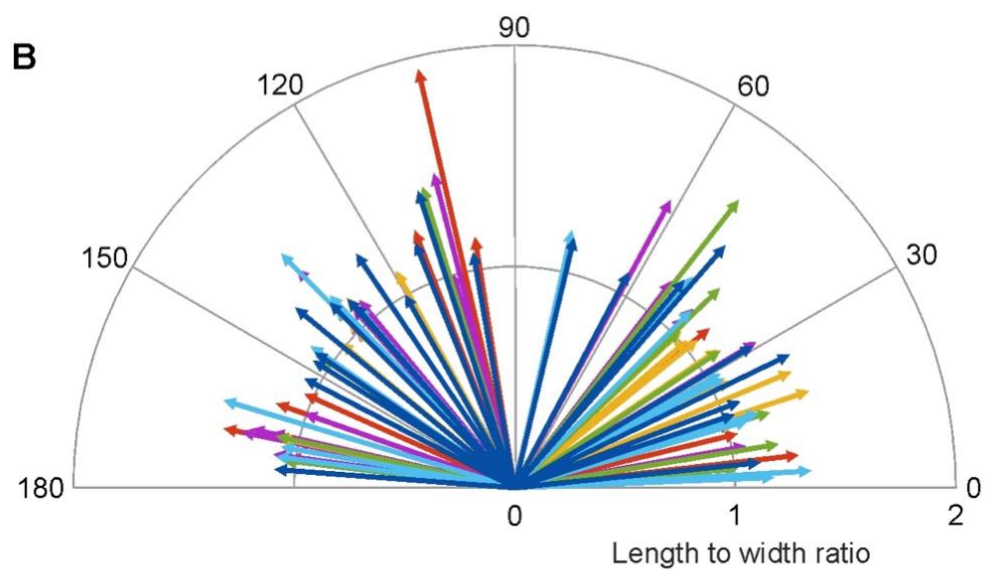
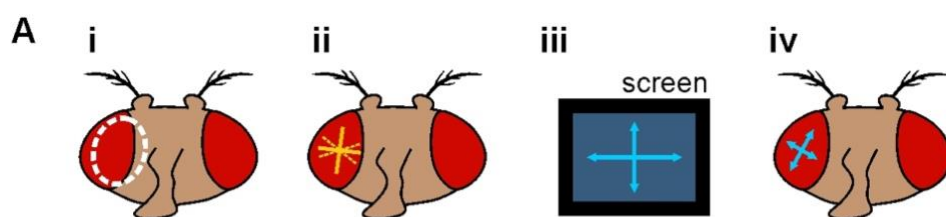


Figure 5.9 Orientation preference of receptive fields in the medulla.

(A) Diagrams presenting (i) the region of the eye stimulated by the screen (dotted white line), (ii) the v- and h-row axes of the eye (yellow lines) after Krapp (2010), (iii) the cardinal axes of the screen (cyan arrows) and (iv) the approximate orientation of those cardinal axes as sampled by the fly's eye (cyan arrows). (B) Orientation properties of receptive fields are plotted as vectors in a polar plot, with orientation preference coded by vector direction and strength of orientation selectivity by length of vector. Data is categorised according to layer groupings in the medulla: M1 (magenta), M2 (red), M3-M5 (yellow), M6-M7 (green), M8 (cyan) and M9-M10 (blue). (C) Polar plots as in (B) showing orientation properties of receptive fields for three example fly preparations (i-iii). Black arrows represent individual receptive fields and the two purple arrows show the sum of vectors within the left and right 90-degree quarter of the polar plot. The angle between both summed vectors for each individual fly preparation is plotted in (iv).

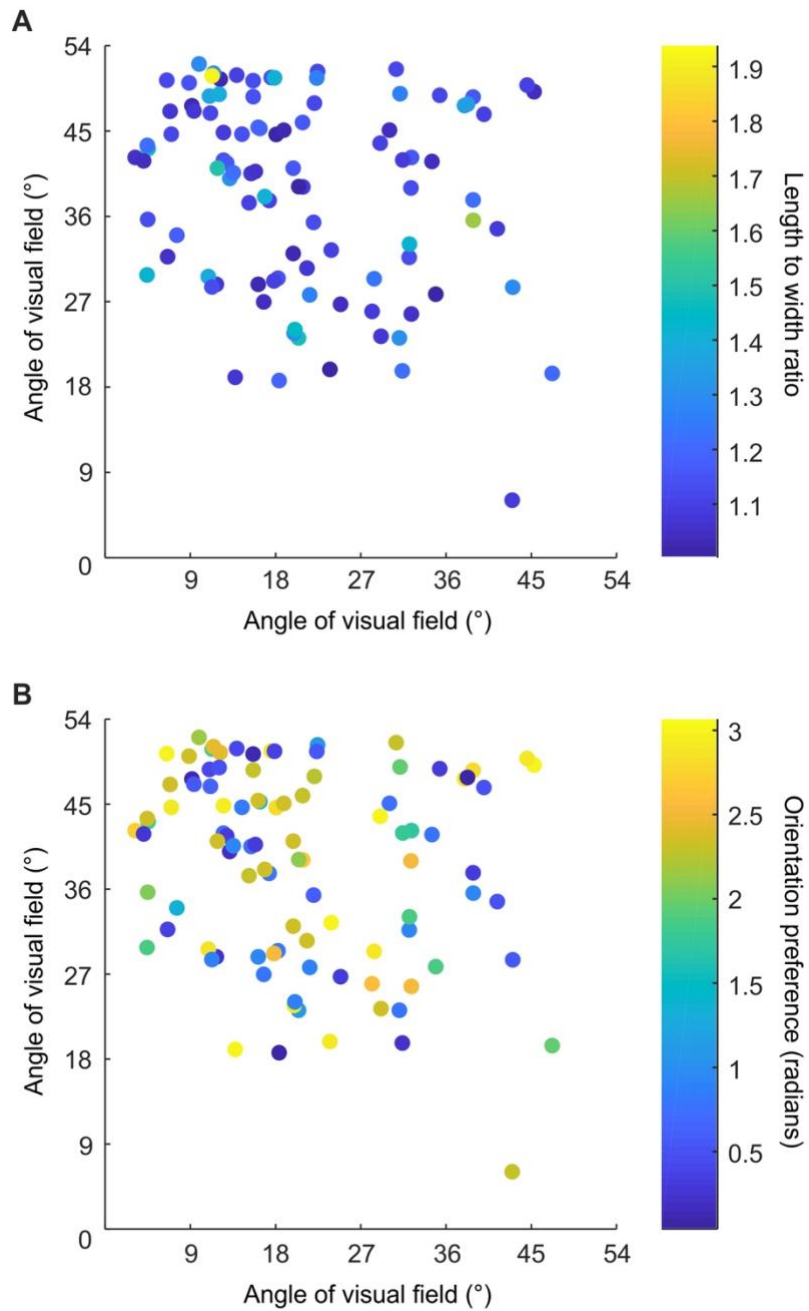


Figure 5.10 Receptive field properties exhibit no dependency on screen optics.

Length to width ratio (**A**) and orientation preference (**B**) of receptive fields plotted as a points representing the screen coordinates of their centroids. Varying measures for both parameters are randomly distributed across the screen.

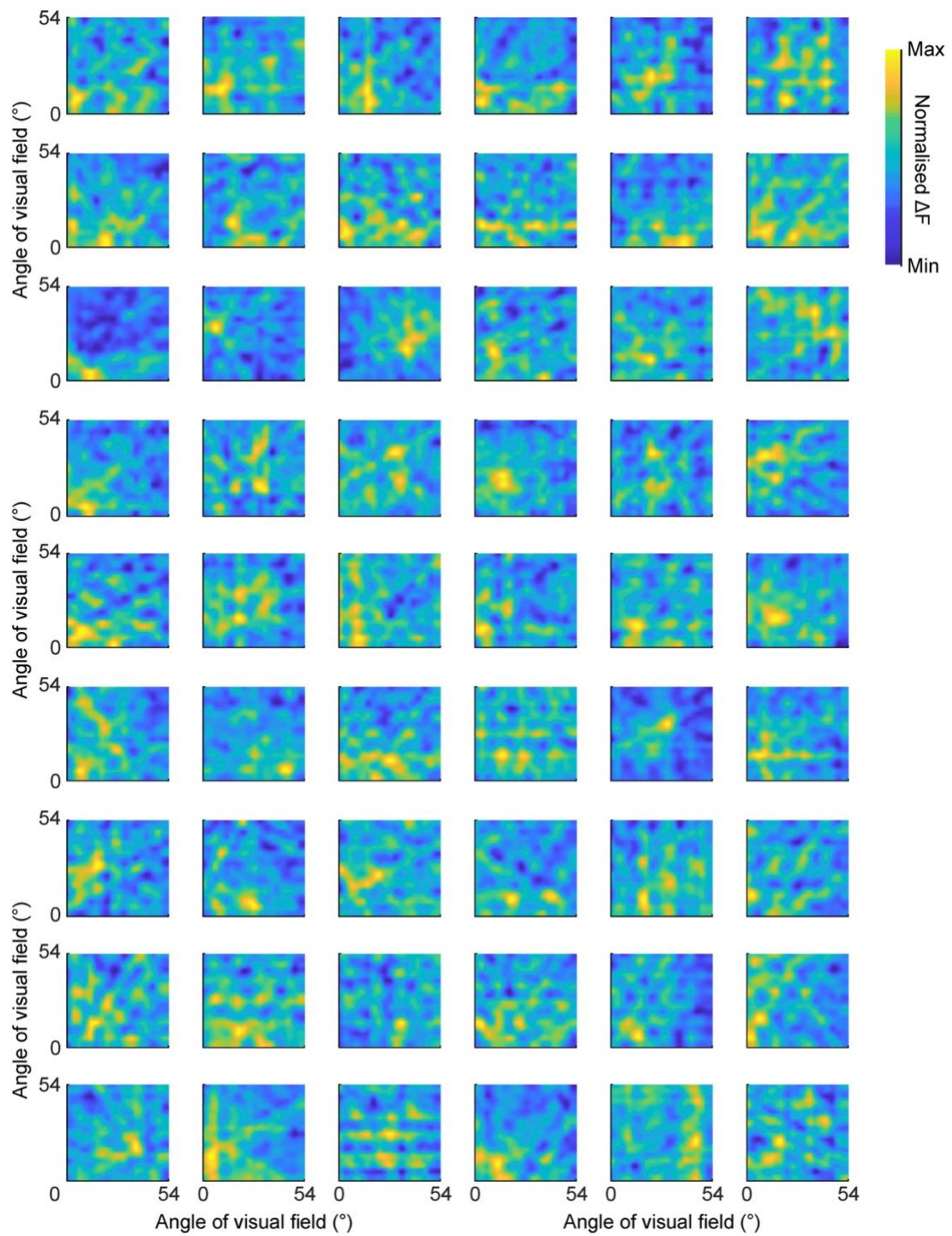


Figure 5.11 Example spatial maps for receptive fields.

Randomly generated set of example spatial maps from the pool of receptive fields extracted using the criteria described in section 5.2.4 ('Receptive field extraction').

5.4 DISCUSSION

In this study we describe spatio-temporal properties of the summed activity of neurons in the medulla. Only blue light was used for this spatial mapping project, matching Rh1 peak sensitivity. However, if circumstances had permitted, a selection of colours from the full range of wavelengths available in our monochromator/projector/2-photon microscope system could also have been applied to this visual stimulation protocol. Some evidence points towards the contribution of colour cells to spatial processing (Buzás *et al.*, 2013), thus investigating the combined spatial and spectral properties of cells could reveal interesting responses. I find that the temporal profiles of individual ROIs are layer specific and match the responses to full-field stimuli reported in the previous chapter (Chapter 4). Spatial profiles, in contrast, appear more diverse, ranging from widespread visually-induced excitation across the spatial map to readily discernible localised regions of excitatory activity. I chose to characterise the latter and found these receptive field dimensions to match the expected size predicted by the conservation of a columnar organisation in the medulla, with little variation from layer to layer. Furthermore, in a subset of these cells I see an elongated receptive field suggestive of static orientation selectivity. I observe an apparent split in the preferred axis of orientation of these receptive fields, with a near-orthogonal angle between the summed vectors of the split populations.

5.4.1 Experimental considerations

Although pan-neuronal labelling of neurons provides the unique advantage of recording from many medulla cells simultaneously, it also introduces an additional dimension of complexity to the data. Many spatial maps showed complex response patterns, often with many different regions across the map exhibiting strong excitatory activity. This makes it difficult to establish with full certainty that we have in fact identified receptive fields. The careful and very stringent methodology used to categorise a responsive portion of a spatial map as a receptive field (see section 5.2.4), as well as visual inspection of the data, leaves me confident that although some receptive fields might have been eliminated in the process, all retained data is appropriate. A further ramification of pan-neuronal labelling lies with the impossibility to gauge how many different neurons are contributing to the dendrite mass of the selected ROI. Naturally, single cell labelling would clarify many of these findings, however this study of the population-level neuronal activity is interesting in its own right.

One important requirement with this recording paradigm is that the section of the fly preparation selected by the ROI is identical from start to end of the recording, in other words that no lateral or horizontal shift occurs over time. The mapping stimulus is rapid, with five repetitions cycled within 20 minutes. As previously specified, I also use a motion correction algorithm to realign images that have shifted as a result of natural movement in the live preparation (See Chapter 2, section 2.3.2). Finally, I have checked both the decay in fluorescence and the correlation between images at the start and end of the recording and discarded experiments as necessary (see Appendix 2).

5.4.2 Receptive fields reflect the columnar structure of the medulla

The acceptance angle of photoreceptors in *Drosophila melanogaster* is approximately 8 degrees of visual field (Gonzalez-Bellido *et al.*, 2011). The average receptive field width in this study is just a couple of degrees wider than the photoreceptor angle, suggesting that photoreceptors inputs to the medulla are largely confined to their designated cartridge, in line with previous reports (Fischbach and Dittrich, 1989; Takemura *et al.*, 2013). Additionally, our results do not contradict the rough receptive field mapping performed on medullary cells by Strother *et al.* (2017) that outlines small receptive fields for Tm4 and Tm9 cells, as well as evidence that Mi1 and Tm3 cells respond well to small objects. This is in line with widely-understood notion that for motion vision and feature detection circuits, spatial pooling does not arise until post-medullary processing. Whether the wide-spread visually-driven excitatory activity observed across spatial maps in numerous ROIs reflects more extensive receptive fields that might arise from inter-columnar connectivity remains elusive. Nonetheless, this pattern of activity suggests that if receptive fields were characterised for individual cell types, we would likely encounter a much larger array of spatial receptive field dimensions than reported here.

5.4.3 Defining orientation selectivity

When Hubel and Wiesel (1962) first encountered orientation selectivity of visual cells in the primary visual cortex of cats, they described neurons that respond with increased firing to elongated stimuli oriented along a specific axis in the visual field while cell firing was maximally inhibited when an elongated stimulus was presented in the orthogonal to preferred orientation. Classically, orientation tuning is characterised by establishing an orientation tuning curve of the response to a grating presented over a range of

orientations. The relationship between the orientation eliciting the strongest response (preferred orientation) and weakest response (least preferred orientation, usually orthogonal to preferred orientation) is used to establish the orientation selectivity index (OSI). In this study, I show elongated receptive fields from single bar presentations, as performed by Hubel and Wiesel, however I was unable to characterise the orientation selectivity via the OSI methodology as pan-neuronal labelling of cells does not allow us to distinguish single cell responses. Instead, I elucidated orientation tuning from the shape of the receptive field. Receptive fields which respond to a static object of a particular orientation are likely to contribute to motion-independent feature detection.

5.4.4 How does orientation selectivity arise?

Earlier studies of orientation selectivity in mammals depict orientation selectivity as the classic example of the transformation of visual information throughout the visual pathway. In this model, the receptive field properties of lateral geniculate nucleus cells that exhibit no preference for orientation are pooled by neurons in the primary visual cortex (V1) to produce elongated receptive fields. Thus, from simple to complex cells, orientation selectivity emerges as a property of cortical cells, reviewed by Priebe (2016). In recent years, however, studies have shown that orientation selectivity exists much earlier in the visual pathway at the level of the retina (reviewed by Antinucci and Hindges, 2018). In the vertebrate retina, a subset of amacrine cells display dendritic arbors that extend considerably along a specific axis. Interestingly, this axis correlates strongly to the preferred stimulus orientation of the cell (rabbit: Bloomfield, 1994; zebrafish: Antinucci *et al.*, 2016, mouse: Nath and Schwartz, 2017). Bloomfield suggests the mechanism behind these are different than the excitatory/inhibitory interplay usually seen. This type of orientation selectivity arises too early in the visual field to rely on antagonistic surround properties of receptive fields to restrict the shapes detected by said receptive field. Instead, spiking of the cell simply occurs if the stimulus crosses any location of the receptive field, but the strength of the response will increase when receptive field is maximally covered.

When considering the neural mechanisms necessary to produce an elongated receptive field in flies with a compound eye and early neuropil exhibiting a columnar organisation, the most intuitive solution is the combination of input from two presynaptic cells. Fischbach and Dittrich (1989) describe how widespread lateral interconnectivity appears

at the level of the second neuropil, the medulla, with a substantial network of interneurons connecting neighbouring cartridges, which supports the hypothesis of a receptive field constructed from the sum of responses from different cells in different columns with slightly offset receptive fields. The length of the receptive fields characterised here, however, nearly never surpasses one and a half times the width. One might expect receptive field length to be double the width if the inputs of photoreceptors from adjacent ommatidia are combining. However, interommatidial angles in *Drosophila* average around 4.6, thus the ratio between the acceptance angle and the interommatidial angle (higher than 1) reveals an extended overlap between photoreceptor visual fields (Gonzalez-Bellido *et al.*, 2011). Consequently, it is a distinct possibility that the orientation selectivity we observe in the receptive fields in this study is formed in a similar manner to that described in the mammalian retina.

It has occurred to me that an ROI might overlap two cartridges and that consequently, the elongated receptive fields we describe arise from the summed activity of dendrites from distinct columns of the medulla. This is highly unlikely to occur, however, as ROIs are considerably smaller than the cartridge width, but also because carefully movement correction and assessments are applied in the x-y plane of the image sequence, but also along the y-stack.

5.4.5 Compound eye optical axes and preferred orientation

Petrowitz *et al.*, (2000) determined a map of optical axes in equatorial region of the frontal part the eye in the female blow fly (*Calliphora*). Due to the hexagonal lattice structure of the compound eye, each ommatidia can be linked to its neighbouring ommatidia via one of three axes. Thus, parallel rows of ommatidia can be traced across the eye: the *v*-rows, oriented vertically, and the *x*- and *y*-rows that are oriented along the diagonal axes. Petrowitz and his team also specify a *h*-row that falls at the midline between the *x*- and *y*- rows (a horizontal row) connecting two ommatidia that are separated by just one intermediate ommatidia. Elementary motion detectors (EMDs) in the early visual neuropil correlate luminance changes between neighbouring ommatidia to detect highly localised motion changes (Borst, 2014). Previous studies investigating the neural circuitry that form the elementary motion detector in flies have demonstrated that a robust response can be elicited in motion-sensitive neurons of the lobula plate by sequential stimulation of only two adjacent photoreceptors in *Musca* (Riehle and Franceschini, 1984). Thus, it

seems highly probable that each cartridge in the medulla shares an independently-functioning elementary motion detector component with every neighbouring cartridge. Krapp (2010) lays out how these thousands of EMDs integrate visual information along the *v*-rows and *h*-rows. It is interesting to consider how the orientation of the elongated receptive fields we find here match these optical axes, with a near orthogonal angle between both direction clusters. It is entirely possible that the slightly wider angle we find in our study is a distortion artefact resulting from the curvature of the eye sampling a stimulus presented on a flat screen.

Krapp (2010) also discusses the value of exploiting optic flow for estimation of self-motion, with a particular emphasis on the necessity of extracting motion cues that “fit the pulling plane of the muscles controlling the head and body movements”. The *v*- and *h*-rows appear to fit neatly with the translational motion across the retina for pitch and yaw. It also seems that the direction selectivity of the T4 and T5 wide-field motion-sensitive neurons could match these axes, as each of the four subpopulations exhibits strong selectivity for a different direction along the cardinal axes (Maisak *et al.*, 2013).

5.4.6 Elongated receptive fields could potentially arise from eye movements

Another possible explanation for the elongated shape of the receptive field is linked to the movement of the eyes. Not unlike the movements of vertebrate eyes, flies also present retinal saccades (Land, 1999). At the level of individual ommatidia, a recent study suggests that photomechanical contraction of individual photoreceptor cells can improve visual acuity both spatially and temporally (Juusola *et al.*, 2017). At the scale of the entire eye, a pair of muscles attached to the cuticle at the edge of the eye are responsible for eye movements along two near-perpendicular axes. Unpublished data presented by L. Fenk at the Fourth International Conference on Invertebrate Vision (August 2019) suggests that these saccade-like movements are performed in an active manner to improve vision. Her data also suggests that these saccades can have an amplitude of nearly ten degrees at their maximum but are generally smaller than that. This leads me to consider the possibility that these eye movements might have an influence on the receptive field properties we measure here. The average receptive field size we have reported is a few degrees larger than would be expected from previously reported acceptance angles (see section 5.4.2), however jitter of the eye might be the underlying cause of this. If this is the case, it would also provide a solid explanation for

the spread of width to length ratios I sampled, as the elongation would occur as a result of bigger saccades from one muscle over the other. Irregularity of the amplitude of the movement would be sufficient to create an elongated profile. In order to establish the contribution of eye saccades to spatial and temporal visual properties of neurons, further experiments where receptive fields are mapped in fly preparations with severed or inactivated muscles are needed, but it is nonetheless an interesting interpretation to consider. As is the possible role played by the microsaccades described by Juusola *et al.* (2017). The implications of eye movements resulting in elongated receptive fields for visual perception, however, remain unclear.

5.4.7 Previous reports of orientation selectivity in *Drosophila*

Orientation selectivity has been found at several locations along the visual pathway in flies. Initially, cells found to exhibit orientation selective properties in the central complex (Seelig and Jayaraman, 2013) were thought to be an emergent property in this higher processing centre which is known to be involved in spatial navigation including the spatial representation of visual cues (Pfeiffer and Homberg, 2014). Seelig and Jayaraman posited that these neurons encoded orientation properties in order to represent behaviourally relevant visual features to allow the fly to navigate its environment accordingly. More recently, however, it has been shown that orientation selectivity appears much earlier in visual system: Fisher *et al.* (2015) recorded orientation preference in T4 and T5 cells in the lobula plate. Furthermore, the authors specify receptive fields in T5 to be elongated with a preference for 15°-wide bars, with a centre-surround organisation reminiscent of cortical complex cells in primates. Interestingly, in *Calliphora*, orientation preference for moving gratings has been reported in the medulla (Spalthoff *et al.*, 2012).

5.5 REFERENCES

- Adelson, E. H. and J. R. Bergen (1985). "Spatiotemporal energy models for the perception of motion." *J Opt Soc Am A* 2(2): 284-299.
- Antinucci, P. and R. Hindges (2018). "Orientation-Selective Retinal Circuits in Vertebrates." *Front Neural Circuits* 12: 11.
- Antinucci, P., O. Suleyman, C. Monfries and R. Hindges (2016). "Neural Mechanisms Generating Orientation Selectivity in the Retina." *Curr Biol* 26(14): 1802-1815.
- Barlow, H. B., R. Fitzhugh and S. W. Kuffler (1957). "Change of organization in the receptive fields of the cat's retina during dark adaptation." *J Physiol* 137(3): 338–354.
- Berry, M. J., I. H. Brivanlou, T. A. Jordan and M. Meister (1999). "Anticipation of moving stimuli by the retina." *Nature* 398(6725): 334-338.
- Bloomfield, S. A. (1994). "Orientation-sensitive amacrine and ganglion cells in the rabbit retina." *J Neurophysiol* 71(5): 1672-1691.
- Brand, A.H., and N. Perrimon (1993). "Targeted gene expression as a means of altering cell fates and generating dominant phenotypes". *Development* 118, 401-415.
- Buzás, P., P. Kóbor, Z. Petykó, I. Telkes, P. R. Martin and L. Lénárd (2013). "Receptive Field Properties of Color Opponent Neurons in the Cat Lateral Geniculate Nucleus." *Journal of Neuroscience* 33 (4) 1451-1461.
- Chen, T. W., T. J. Wardill, Y. Sun, S. R. Pulver, S. L. Renninger, A. Baohan, E. R. Schreiter, R. A. Kerr, M. B. Orger, V. Jayaraman, L. L. Looger, K. Svoboda and D. S. Kim (2013). "Ultrasensitive fluorescent proteins for imaging neuronal activity." *Nature* 499(7458): 295-300.
- Fischbach, K. F. and A.P.M. Dittrich (1989). "The optic lobe of *Drosophila melanogaster*. Part I. A Golgi analysis of wild-type structure." *Cell Tissue Res* 258:441–475.
- Fisher, Y. E., M. Silies and T. R. Clandinin (2015). "Orientation Selectivity Sharpens Motion Detection in *Drosophila*." *Neuron* 88(2): 390-402.
- Gonzalez-Bellido, P. T., T. J. Wardill and M. Juusola (2011). "Compound eyes and retinal information processing in miniature dipteran species match their specific ecological demands." *Proc Natl Acad Sci U S A* 108(10): 4224-4229.
- Hartline, H. K. (1940). "The receptive fields of optic nerve fibers." *American Journal of Physiology* 130: 690–699.

- Hubel, D. H. and T. N. Wiesel (1962). "Receptive fields, binocular interaction and functional architecture in the cat's visual cortex." *J Physiol* 160: 106-154.
- Johnston, J., H. Ding, S. H. Seibel, F. Esposti and L. Lagnado (2014). "Rapid mapping of visual receptive fields by filtered back projection: application to multi-neuronal electrophysiology and imaging." *J Physiol* 592(22): 4839-4854.
- Juusola, M., A. Dau, Z. Song, N. Solanki, D. Rien, D. Jaciuch, S. A. Dongre, F. Blanchard, G. G. de Polavieja, R. C. Hardie, J. Takalo (2017). "Microsaccadic sampling of moving image information provides *Drosophila* hyperacute vision". *Elife* 6
- Keleş, M. F. and M. A. Frye (2017). "Object-Detecting Neurons in *Drosophila*." *Curr Biol* 27(5): 680-687.
- Krapp, H. G. (2010). "Sensorimotor transformation: from visual responses to motor commands." *Curr Biol* 20(5): R236-239.
- Kuffler, S. W. (1973). "The single-cell approach in the visual system and the study of receptive fields." *Invest Ophthalmol* 12(11): 794-813.
- Land, M. F. (1999). "Motion and vision: why animals move their eyes". *Journal of Comparative Physiology A: Sensory, Neural, and Behavioral Physiology*. 185:341–352
- Lettvin, J. Y., H. R. Maturana, W. S. McCulloch and W. H. Pitts (1959). "What the frog's eye tells the frog's brain". *Proceedings of the Institute of Radio Engineers* 49:1940-1951.
- Maisak, M. S., J. Haag, G. Ammer, E. Serbe, M. Meier, A. Leonhardt, T. Schilling, A. Bahl, G. M. Rubin, A. Nern, B. J. Dickson, D. F. Reiff, E. Hopp and A. Borst (2013). "A directional tuning map of *Drosophila* elementary motion detectors." *Nature* 500(7461): 212-216.
- Melnattur, K. V. and C. H. Lee (2011). "Visual circuit assembly in *Drosophila*." *Dev Neurobiol* 71(12): 1286-1296.
- Nath, A. and G. W. Schwartz (2017). "Electrical synapses convey orientation selectivity in the mouse retina." *Nat Commun* 8(1): 2025.
- Petrowitz, R., H. Dahmen, M. Egelhaaf and H. G. Krapp (2000). "Arrangement of optical axes and spatial resolution in the compound eye of the female blowfly *Calliphora*." *J Comp Physiol A* 186(7-8): 737-746.
- Pfeiffer, K. and U. Homberg (2014). "Organization and functional roles of the central complex in the insect brain." *Annu Rev Entomol* 59: 165-184.

- Priebe, N. J. (2016). "Mechanisms of Orientation Selectivity in the Primary Visual Cortex." *Annu Rev Vis Sci* 2: 85-107.
- Riehle, A. and N. Franceschini (1984). "Motion detection in flies: parametric control over ON-OFF pathways." *Exp Brain Res* 54(2): 390-394.
- Seelig, J. D. and V. Jayaraman (2013). "Feature detection and orientation tuning in the *Drosophila* central complex." *Nature* 503(7475): 262-266.
- Sher, A. and S. H. DeVries (2012). "A non-canonical pathway for mammalian blue-green color vision." *Nat Neurosci* 15(7): 952-953.
- Sherrington, C. S. (1906). "Observations on the scratch-reflex in the spinal dog." *J Physiol* 34(1-2): 1-50.
- Spalthoff, C., R. Gerdes and R. Kurtz (2012). "Neuronal representation of visual motion and orientation in the fly medulla." *Front Neural Circuits* 6: 72.
- Strother, J. A., S. T. Wu, A. M. Wong, A. Nern, E. M. Rogers, J. Q. Le, G. M. Rubin and M. B. Reiser (2017). "The Emergence of Directional Selectivity in the Visual Motion Pathway of *Drosophila*." *Neuron* 94(1): 168-182.e110.
- Takemura, S. Y., A. Bharioke, Z. Lu, A. Nern, S. Vitaladevuni, P. K. Rivlin, W. T. Katz, D. J. Olbris, S. M. Plaza, P. Winston, T. Zhao, J. A. Horne, R. D. Fetter, S. Takemura, K. Blazek, L. A. Chang, O. Ogundeyi, M. A. Saunders, V. Shapiro, C. Sigmund, G. M. Rubin, L. K. Scheffer, I. A. Meinertzhagen and D. B. Chklovskii (2013). "A visual motion detection circuit suggested by *Drosophila* connectomics." *Nature* 500(7461): 175-181.

Chapter 6 – Stereoscopic vision in the European cuttlefish

6.1 INTRODUCTION

6.1.1 Evidence for stereopsis in cuttlefish

Despite a large body of research into vertebrate depth perception, notably in primates (Cumming and DeAngelis, 2001; Welchman, 2016), little is known about this type of visual processing in the rest of the animal kingdom, especially in non-mammalian species. One such invertebrate that has long been postulated to have stereopsis is the cuttlefish (Messenger, 1968), as outlined in the introductory chapter of this thesis (Chapter 1, section 1.5.4). We already know that cuttlefish can perceive depth through non-stereopsis cues (section 1.5.4), and they are not alone in this ability amongst the molluscan class of cephalopods. Chung and Marshall (2014), uncovered a novel mechanism that allows squid to judge distances accurately with minimal neural processing. A portion of the retina is intentionally blurred, and the focus of an object will change markedly as it moves from the ‘retinal bump’ to a different region of the retina if the object is within tentacle reach. In contrast, octopuses have a limited overlap of visual fields from both eyes which makes the use of stereopsis unlikely (Byrne *et al.*, 2002). Cuttlefish, however, can produce a significant binocular overlap through ocular vergence, a phenomenon generally observed as eye rotation to improve the resolution of the target during a predatory hunt (Messenger, 1968).

In primates, depth perception requires multiple levels of processing in separate parts of the brain to finally combine in the cortex for a single representation of depth (Welchman *et al.*, 2005). This poses the problem of how a species such as the cuttlefish, which diverged more than 500 million year earlier (Kröger *et al.*, 2011), might have evolved the necessary neural circuitry to implement such a refined computational output. The concept of alternative forms of stereopsis is not a novel one. In fact, stereoscopic vision

has been demonstrated in one invertebrate species, the praying mantis (Rossel, 1983; Nityananda *et al.*, 2016), and a part of the neural circuitry subservient to mantid stereopsis has been revealed (Rosner *et al.*, 2019). Thus, we have evidence of an insect brain substantially smaller than its mammalian counterpart performing a task that sceptics once argued was too neuronally expensive for such a nervous system, not least because of the sheer number of neurons implicated in primate stereoscopic vision (Cumming and DeAngelis, 2011; Welchman, 2016). Nevertheless, mantids have neurons that exhibit visual response properties that are directly comparable to disparity-tuned cortical cells in vertebrates (Rosner *et al.*, 2018), although much remains to be elucidated about this neural circuit. Nityananda *et al.* (2018) have shown that mantid stereopsis employs a completely different set of visual cues when comparing retinal images: local luminance changes provide a sufficient basis to compute disparity, in contrast with mammalian stereopsis that requires a more global approach to matching images. Thus, despite extensive research into vertebrate stereopsis, little is known about this type of visually processing in animals with different brains.

6.1.2 Project aims

Despite the strong body of evidence suggesting that cuttlefish can extract binocular cues and use these for stereoscopic vision, it is still unknown whether their striking predatory attack relies on stereopsis for a precise tentacle to prey distance estimation, as hypothesised by Messenger (1968). Here, we aimed to address this deficit. In order to conclusively demonstrate whether cuttlefish employ stereopsis, we required a paradigm that allows for the independent manipulation of visual input to each eye so as to control the disparity of a stimulus between the two eyes. To this end, we adapted the 3D cinema experimental paradigm developed by Nityananda *et al.* (2016) and fitted the cuttlefish with anaglyph (coloured-filter) glasses to present a disparate shrimp stimulus to the left and right eye, thus creating an illusory sense of depth, but only if the animal has stereoscopic vision. Our behavioural assay explores how various parameters of the cuttlefish predatory hunt are affected when we modify the stimulus disparity in both uniform and cluttered backgrounds, but also how these parameters might be affected if the target prey is presented monocularly versus binocularly.

6.2 METHODS

6.2.1 Animals

Experiments were conducted on adult cuttlefish, *Sepia officinalis*, provided by Prof. Roger Hanlon, aged 18-24 months and originating from wild-collected eggs retrieved in the southern region of England, UK. Animals were housed, fed and reared in accordance to methods detailed by Panetta *et al.* (2017). Data was collected from eleven adults.

6.2.2 Experimental setup

A bioassay was developed whereby cuttlefish were trained to hunt the image of shrimp presented on a screen. The setup (**Figure 6.1 A**) consisted of a computer monitor (Dell UltraSharp LED U2413 24" Premier Colour) positioned against the side of a plastic tank (IRIS USA File Box, Model# 586490, 10.75"H x 13.88"W x 18.25"D) used as the experimental arena. Two cameras monitored the behaviour of the animal. A high-speed camera (Photron SA3 or Photron Fastcam mini WX100 with Canon EF 24-70 mm f/2.8L USM macro lens) positioned over the tank captured the entirety of the arena at 250 or 500 frames/s. Additionally, an underwater camera (GoPro Hero5 or Hero7 with Super Suit) placed inside the tank on the side opposite to the monitor provided an additional vantage point. Each day after the camera location and lens focus had been established, but before experiments started, an image was taken of a ruler in the tank. This served as the scale bar that allowed us to measure distances in x-y dimensions in the tank.

Over the course of the day, we exchanged the behaviour arena seawater several times with water sourced from the MRC recirculating seawater system. Temperature varied by ~5°C maximum. We did not measure Ammonia and pH throughout. Water quality changes were likely to be slow and we noticed no trend with increased time out of the recirculating water system (in fact hunting improved over time as the animals acclimated to the tank). Animals were motivated with live shrimp rewards and ate up to 30 grass shrimp (1.5-3 cm in length) per day.

6.2.3 Behavioural training

Food was withheld for 2 days prior to training beginning to motivate hunting and expedite learning. During initial training stages, a live grass shrimp (*Palaemonetes vulgaris*)

reward was delivered to the cuttlefish for each attempt by the animal to engage with the image of a moving shrimp presented on the screen. In subsequent training stages, shrimp rewards were restricted to trials during which the cuttlefish responded to the onscreen target by extending its tentacles i.e. it entered hunting mode and was preparing to strike at a target deemed suitable to capture. Once this behaviour became consistent, a Velcro patch (approximately 1 cm²) was affixed to the dorsal surface of the animal's head. This was achieved by netting the animals out of the tank, patting the skin dry with a paper towel three times and applying a superglue-covered Velcro patch directly to the skin and holding in place for 10 seconds. Animals were immediately returned to the tank with care and fed with a large mysid shrimp. Training as detailed above was repeated, following which a custom-made pair of glasses (see below) was attached via a Velcro patch and training was repeated. Trained animals were tested repeatedly over the course of several days.

6.2.4 Visual stimuli

We crafted “anaglyph” style glasses for the cuttlefish, adapted from the mantis glasses described by Nityananda *et al.* (2016). Experiments were conducted over the course of two field trips with an evolution in glasses design from the first trip to the second. Original glasses were made using a double layer of red and blue filters (**Figure 6.1 B**, Right Eye: Red = Lee 135 Deep Golden Amber; Left Eye: Blue = Lee 797 Purple). Light and transmission measurements made upon the return to the lab showed that the red filter was suboptimal in matching cuttlefish spectral sensitivity (**Figure 6.3**) creating a large difference in the luminance of the stimulus reaching each eye. Although we find no evidence that this affects the animal's ability to perceive the stereoscopic stimulus, in line with previous reports that the shape of the prey is more strongly discriminated for than the brightness of the prey (Guibe *et al.*, 2012), we chose to remedy this discrepancy by improving the glasses design with more adequate filters. Thus, second generation glasses were made with a double layer of blue and green filters (Right Eye: Green = Lee 736 Twickenham Green; Left Eye: Blue = Lee 071 Tokyo Blue). A Velcro patch on the underside of the glasses allowed easy attachment or removal of the glasses to the animals. Each filter allows transmission of a subset of the spectrum of light while blocking or reducing all other wavelengths. This paradigm allowed us to selectively stimulate both left and right eye and create an offset between right and left images to produce an illusory depth percept for animals that use stereopsis (**Figure 6.1 C**). We refer to a positive

disparity as disparity between images that causes the illusory depth percept to appear anterior to the screen, whereas a negative disparity will create a percept behind the screen. The value attributed to a disparity stimulus (1, 2 or 3 cm) indicates the offset between the images presented to each eye.

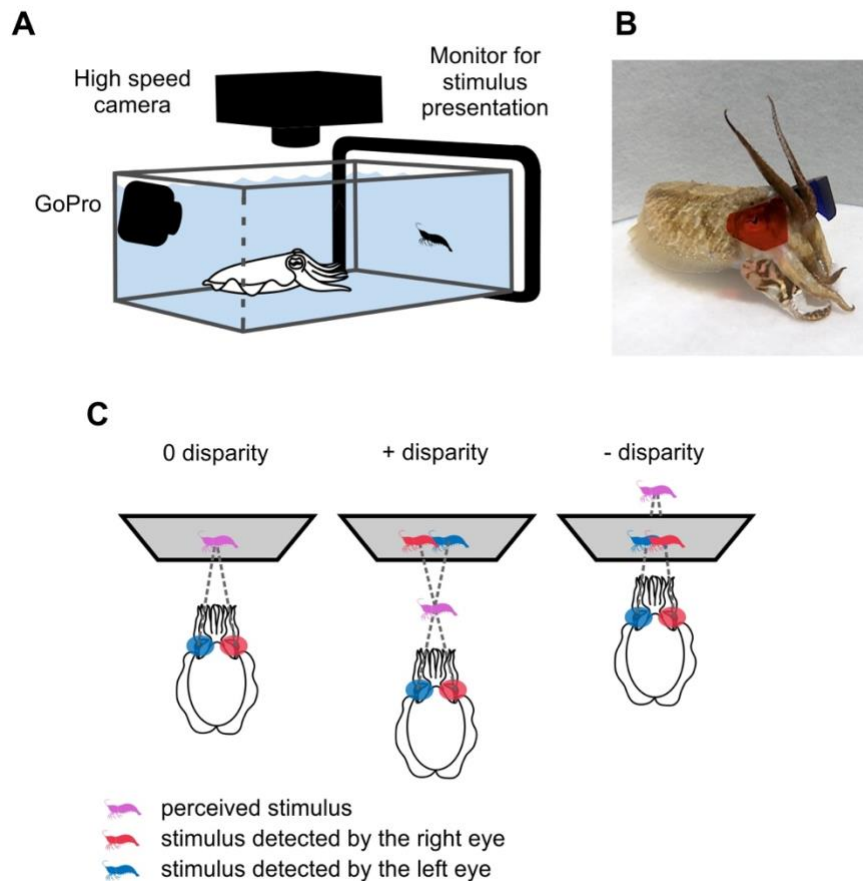


Figure 6.1 Experimental setup and stereoscopic stimuli.

(A) Experimental setup for tracking cuttlefish hunting behaviour when presented with a prey stimulus. (B) Cuttlefish fitted with experimental 3D coloured glasses. (C) Stereoscopic stimulus geometry for the three disparity conditions.

The shrimp stimulus presented to the cuttlefish via the screen was created from videos of grass shrimp recorded with the GoPro camera. A clip of a shrimp travelling the full width of the screen was selected and a thresholding method followed by binary conversion was used to remove the background to generate the outline of a shrimp against a uniform background. The three LED channels of the screen (Figure 6.2 A) were used individually or as a combination of two LEDs to create six possible colours of shrimp stimulus presented against a white or a black background (Figure 6.2 B).

Radiance spectra were measured using a NIST calibrated Avantes AvaSpec 2048 Single Channel spectrometer coupled to an Avantes UV-VIS 600 μm fibre (numerical aperture $\text{NA} = 0.22$, acceptance angle $= \text{AA} = 25.4^\circ$ and solid angle $\text{SA} = 0.1521^\circ$) positioned at a distance of 125 mm from the tank wall and monitor. Spectra were collected by averaging 100 repetitions of 50-millisecond light integration time, and smoothed using an 8-point moving average filter. Measurements were made in air rather than water for equipment preservation purposes. All stimuli spectra were measured from a full-screen of colour matching RGB values for individual components of all stimuli videos (**Figure 6.2 C**). Measurements were repeated with the addition of either blue or red original filters (**Figure 6.3 A and B**) or blue and green new generation filters (**Figure 6.4**) by positioning the glasses in the light pathway from the screen to the fibre, a few millimetres from the fibre end.

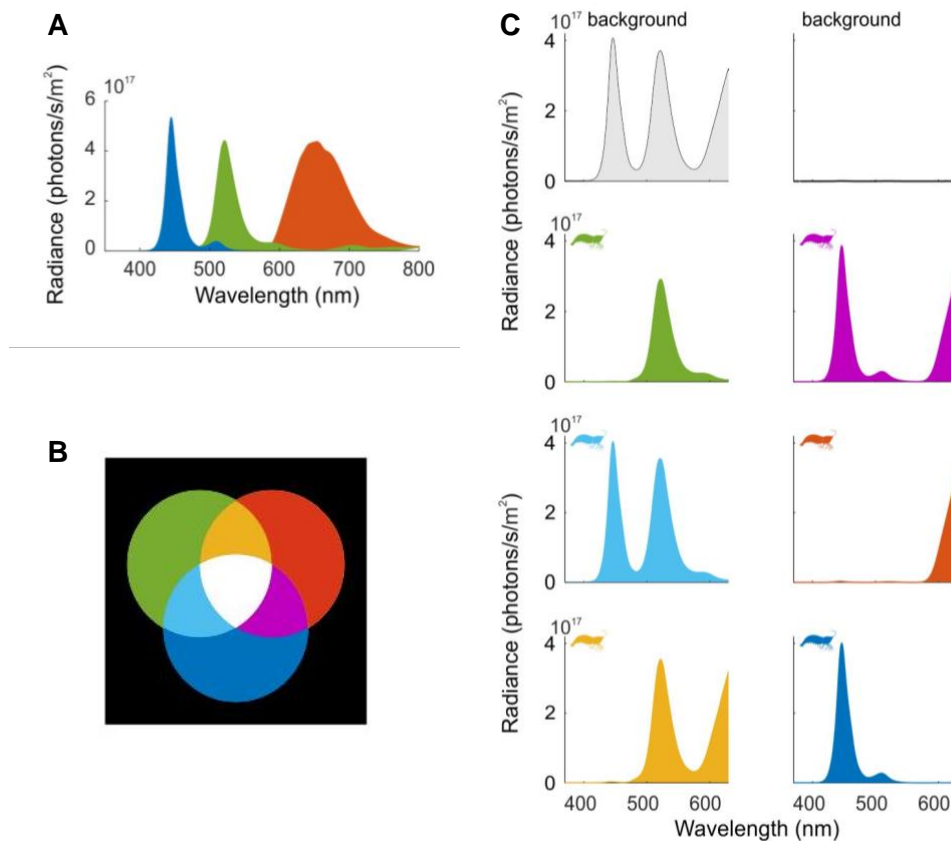


Figure 6.2 Screen and stimulus spectra.

(A) Radiance spectra of the three primary LEDs of the screen display. (B) Additive colour system of an LCD display. (C) Spectral radiance of light emitted by each colour of background and shrimp stimulus.

The spectral sensitivity of the *Sepia officinalis* visual pigment was calculated using the equations formulated by Stavenga *et al.* (1993), using a peak wavelength $\lambda_{\max} = 492$ nm for the alpha wave of the template, and a peak wavelength $\lambda_{\max} = 360$ nm for the beta wave (Brown and Brown, 1959). The relative photon catch for each colour of shrimp stimulus, in other words the number of photons (N) absorbed by a cuttlefish photoreceptor for a given stimulus, was obtained using the following equation (from Warrant, 2004:

$$N = \int (1 - \exp(-kS(\lambda)l)) \times R(\lambda)d(\lambda)$$

k is the quantum efficiency of transduction = 0.0067/ μm (Warrant and Nilsson, 1998), $S(\lambda)$ corresponds to the spectral sensitivity of the visual pigment, l is the length of the rhabdom = 400 μm (Hanlon and Messenger, 1996), and $R(\lambda)$ is the measured radiance spectra of the stimulus on the screen. As our goal was to produce stimuli that would only be detected by either the left or the right eye of the cuttlefish when wearing the glasses, we assessed the crosstalk of these stimuli by establishing the ratio of the quantum catch by the eye supposedly blind to the stimulus and the quantum catch of the eye intended for the stimulus (Figure 6.3, bottom row and Figure 6.4, bottom row). Our physical measurements show minimal crosstalk between stimuli (1-24%) for first generation glasses, reduced even further (1-5%) for second generation glasses.

For experiments in which we presented a video of a shrimp against a uniform background, we tested a dark silhouette against a white background as well as a light silhouette against a dark background (Figure 6.3). The 4 cm wide shrimp, when viewed at 18 cm, subtends 12.53° and when viewed at 12.5 cm subtends 17.74° . In the case of a white background, the band of light reflected from a green shrimp was not transmitted through either blue or red filter, resulting in a contrast between the absence of light of the shrimp appearing dark against a light background. If the shrimp is presented as cyan, this effect will be created with the red filter, however the blue filter will transmit the light thus removing the contrast in the image and rendering the shrimp indistinguishable from the background. This same effect is reversed for blue and red filters with a yellow shrimp. In the case of a dark background, a magenta shrimp will transmit light to both eyes thus contrasting against the absence of light from the surrounding black. Blue and red light, however, will only be transmitted through blue and red filters respectively. For simplicity's sake, stimuli for blue-green glasses only included a dark shrimp against a light background.

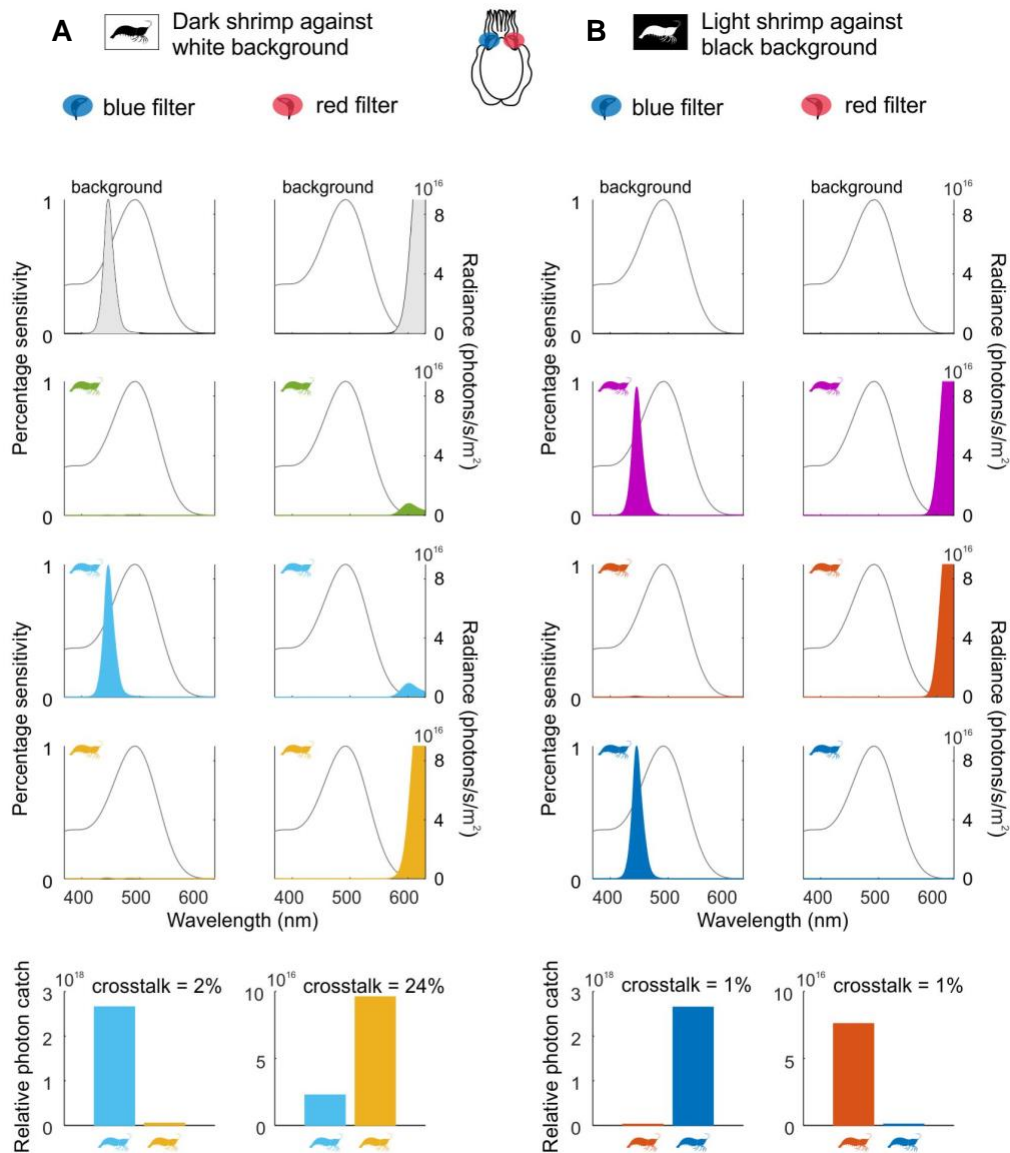


Figure 6.3 Stimulus spectra, filter properties and spectral content crosstalk measurements – first generation glasses.

Shrimp stimulus appears in (A) as dark against a white background and in (B) as light against a dark background. Spectral radiance of light emitted by each stimulus colour as transmitted through the blue and red filters of the first generation glasses (y-axis on the left) overlaid on the cuttlefish spectral sensitivity curve calculated after Stavenga et al. (1993). Such curves provide a measure of relative photon catch for each stimulus type through the filters. The crosstalk is the ratio of the relative photon catch of the stimulus intended for one eye by the other.

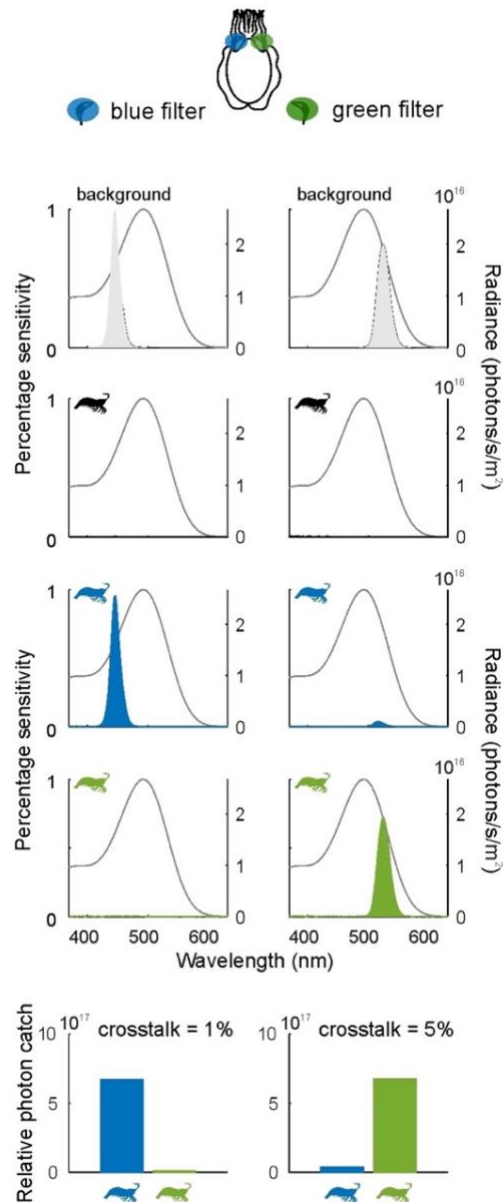


Figure 6.4 Stimulus spectra, filter properties and spectral content crosstalk measurements – second generation glasses.

Spectral radiance of light emitted by each stimulus colour as transmitted through the blue and green filters of the second-generation glasses (y-axis on the left) overlaid on the cuttlefish spectral sensitivity curve calculated after Stavenga et al. (1993). Such curves provide a measure of relative photon catch for each stimulus type through the filters. The crosstalk is the ratio of the relative photon catch of the stimulus intended for one eye by the other.

We also varied other parameters of the visual scene: the shrimp moving across the visual scene either walked or swam, and we also presented the cuttlefish with videos consisting of a shrimp dissimulated in a background of dots that were either correlated (same contrast polarity), anticorrelated (flipped contrast) or uncorrelated (different pattern) between both eyes. The 1.4 mm dot stimuli, when viewed at 18 cm, subtends 0.44° . The 5 mm dot stimuli, when viewed at 18 cm, subtends 1.59° . Data from both size dot patterns were combined in [Figure 6.10](#) as we found no significant difference between these data sets (Correlated 0 cm and 2 cm disparity, $p = 1.0$ and 0.1074 ; Anti-correlated 0 cm and 2 cm disparity, $p = 0.9986$ and 0.5313). This methodology was adapted from Nityananda *et al.* (2016). All visual parameters were tested for a range of stimulus disparities and experimental protocols were applied in a random order over the course of each experimental day.

6.2.4 Data digitisation

Images from the high-speed camera were scaled by placing a calibration ruler at the bottom of the tank at the start of the experimental day to identify the pixel to millimetre conversion. Coordinates corresponding to the locations of the monitor, the animal's two eyes, the anterior and posterior edge of the mantle and the tip of the tentacles, were identified and extracted manually for the high-speed camera recordings of each cuttlefish hunt. These points were recorded for five time points corresponding to the transitions between stages of the attack sequence detailed by Messenger (1968): (1) the appearance of the prey on the screen, (2) the detection of the prey by the cuttlefish, (3) the first appearance of the tentacles beyond the arms, (4) the initiation of the ballistic tentacle extension and (5) the maximal tentacle extension.

6.2.5 Data analysis

A trial was only included in the dataset if a hunt occurred and was completed such that all five stages outlined above could be identified. Furthermore, trials were discarded if the animal was closer than 125 mm to the screen upon stimulus detection to ensure the target was within the field of view of both eyes. Coordinates extracted from data digitisation were used to calculate the distance from the midpoint of the eyes to the screen along the tentacle extension axis and to full tentacle extension. Once a stimulus disparity is introduced, however, the distance from predator to perceived prey location is determined using the value of the disparity, the interocular distance and the distance

from the eyes to the screen (**Figure 6.5**). Using this methodology, we calculated the distance from eyes to illusory prey for all non-zero disparities. We also calculated the angle of the eyes to the screen and the angle of the tentacles to the screen (**Figure 6.7**). For zero disparity trials, the animal's position was tracked over the course of the hunt to measure the distance travelled (**Figure 6.8**). For these analyses, high speed videos were shortened by retaining every 1 in 10 frames and any trial where the animal took longer than 10 seconds to detect the stimulus was discarded. All analyses and tracking were conducted in Matlab 2015b (The MathWorks, Inc., Natick, Massachusetts, United States).

Statistics

All stages of data analysis including statistical analysis were conducted using custom-made programmes and statistical packages available in Matlab 2015b (The MathWorks, Inc., Natick, Massachusetts, United States). Individual statistical tests are reported in figure legends and the results of post hoc tests, original data points, mean, standard deviation, and standard error of the mean are reported throughout using notBoxPlot Matlab function (version 1.31.0.0, Rob Cambell).

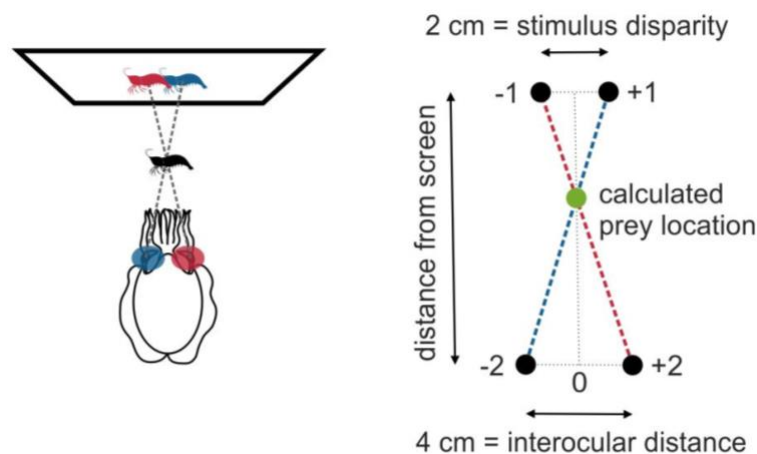


Figure 6.5 Establishing the calculated prey location for stimuli with disparities.

The disparity of the shrimp stimuli between the left and right eye creates the illusion of the prey in a different plane than the screen. Here an example of the methodology used to calculate the illusory prey location using the value of the disparity, the interocular distance and the eyes to screen distance.

6.3 RESULTS

6.3.1 Cuttlefish are tricked by a stereoscopic illusion

Our investigation aimed to probe for a role for stereoscopic vision in the cuttlefish hunting behaviour. To this end, we monitored the animal's response to a shrimp presented via a screen. We used coloured glasses fitted to the cuttlefish to deliver a stereoscopic stimulus in which images the right and the left eye were disparate laterally. When delivered to a subject capable of stereopsis, this stimulus creates an illusion that places the perceived target closer or further than the screen. In our cuttlefish experiments, we found that they significantly increased the distance of their eyes relative to the screen, proportional with the increasing stimulus disparity (**Figure 6.6 A**, 1-way ANOVA $p = 0.0123, 0.0041, 0.0161$ and <0.0000 respectively). Furthermore, the stimulus disparity and cuttlefish's position were correlated (**Figure 6.6 A**, Pearson's correlation $r^2 = 0.74$). Next, we established an expected distance from the perceived illusory prey using the mean eye to target distance at zero disparity. By subtracting this value from the calculated distance for other disparity conditions, we were able to compare the accuracy of positioning for each stimulus disparity relative to the absence of disparity. No stimulus disparities were found to be significantly different from the zero-disparity condition (**Figure 6.6 B**, Bootstrap test, $p > 0.05$ for all groups).

6.3.2 Tentacle extension is precisely calculated

We measured the maximal length of the fully extended tentacles (from the tip of the clubs) across the range of stimulus disparities. Using the zero-disparity condition as our reference, we observed that positive stimulus disparities induced a consistent overshoot of the tentacles of approximately 20 mm (**Figure 6.6 C**, 1-way ANOVA $p = 0.0041, <0.0000$ and <0.0000 respectively and **Figure 6.6 D**, Bootstrap test, $p = 0.2236, 0.0356$, and <0.0000 for increasing positive disparities). In the case of the negative disparity conditions, the tentacle extension was impeded by the edge of the tank and although data is reported in **Figure 6.6**, no statistical analyses were conducted for this subset of data.

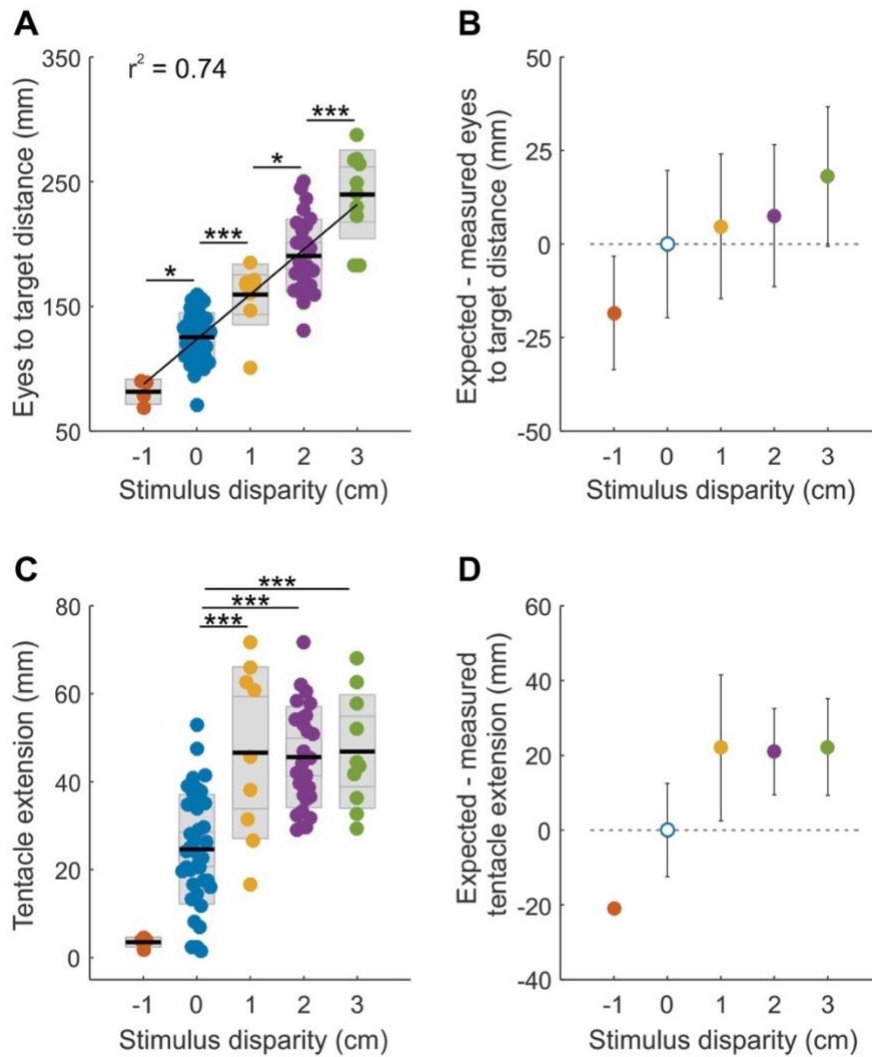


Figure 6.6 Cuttlefish have stereoscopic vision.

(A) Distance of the animal's eyes from the screen at prey strike for a range of stimulus disparities and (1-way ANOVA, p -values from left to right: 0.0123, 0.0041, 0.0161 and <0.0001). (B) the difference from the expected positioning for each stimulus disparity (Bootstrap test, $p = 0.2490$, $p = 0.8897$, $p = 0.7498$ and $p = 0.4008$). (C) Length of full tentacle extension for each disparity (1-way ANOVA, p -values from left to right: 0.0041, <0.0000 and <0.0000) and (D) the difference from the expected length in tentacle extension for each disparity condition (Bootstrap test, $p < 0.0001$, $p = 0.2236$, $p = 0.0356$, and $p < 0.0001$). Black, solid lines represent the mean value. From the mean outwards, the first grey line of the background box shows the 95% confidence interval (or 1.96 standard error of the mean) and the second grey line represents 1 standard deviation from the mean. $n = 2, 5, 2, 5, 2$ for -1, 0, 1, 2, 3 cm disparities, respectively.

6.3.3 Control parameters of the hunting behaviour

We found no evidence of differences in the hunting behaviour for the when the stimuli presented was a walking or swimming shrimp and whether the stimuli had a white or black background (**Figure 6.7 A**, data only shown for the zero-disparity condition), and as such the data presented in this chapter combines trials from all of these conditions. Furthermore, apart from a change in head position relative to the screen as correlated to altered disparity, our analyses did not reveal any other modification of the animal's behaviour during the attack sequence. The angle of the eyes to the screen at the start of the ballistic shoot does not exhibit any relationship to the distance between eyes and target across the range of disparities (**Figure 6.7 B**), and the strong 90° tentacle to eyes angle is consistent with the exception of a few trials at either end of the disparity spectrum (**Figure 6.7 C**, Pearson's correlation $r^2 = 0.908$).

6.3.4 Impact of binocular vision on the hunting behaviour

To investigate how stereoscopic cues might improve the cuttlefish predation, we compared the behaviour of animals presented with monocular and binocular visual stimuli. Note that all monocular experiments used stimuli filtered to one eye only through the glasses rather than monocular occlusion. The second phase of the hunt, during which the animal chooses the optimal location from which to strike, exhibits a significant difference between monocular and binocular experiments, whereas other stages did not. Specifically, monocularly presented prey causes the animal to spend more time positioning itself before striking as well as travelling a greater distance during this phase than animals hunting a binocular stimulus. Furthermore, monocularly-driven cuttlefish position themselves closer to the screen than their binocular counterparts (**Figure 6.8**, 1-way ANOVA $p < 0.0000$, $p < 0.0000$ and $p = 0.0018$ respectively).

Our data suggest that timings from each phase of the hunt are not affected by the previous phase. Indeed, a longer target detection delay does not predict a longer striking delay (**Figure 6.9 A**). Similarly, the initial distance from the target does not have any bearing on the time to strike (**Figure 6.9 B**). These findings are the same for the monocular and binocular group, suggesting that the monocular group is not disadvantaged by the higher probability of increased stimulus detection time resulting from the reduced field of view. The shrimp stimulus presented to the cuttlefish moves

across the screen from left to right and reverses its direction of travel once it reaches the edge of the screen. The dataset was divided into animals that shot at the target before and after the direction flip. Although this analysis does not reveal a significant difference between monocular and binocular groups, the delay to striking of monocularly driven animals appears to be affected more by the stimulus flip than binocular animals (**Figure 6.9 C**).

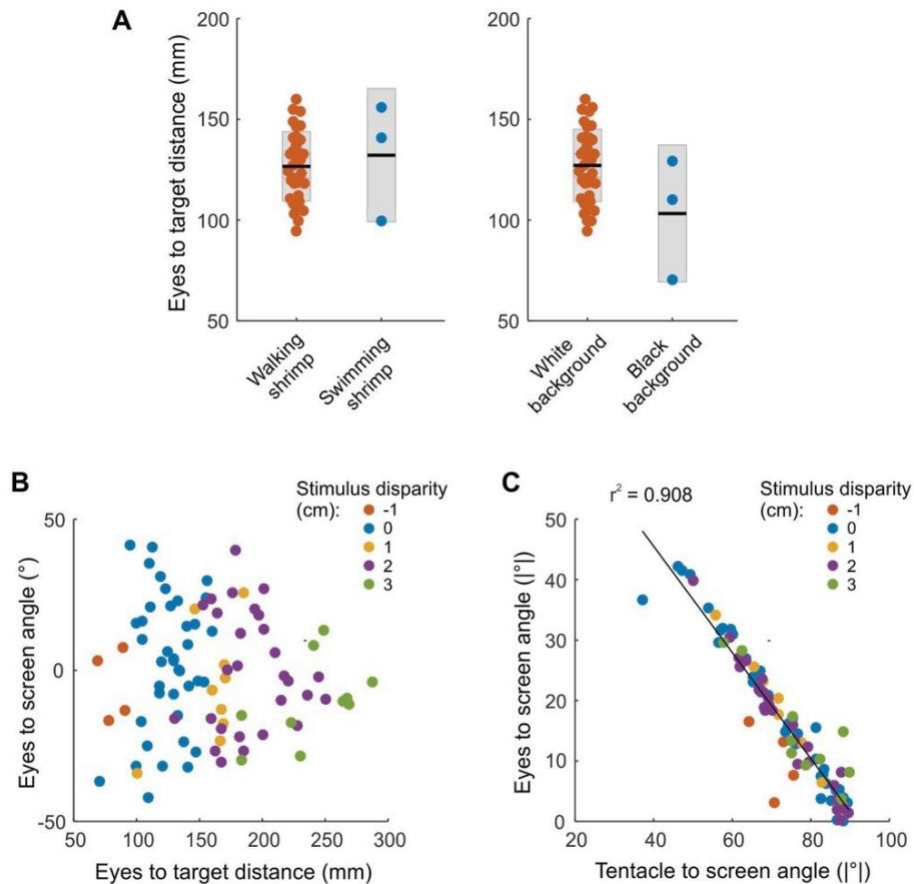


Figure 6.7 Control data for different parameters of the hunting behaviour.

(A) Eyes to target distance for varying parameters of the visual stimulus, such as shrimp movement and background for the zero-disparity condition. Black, solid lines represent the mean value. From the mean outwards, the first grey line of the background box shows the 95% confidence interval (or 1.96 standard error of the mean) and the second grey line represents one standard deviation from the mean. (B) Scatter plot illustrating the relation between the eye to target distance and the angle of the eyes to the screen for all stimulus disparities. (C) Scatter plot illustrating the relationship between the absolute angle of the tentacles to the screen and the absolute angle of the eyes to the screen for all disparity conditions. $n = 2, 5, 2, 5, 2$ for $-1, 0, 1, 2, 3$ cm disparities, respectively.

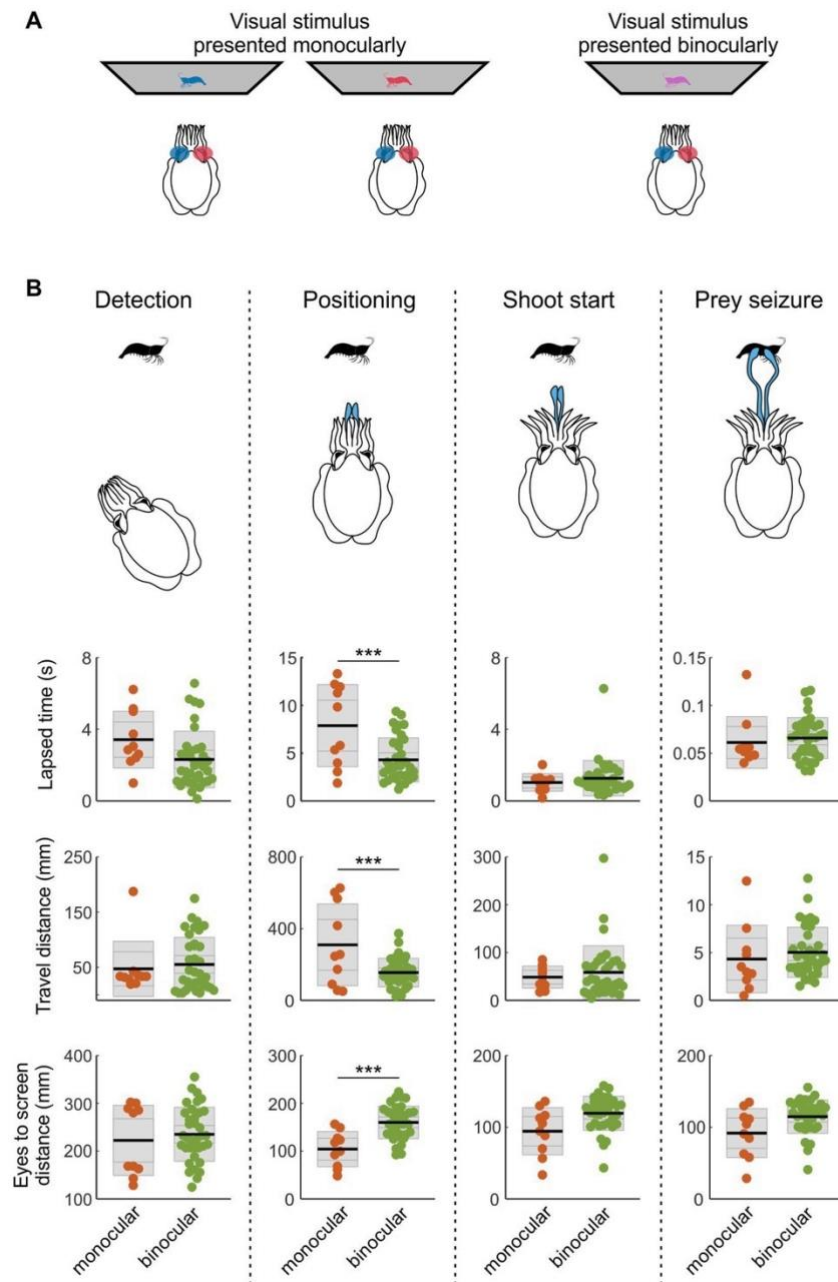


Figure 6.8 Binocular vision improves hunting behaviour.

(A) Cuttlefish fitted with anaglyph 3D coloured glasses can be presented with monocular and binocular visual stimuli. (B) Boxplots detailing lapsed time, distance of travel and distance of the animal to the screen for the different stages of the hunt for monocular ($n = 3$) and binocular ($n = 5$) experiments. Black, solid lines represent the mean value. From the mean outwards, the first grey line of the background box shows the 95% confidence interval (or 1.96 standard error of the mean) and the second grey line represents 1 standard deviation from the mean.

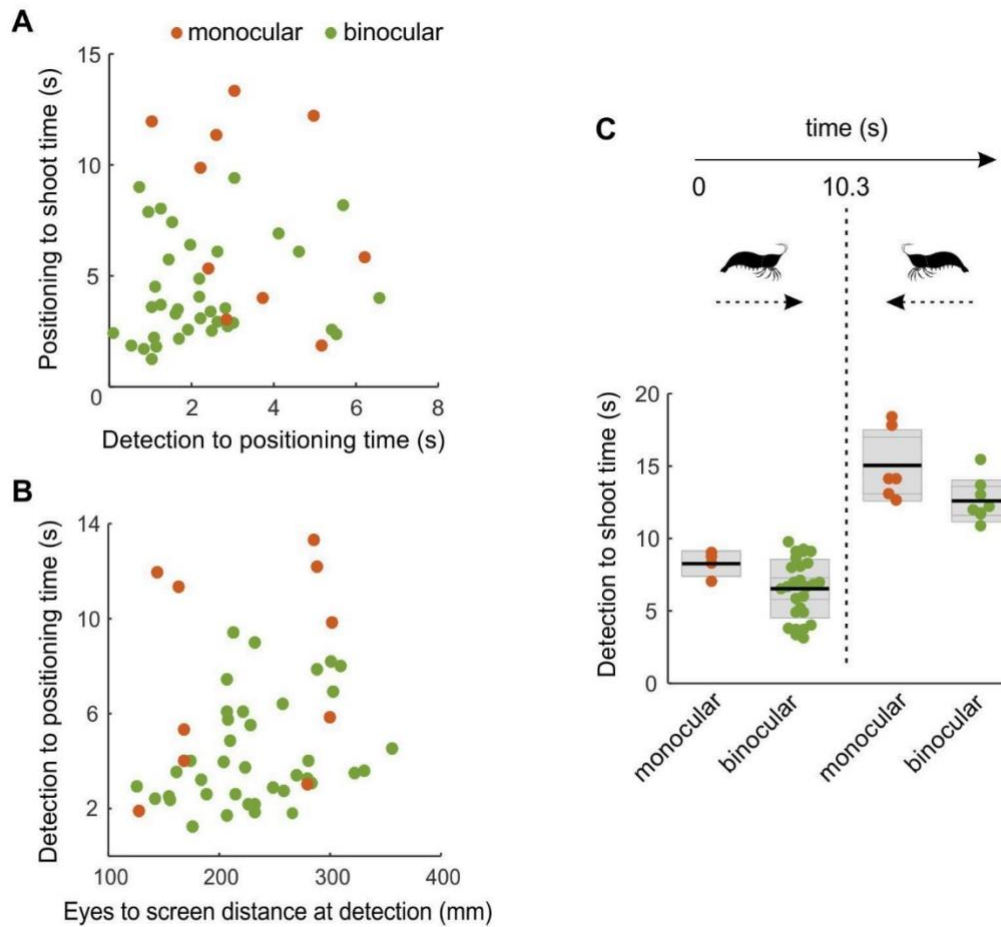


Figure 6.9 Control analyses for monocular and binocular behaviour timings.

(A) Scatter plot illustrating the relationship between time lapsed during the detection phase and the positioning phase of the hunt, combined monocular and binocular data: $r^2 = 0.0114$, monocular alone ($n = 3$): $r^2 = 0.1331$, binocular alone ($n = 5$): $r^2 = 0.0162$. (B) Scatter plot illustrating the relationship between eyes to screen distance and time lapsed during the detection phase, combined monocular and binocular data: $r^2 = 0.0436$, monocular alone: $r^2 = 0.0679$ ($n = 3$), binocular alone: $r^2 = 0.0860$ ($n = 5$). (C) Total time to shoot start shown for animals that strike before and after the direction of travel of the stimulus is reversed for monocular and binocular experiments. Black, solid lines represent the mean value. From the mean outwards, the first grey line of the background box shows the 95% confidence interval (or 1.96 standard error of the mean) and the second grey line represents one standard deviation from the mean.

6.3.5 ‘Static’ and ‘kinetic’ luminance correlation between eyes

Stimuli videos with a random-dot pattern background were used to probe the mechanisms underlying stereopsis in cuttlefish. Interestingly, we were only able to train six of the eleven animals to shoot at the target in this stimulus configuration. The remaining five animals appeared to notice the dotty-pattern stimulus, engaged positioning behaviour on occasion but seemed did not strike at the on-screen stimuli.

The three different dotty-pattern stimuli were applied to tease apart the importance of cross-correlating global versus local luminance patterns between both eyes in cuttlefish stereopsis. For all three conditions, the shrimp silhouette, dissimulated in the dot pattern, was indistinguishable from the background in any one monocular frame. In the case of correlated stimuli, the visual scene is identical for both eyes. We found that the position of the cuttlefish prior to striking is significantly different between a zero-disparity and a 2 cm disparity stimulus (**Figure 6.10 A** middle panel, 1-way ANOVA $p = 1.483\text{e-}07$), and the position of the animals for this latter disparity is not different from expected (**Figure 6.10 A** lower panel, Bootstrap test $p = 0.730$). Thus, as shown above for uniform background, cuttlefish positioning is also dependent on the stimulus disparity in the presence of a cluttered background. The same outcome was observed when the stimulus background was uncorrelated such that the luminance of the dots was reversed between eyes (**Figure 6.10 B** middle panel, 1-way ANOVA $p = 2.378\text{e-}06$; **Figure 6.10 B** lower panel, Bootstrap test $p = 0.499$). This indicates that cuttlefish are able to resolve a stereoscopic stimulus even when the static disparity of the background is disrupted. In the presence of an uncorrelated background, the static disparity is removed from the image completely as the background dotty pattern is different from one eye to another. We found that despite taking an interest in the stimulus and engaging in the early stages of the hunt, the cuttlefish consistently gave up during the positioning phase and didn't strike at the screen.

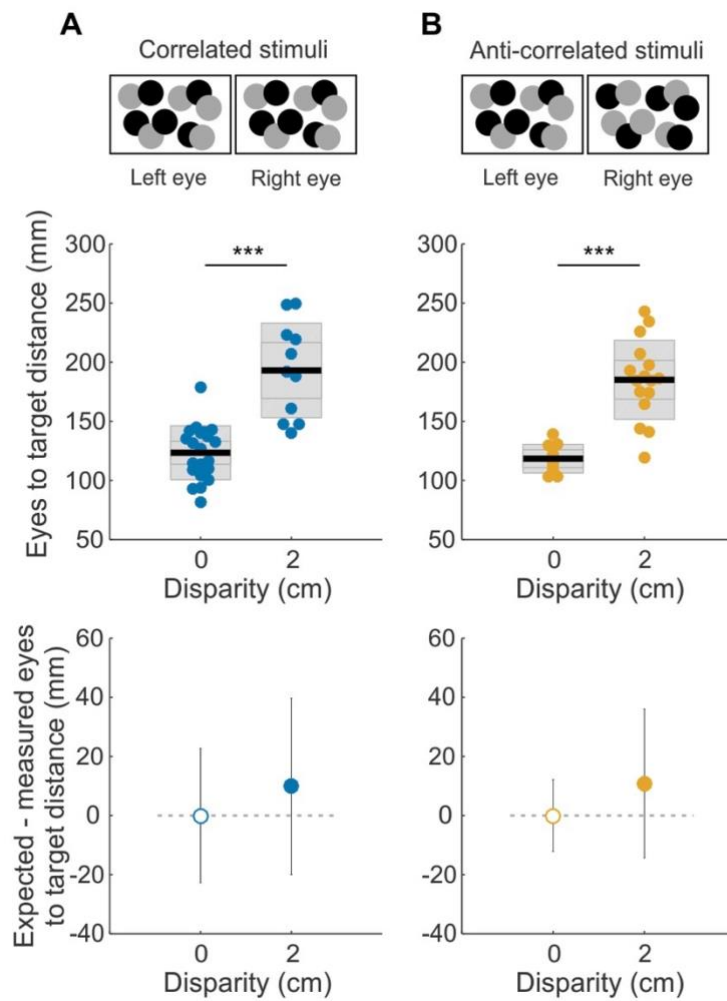


Figure 6.10 Stereopsis and luminance correlation.

(A) Cuttlefish can resolve the disparity of the target shrimp stimulus when camouflaged within a random pattern of dark and bright dots, correlated between the left and the right eye, which was indistinguishable from the background in any one monocular frame. Schematic of the stimulus presented (top), the distance from eyes to target just prior to the shoot (middle, 1-way ANOVA $p = 1.483\text{e-}07$) and the distance of each group from the expected value (bottom, Bootstrap test $p = 0.730$). (B) The same result was found when the patterns of dots were anti-correlated between the left and the right eye (middle, 1-way ANOVA $p = 2.378\text{e-}06$, bottom, Bootstrap test $p = 0.499$). Black, solid lines represent the mean value. From the mean outwards, the first grey line of the background box shows the 95% confidence interval (or 1.96 standard error of the mean) and the second grey line represents one standard deviation from the mean. $n = 6$ & 3 for 0 & 2 cm correlated disparities, $n = 5$ & 4 for 0 & 2 cm anti-correlated disparities.

6.4 DISCUSSION

Cuttlefish require accurate knowledge of the location of their prey in order to ensure they direct their tentacles to successfully hit the target. Here we show that cuttlefish use left and right eye stimulus disparity to perceive depth so that they can determine the optimal position to range-find their prey before shooting, and that binocular vision increases the efficiency of the attack sequence. We also show that cuttlefish consistently overshoot their tentacle extension when they do not encounter a physical object (expected prey or screen). Taken together, these results provide strong evidence that cuttlefish perceive the stereoscopic illusion and adjust their prey striking position accordingly. Thus, cuttlefish use stereopsis to improve their hunting behaviour. Furthermore, we demonstrate that cuttlefish compute stereopsis in a fundamentally different manner to humans but similar to praying mantids, the only other invertebrate species currently known to use stereopsis (Nityananda *et al.*, 2016; Nityananda and Read, 2017).

6.4.1 Experimental considerations

Stereopsis in cuttlefish has long been postulated, notably by Messenger (1968), who stipulates that the ballistic tentacle extension for prey capture is too rapid for visual feedback about tentacle position. As such, estimating the distance relative to the target prior to the attack is critical if the hunt is to be successful. Although we were able to show stereopsis is employed for prey capture, a few experimental considerations should be discussed. The “anaglyph” style stimulus is particularly appropriate for the monochromatic cuttlefish visual system as different coloured stimuli are unlikely to cause complications in visual processing. However, the use of blue and red filters for the glasses is not the most appropriate design as red is at the far end of the cuttlefish opsin sensitivity and as such luminance is not matched between eyes. This, however, did not appear to affect the cuttlefish’s ability to detect a stereoscopic stimulus, and it has been previously reported that the shape of the prey is more strongly discriminated for than the brightness of the prey (Guilbe *et al.*, 2012). Nonetheless, the red filter was swapped out for a green filter for the second field trip to ensure optimal luminance matching between eyes (see methods section 6.2.4). Furthermore, we observe a small drift from the expected distance from eye to screen distance as the stimulus disparity increases. This is most likely a consequence

of the diffraction of light in the water medium that will affect the crossover point of perceived illusory stimulus. As the disparity increases, this diffraction phenomenon will be amplified.

We observed differences amongst cuttlefish individuals in the rate of task learning and willingness to engage with the stimulus in tougher tasks. These discrepancies were most obvious for random-dot pattern experiments where a subset of the cuttlefish displayed no willingness to attempt a hunt, even in the simplest stimulus configuration where the luminance pattern was correlated between the eyes. It is unlikely that this subset of animals lacks the ability to perform a task that other cuttlefish have no trouble completing. Furthermore, general performance (for both uniform and cluttered backgrounds) did not appear to be affected by hunger states and was consistent for individuals across experimental days. Thus, the interpretation I propose for these differences is distinctive character traits present in each cuttlefish that may drive differences in motivation, something I have observed from working with these animals, which has also been suggested by other cephalopod researchers (Sinn *et al.*, 2008; Carere *et al.*, 2018; Zoratto *et al.*, 2018).

6.4.2 Stereopsis is used in addition to other depth cues

Interestingly, our monocular data set is not homogenous. A subset of animals exhibited increased time latency and travel distance in addition to misestimation of target location in the prey range-finding phase of the hunt. This is unsurprising and although we are unable to assess the success of prey capture with these data (the setup does not enable us to track the location of the shrimp on the screen), we know from Messenger (1968) that in unilaterally blinded animals the success of an attack decreases to 56% (91% in binocular animals). Messenger notes that, frequently, monocular animals badly estimate the distance, as well as the direction. However, in Messenger's study and in ours, several of the monocularly stimulated cuttlefish do not appear to hunt with less precision compared with their binocularly stimulated counterparts. This suggests that stereopsis is not the only depth perception mechanism used by the cuttlefish for this task. The absence of pictorial cues in the stimulus (the shrimp silhouette lacks any shadowing, shading or occlusion thus removing any illusion of depth) leads us to consider that for monocular depth perception, cuttlefish may rely on motion cues such as parallax (Helmer *et al.*, 2017) and/or motion-in-depth (Thompson *et al.*, 2019). With repeated exposure to an

identical shrimp outline in all stimulus videos (with the exception of the few trials comprising a swimming shrimp rather than a walking shrimp), it is interesting to consider that the cuttlefish might learn to gauge the distance of the target using the angular size of the stimulus. This could be an alternative explanation for the successful monocular hunts.

6.4.3 Cuttlefish stereopsis requires ‘static’ background disparity

A fundamental principle of vertebrate stereoscopic vision lies in the ability to perceive a camouflaged object within the single binocular frame of two static images (Julesz, 1986). Praying mantids, however, are able to resolve targets based on the so-called ‘kinetic disparity’, the difference in location of moving object between both eyes. They can do this in the absence of ‘static disparity’ provided by the surrounding visual scene, something which humans are unable to do (Nityananda *et al.*, 2018). Although cuttlefish stereopsis appears to bear some hallmarks of insect stereopsis, our results suggest that the ability to resolve kinetic disparity in the absence of static disparity is limited. An interesting question for further investigation is whether stereopsis in cuttlefish can be motion-independent.

6.4.4 Stereopsis and eye movement control

An intriguing outcome of this study lies with the correspondence problem. Despite numerous similarities between primate and cuttlefish eyes such as camera-type, accommodating lens, eye mobility, etc., one fundamental difference is especially problematic when considering stereopsis: cuttlefish eyes move independently of each other. In mammals, it is known that tight coordinated control of eye movements is necessary for stereopsis, as independent movements will result in unresolvable differences when comparing both retinal images leading to fusion failure (Otero-Millan *et al.*, 2014). Therefore, even in the case of binocular overlap, the question remains – can distance computations from retinal disparity be accurate if the overlap of the eyes is constantly changing? The resolution of the cuttlefish retina is relatively low, estimated around 0.57 to 2.5° per photoreceptor (Groeger *et al.*, 2005). Thus, it is plausible that the varying overlap between the eyes falls within a magnitude range comparable to vertebrates for their respective resolution. Eye mobility and stereopsis have previously been investigated in chameleons who appear to lack stereopsis (Ott, 2001) and use accommodation cues instead (Harkness, 1977; Ott *et al.*, 1998), a

strategy that may well be implemented by cuttlefish too. However, Messenger (1968) notes that the convergence of the eyes for prey fixation is such that the image of the shrimp always falls on the same location of the retina. Furthermore, he observes that the eyes converge further as the distance to the prey diminishes, which is suggestive of a specialised fixation point on each retina to align the image of the target.

It is interesting to consider whether the correspondence problem is the underlying reason for which cuttlefish perform well in the anti-correlated background task but are unable to resolve the target for the uncorrelated stimulus. In the case of anti-correlation, the static background maintains an identical pattern of shapes as only the luminance is reversed between eyes. A lack of uniformity between eyes in the background of uncorrelated stimuli might lack the necessary landmarks to align retinal images. Further investigation is required to establish the properties of stereoscopic vision in cuttlefish and to uncover the neural mechanisms underlying the computation of stereopsis in these animals.

6.4.5 Alternative depth perception cues

As suggested by Messenger (1968), other depth estimation strategies, such as oculomotor proprioceptive cues provided by the vergence of the two eyes (Gonzalez and Perez, 1998; Donaldson, 2000) could be at play. Accommodation cues, as employed by chameleons to judge distance (Harkness, 1977) provide an additional explanation. However, if proprioceptive or accommodation cues were being used by cuttlefish for such purpose, depth estimation should not fail as it did when presented with a completely uncorrelated stimulus. i.e. each eye should still fixate and converge on the moving target without requiring correspondence between the images. Importantly, we observed that cuttlefish consistently engaged and reached the positioning phase when presented with uncorrelated stimuli, but they quickly aborted and never advanced to the shooting phase of the hunt. Therefore, our results suggest that cuttlefish must rely on binocular disparity (stereopsis), and not simply on binocular optomotor cues (vergence) or accommodation to estimate depth.

Harris *et al.* (2008) propose an alternative binocular depth perception mechanism: the use of use a different algorithm for computing depth that doesn't require precise knowledge of the location on both retinas that correspond to the same object. Instead, the velocity of a given object on the two retinas can be compared. It seems unlikely that the cuttlefish employ this strategy, however, as the cuttlefish were also positioned

in close proximity to the target, and the tentacles strike at a perpendicular orientation to the line between the eyes. As such, the velocity of the target on each retina would be largely similar, thus limiting the implementation of such a strategy.

6.4.6 Conclusions

The evidence presented here establishes that the European cuttlefish, *Sepia officinalis*, makes use of stereopsis when hunting in order to resolve the distance to the prey, and that this improves hunting performance by shortening the time and distance covered prior to striking at the target. We have uncovered an independently-evolved form of stereopsis in a non-vertebrate group with camera-type eyes. Further investigation is required to uncover the neural mechanisms underlying the computation of stereopsis in these animals, which appears to be different to both mantid and human stereopsis.

6.5. ACKNOWLEDGMENTS

This chapter is the product of a study conceived by Dr Paloma Gonzalez-Bellido and Dr Trevor Wardill. I joined the project after the completion of the first field trip and undertook glasses characterisation (and made the new design), visual stimulus refinement and behavioural experiments for the second field trip. I undertook the large majority of the data analysis and all of the figure generation. Data digitisation was kindly performed by Mary Sumner and Trevor Wardill.

6.6 REFERENCES

- Brown, P. K. and P. S. Brown (1958). "Visual pigments of the octopus and cuttlefish." *Nature* 182(4645): 1288-1290.
- Byrne R. A., M. Kuba and U. Griebel (2002) "Lateral asymmetry of eye use in *Octopus vulgaris*". *Anim Behav* 64, 461-468.
- Carere C., G. Grignani, R. Bonanni, M. DellaGala, A. Carlini, D. Angeletti, R. Cimmaruta, G. Nascetti and J. A. Mather (2015). "Consistent individual differences in the behavioural responsiveness of adult male cuttlefish (*Sepia officinalis*)". *Applied Animal Behaviour Science* 167, 89-95.

- Chung, W. S. and J. Marshall (2014). "Range-finding in squid using retinal deformation and image blur." *Curr Biol* 24(2): R64-65.
- Cumming, B. G. and G. C. DeAngelis (2001). "The physiology of stereopsis." *Annu Rev Neurosci* 24: 203-238.
- Donaldson, I. M. (2000). "The functions of the proprioceptors of the eye muscles." *Philos Trans R Soc Lond B Biol Sci* 355(1404): 1685-1754.
- Gonzalez, F. and R. Perez (1998). "Neural mechanisms underlying stereoscopic vision." *Prog Neurobiol* 55(3): 191-224.
- Groeger G., P. A. Cotton and R. Williamson (2005). "Ontogenetic changes in the visual acuity of *Sepia officinalis* measured using the optomotor response". *Canadian Journal of Zoology-Revue Canadienne De Zoologie* 83, 274-279.
- Guibe M., N. Poirel, O. Houde and L. Dickel (2012). "Food imprinting and visual generalization in embryos and newly hatched cuttlefish, *Sepia officinalis*". *Anim Behav* 84, 213-217.
- Hanlon R. T. and J. B. Messenger (1996). "Cephalopod behaviour". Cambridge University Press, Cambridge, pp. 232.
- Harkness, L. (1977). "Chameleons use accommodation cues to judge distance." *Nature* 267(5609): 346-349.
- Harris, J. M., H. T. Nefs and C. E. Grafton (2008). "Binocular vision and motion-in-depth." *Spat Vis* 21(6): 531-547.
- Helmer, D., B. R. Geurten, G. Dehnhardt and F. D. Hanke (2016). "Saccadic Movement Strategy in Common Cuttlefish." *Front Physiol* 7: 660.
- Julesz, B. (1986). "Stereoscopic vision." *Vision Res* 26(9): 1601-1612.
- Kröger, B., J. Vinther and D. Fuchs (2011). "Cephalopod origin and evolution: A congruent picture emerging from fossils, development and molecules: Extant cephalopods are younger than previously realised and were under major selection to become agile, shell-less predators." *Bioessays* 33(8): 602-613.
- Messenger, J. B. (1968). "The visual attack of the cuttlefish, *Sepia officinalis*." *Anim Behav* 16(2): 342-357.
- Nityananda, V. and J. C. A. Read (2017). "Stereopsis in animals: evolution, function and mechanisms." *J Exp Biol* 220(Pt 14): 2502-2512.
- Nityananda, V., G. Tarawneh, S. Henriksen, D. Umeton, A. Simmons and J. C. A. Read (2018). "A Novel Form of Stereo Vision in the Praying Mantis." *Curr Biol* 28(4): 588-593.e584.

- Nityananda, V., G. Tarawneh, R. Rosner, J. Nicolas, S. Crichton and J. Read (2016). "Insect stereopsis demonstrated using a 3D insect cinema." *Sci Rep* 6: 18718.
- Otero-Millan, J., S. L. Macknik and S. Martinez-Conde (2014). "Fixational eye movements and binocular vision." *Front Integr Neurosci* 8: 52.
- Ott, M., F. Schaeffel and W. Kirmse (1998). "Binocular vision and accommodation in prey-catching chameleons". *J. Comp. Physiol. A* 182: 319-330.
- Ott, M. (2001). "Chameleons have independent eye movements but synchronise both eyes during saccadic prey tracking." *Exp Brain Res* 139(2): 173-179.
- Panetta D., M. Solomon, K. Buresch and R. T. Hanlon (2017). "Small-scale rearing of cuttlefish (*Sepia officinalis*) for research purposes". *Mar Freshw Behav Phy* 50, 115-124.
- Rosner, R., J. von Hadeln, G. Tarawneh and J. C. A. Read (2019). "A neuronal correlate of insect stereopsis." *Nat Commun* 10(1): 2845.
- Rossel S. (1983). "Binocular stereopsis in an insect". *Nature* volume 302, 821–822.
- Sinn D. L., S. D. Gosling and N. A. Moltschaniwskyj (2008). "Development of shy/bold behaviour in squid: context-specific phenotypes associated with developmental plasticity". *Anim Behav* 75, 433-442.
- Stavenga, D. G., R. P. Smits and B. J. Hoenders (1993). "Simple exponential functions describing the absorbance bands of visual pigment spectra." *Vision Res* 33(8): 1011-1017.
- Thompson, L., M. Ji, B. Rokers and A. Rosenberg (2019). "Contributions of binocular and monocular cues to motion-in-depth perception." *J Vis* 19(3): 2.
- Warrant, E. (2004). "Vision in the dimmest habitats on earth." *J Comp Physiol A Neuroethol Sens Neural Behav Physiol* 190(10): 765-789.
- Warrant, E. J. and D. E. Nilsson (1998). "Absorption of white light in photoreceptors." *Vision Res* 38(2): 195-207.
- Welchman, A. E. (2016). "The Human Brain in Depth: How We See in 3D." *Annu Rev Vis Sci* 2: 345-376.
- Welchman, A. E., A. Deubelius, V. Conrad, H. H. Bülthoff and Z. Kourtzi (2005). "3D shape perception from combined depth cues in human visual cortex." *Nat Neurosci* 8(6): 820-827.
- Zoratto, F., G. Cordeschi, G. Grignani, R. Bonanni, E. Alleva, G. Nascetti, J. A. Mather and C. Carere (2018). "Variability in the "stereotyped" prey capture sequence of male cuttlefish (*Sepia officinalis*) could relate to personality differences." *Anim Cogn* 21(6): 773-785.

Chapter 7 – Concluding remarks and future directions

7.1 EXPLORING FACETS OF INVERTEBRATE VISION

Despite the somewhat eclectic nature of this thesis, from engineering an optical setup to recording physiological responses in the optic lobes of *Drosophila* to behavioural testing of cuttlefish binocular vision, my PhD journey has provided me with a diverse experience studying how animal undertake processing of visual information.

7.1.1 General conclusions

As detailed in Chapter 3, we developed and build a setup for simultaneous spectral stimulation and two-photon imaging, overcame the complexities of producing a stimulus with both high spatial and high spectral resolution while maintaining spectral constancy across a rear projection screen. The data I present in Chapter 4 may not provide a definitive answer to a newly uncovered neural mechanisms underpinning colour vision in *Drosophila*, but it does show that variability in spectral responses exist across different medulla layers. Furthermore, this study confirms the adequacy and precision of my setup, as well as my visual stimulation paradigms. I was also able to confirm the influence of screening pigment on spectral processing. In Chapter 5, I recorded spatial maps of summed medulla activity with identifiable receptive fields of expected size predicted by the conservation of a columnar organisation, as well as evidence for an elongated shape in a subset of cases. Thus, through these three chapters, I have developed the necessary tools for probing spectral response profiles, intensity response relationships and receptive field characterisation in one unified experimental setup. Furthermore, this could be applied to a variety of small insects that fit in the microscope holder if neuronal labelling is achievable (through electroporated dyes for example).

Chapter 6 took an unexpected turn into a different branch of vision science, with a new model organism, a new visual processing feature and a new methodological approach (not to mention a whole new continent with the lab move to the University of Minnesota).

Nonetheless, the necessity to design precise colour stimuli for isolated stimulation of either eye through the coloured-filter glasses created an amusing bridge between both segments of my thesis, thus allowing me to apply skills developed during the earlier phase of my PhD. This section of my thesis demonstrated the use of stereoscopic vision in cuttlefish, which has evolved through convergence in this species and appears to use alternate neural processing from that used by humans or mantids.

Interestingly, the two visual processing mechanisms I have studied, colour vision and stereopsis, do not coexist in any invertebrate species to our knowledge. Both the praying mantis and the cuttlefish only express one class of photoreceptor, and we have yet to attribute stereoscopic vision to any other invertebrate. It is interesting to consider how stereopsis and colour processing, both expensive neural processes involving a comparative computation, might be competing features with invertebrate species evolving just one of the two (Nityananda and Read, 2017).

7.1.2 Future directions for studying fly spectral processing

The investigation of spectral processing in *Drosophila* requires the development of many different experimental components, especially in a newly formed colour vision lab where the project has to be developed from square one. The work from my PhD has established a functionally dissected and physiologically stable fly preparation, a precisely engineered visual stimulation setup as well as operative visual stimulation paradigms and analysis methodology. This provides the essential framework for future work characterising medulla (or other optic lobe) neuron responses.

Our understanding of the spectral quality of visual information transmitted by the different photoreceptive cells to downstream visual neurons is primarily based on the generation of spectral sensitivity curves for opsins or electroretinogram measurements of the surface of the eye (Salcedo *et al.*, 1999; Stavenga *et al.*, 2010). The recent breakthrough study by Schnaitmann *et al.* (2018), however, demonstrated that R7 and R8 terminals interact to transform the inner photoreceptor output to a biphasic sensitivity curve, exemplifying the modification of spectral tuning at the early stages of visual processing. Very little is known about how outputs of different photoreceptors might be combined by colour-encoding circuits, highlighting the need for high resolution spectral stimulus capabilities. Our system uses narrow bands of monochromatic light well suited to our

investigation into spectral response properties, but it is entirely possible to modify the light source to produce multispectral light using a system such as the LED-based monochromator (Belušič *et al.*, 2016). Methods commonly employed in mammalian vision research, such as the sophisticated combination of multispectral light to effectively target only one class of photoreceptors (Estévez *et al.*, 1982), are limited in invertebrates. Further characterisation of the effect of pre-receptor filtering, such as eye pigment screening, as well as instability and adaptation properties of visual pigments, is required. With this information, a smaller, but carefully selected, array of colour channels can be coupled to a display technology (screen or panel) such as the modified projector system with a five-primary light engine used in mouse vision research (Allen *et al.*, 2017) or the arbitrary-spectrum spatial visual stimulator presenting up to six chromatic channels (Franke *et al.*, 2019).

An ideal spectral stimulation range would extend further into the UV portion of the spectrum to match the known spectral sensitivities of Rh1, Rh3 and Rh4. Monochromators providing this range of UV light exist. However, the high-energy photons of the shorter wavelengths are lost by transmission throughout the optical pathway, with the DLP chip in the projector, in particular, drastically reducing the UV content of light. The ongoing progress in the development of UV transmitting projectors (e.g. Texas Instruments) and optics might soon provide an adequate and affordable solution and extend the capabilities of our system to include UV visual stimulation.

One of the reasons I chose to record neural activity from the pan-neuronally labelled optic lobes was the absence of any obvious specific colour vision circuitry to target via single cell labelling. I hoped to locate colour responses in specific layers of the medulla to serve as guidance for a more selective approach. I also intended to establish spectral response properties of R7 and R8 photoreceptor terminals projecting to the medulla as this would provide a better indication of response dynamics etc to be expected in postsynaptic colour cells. Issues arose with the genetics of our labelled photoreceptor *Drosophila* model due to Gal4 toxicity which were subsequently solved through a promoter fusion to bypass Gal4, but time constraints left me unable to finish this work. Thus, future work should include detailed characterisation of photoreceptor terminal properties, including establishing intensity-response relationship and spectral sensitivity interactions to complete the work started by Schnaitmann *et al.* (2018). Spectral properties of any readily-labelled cell in the medulla can now be determined, however in

the absence genetic lines that enable targeting of cell specific targeting in accordance with the reconstructed neural circuitry, an exploratory approach might prove lengthy. Once these lines are made available to the public from HHMI Janelia or other labs, the field of colour vision in insects will be transformed, and more specific questions can be targeted.

7.1.3 Future directions for studying cuttlefish visual processing

A key motivation for studying cuttlefish and their neural system is that cephalopods present as a uniquely ideal model to investigate features of the convergent evolution of advanced cognition. Their visual system, in particular, is of interest, through its many parallels to primate vision, not just in terms of eye structure but also in its role as the primary sense by which both we and cuttlefish interact with the world. We have demonstrated that cuttlefish and primates share the capacity for stereopsis, but that the implementation algorithm is different in both species. This is just one example of a convergent neural response, with countless more to be uncovered to increase our understanding of the different mechanisms cuttlefish might have evolved to tackle various visual challenges.

The behavioural assay outlined in Chapter 6 opens many avenues for future work. The innate and robust hunting behaviour of the cuttlefish, with its clearly identifiable stages, provides an excellent platform for relating visual input to behavioural output. Our assay demonstrates that cuttlefish can be trained to track and strike at targets displayed on a computer monitor. In this way, visual input to the animal can be carefully controlled to tease apart distinct visual cues and the modifications they cause in the hunting behaviour. For example, by transforming the current setup into a closed-loop system, tracking strategies could be tested such a predictive eye or body movements to target prey moving behind an occluding object or the modification of target trajectories (change of speed or direction). Furthermore, the paradigm of fitting glasses to cuttlefish can be employed in many ways. For example, switching out the coloured filter lenses for prisms that laterally shift the field of view of the observer can be used to test behavioural adaptation mechanisms with a potential insight into neural plasticity capabilities, and allow us to compare how these processes might compare to their mammalian counterparts.

7.2 THE BIGGER PICTURE

7.2.1 Impact in the field of biological science

The overall importance of this investigation is emphasised by the growing field of visual studies in invertebrates. The emergence of *Drosophila* as a key neuroscience model has increased the impact of invertebrate visual studies and has taken on an important role of bridging the gap between neuroethological studies in non-model invertebrates and so called “classical” mammalian neuroscience. In the same vein, the view that a variety of species need to serve as model organisms is becoming more widely accepted. Thus, although the study of cephalopod biology has long been popular, recent years have seen a revival of visual and neural studies in cuttlefish, squid and octopus.

Although invertebrate neural biology is sometimes dismissed as “simpler” or “less sophisticated” than that of mammals, some invertebrate visual systems provide their hosts with sensory experiences that will never be accessible to mammals. For example, *Drosophila* possess the ability to see into the UV range of the spectrum, and cuttlefish are sensitive to the polarisation of light. In this way, these model organisms provide a whole new wealth of diversity in their visual processing abilities. In its current state, the field of colour vision is further advanced in primates than flies, primarily through a century of human visual psychophysics. However, to delve not only into colour vision but also more generally the influence of spectral information on other visual processes and visually guided behaviours, the fly and its neurogenetic and behavioural toolbox appears a more conducive model organism. Understanding the evolution of a visual feature, such as stereopsis, as well as the similarities and variances of that visual feature in the differently evolved versions, is important to unpick the selective pressures and adaptations on neural circuits encoding such a feature. Thus, visual studies in both flies and cuttlefish can provide valuable insights to the general field of visual neuroscience.

7.2.2 Impact in the field of technological science

Visual processing serves as a case study in information encoding and its underlying machinery. In other words, the information flow from the biochemical transformation of light information at the level of the photoreceptors through to the extraction of a salient visual feature can be studied by piecing apart the stages of that information processing in individual neurons and how these neurons form the building blocks of a larger network.

Visual circuits, or more general neural circuits in insects are very useful examples of the ways in which smaller brains and often much more compact circuits containing fewer cells can nonetheless process and extract complex information. This provides us with unique insights for developing new bioengineering solutions. For example, Lambrinos *et al.* (1997) have developed a robotic polarise light detector based on the dorsal rim area of ant eyes, Song *et al.* (2013) have pioneered a new camera design based on arthropod vision and navigation, sensory-motor control and visual strategies in flies have inspired many robotic designs (reviewed by Franceschini, 2014). Cephalopods might not have comparatively small brains, however their unique characteristics are nonetheless providing much inspiration in the field of technology including propulsion and buoyancy systems for Autonomous Underwater Vehicles (Song *et al.*, 2016), distributed cognitive control systems for artificial intelligence (Íñiguez, 2017).

Generally speaking, colour vision and depth perception are both very relevant to today's technological developments. Indeed, much effort has been directed towards creating displays that provide good colour capabilities. Not to mention the important milestones in the evolution of 3D cinematography over the past couple of decades, with a focus on creating a near-realistic experience to the viewer (Banks *et al.*, 2016). As discussed above, stereoscopic vision in cuttlefish is an important discovery from the perspective of the convergent evolution of neural processing. In addition, however, alternative neural implementations of stereopsis (e.g. in the praying mantis or cuttlefish) could provide technological advances to machine vision with a potentially simpler and less costly computational algorithm (Nityananda and Read, 2017), thus adding to the growing list of technology-inspiring cephalopod characteristics.

7.3 REFERENCES

- Allen, A. E., R. Storchi, F. P. Martial, R. A. Bedford and R. J. Lucas (2017). "Melanopsin Contributions to the Representation of Images in the Early Visual System." *Curr Biol* 27(11): 1623-1632.e1624.
- Belušič, G., M. Ilić, A. Meglič and P. Pirih (2016). "A fast multispectral light synthesiser based on LEDs and a diffraction grating." *Sci Rep* 6: 32012.
- Estévez, O. and H. Spekreijse (1982). "The "silent substitution" method in visual research." *Vision Res* 22(6): 681-691.

- Franceschini N. (2014). "Small brains, smart machines: from fly vision to robot vision and back again." *Proc. IEEE*, 102:751-781
- Franke, K., A. M. Chagas, Z. Zhao, M. J. Y. Zimmerman, P. Bartel, Y. Qiu, K. P. Szatko, T. Baden and T. Euler (2019). "An arbitrary-spectrum spatial visual stimulator for vision research". *Elife* 8: e48779.
- Íñiguez, A. (2017). "The octopus as a model for artificial intelligence-a multi-agent robotic case study," in *Proceedings of the 9th International Conference on Agents and Artificial Intelligence*.
- Lambrinos, D., H. Kobayashi, R. Pfeifer, M. Maris, T. Labhart and R. Wehner (1997). "An autonomous agent navigating with a polarized light compass." *Adaptive behavior*, 6(1):131–161, 1997.
- Nityananda, V. and J. C. A. Read (2017). "Stereopsis in animals: evolution, function and mechanisms." *J Exp Biol* 220(Pt 14): 2502-2512.
- Salcedo, E., A. Huber, S. Henrich, L. V. Chadwell, W. H. Chou, R. Paulsen and S. G. Britt (1999). "Blue- and green-absorbing visual pigments of *Drosophila*: ectopic expression and physiological characterization of the R8 photoreceptor cell-specific Rh5 and Rh6 rhodopsins." *J Neurosci* 19(24): 10716-10726.
- Schnaitmann, C., V. Haikala, E. Abraham, V. Oberhauser, T. Thestrup, O. Griesbeck and D. F. Reiff (2018). "Color Processing in the Early Visual System of *Drosophila*." *Cell* 172(1-2): 318-330.e318.
- Song, Y. M., Y. Xie, V. Malyarchuk, J. Xiao, I. Jung, K. J. Choi, Z. Liu, H. Park, C. Lu, R. Kim, R. Li, K. B. Crozier, Y. Huang and J. A. Rogers (2013). "Digital cameras with designs inspired by the arthropod eye." *Nature*, 497(7447): 95–99.
- Song, Z., C. Mazzola, E. Schwartz, R. Chen, J. Finlaw, M. Krieg and K. Mohseni (2016). "A compact autonomous underwater vehicle with cephalopod-inspired propulsion." *Mar. Technol. Soc. J.* 50 88–101.
- Stavenga, D. G. (2010). "On visual pigment templates and the spectral shape of invertebrate rhodopsins and metarhodopsins." *J Comp Physiol A Neuroethol Sens Neural Behav Physiol* 196(11): 869-878.

Appendix 1

Abbreviations for fly stocks:

RE-WT – red eye/ wild type photoreceptor function/ GCaMP (Stock 1)

RE-Rh1 – red eye/ Rh1 photoreceptors only/ GCaMP (Stock 3)

OE-Rh1 – orange eye/ Rh1 photoreceptors only/ GCaMP (Stock 4)

Table A1. 1-way ANOVA p-values from Figure 4.8

	RE-WT/RE-Rh1	RE-WT/OE-Rh1	RE-Rh1/OE-Rh1
396	1	3.2094e-05	3.2094e-05
398	1	3.2094e-05	3.2094e-05
401	0.8996	3.2094e-05	3.2094e-05
406	0.9999	3.2094e-05	3.2094e-05
411	1	3.2094e-05	3.2094e-05
416	1	3.2094e-05	3.2094e-05
421	1	3.2094e-05	3.2094e-05
425	1	3.2094e-05	3.2094e-05
430	1	3.2094e-05	3.2094e-05
435	1	3.2094e-05	3.2094e-05
440	1	3.2094e-05	3.2094e-05
445	0.0294	0.6676	3.2094e-05
451	1.9732e-04	4.3811e-05	1
569	0.0283	3.2094e-05	3.2094e-05
574	0.0098	3.2094e-05	3.2094e-05
578	0.1550	3.2094e-05	3.2094e-05
583	0.9891	3.2094e-05	3.2094e-05
589	1	3.2094e-05	3.2094e-05
593	1	3.2094e-05	3.2309e-05
598	1	2.5220e-04	0.2610

Table A2. 1-way ANOVA p-values from Figure 4.10

		RE-WT/RE-Rh1	RE-WT/OE-Rh1	RE-Rh1/OE-Rh1
M1	UV	1	1	1
	Blue	1	0.0039	0.6421
	Green	1	7.2533e-06	7.2533e-06
M2	UV	7.2533e-06	1	7.2533e-06
	Blue	7.2533e-06	0.7172	7.2533e-06
	Green	7.2533e-06	7.2533e-06	7.2533e-06
M3	UV	0.9962	1	0.9960
	Blue	0.4919	1	0.9999
	Green	0.9957	0.3603	1
M5	UV	1	0.1753	0.9403
	Blue	1	1	1
	Green	1	7.2534e-06	7.2534e-06
M6-M7	UV	1	0.0335	0.9671
	Blue	1	0.2098	0.9167
	Green	1	1	1
M9-M10	UV	1	0.0022	0.8434
	Blue	0.9999	1	0.9981
	Green	1	7.2534e-06	7.2534e-06

Appendix 2

Table A3. Fly preparation selection parameters for receptive field mapping.

Mean fluorescence change and cross-correlation values for reference images corresponding to averaged frames across the response period for all bars of a given orientation for the first and the last stimulus set repetition of an experiment.

	Mean fluorescence change	Start-end image correlation
Experiment 1	0.0472	0.9699
Experiment 2	0.1011	0.9488
Experiment 3	0.0521	0.9961
Experiment 4	0.0973	0.9859
Experiment 5	0.0763	0.9757
Experiment 6	0.00058	0.9732
Experiment 7	0.0969	0.9735
Experiment 8	0.0958	0.9958
Experiment 9	0.0788	0.9905
Experiment 10	0.064	0.9798